BEYOND ARROWS: ENERGY PERFORMANCE OF A NEW, NATURALLY VENTILATED DOUBLE-SKIN FACADE CONFIGURATION FOR A HIGH-RISE OFFICE BUILDING IN CHICAGO

BY

MONA AZARBAYJANI

DISSERTATION

Submitted in partial fulfillment of the requirements
for the degree of Doctor of Philosophy in Architecture
in the Graduate College of the
University of Illinois at Urbana-Champaign, 2010

Urbana, Illinois

Doctoral Committee:

Professor James R. Anderson, Chair, Director of Research
Associate Professor Richard Strand
Associate Professor Ralph Hammann
Professor Ty Newel

ABSTRACT

Designers tend to rely on their intuition when designing naturally ventilated buildings without detailed analyses for the long term. It may be argued that for many standard and smaller buildings, designing for natural ventilation is straightforward: a simple process of drawing diagrams to illustrate how air flows within the building, which can achieve satisfactory comfort conditions. However, there is a significant lack of information in the current literature to demonstrate the complexity and challenges in designing large, naturally ventilated buildings. This is especially true when the new double-skin facade (DSF) configuration is used as a means of conserving energy while providing superior thermal comfort. For these types of buildings, it is important to have the tools to evaluate a design's predicted performance to achieve successful natural ventilation concepts.

It has been learned that significant energy saving is possible by exploiting natural ventilation in a DSF configuration. To determine if a DSF configuration will provide a better thermal comfort through natural ventilation, this research uses building simulation tools (EnergyPlus) and Computational Fluid Dynamics (CFD) to analyze various thermal-comfort parameters through parametric studies in the facade.

This thesis presents three significant contributions for the evaluation of natural ventilation in high rise office buildings with DSF configuration:

- A methodology for assessing the performance of naturally ventilated DSF buildings through an airflow modeling was developed by three-dimensional analysis using Fluent. Buoyancy, wind, and combined ventilation strategies for a commercial office building with an open floor plan layout were evaluated using the k-ε model.

- Models to simulate the specific DSF typology and couple the envelope-level results to a building simulation program.

- A framework for comparing and evaluating the conventional facade solution with a new configuration of naturally ventilated DSF.

Acknowledgements

I would like to thank my advisor, Professor Jim Anderson, Your insight and our discussions were invaluable in the advancement of this research. I would like to thank Professor Hammann, for his unfailing guidance and patience throughout my quest to fulfill my research.
I am indebted to my thesis committee members for their support and insight during my research, and for their time, effort, and encouragement. Your suggestions and consideration was greatly appreciated.

My thanks and appreciation also go to those who gave up their valuable time and effort to guide, advise, and teach me, especially Professor Strand, Professor Bill Rose, and Professor Dimitrios Kyritsis.

I am also thankful to Jeaongli Kim, who patiently resolved and explained my Fluent problems.
I want to be sure to thank the Smart Energy Design Center for the many discussions, laughs, and moral support through the past four years. In particular, I would like to thank Ben Sliwinski: you have always been a true friend, willing to discuss and review my research, and have been supportive throughout.

I would like to thank all the experts who, by making available their theses, reports and articles, have provided easy access to knowledge.
To my friends, thank you for always listening, supporting, and reviewing my efforts over the past four years. My brother, you have my gratitude for always pushing me to succeed for being supportive.

Last but definitely not least, I would like to express my greatest gratitude to my parents for their support during all the years of my study. I wish to thank them for believing in me and supporting my choices without considering any cost.

Table of Contents

List of Figures

List of Tables and Graphs

Chapter 1.0

Introduction

With the emergence of energy-consumption reduction as a major national concern, the search for better approaches in improving both thermal comfort conditions and the energy efficiency of buildings is intensifying. Currently, low-energy building design features include lighting and controls, ventilation systems, and an improved building envelope. Lighting energy can be reduced through the use of natural daylighting, high efficiency fixtures and controls, such as occupancy sensors that turn lights off when there is no movement, and photosensors that reduce light output as needed to maintain a minimum level. These technologies, combined with architectural details like light shelves, high windows, external shading, and double-skin facades, increase natural daylight while reducing energy consumption associated with artificial light. Energy-consuming systems required for providing fresh air to meet indoor air quality requirements can be reduced or eliminated with the use of passive or hybrid technologies. Hybrid ventilation, or the use of natural and mechanical systems to cool and ventilate buildings, offers opportunities to take advantage of external conditions, but require a backup system to maintain the indoor environment when these conditions are not adequate. Additionally, the building facade plays an important role in achieving energy conservation. Due to technological advances, transparency and the use of glass has become an attractive envelope option in architectural design. Building glass facades can provide outdoor views and an excellent level of natural light as well as the potential for natural ventilation. However, with the use of glass, heat loss during the winter and solar gain during the summer will increase energy loads. In central Europe, which has moderate-to-cold climates, new concepts were tested that used outdoor conditions in creating climatic-responsive buildings (Givoni, 1998; Szokolay, 1980; Wigginton, 1996). Advanced

facade technologies were developed for the high-end office building sector, in particular (Wigginton, 2002), and designers tried to integrate more building services into the facade system. By integrating the use of thermal mass, building-envelope systems can help temper the internal environment, and reduce the amount of supplementary heating or cooling needed to maintain occupant comfort.

In addition to overall building performance, indoor environment conditions and occupant comfort have emerged as important design considerations in both mechanically and naturally ventilated buildings. Passively cooled and ventilated buildings have many benefits not only in reduced energy consumption and reduced ventilation-equipment first costs, but also in terms of occupant environment. Occupant comfort, though difficult to measure quantitatively, has been evaluated through tools such as the PROBE studies. These surveys indicate that indoor temperature associated with occupant thermal comfort has a larger range in naturally ventilated buildings (de Dear and Brager ,2000) extending the range of exterior temperatures over which natural ventilation is usable. Interior temperature is only one aspect of the indoor environment, which also includes air velocity and surface temperatures. Although high air velocity has prompted concern over paper disturbances in naturally ventilated building designs, slightly higher velocities can help maintain comfort when higher internal temperatures are experienced. With slight increases in velocities—0.1 m/s to 0.25 m/s—occupants can tolerate a temperature increase of 3.6°C without any additional discomfort (Chandra et al., 1986). For air velocities within the occupied space up to 0.4m/s, occupants can tolerate interior temperatures of 28°C or 30°C(with relative humidity range 50-80%) as long as there are cooler surface temperatures on surrounding walls, floors, or ceilings (Allard, 2002 and Brager, 2004). Cooler surface temperatures can be achieved through proper use of thermal mass in the building design.

Passively cooled and ventilated environments have increased occupant satisfaction when occupants have the ability, or perceived ability, to control their own environment through the use of operable windows (Jones and West 2001).

The location of the building affects performance as well. Climate influences the feasibility and usage period of natural ventilation as a means of cooling. Buildings in temperate climates can use natural ventilation for most of the cooling season, which is usually from May through October. In climates with a wider temperature range, including hot summers, passive cooling is still possible, but greater attention to detail and design must be made. US has been divided into 17 different climate regions based on maximum, minimum, average monthly temperatures, humidity, wind, sunshine and degree days. Of the 17 climates identified, 12 regions could benefit from natural ventilation, at least for a portion of the cooling period (Jones and West, 2001).

1.1 Building Energy Use

Energy use in the building sector accounts for a large proportion of total energy use in most developed countries. In the U.S., buildings are responsible for half of all energy consumption, while industry and transportation consume 27 percent and 29 percent, respectively. Because the built environment consumes the largest amount of energy, developing building designs that consume less operational energy during their lifecycle is critical. The breakdown of sub-system energy usage in commercial office buildings in the U.S. is presented in Figure1.1. The majority of energy is used in heating, cooling, and ventilating occupied spaces. The situation is even more critical for office buildings, which consume the highest amount of energy across the building spectrum, as shown in Figure1.1. A study done by EIA in 2005 showed that commercial buildings consumed 21 percent of total U.S. energy. Although heating comprises most of the

country's energy usage, cooling is also a significant portion, representing almost 23 percent of total building primary-energy use (EIA, 2005).

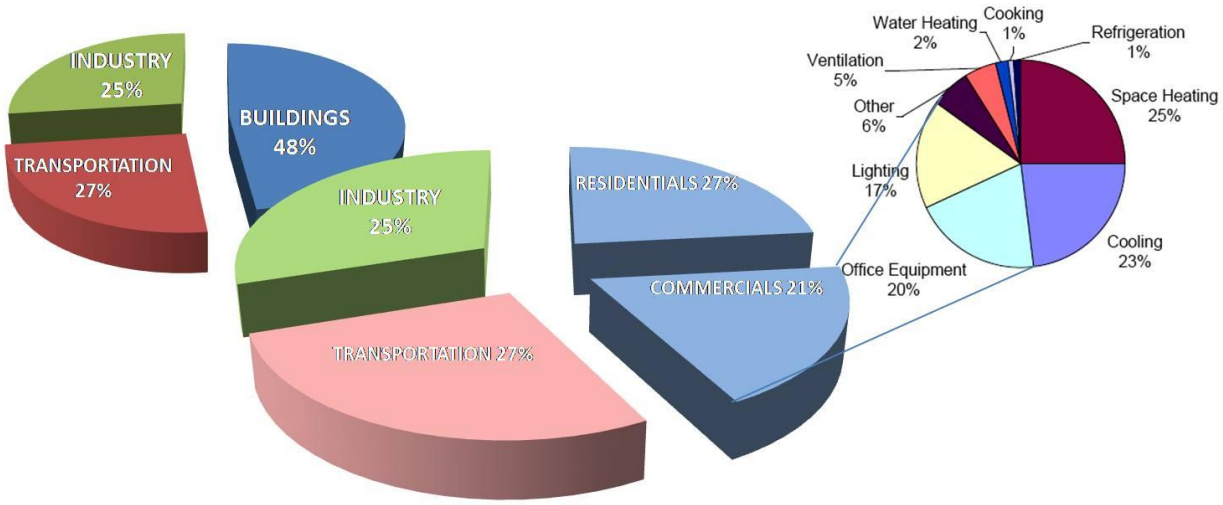

Figure 1.1 Statistical average energy consumption breakdown in U.S. office buildings

In office buildings, the use of natural ventilation techniques can be a potential design-strategy component. Heating and cooling loads could be decreased by incorporating energy efficient technologies, control schemes, and improved building-envelope design. Designers and engineers can continue to improve the building envelope and facade treatments to reduce heat loss and solar gains through the windows, thereby decreasing heating and cooling requirements and minimizing differences between indoor air and surface temperatures that may cause occupants discomfort. The increased use of thermal mass to temper indoor air temperature has become more widely used in commercial building design. In hot summer continental climates like Chicago, the energy consumption required to cool and ventilate a building can be reduced by incorporating natural ventilation in the building design during the shoulder seasons, though it is

not often done. In most climates suitable for natural ventilation, there are only a handful of buildings with this type of system.

Transparency and the use of glass has also become an attractive envelope option primarily in high-rise buildings. The challenge is to improve building performance while providing a more comfortable and healthier place for users. Fortunately, there are numerous methods and techniques that can be employed to achieve these goals.

New enclosures that can substantially reduce energy usage by allowing natural ventilation is a promising development. Aesthetics aside, a double-skin facade (DSF) is believed to reduce cooling loads, allow for more or better natural ventilation, and provide natural ventilation in high-rise buildings. The aim of this study is to propose an effective way to reduce energy consumption in an office building during cold and hot seasons. Therefore, it will focus on how DSF works in such climates. The primary goal of the dissertation is to clarify the state-of-the-art performance of DSFs, so that designers can assess the value of these building concepts in meeting design goals for energy efficiency, ventilation, productivity, and sustainability.

1.2 Problem statements and difficulties

Developing new facade technology is necessary for more environmental friendly and energy-conscious building design. While a great deal of interest exists in learning how to integrate DSFs into our current architecture, there is little knowledge or demonstration of how the concept might work in a city such as Chicago. Studies on DSF energy performance have been mostly limited to the colder and more temperate climates of central Europe. However, the use of DSFs in hot summer continental climates is not well documented. In addition, numerous papers describe how DSFs should improve a building's energy efficiency through principles and ideas yet provide no calculated or experimental results (Lieb, 2001; Arons and Glicksman, 2001). Other researchers

have provided simulation models to specific DSF typologies, but have not linked the envelope-results level to the building energy performance or do not couple the model to a building-energy simulation program (Saelens, 2003). Most of the papers regarding a facade and energy-modeling combination are restricted to only one DSF typology (Saelens, 2003). This study attempts to analyze a new DSF configuration (a combination of two current typologies: corridor and shaft) in a Chicago office building in terms of energy and thermal comfort. A base case with conventional skin will be simulated. Then the building's performance will be simulated with the proposed new DSF (combined corridor-shaft) configuration. A series of varied parameters will provide the maximum thermal comfort. Final comparisons will be made between the proposed options and the base case to find the most efficient strategy with maximum thermal comfort.

Although natural ventilation has the potential to significantly reduce energy consumption in relation to cooling buildings, several factors impede its application in commercial office buildings. There is concern over building performance and occupant comfort, particularly in regards to warm temperatures outside occupants' comfort areas or other interior environmental aspects. There is not only a lack of understanding of natural ventilation and the resulting temperatures and airflows for specific climates, but also a lack of comprehensive tools to analyze detailed design strategies effectively.

1.3 Goals of this Research

The use of either fully naturally ventilated, or partially, when mixed with mechanical ventilation, has, so far, not been attempted in large office buildings in hot summer continental climates. This type of ventilation is more preferable to a mechanically ventilated counterpart because of the possibility of reducing high air-conditioning energy demands, and can also provide a comfortable and healthy indoor environment.

In high-rise buildings, natural ventilation is not viable in the upper levels due to high wind speeds. The main problem with applying natural ventilation to high-rise buildings arises from the high pressure differences that can be generated by buoyancy, due to the large value of H in equation $\Delta p = \Delta T \rho g h$ i.e. since the building acts as a single space, the overall height H is the determinant of the buoyancy force. Taking H = 180 m and ΔT = 20 K the pressure difference across the envelope at ground level could be up to 140 Pa. Such pressures could cause problems in opening doors and windows (the force on a 1.5 m^2 opening would be 210 N) (Etheridge, 2008). However, double facades are built to allow natural ventilation in high-rise buildings, which is a great benefit. The possibility of exploiting natural ventilation due to the complexity of physical phenomena that is non-linearity or left to the chaotic behavior of air movement is not characterized by one solution. Therefore, the major tool necessary for design analyses is Computational Fluid Dynamics (CFD).[1] CFD is used to study the airflow and temperature distribution in occupied spaces and evaluates different combinations of window openings and outside conditions.

In exploiting natural ventilation, the challenge is to design a window-opening system that provides a good supply of air across a narrow-width, European-type floor plate without causing draughts near openings. Even with building mock-ups and wind tunnel models can be time-consuming and expensive, there is substantial risk of getting the design wrong. Using the type and level of technology normally reserved for Formula One racing cars, CFD has the potential to test numerous design modifications before construction begins.

The aim of this study is to investigate the performance of a new DSF configuration for an office building in terms of thermal comfort and energy consumption in a climate that is both cold and

[1] CFD codes numerically solve the differential equations, which govern fluid dynamics (Navier-Stokes equations). It is solving for three-dimensional, fluid flow problems by solving conservation of heat, mass, momentum, and other transport equations using control-volume technique.

humid. The significant lack of information describing the complexity and challenges of designing large, naturally ventilated buildings with DSF as a means to save energy with better thermal comfort is addressed in the literature review.

The following questions hope to be answered satisfactorily in this study:

a) Can we take the design strategies that performs well in central Europe to a new location and climate, such as Chicago?

b) Is it possible to use DSF technology to achieve natural ventilation in a commercial building?

c) How well does DSF technology perform in high-rise buildings in hot summer continental climates?

1.4 Scope of document

This thesis presents the foundation of a methodology for modeling natural ventilation airflow in high-rise office buildings with a new DSF configuration (combined shaft-corridor). This thesis also explores the viability of combined shaft-corridor DSF designs to provide natural ventilation as an energy efficient solution by means of numerical simulations using CFD coupled with dynamic energy-simulation tools. Actual measured data of the building's energy performance based on a full-scale model is not in the scope of study. Therefore, the base case is essentially a simulated base case and is not calibrated with an actual model.

- The simulated combined shaft-corridor strategy is compared with the simulated base case.

In addition, the issue of condensation of the facade system has not been taken into account.

As there is no exact method of local comfort measurements, the predicted-mean vote was used to evaluate the comfort performance.

The organization of this thesis is as follows:

- Chapter 2: Natural Ventilation Strategies.

This chapter presents the three types of natural ventilation and building characteristics that are often considered in the design of naturally ventilated buildings. It also describes the various natural ventilation strategies and their positive impact on reducing energy consumption in high-rise office building design, and the use of DSF technologies in achieving naturally ventilated buildings.

- Chapter 3: Double Skin Facade and Natural Ventilation.

This chapter provides a detailed look at the research and findings of various aspects of DSFs through a literature review. It illustrates the history, categories, functioning, and applications of DSFs.

- Chapter 4: Application of CFD in Built Environment.

This chapter describes the application of CFD in architecture**.** There is a short description of the use of Gambit and Fluent to model buildings' airflow and how to simulate the buoyancy and wind effects as driving forces.

- Chapter 5: Methodology.

This chapter presents the modeling process of the high-rise with the combined shaft-corridor configuration using CFD simulation (Fluent) coupled with a dynamic-building energy simulation tool (EnergyPlus). The knowledge gap and goals for research will be explained.

- Chapter 6: Energy Performance Assessments.

This chapter describes the base case model through two facade types, and the newly designed DSF type. It also assesses the energy and thermal comfort DSF performance in comparison with a typical single-facade system.

- Chapter 7: Air Flow Modeling of a combined shaft-corridor DSF Configuration

This chapter explains natural ventilation in the combined shaft-corridor DSF configuration and demonstrates results of temperature and velocity profile through the building.

- Chapter 8: Parametric Studies of the combined shaft-corridor DSF configuration

This chapter studies the different parameters that enhance the combined shaft-corridor DSF configuration's energy and thermal performance. The modeling and simulation are employed to support the design process comprising an iterative process of performing simulations based upon ambient boundary conditions. Also included are analyses and comparisons of alternative design processes. A summary of the methods developed for evaluating natural ventilation in high-rise buildings with DSF using an airflow analysis coupled with energy simulation are also presented.

- Chapter 9: Contributions and Future Work.

Regarding the complexity of analyzing DSFs, a few assumptions have been made and limitations are acknowledged. In this chapter, contribution and limitations of the research are discussed and the future work areas are also presented.

Chapter 2.0
Natural Ventilation Strategies

2.1 Introduction

Natural ventilation has been used as a healthy solution for ventilating and has the potential to reduce energy costs required for air conditioning. The possibilities of incorporating natural ventilation should be reconsidered, as the effort of the last half century have been almost solely on optimizing mechanical rather than natural ventilation. The goal of modern natural ventilation is to utilize natural driving forces as effectively as possible, for as long as possible, to minimize the use of energy for cooling.

With the advent of more densely populated office buildings that have more computers, higher internal heat loads, and deeper floor plans, there has been a shift toward tighter construction which controls the air introduced into the building, usually cooled mechanically. Increased heat loads and concerns over occupant comfort have often restricted the use of natural ventilation in commercial office buildings, even in temperate climates. Achieving a uniform internal temperature for occupant comfort was thought to be possible only by controlling the amount of air being supplied to an occupied space and its temperature.

Summer conditions are usually the primary occupant-comfort concern. During that time, the goal is to ventilate to meet comfort requirements and cool the space using purpose-provided openings. A well-designed and naturally constructed ventilated building should be able to perform satisfactorily year round. A focus of this research is on evaluating airflow patterns and velocities that can be created by natural ventilation in a commercial office building during shoulder season.

This chapter provides an overview of ventilation strategies from the types of ventilation to specific design elements. First the types of ventilation, buoyancy-driven and wind-driven, are presented. Then DSF design characteristics in naturally ventilated high-rise buildings are outlined, followed by a brief description of the reference building and its specific characteristics.

2.2 Natural ventilation mechanism: Driving forces

There are two main forces that drive natural ventilation: stack or buoyancy-driven ventilation and wind-driven ventilation. The properties of these two are elaborated in the following section; both individual and combined effects are described.

2.2.1 Stack pressure: Thermal buoyancy

Buoyancy-driven ventilation is prevalent in many naturally ventilated buildings, with air flow caused by pressure differences across the building envelope. With this type of ventilation the pressure differences are due to air density differences, which in turn are due to temperature differences. It is the magnitude of these temperature and resulting pressure differences, as well as the building-opening characteristics that determine the magnitude of the buoyancy airflow. In stack-driven ventilation, height is increased and therefore the pressure difference between an inlet and outlet is increased.

A neutral pressure level (NPL) is created at the point where internal pressure is equal to the external pressure, resulting in no airflow in or out of an opening at that particular height. Above or below the NPL, airflow and direction can be determined; it is always from the higher-pressure region to the area of lower pressure. In other word, a temperature difference between the inlet and outlet can enhance the effects of buoyancy-driven ventilation. When the inside air temperature is greater than the outside air temperature, air enters through openings in the lower

part of the building and escapes through openings at a higher level. The flow direction is reversed when the inside air temperature is lower than the outside temperature. Calculation of stack pressure is based on the temperature difference between the two air masses and the vertical spacing between the openings.

The NPL can be calculated based on the total inlet and outlet areas and respective resistances, and their relative height if more than one floor level exists. Roof openings and chimneys or raised stacks can shift the NPL, usually to higher levels. For buoyancy-driven flow, the NPL is presented graphically in Figure 2.1.

The Bernoulli equation is used to derive the flow from buoyancy-driven ventilation, calculating the pressure differential due to height—i.e., the hydrostatic head, for both the exterior and the interior environment. The overall pressure difference between the interior and exterior can be expressed in terms of the height difference, H, gravitational constant, g, density at a reference temperature, ρ_o, and the interior and exterior temperatures. The Bernoulli equation is given as:

$$\frac{v_O^2}{2} + \frac{P_O}{\rho} + gz_O = constant \qquad (2.1)$$

For the buoyancy-driven case, there is no external velocity so the relationship reduces to:

$$\frac{P_O}{\rho_O} + gz_O = constant \qquad (2.2)$$

The pressure difference is applied to the outside environment, using subscript E, and the internal environment, using subscript I. The resulting pressure differences due to height between an origin height, z_O, and at some height H, z_H, for the outside and inside become:

$$\Delta P_E = \rho_E g(z_H - z_O) \qquad (2.3)$$

$$\Delta P_I = \rho_I g(z_H - z_O) \qquad (2.4)$$

To determine the total pressure difference, ΔP_T, the difference across the inlet and outlet openings is calculated. Figure 2.1 illustrates this, with it resulting in:

$$(P_{I,H} - P_{O,H}) + (P_{O,0} - P_{I,0}) = gH(\rho_O - \rho_I) \qquad (2.5)$$

It is assumed that air is a perfect gas, so the ideal gas law is used:

$$\rho = \frac{P}{RT} \qquad (2.6)$$

and substituted into equation 2.5 for the ρ_O and ρ_I terms. Since the difference between P_O and P_I is negligible compared to atmospheric pressure, the term P/RT_B is moved outside of the parenthesis, and the ideal gas law is again applied. Equation 2.5 to describe the pressure difference due to buoyancy-driven flow then becomes:

$$\Delta P_T = \rho_O gH\left(\frac{T_I - T_O}{T_I}\right) \qquad (2.7)$$

The Boussinesq approximation is used for ideal gases, so that $\beta=1/T_I$. The density differences are assumed to be negligible in the Boussinesq approximation except to determine ΔP_T, since the density of air does not vary significantly with temperature over the range of temperature differences found in the reference building. The value for β used is the inverse of an average internal temperature. The Boussinesq approximation is generally valid as long as $\Delta T<30°C$ (Etheridge, 1996).

The ventilation rate is calculated by using the square root law (Etheridge, 1996), and the Boussinesq approximation, and substituting in equation 2.7 to yield:

$$Q = c_d A\sqrt{2\frac{\Delta P}{\rho}} = c_d A^*\sqrt{gH\frac{T_I - T_O}{T_I}} = c_d A^*\sqrt{g\beta H T_I - T_O} \qquad (2.8)$$

Where Q is the flow rate through a building or space, C_d is the coefficient of discharge, and A^* is the contribution of inlet and outlet areas. A* is defined by:

$$A^* = \sqrt{\frac{A_1^2 + A_2^2}{A_1^2 A_2^2}} \qquad (2.9)$$

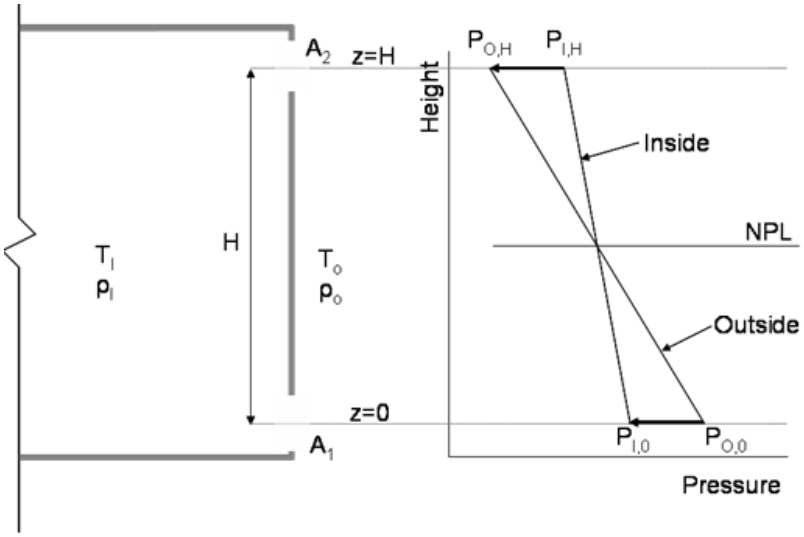

Figure 2.1 Neutral pressure level for buoyancy-driven ventilation

When natural ventilation is used in a buoyancy-driven case, the airflow is not assisted by forced air from wind or mechanical systems. This is often considered a critical design situation during warm summer months for applying this passive technique in buildings. In a buoyancy-driven case, the following parameters are somewhat interdependent, making the analysis of this ventilation scheme more complicated. The parameters include:

- Size of inlets and outlets
- Height of the space
- Strength of the heat sources driving the airflow
- Resulting temperature difference between the interior and exterior spaces due to the interior heat source(s).

Additionally, complex building geometries, such as multiple floors that are directly or indirectly connected, increase the difficulty of evaluating the forces that drive natural ventilation flow. It is in part this complexity, combined with a lack of understanding of the physical mechanisms involved in both buoyancy- and wind-driven natural ventilation that reduces the effective use of natural ventilation in building design.

2.2.2 Wind-driven ventilation

Natural ventilation is influenced by several environmental conditions, the most unpredictable being wind velocity—its speed and direction. Both of these factors are difficult to control and analyze, especially in a full-scale building. In the actual environment, instantaneous wind speed varies with time, and the pressure difference varies with building geometry and location on the building surface. In most wind-driven natural ventilation experiments, a constant, uniform wind speed is used. These design-wind speeds are often the mean wind speeds for a given location over a specific period of time, often years or decades (Awbi, 2003).

Several equations have been developed to describe pressure differences due to wind-driven flow. The equations below describe a case with a constant wind speed where wind pressure does not fluctuate with time. However, for single-sided ventilation, fluctuations in wind speed may be important. A diagram portraying wind-driven ventilation, airflow direction, and resulting pressure versus height is presented in Figure 2.2. If the openings on opposite sides are identical, pressure differences across the openings are equal to half the pressure difference across the building when it is assumed there is negligible-pressure differential through the building's interior. The Bernoulli equation, applied between a point at some distance from the face of the building containing the window and the facade, then reduces to the ideal equation:

$$P_w = P_O + \rho_O U_O^2/2 \qquad (2.10)$$

where P_w is the pressure due to wind at the facade and P_O is the pressure away from the building, and U_O is a reference velocity away from the building. Any height differential for flow along a particular streamline is neglected, so both gz terms are zero, and the velocity at the face of the building is zero as it is the stagnation point. A pressure coefficient, c_p, is used in the actual case, and is a function of wind direction and measurement location on the building facade. The resulting equations are:

$$P_w = P_O + C_P \rho_O U_O^2/2 \qquad (2.11)$$

$$Q = C_d A U_O \sqrt{\Delta C_P/2} \qquad (2.12)$$

where Q is the flow entering or leaving through the openings. The value of c_p depends on the geometry of the building and the location on the facade, and values are often obtained through the use of wind tunnel experiments (Orme, 1999). The pressure on the exterior of the building in Figure 2.2 is assumed to not vary significantly with height.

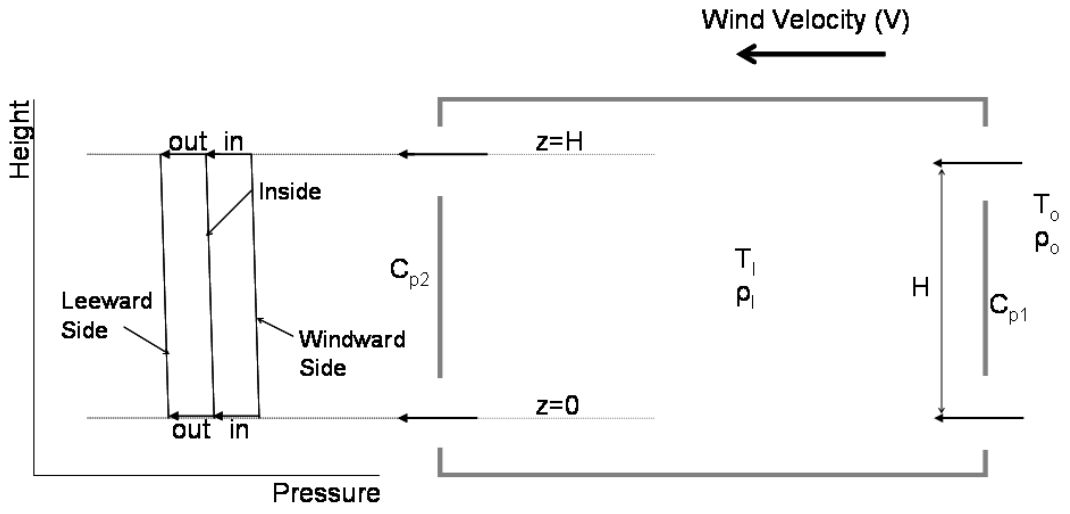

Figure 2.2 Wind-driven ventilation: Airflow direction and pressure versus height

2.2.3 Thermal buoyancy and wind in combination

Combined wind-buoyancy flow is more readily found in full-scale buildings, and these two natural ventilation types can work together or in opposition. Figure 2.3 presents the airflow direction and relation of pressure versus height in a combined buoyancy-wind natural ventilation case. The total case pressures are added together to determine an opening:

$$\Delta P_T = \Delta P_W + \Delta P_B \quad . \qquad (2.13)$$

Using the square root law presented in equation 2.8, the total flow rate through an opening is calculated by:

$$Q_T = C_D A \sqrt{2 \Delta P_T / \rho} \qquad (2.14)$$

Substituting the pressure differences for each case into equation 2.12, and then the total pressure difference into equation 2.13, the total flow rate, Q_T, becomes:

$$Q_T = C_D A \sqrt{\Delta C_P U_O^2 / 2 + g \beta H (T_B - T_O)} \qquad (2.15)$$

$$Q_T = \left[Q_W^2 + Q_B^2 \right]^{1/2} \qquad (2.16)$$

where Q_w is the flow rate component due to wind and Q_B is the component due to stack, or buoyancy flow (Awbi, 2003).

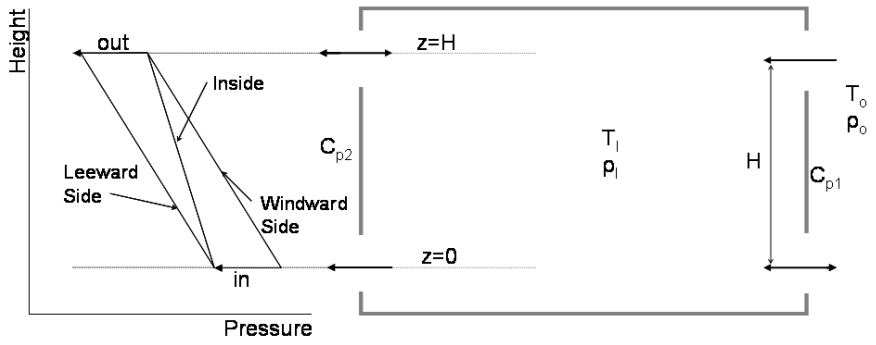

Figure 2.3 Combined wind-buoyancy ventilation: Airflow direction and pressure versus height

There are concerns with the accuracy of this equation (Etheridge, 1996) in part due to the relative effects of wind and buoyancy. When the buoyancy and wind effects were approximately equal, the error in using equation 2.15 was usually 50 percent (Etheridge, 1996). The magnitude of the errors associated with equation 2.15 depends on the distribution of both inlet and outlet openings and the flow characteristics of those openings. At present, however, there are not many simplified methods available for calculating the ventilation rate when wind and buoyancy are simultaneously active.

Air change is driven in part by thermal conditions, so it is important to include a ventilation component in the energy balance of a space. In a simple room, the total airflow, ρcPQTΔT, added to the heat conduction through the building envelope must equal the interior-heat loads under steady state conditions. The material properties, surface areas, and temperature difference between the interior and exterior environment are used to calculate the conduction through the walls and windows, Qwalls+windows=UAΔT. The internal loads, Qloads, typically include heat due to occupants, equipment and lights. For steady state conditions, the energy balance equation is:

$$Q_{loads} = UA(T_I - T_O) + \rho c_P (T_I - T_O) \qquad (2.17)$$

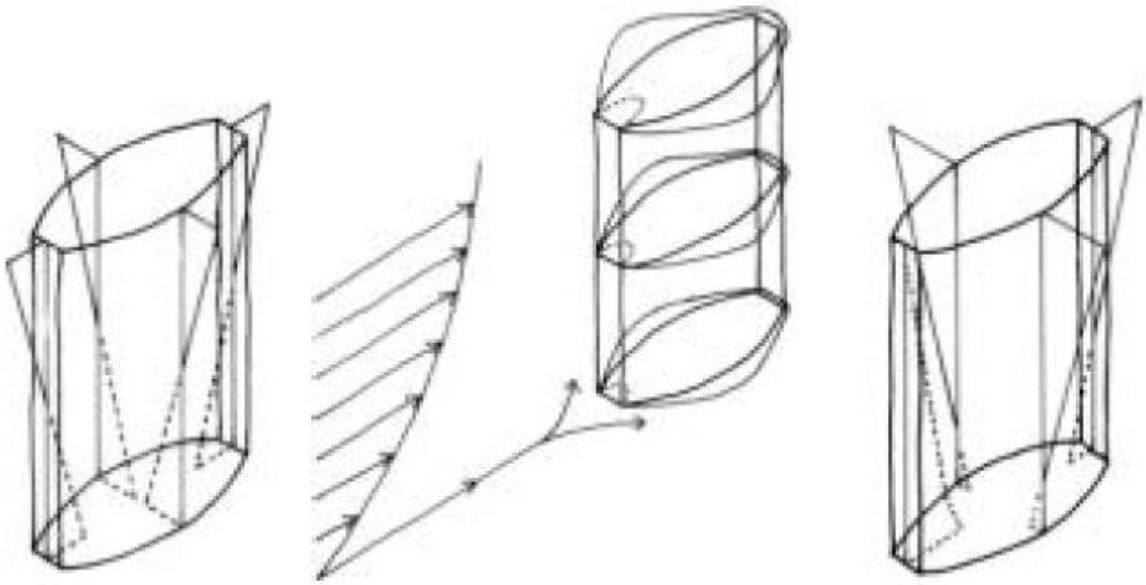

Figure 2.4 Left: Buoyancy-induced airflow. Middle: Wind-induced airflow. Right: Combination of both driving forces(Daniels, 1998)

The schematic drawing (*left*) shows buoyancy-induced pressure distribution upon the envelope of a high-rise building with an oval shape. The inward-pointing dotted lines indicate under pressure, and the outward-pointing solid lines indicate over pressure. Because of the interior and exterior temperature differences, a pressure differential over the building envelope is created. The schematic drawing (*middle*) shows the wind-induced pressure distribution upon the same high-rise building. The inward-pointing dotted lines indicate the positive pressure created on the windward side of the building envelope, and the outward-pointing solid lines indicate the under pressure created on the building envelope on the leeward side. Both the positive and negative pressure increase towards the top of the building as a result of the wind profile. The schematic drawing (*right*) illustrates the combined effect of wind and buoyancy, and the distribution of pressure differentials on the building envelope. The Figure 2.4 illustrates that pressure gradients derived from buoyancy and wind forces can be summed. They either strengthen or neutralize each other (Daniels, 1998).

2.3 Natural ventilation principles

The shape of a building together with the location of the ventilation openings dictates the natural ventilation's manner of operation. One usually differentiates between three different ventilation principles for natural ventilation:

- Single-sided ventilation
- Cross ventilation
- Stack ventilation

The ventilation principle indicates how the exterior and interior airflows are linked, therefore, how the natural driving forces are utilized to ventilate a building. The principle also indicates how air is introduced into the building, and how it is exhausted. Infiltration through the building envelope can also play a role, depending on how airtight it is. This form of ventilation is, however, usually both unintended and unwanted.

2.3.1 Single-sided ventilation

Single-sided ventilation relies on opening(s) on only one side of the ventilated enclosure. Fresh air enters the room through the same side as used air is exhausted. Rooms within a cellular building with openable windows on one side and closed internal doors on the other side is an example of this type of ventilation.

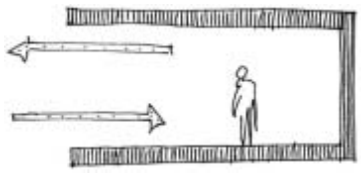

Figure 2.5 Sketch of single-sided ventilation system

As a rule of thumb, single-sided ventilation is effective to a depth of about 2–2.5 times floor-to-ceiling height (CIBSE Application Manual AM10, 1997). With a single ventilation opening in a room, the main driving force in summer is wind turbulence. In cases where ventilation openings are provided at different heights within the facade, the ventilation rate can be enhanced by the buoyancy effect. The contribution from thermal buoyancy depends on the temperature difference between the inside and the outside, the vertical distance between the openings, and where the openings are located. The greater vertical distance between the openings and the greater temperature difference between the inside and the outside, the stronger the effect of the buoyancy. Compared with other strategies, lower ventilation rates are generated, and air does not penetrate far into the space.

2.3.2 Stack ventilation

Stack ventilation occurs when driving forces promote an outflow from the building, thereby drawing in fresh air through lower-level ventilation openings. Fresh air typically enters through lower-level openings, while used and contaminated air is exhausted through higher-level openings (a reverse flow can occur during certain conditions). Designing the outlet to be in a wind-induced underpressure region can enhance the effectiveness of stack ventilation.

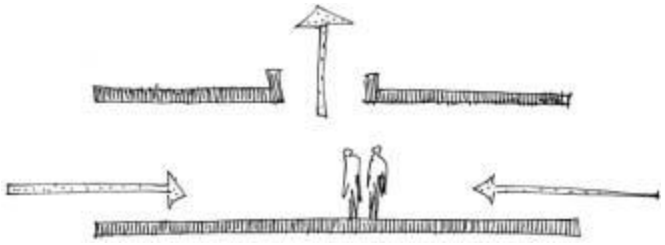

Figure 2.6 Sketch of stack ventilation

As a rule of thumb, stack ventilation is effective across a width of 5 times floor-to-ceiling height from the inlet to where the air is exhausted.

A typical example is a building with an elevated central area, in which warm and contaminated air from the surrounding spaces rises to be exhausted through rooftop wind towers.

Due to its physical nature, the stack effect requires a certain height between the inlet and the outlet. This can be achieved by a variety of methods, including increasing the floor-to-ceiling height, tilting the profile of the roof, or applying a chimney or atrium. Stack ventilation also resembles cross ventilation as far as some individual spaces are concerned, in that air enters one side of the space and leaves from the opposite side. The air may flow across the whole width of the building or from the building's edges to its middle to be exhausted via a central chimney or atrium.

2.4 Elements of Natural Ventilation

Characteristic elements are utilized to enhance natural ventilation principles. These elements distinguish natural ventilation concepts from other ventilation concepts and have consequences with regard to architecture, economy, and performance.

However, natural ventilation can be realized without the use of dedicated elements. The building itself can double as a ventilation element, which might be named, "building integrated element". In this case, the building is designed to harness natural driving forces and direct ventilation air through its spaces without the need for specific ventilation elements. In this sense, a building's integrated-ventilation element is really not an element, but rather an absence of one. As the ventilation system and occupants share the same spaces (rooms, corridors, stairwells, etc.), and windows and doors are utilized as part of the air paths, the most characteristic feature of this type of system is the appearance of no system at all. There are no traditional natural ventilation elements, nor mechanical ones. The main advantage of a building integrated-element system is that it represents no additional use of building space. Most naturally ventilated buildings do,

however, make use of dedicated ventilation elements to harness natural driving forces and to support airflow through the building. The elements used in this research are described in the following section. A description of the advantages and drawbacks of the individual element system is included.

2.4.1 Double facades

A double facade system involves the addition of a second glazed envelope, which can create opportunities for maximizing daylight and improving energy performance. A double facade thus has many properties in common with an atrium. However, the cavity in a double facade does not offer space for occupation.

A natural ventilation double facade can be used as an outlet or inlet path in any of the three natural-ventilation principles. They offer many important advantages such as:

- The cavity is protected against wind and outdoor noise. Thus, open windows can be utilized irrespective of wind and noise from the outside, even on the upper floors of high-rise buildings.
- Solar shading devices are protected from wind when placed in the cavity.
- Solar preheating of the supply air is provided on sunny days, when the cavity is used as an air supply path.
- Due to the protected environment in the cavity, transmission losses through the wall are reduced compared with an ordinary external wall. When used as a supply air path, some of the transmission heat losses through the wall will be captured by the inlet airflow in the cavity, thus providing a heat recovery effect.
- Due to the protected climate in the cavity, inside window surfaces will be warmer, reducing cold downdrafts and asymmetric radiation.

Drawbacks:

- High cavity temperatures can be a problem on hot days, if the external glazing is not operable. This is particularly a problem in the upper floors of a building, when the double facade is used as an exhaust stack.
- Noise can be transferred between adjacent rooms by reflection in the glazed cavity surfaces.
- Cleaning of the cavity is important, especially when used as a supply air path. This implies higher operation costs than a normal facade.
- A double facade represents significantly higher construction costs than a normal facade; however, because they are usually not built solely for ventilation purposes, the costs can be distributed for other functions, e.g., daylight and visual amenity.

2.4.2 Chimneys

Cylindrical-shaped chimneys are another common type of roof element in natural ventilation systems. Most chimneys extract the ventilation air while providing an increased buoyancy effect. Due to where chimneys are usually located—well above a building's roof—the opening is conducive to strong, more stable winds thus increasing the potential to function as a driving force for ventilation. Careful attention should be paid when designing the chimneys opening section to maximize a building's underpressure. The simplest design is an open top, which ensures negative pressure and provides suction in all wind directions due to the Bernoulli effect. To avoid ingress of rain, a cover can be placed above the top. Alternatively, a combination design with roof cowls might provide a greater degree of protection from the weather and increase the chimney's effect.

Figure 2.7 The BRE building with chimneys extending well above roof level to increase the stack potential and achieve stabile wind-induced suction

An advantage of chimneys is that they offer an uncomplicated and efficient way of taking advantage of both thermal buoyancy and wind, independent of wind direction.

2.5 Natural ventilation and high-rise buildings

Buildings are considered high rise when they are taller than ten stories. Several low energy concepts can be incorporated into a high-rise building, including natural ventilation. The high rise is therefore of particular interest and constitutes the focal point of this research.

Facades are the most important element of the low energy concept. A high degree of transparency allows for maximum daylight and exterior views. Heat and light interior transmission is controlled through the use of solar shutters and blinds; the double facade-buffer zone contributes to good insulation values. The biggest factor to take into consideration when deciding upon a high-rise ventilation is that the building's velocity profile increases with height. The conventional way to solve this issue has been to seal the facade and put a mechanical-ventilation plant into it. Due to the building's height, windows cannot be open and there is no shading because it flaps around in the wind. Being in the middle of a city presents other issues

such as traffic, noise and air pollution. Therefore our concept was to close the facade with the second skin and ventilate the offices into the double facade.

A number of interesting investigations and findings are reported in the literature pertaining to passive ventilation in buildings with double-skin facades.

It was found that significant energy savings are possible if natural ventilation could be exploited through the use of a double-skin facade (DSF). For example, the Loyola University Information Commons and Digital Library in Chicago integrated natural ventilation with a DSF to cool the buildings. The results indicated that an integrated facade can reduce 30 percent of energy consumption (52 days operated in natural mode) (Frisch, 2005).

Even though most of the research has been done in temperate climate conditions, studies have revealed a close link between natural ventilation design and the DSF function. Grabe et al. (2002) developed a simulation algorithm to investigate the temperature behavior and flow characteristics of natural-convection DSFs through solar radiation. It was found that the air temperature increased near heat sources that are close to window panes and shading device. Gratia and Herde (2004a, 2004b, 2004c, 2004d, 2004e, 2007a, 2007b, 2007c, 2007d) attempted to look at natural ventilation strategies, greenhouse effects, and the optimum position of sun-shading devices for DSFs facing south in a northern hemisphere temperate climatic. They found that a sufficient day or night ventilation rate can be reached by a window opening, even if wind characteristics are unfavourable. They also argue that with a south- facing DSF, there is a danger when using the cavity air to ventilate the building during the cooling season when air flows downward due to higher wind pressure at the upper openings. In this situation, air that has been warmed in the cavity is drawn into the building and adds to the cooling load. During daytime hours when there is incident isolation, the cavity air temperature is always higher than that of the

outdoor air. This suggests that a sophisticated louver control system is necessary to ensure that cooling loads are not increased with natural ventilation in the case of a south-facing DSF. Care must be taken to prevent greater wind pressure at the top cavity opening than at the bottom. On a windward facade, airflow within the cavity is almost always determined by wind pressure rather than buoyancy; therefore air flows downward, without a careful design to prevent it. This phenomenon might lead to a northern-orientation DSF, if ventilation from operable windows is the main goal. The authors further provided some general guidelines in improving natural daytime ventilation in office buildings with a DSF and demonstrated that efficient natural cross ventilation is possible in temperate climatic conditions.

2.6 Conclusion

Buoyancy and wind velocity are the two driving forces by which the outdoor fresh air can be brought into an interior space and unwanted radiant heat (solar radiation and internal heat gains) can be expelled externally. These principles are understood but more research needs to be done to explore the full extent of DSFs' capabilities in reducing energy usage. In particular, there is a great possibility for a shaft type facade system that reduces energy usage in high-rise buildings through the use of natural ventilation strategies.

Chapter 3.0

Double Skin Facade and Natural Ventilation

3.1 Introduction

In the previous chapter the possibilities and issues of incorporating natural ventilation in different facade system and high rise building presented. The main purpose of this chapter is to provide an overview of various theoretical backgrounds regarding different aspects of building facade systems (building science and aesthetic) and their impact on building performance. First, a general definition of double skin facade system is presented. Then a brief history, which describes the facade's evolution from early concepts to the present, is highlighted. The next section explains different DSF typologies and classifications in terms of airflow driving force, facade divisions, and the airflow modes, as well as the presentation of previous work. The final section gives an overview of thermal performance considerations and envelope performances during summer and winter seasons.

3.2 Definition Single Skin Vs Double

Single skin facade in typical buildings consists of different functional layers including cladding, structure, insulation, etc which separates building interior from exterior. The emergence of curtain walls in the nineteenth century which did not have a load bearing function, made it possible to from an envelope made entirely of glass. Nevertheless, the issues related to thermal comfort condition and low thermal performance of those lightweight single skin envelope supported by the invent of mechanical system. The energy crisis of 1973 necessitates the designer to exploit renewable energy sources for cooling, heating, lighting and ventilating a building. Those issues resulted in developing new products in the glass industry to protect

unwanted heat gain in summer and optimize the use of daylight. Examples of such products include glasses with different coatings. At the moment the architects tried to incorporate the use of natural ventilation and solar energy which resulted in emergence of new concepts in the facade system such as double skin facade.

A double skin facade (DSF) consists of a multilayered facade, which has an external and internal layer that contains a buffer space used for controlled ventilation and solar protection (Arons, 2001). The use of multilayered skins uses building insulation against thermal variation and external noise. As illustrated in Figure 3.1, a DSF could provide outdoor air through operable windows, and preheat or precool the air introduced to the interior space by HVAC system. It can integrate the mechanical ventilation with natural ventilation during the mild seasons. Psychologically speaking, it can reconnect inhabitants with the outdoor and provide a healthy environment while using a substantially smaller mechanical system.

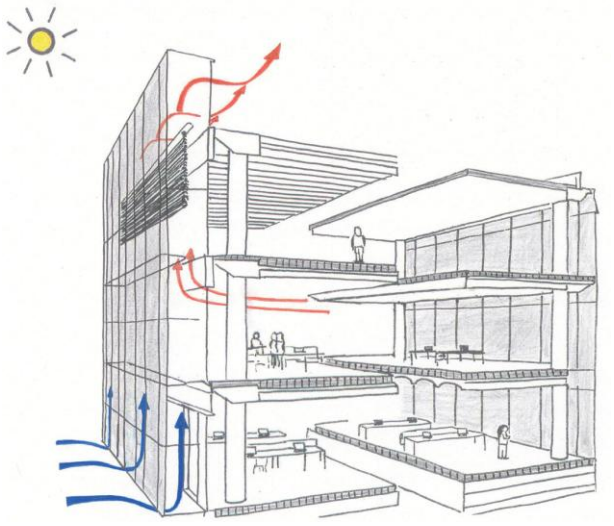

Figure 3.1 Typical DSF (Angus. 2001)

3.3 History and background

The concept of DSF dates back to when many central European houses utilized box-type windows to increase thermal insulation (Oesterle, 2000). In 1849, Jean-Baptiste Jobard, at that time director of the Industrial Museum in Brussels, described an early version of a mechanically ventilated multiple skin facade. He mentioned that in winter, hot air could be circulated between two glazings; while in summer, cold air could be used (Saelens, 2002). Crespo and Neubert mentioned that a doubleskin curtain wall appeared first in 1903, in the Steiff Factory in Giengen, Germany, where priorities were to maximize daylight while taking into account the cold weather and strong winds of the region. A DSF was assumed to be energy efficient and environmental friendly, providing a 40-60 percent reduction in energy consumption, external noise reduction, and natural ventilation even in skyscrapers (Oesterle et al., 2001). Aside from an aesthetic viewpoint, such concepts are often chosen—particularly in high-rise buildings—for shading-device protection from high wind pressure and the possibility of natural ventilation due to lower pressure in the facade cavity.

3.4 Overview of the system

3.4.1 Thermal performance

This section discusses how DSFs perform in two different climate scenarios (winter and summer):

1) During the winter, the external additional skin provides improved insulation by increasing external heat-transfer resistance. Although the equivalent thermal transmission coefficient U-Value for a permanently ventilated facade will be poorer in part (than with a single skin facade), the results will improve if the intermediate space (cavity) is closed (partially or completely) during the heating period. The reduced air-flow speed and increased temperature inside the

cavity lowers the heat transfer rate on the surface of the glass which leads to a reduction of heat loss. This has the effect of maintaining higher temperatures on the inside part of the interior pane. Oesterle et al. (2001) describe the proportion of the opening area in order to improve thermal insulation.

2) During the summer, once radiation passes into the building, it is absorbed by the building fabric and re-radiated as long-wave infrared energy that does not pass back through the glass. As a result, the air in the cavity will be heated via convection. The hot air flow in the cavity can pass through the glazing outside and inside the space via conduction. As the cavity warms up the stack effect is improved respectively. Figure 3.3 shows the effect of various factors on heat transfer through the building's envelope and illustrates the impact of solar radiation, conduction, and convection on the airflow through the DSF cavity. A DSF system results in less heat transferred from outside to inside, and less energy required to cool the space. The rate of heat transfer under steady-state conditions is known as the U-value (coefficient of thermal transmission). The U-value expresses the heat flux (in W/ m^2K) through a building component (or a combination of components) with a temperature difference of one degree across several components under steady-state conditions. Figure 3.2 shows the heat transfer mechanism through single pane glass; the heat transfer mechanism through DSF is illustrated in Figure 3.3. A low U-value indicates that the building component has a high thermal resistance and can be expressed in a case for a multiple-glassing unit by the following equation (Osterle, 2001):

$$U = \frac{1}{\frac{1}{h_e} + \frac{1}{h_i} + \frac{1}{h_t}} \qquad (3.1)$$

Where: U= W/m^2K
h_e= External heat transfer coefficient (W/m^2K)
h_i= Internal heat transfer coefficient (W/m^2K)
h_t= Conduction of multiple glazing units (W/m^2K)

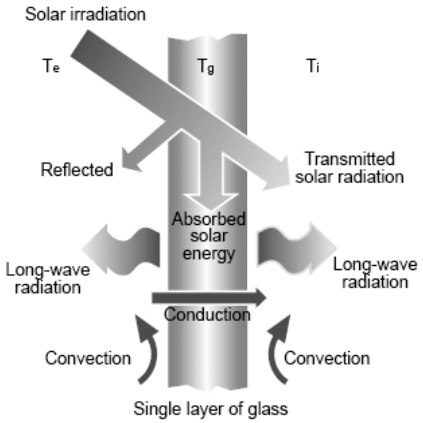

Figure 3.2 Heat transfer through a single pane of glass (Yellamraju, 2004)

The exterior heat source is solar radiation, which is initially reflected on the external glazed skin in this process and, depending on external conditions, determines the external heat transfer coefficient h_e . The remaining radiation passes through the glass. The reflection with the inner glass and inner walls of the cavity creates processes of convection and conduction, which determine the heat transfer coefficient inside the cavityh_i. The accumulated and remaining heat by radiation and conduction received by the room determines the heat transfer coefficient h_t.

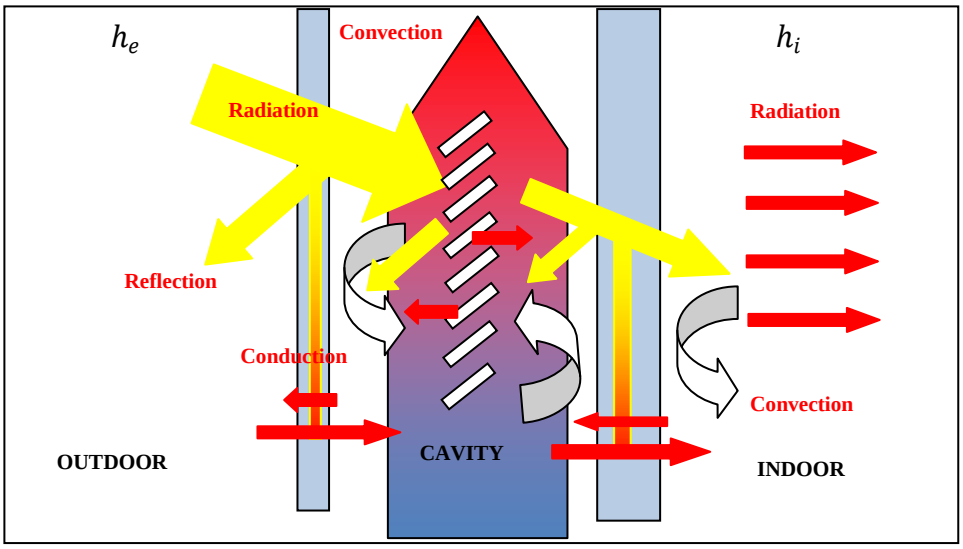

Figure 3.3 Heat transfer through a DSF on a summer day (Haase, 2006)

Three characteristics identify types of double skin facades. These are based on geometric characteristics and also the ventilation mode and type.

As presented in Figure 3.4 these criteria are:

1. Type of ventilation

2. Partitioning of the facade

3. The modes of cavity ventilation

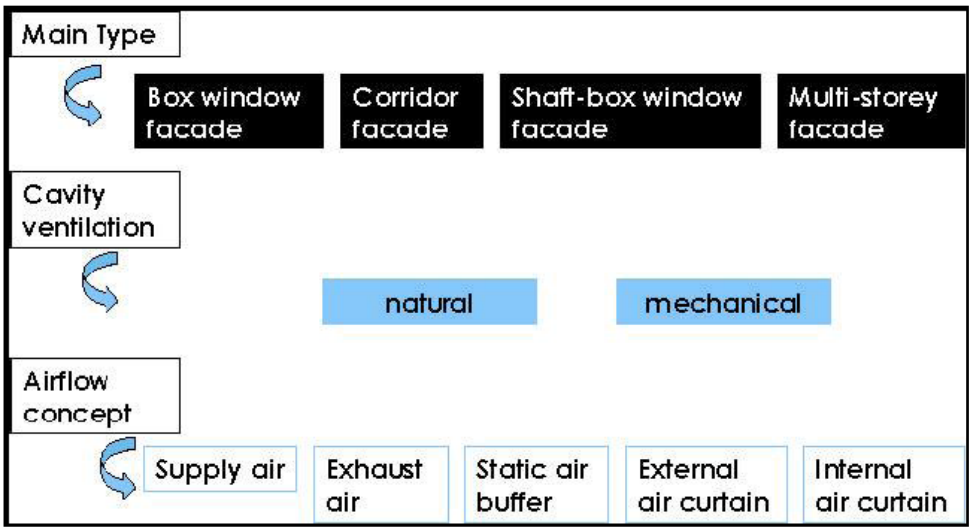

Figure 3.4 The three main criteria for classifying DSFs (Hasse, 2006)

3.4.2 Type of cavity ventilation

The two main driving forces of natural ventilation are the differences between the pressure created by the stack effect and wind effects. Natural ventilation drives the air through a space by taking advantage of the pressure differences caused by these two factors due to internal temperature differences or a combination of both. Hybrid ventilation is a controlled compromise between natural and mechanical ventilation. In hybrid ventilation, natural ventilation is generally used; mechanical ventilation is only triggered when the driving forces of natural ventilation become inadequate and make it no longer possible to achieve the desired performances.

"Note: The stack effect (or chimney effect) is a phenomenon related to the rising of hot air. Applied to a DSF, the concept of stack effect expresses the fact that air is lighter than cold air. As the cavity is generally hotter than the outside, air has a tendency to escape at the top (Loncour, 2002).

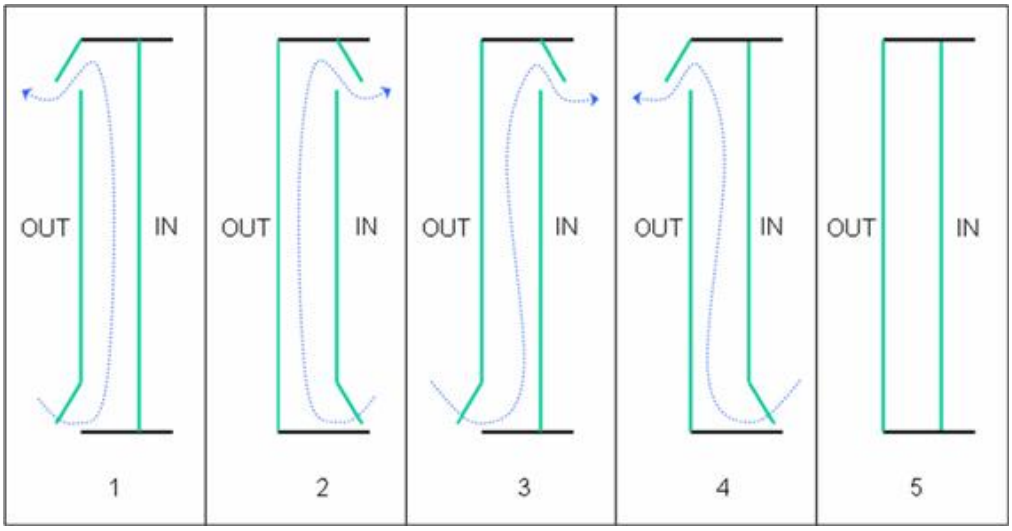

Figure 3.5 The five ventilation modes: outdoor air curtain; indoor air curtain; air supply; air exhaust, and air buffer

3.4.3 Airflow concept

Based on the ventilation mode, the DSF was categorized into five groups. The ventilation mode is independent of the type applied (the first classification presented). Not all facades are capable of adopting all the ventilation modes described here; a facade is characterized by a single ventilation mode. However, a facade can adopt several ventilation modes at different moments, depending on whether or not certain components integrated into the facade permit it (i.e. operable openings). One must distinguish between the following five main ventilation modes:

- ***Outdoor air curtain***

In this ventilation mode, outside air introduced into the cavity is immediately turned back outside. The cavity ventilation thereby forms an air curtain enveloping the outside facade.

- ***Indoor air curtain***

The air comes from the inside of the room and is returned to the same place or via the ventilation system. The cavity ventilation forms an air curtain enveloping the indoor facade.

- ***Air supply***

The ventilation of the facade is created with outdoor air. The air then travels to the interior room or into the ventilation system. This makes it possible to supply the building with air.

- ***Air exhaust***

Air inside the room is evacuated towards the outside. The ventilation of the facade thus makes it possible to evacuate air from the building.

- ***Buffer zone***

This ventilation mode is distinctive as each of the double facade skins is made airtight. The cavity thus forms a buffer between the inside and the outside, with no possible cavity ventilation.

3.4.4 Partitioning of the facade

Based on the geometry of the facade (width openings, cavity height and width, etc.), Oesterle et al.(2001) categorized DSF into the following groups: box window, shaft window, corridor facade and multi-story.

If the DSF extends over the entire height and width of the building, the term, *facade,* is appropriate. If the facade is divided into smaller units, three main categories can be defined. If the partitioning consists of vertical ducts, the expression *shaft facade is* adopted. When the facade is horizontally partitioned, the term *corridor facade* is usually employed. If the facade is

both horizontally and vertically subdivided, the DSF is called *window* or *box*. The term *windows* can be used for systems in which the windows act as DSFs. The term *box* is more appropriate for entirely transparent envelopes with horizontal as well as vertical partitioning.

3.4.4.1 Box window

In this type, the facade is horizontally and vertically subdivided, with entirely transparent envelopes. Horizontal and vertical partitioning divides the facade into smaller and independent boxes. A box window is the oldest form of a DSF, and consists of a frame and inward-opening casements. The cavity between two facade layers is divided horizontally and vertically along constructional axes and floors, respectively. This type of window is common in areas with high external sound levels and special requirements relating to sound insulation between adjoining rooms. This form is the only type that provides the function of a DSF with a conventional way of opening (Osterle, 2001).

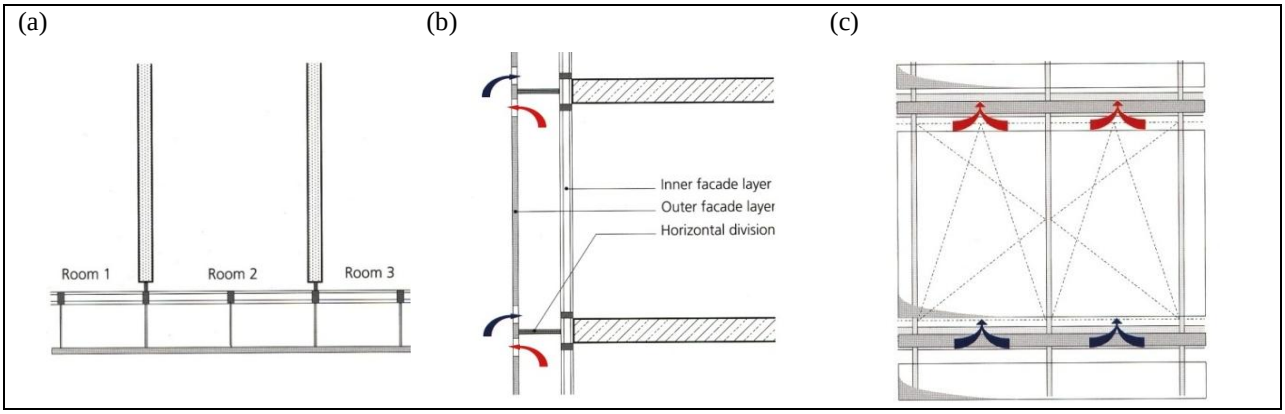

Figure 3.6 Box-window type: Plan (a); section (b); elevation(c) (Osterle, 2001)

The Telus Headquarters (William Farrell Building)

Location: Vancouver, British Columbia, Canada
Building size: 130,000 ft^2 , 7 stories
Architect: Busby + Associates Architects Ltd.

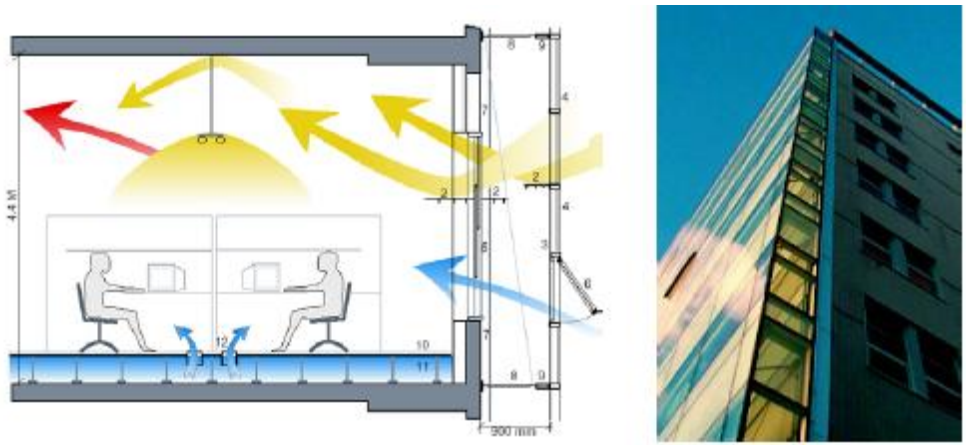

Figure 3.7 William Farrell Building: (a) section showing DSF (b) northeast corner of building

This project was a renovation of an existing brick-face building in which the south and east orientations were covered with a second glazed facade. The second facade provided a buffer between the building interior and a busy Vancouver street, and the system allows for natural ventilation through manually operable windows, the interior facade, and mechanically controlled exterior windows. Occupants can control the exterior windows with switches at each floor. Providing daylight access was also a driving force behind this new facade design, and light shelves within the cavity and space helped to achieve this. In the heating season, the cavity functions similar to a Trombe wall, with the masonry-interior facade storing heat from absorbed solar radiation and transferring it to the building's interior space. Details of the cavity and adjoining space are shown in Figure 3.13. Information about the cavity's performance was not available.

3.4.4.2 Shaft type

In this case, a set of box-window elements are placed in the facade with continuous vertical shafts that go along a number of stories to create a stack effect. On every story, the vertical shafts are linked with the adjoining box windows by an opening. The stack effect draws the air from the box window into the vertical shafts. The air also can be sucked out mechanically. This type of

DSF is suited for low-rise buildings, since the height of stacks is limited (Osterle, 2001). Figure 3.7 shows the plan, elevation, section, and diagram of ventilation in the shaft type. The arrows indicate the route of the airstream through the box windows and the common shaft.

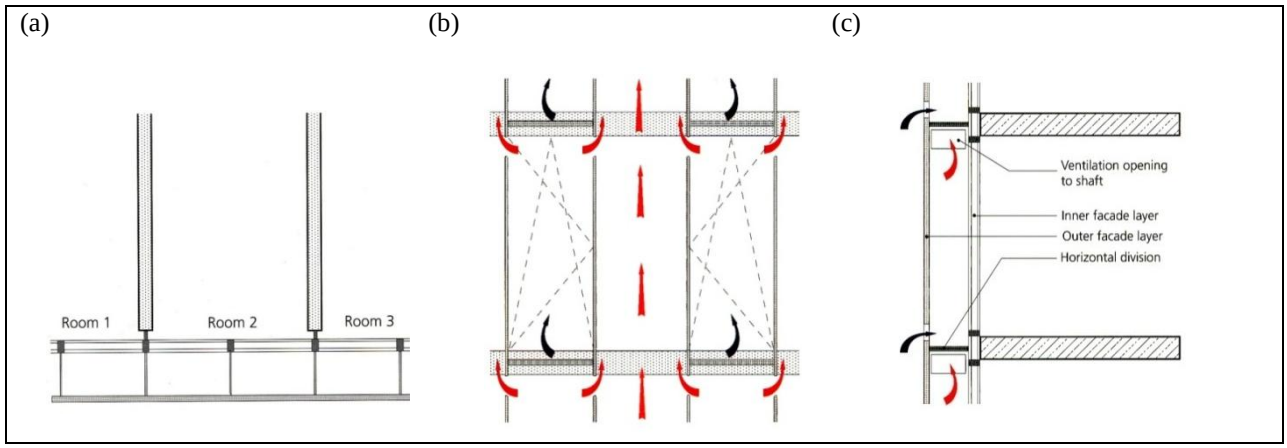

Figure 3.8 Shaft box facade: Plan (a), section (b) and elevation(c) (Osterle, 2001)

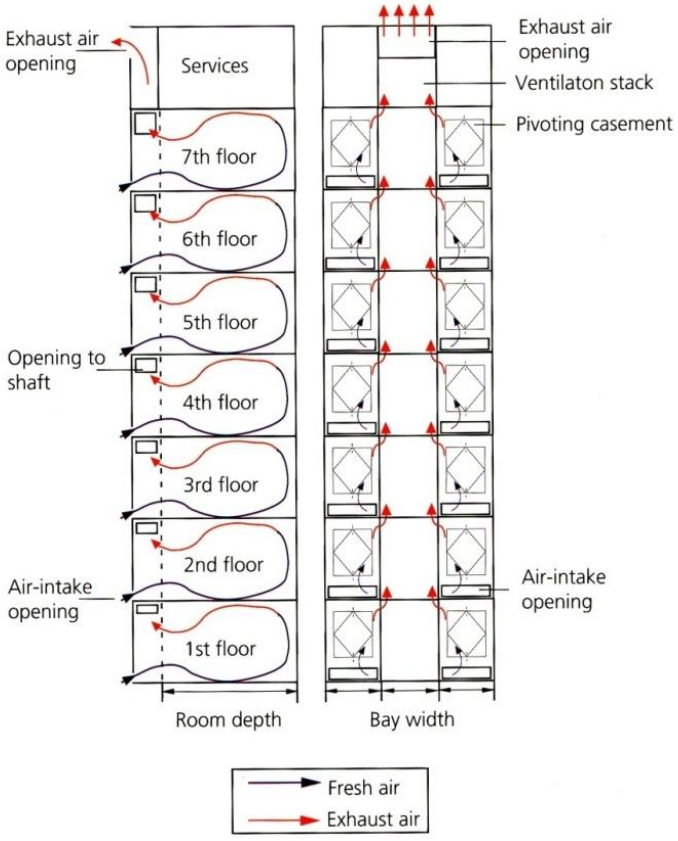

Figure 3.9 Shaft box facade: Plan (a), section (b) and elevation(c) (Osterle, 2001)

Center for Cellular and Biomedical Research

Location: Toronto, Canada
Architect: Behnisch, Behnisch & Partner

Figure 3.10 CCBR south elevation (a) South facade section (b) west facade section

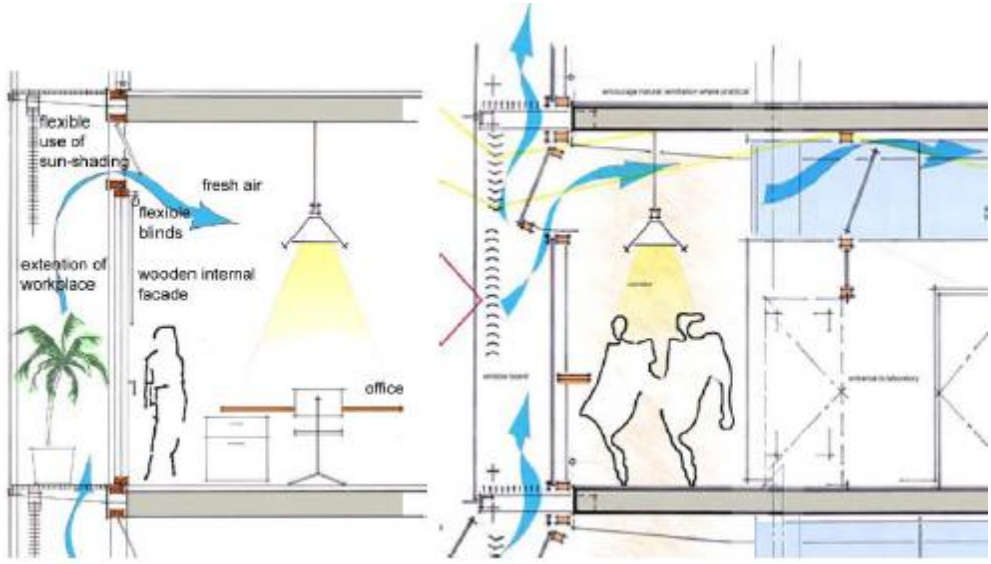

Figure 3.11 CCBR cavity details

The proposed design for this building has a DSF on the south facade, adjacent to office spaces, as well as on the west facade. The design intentions of both facades include: providing natural ventilation while shielding from the elements, providing building security, reducing heat loss in the heating season, increasing indoor comfort by tempering the interior wall temperature,

buffering sound pollution, providing an additional space that can be occupied, and allowing for sufficient daylight access and control system.

As shown in Figure 3.16, the 3-feet wide cavity is large enough to serve as an occupied space. Along the north facade, this space is an addition to the office workspaces, while on the west facade, the cavity acts as an extension to the corridor. In both cases, the designers took advantage of the cavity for the placement of shading devices, which are located both within the cavity and in the office space for easy adjustment. Airflow through the cavity is driven only by natural forces; catwalks at each floor allow air flow and provide shading. Occupants are able to manually control the windows on the interior facade as well as cavity vents.

Given that 75 percent of the building's occupants will use natural ventilation when the ambient temperature is above 15° C in the heating season and below 15° C in the cooling season, the engineers predicted that savings would be 58 percent of annual energy costs over a conventional facade.

3.4.4.3 Corridor type

When necessary, divisions occur horizontally along the corridor for fire protection or ventilation reasons. The intake and extract openings are situated near the floor and the ceiling. They are usually staggered to prevent extracted air on the floor from entering the space on the floor immediately above (Osterle, 2001).

A plan, section, and elevation of a corridor facade are illustrated in Figure 3.9. As shown, the intermediate space is not divided at regular intervals along its horizontal length and air flows diagonally to prevent extracted air from the lower story being sucked in with the air supply of the above floor. The section of corridor facade shows the separate circulation for each story.

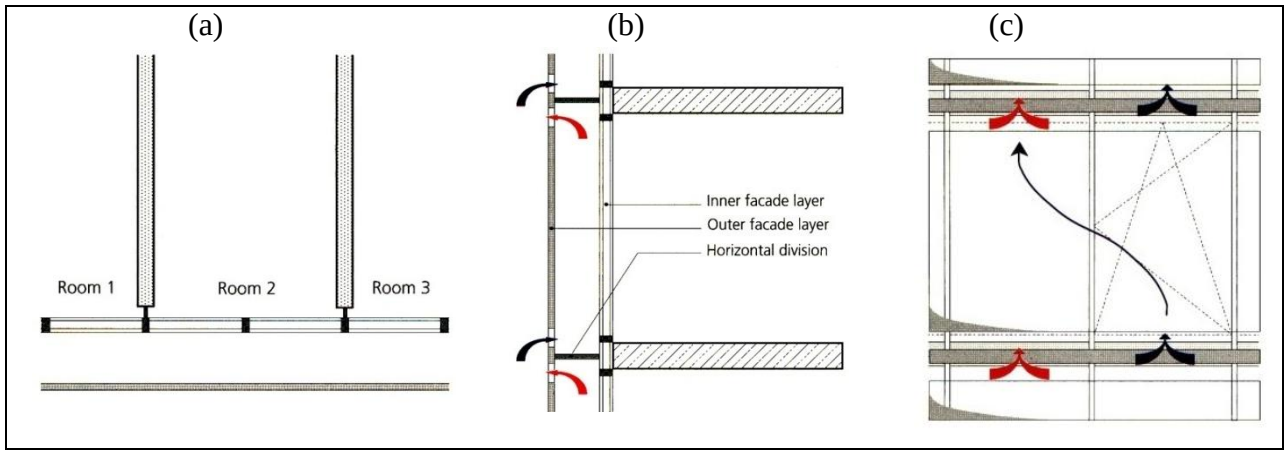

Figure 3.12 Corridor facade: plan (a); section (b) and elevation (c) (Osterle, 2001)

Example of Corridor type in the US : Seattle Justice Center
Location: Seattle, WA.
Building size: 310,500 ft^2,12 stories
Building description: Police headquarters and municipal courts
Construction date: 2002
Architect: NBBJ Architects
Facade Engineer: Arup Consulting Engineers

Figure 3.13 Seattle Justice Center: (a) model of cavity section (b) model of building from south

This project had sustainable-design proponents behind it from the beginning; the mayor of Seattle, Paul Schell, is a former dean of architecture at the University of Washington. In addition, there was an architect on the city council who approved the project. Seattle had a goal of achieving LEED silver ratings for all city-owned buildings, and wanted to make sustainable aspects evident to both users and the general public.

The DSF covers the southwest facade of the building and it was designed to allow for maximum-daylight penetration while minimizing heat gain. The 30-in deep cavity is ventilated with a single opening near ground level, and there is one above the roof height. Openings are controlled by automatic louvers that close when in heating mode. The interior facade is double-pane low-E glazing, and the exterior is single-pane clear glazing. Catwalks at each floor level allow access to the cavity for maintenance, and also serve as shading devices. Light shelves and a movable shading device within the cavity also serve to control light and heat entering the building. There are no operable windows on the interior facade within the cavity, so the DSF serves only to extract heat from the facade. Arup predicted a 21 percent savings in energy in the perimeter zone adjacent from the facade from this configuration.

3.4.4.4 Multi story

In this DSF case, the cavity is adjoined vertically and horizontally by a number of rooms. Ventilation occurs via large openings near the ground floor and roof. The room behind the DSF should be ventilated mechanically (Osterle, 2001). For winter conditions, the cavity can be closed at the top and bottom to take advantage of the greenhouse effect created in the cavity. During summers, the cavity is kept open to exploit cooling buoyancy. Multistory facades are suitable when external noise levels are high. However, high levels of sound transmissions that occur in the intermediate space in this facade type are problematic. As shown in Figure 3.9 the external skin is set independently in front of the inner facade. The intermediate space can be ventilated in all directions. The other problem of such a facade is related to fire protection as all the rooms are linked.

Another issue with this DSF type is that major thermal discomfort exists for the upper floor chimney zone. In a multistory double skin facade, as a result of solar radiation, the air in the

intermediate space between the two skins becomes warmer than the external air. The air in this space will therefore be lighter than outside air. The intermediate space is in contact with external air at the top and bottom, so that a pressure-equalization process occurs. The cooler external air is heavier and thus causes excess pressure at the bottom of the opening, which forces it into the intermediate space. The warmer air within this space is lighter and rises upward, thus causing a state of excessive pressure at the top, whereas the heated air provides less comfort in the upper floors if not totally ejected.

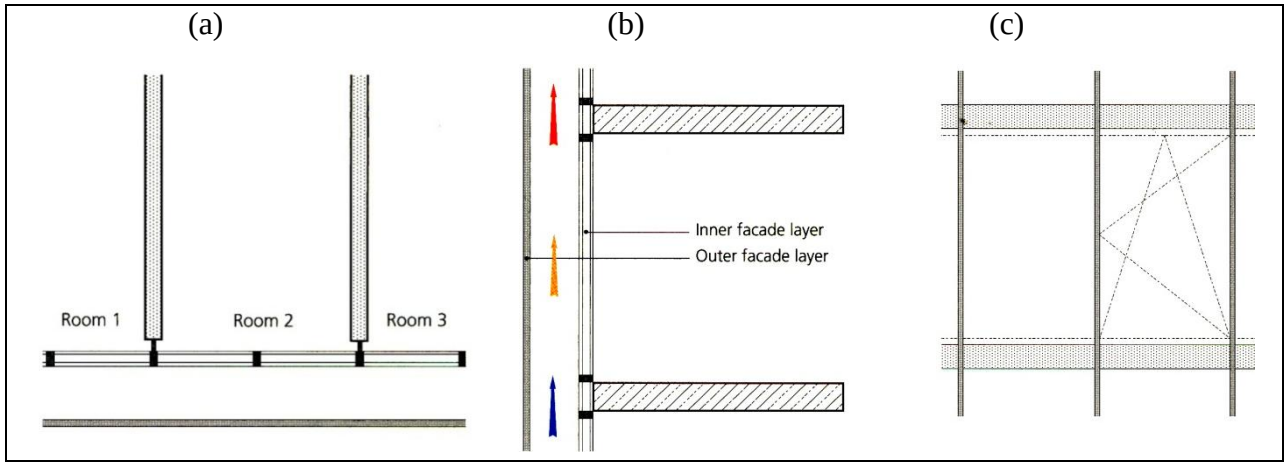

Figure 3.14 Multistory DSF: Plan (a); section (b) and elevation(c) (Osterle, 2001)

Example of multi story DSSF: Occidental Chemical Center
Location: Niagara Falls, N.Y.
Building size: 20,000 m^2 ,12 stories
Building description: Office building
Architect: Cannon Design, Inc.
Consultants: Hellmuth, Obata, & Kassabaum

Figure 3.15 Occidental Chemical Building, southwest corner

This project, a renovation of an existing building with conventional glazed curtain walls, was the first DSF building in North America. A second facade of green-tinted insulating glazing was added to the exterior of all four facades, creating an undivided, and 1.2 meter-wide cavity that extends the full height of the building. Motorized louvers control airflow through the cavity, which is exhausted through an opening at the top above roof height. Details of these opening are shown in Figure 3.12 above. There are wide, horizontal louvers for shading within the cavity controlled by light sensors. The configuration and energy saving intent of this DSF design is similar to that of the Seattle Justice Center, but the cavity is used to preheat air for the HVAC system during the heating season. As in the Justice Center, there are no operable windows.

In 2001, Terri M. Boake and Kate Harrison of the University of Waterloo studied this building to assess the DSF performance. The cavity was quite dirty due to lack of maintenance. The automatically controlled louvers had not been functioning for about four years, and the motorized dampers were covered with plywood. There was no airflow through the cavity, which caused it to overheat; occupants complained of discomfort due to the malfunctioning system. The faults were found to be largely a result of a failed control system.

3.5 Previous work

Double skin facade (DSF) is a concept that is being adopted on many new buildings in Europe with the promise of saving energy while maintaining a transparent facade. Research, studies, and several simulation programs have been carried out to explore solar chimneys—one way to increment natural ventilation and improve indoor air quality—and Trombe walls prior to DSFs. Gan (1998) studied Trombe walls for summer cooling of buildings. He used CFD to simulate ventilation rates resulting from natural cooling. He also investigated the effects of the distance

between wall and glazing, wall height, and type of glazing. He concluded that, using trombe wall for summer cooling by the buoyancy effect increased with the wall temperature, wall height and thickness.

Afonso (2000) compared the behavior and air-exchange rate in a room with both a conventional and solar chimney at different times of the year. He concluded that chimney wall thickness should be chosen according to building utilization. A small thickness is optimal for diurnal operation; for night operation, a larger thickness is advisable. He also mentions that as the nature of wind is variable, the design of the solar chimney can be done without considering the wind effect. Most of the studies using the stack effect idea or the solar chimney concept found that passive summer ventilation is possible even in multi-story buildings. Due to the random nature of the wind, these studies did not consider it in the simulation.

In the U.S., people are reluctant to use DSFs due to high first costs and the lack of a precise airflow model that can accurately predict the facade performance. Arons (2000) developed a model of performance and experimentation verification on a small-scale facade for a Japanese climate.

An experimental study determining the performance of a single-story, south-facing DSF was done at Virginia Technical Institute by Shang Shiou Li (2001). Two modular, full-scale double glazed windows were naturally and mechanically ventilated and monitored for a range of weather conditions. The results showed that the average cavity-heat removal rate of an active system is 25 percent more than a naturally ventilated one. In addition, the temperature difference between the indoor glass surface and indoor air was higher in the passive system.

Saelens (2002) also contributed to the energy performance assessment of single story, multiple-skin facades that are naturally and mechanically ventilated. He undertook a controlled

experimental set-up measure and provided data to compare and validate the numerical model. He found that a traditional facade with shading devices were comparable to a naturally ventilated DSF and a mechanically ventilated one.

Faggembauu (2003) did a numerical study on passive systems in general, and advanced the concept of facades in particular. In the study, a transient code for the simulation of double and single skin facades including advanced technological elements such as phase change materials, transparent insulation, and facade integrated collectors was developed.

Gratia (2004c) attempted to look at the impact of DSFs that face south in a temperate climatic condition. Thermal analysis using simulation software for different seasons of a year was peformed for a low-rise office building with and without a DSF. The results indicated that significant energy savings are possible if natural ventilation can be exploited by using DSFs. Oesterle et al. (2001) compiled DSF typologies, advantages, disadvantages, uses and many examples to prove this point. A parametric analysis of overheating in summer conditions in a full-scale DSF laboratory chamber was carried out for this study. CFD was used to compare the results with full-scale experimental models by Hernandez (2006).

Numerous papers have described how multiple skin facades should work to improve a building's energy efficiency. Manz (2005) mentions that, "Gertis correctly points out that only few simulations have been made and that only few measurements are available to support the claimed benefits. Much of the literature deals with specific topics such as the modeling of the convective heat transfer in cavities or the optical properties of glass layers."

Most researchers provide models to simulate specific multiple skin facade typologies. Only a few models for naturally ventilated multiple skin facades are available. Todorovic and Maric (1998) used a single-zone heat balance representing an entire cavity. Faist (1998) developed a simplified

iterative method to model the airflow due to the stack effect in multi-story envelopes. In this model, the DSF acts like a solar chimney, extracting air through openings in the interior or exterior skin. Wind effects were not considered (Saelens, 2002). He presents a limited evaluation of the model with *in situ* and laboratory measurements. Van Paassen and van der Voorden (2000) developed a network model in which airflow is based mainly on the stack effect. The model had a limited capability to take into account airflow due to wind through joints distributed over the height of the cavity (Saelens, 2002). Airflow from the cavity towards the building was not considered. No comparison with other measurements was given. Results from CFD calculations have become available only recently (Oesterle et al., 2001; McCarthy and Wigginton, 2002). They are mainly illustrative and not yet validated. Moreover, wind effects are not taken into account in these works.

A three-dimensional modeling of a single-story DSF was done with CFD to visualize the airflow within a system (Hernandez, 2006). To date, however, little information is available on how ventilated glazed facades behave during cold winters, or hot, humid summers. At the same time, there has been a significant increase in the number of glazed facades applied to commercial and office buildings. Various experimental and numerical investigations of air flows and heat transfer in glazed cavities such as DSFs and of airflow patterns, temperature distributions, and heat flows at solar-protection devices close to window glazing have been performed (Phillips et al, 2001; Duarte et al., 2001). In the literature, numerous papers describe how DSFs should work to improve a building's energy efficiency. Some authors sum up principles and ideas without providing calculation results or experiments (Lieb, 2001; Den Boer and Ham, 2001; Arons and Glicksman, 2001). Although many other articles representing a tremendous amount of work in this area can be cited, Gertis (1999) stresses a continuing, significant lack of reliable verified

simulation techniques in the DSF domain for high-rise buildings. Other researchers have provided models to simulate specific DSF typologies. However, they do not link envelope-level results to building energy performance or couple the model to a building energy simulation program (Saelens, 2002). Only a few combinations of DSF modeling and energy simulation are available. Most of these papers are restricted to only one DSF typology. In this study, the focus is in the energy saving objectives of a combination of two conventional typologies used in an office in Chicago. The dissertation—which only deals with the thermodynamic and fluid-dynamic behavior of naturally ventilated combined shaft-corridor configuration of DSF during shoulder seasons in high rise office buildings— sets out to make a small contribution toward filling this gap. The goal is to present a numerical investigation and to show an approach to model such facades based on a computational fluid dynamics (CFD) model in a combined shaft-corridor configuration of DSF in cavities with shading devices and to compare simulated results with conventional facades. The dissertation will study natural ventilation in air supply and exhaust mode and a double skin south-facing facade with a combination of two facade types, a shaft and corridor type (the cavity height would be variable), in a high-rise office building.

3.6 Natural ventilation in double skin facade

A number of interesting investigations and findings are reported in the literature pertaining to passive ventilation in buildings and the thermal performance of double skin facades. Even though most of the research has been done in temperate climate conditions, the studies have revealed a close link between natural ventilation design and the DSF function. It was found that significant energy savings are possible if natural ventilation can be exploited through the use of a DSF.

For example, Grabe et al. (2001) developed a simulation algorithm to investigate the temperature behavior and flow characteristics of double facades with natural convection through solar radiation. It was found that the air temperature increased greater near the heat sources that were near the panes of the window and the shading device. Gratia and Herde (2004a, 2004b, 2004c, 2004d, 2004e, 2007a, 2007b, 2007c, 2007d) attempted to look at natural ventilation strategies, greenhouse effects, and the optimum position of sun-shading devices for DSFs facing in a southern direction in a temperate climatic in the northern hemisphere. They found that sufficient day-or night-ventilation rate can be reached by window opening, even if wind characteristics are unfavorable. If natural cooling strategies are used with double facades, the greenhouse effect is favorable if the facade is facing south. Thermal analysis using simulation software was done for a low-rise office building with and without double-skin facade for different seasons. They also provided some general guidelines in improving natural daytime ventilation in office buildings with a DSF and demonstrated that efficient natural-cross ventilation is possible in climatic conditions in Belgium.

3.7 Double skin facades in office buildings

The double skin facade is a system that can create opportunities for maximizing daylight and improving energy performance. There are many issues to be considered in the development of appropriate facade systems for an office building. A natural stack effect often develops in the cavity and the facade can reduce solar gains as the heat load against the internal skin can be reduced through the ventilated cavity. The relatively new double skin facade technology requires greater care in implementation, especially for high-rise buildings.

The effects of wind and strong thermal uplift are two of the more important issues that need to be dealt with in design. A precise survey of wind loads acting on buildings can be obtained through

measurements in a wind tunnel or by using appropriate simulation software. Intelligent control mechanisms have been used in most double skin facade buildings to regulate the admittance of air into the cavity automatically and also closing it up to create a thermal buffer. Further details of important issues in designing double-skin facades for high-rise office buildings are discussed below.

3.8 Conclusion

In this chapter, a definition of double facades is given. A brief history and DSF examples are presented, and existing typologies are outlined. The typology is based on the origin, the driving force of the airflow, and divisions of the facade. It also allows for a description of how a DSF might operate. Based on the literature review, the developments of studies using DSF and other quantitative methods of analysis are reviewed and linked to energy perform. Previous work by various authors has been studied and highlighted in this chapter. A new DSF configuration, which is a combination of two typical facades, follows this chapter. The energy and thermal performance assessment of this configuration in Chapter 6 will put this research into a broader perspective.

Chapter 4.0

Application of Computational Fluid Dynamics in Architecture

4.1 Introduction

Natural ventilation is an essential part of sustainable building design. Energy conscious designers harness the cooling capacity of natural wind to increase indoor thermal comfort and ultimately save energy for active-space conditioning. Wind can cause air movement and perception of cooling, wind can bring in air of a different temperature and humidity. By numerically solving a series of conservation equations related to mass, momentum, and energy, computational fluid dynamics (CFD) tools help designers predict detailed airflow for special design cases and plan a building with optimal natural ventilation. This chapter will describe CFD and how to use two programs commonly involved in CFD: Fluent and Gambit.

4.2 Application of CFD for building design

Knowledge is often needed about the pattern of airflow and distribution of air temperature within an enclosed space. This may be especially important in checking the performance of a natural ventilation system to predict comfort. Different techniques can be used to study the wind effect in building design, such as a model mockup, wind tunnel, nodal/zonal models, and computational fluid dynamics (CFD). It is often inconvenient to evaluate full-scale (model mockup) buildings in the design or occupancy phase of a building, so models are created to simulate the airflow. The goal of modeling is to evaluate systems in feasible, economical way. Modeling techniques have been used to investigate flow around objects and within spaces and buildings in a wide variety of systems.

Three types of models are currently used: mathematical models that provide an analytical solution; computational models that provide a numerical solution; and physical models used for experimental solutions. Analytical solutions are mathematical analyses that describe the phenomena under investigation through a series of equations. An analytical solution is assumed to have a closed-form solution, in that at least one solution can be expressed as a mathematical expression in terms of a finite number of well-known equations. The governing, analytical flow equations for buoyancy, wind, and combined flow were presented in Chapter 2. They are applicable to simple configurations and geometries with well-mixed assumptions and a limited number of zones, such as a single room attached to a double skin facade (DSF) system.

The numerical solution is a more complex version of the mathematical model described above, in that it is a system of algebraic relationships that are solved simultaneously. The computational model provides point-like solutions, with unique values for a series of determined points. A common approach to numerical solution in the area of ventilation is the use of CFD software to quantitatively predict fluid flow in or around objects. CFD software programs such as Fluent have the ability to model temperature interactions, heat flow, buoyancy, and air flow in and around buildings. A grid of boundary surfaces and inclosed space is used to solve the mechanical and thermodynamic relationships throughout the environment under analysis, taking into account the layout, ventilation opening(s), geometry, and heat loads (Szucs, 1980).

CFD applications representing the flow field have become increasingly popular. CFD is a numerical method that approximates the enclosure by a series of control volumes. Air flow in each element must follow fundamental physics laws covering energy transport, conservation of mass, and momentum. These conservation equations are solved for all nodes of a cellular grid that is placed within the domain. Specific applications for CFD include the simulation and

prediction of temperature distribution, air velocity distribution (for comfort, draughts, etc.), pressure distribution, airflow in large enclosures (DSF, atria, airports, etc.) and airflow around buildings (for wind pressure distribution).

4.2.1 CFD approaches in an indoor environment simulation

CFD programs, in particular, can be used to deal with problems associated with the thermal environment, indoor air quality, and building safety as they estimate important parameters such as temperature, airflow, and relative humidity. CFD applications in indoor environments are very diverse and there are many recent examples of its use for natural ventilation design (Carrilho da Grace et al., 2002), the study of building material emissions for indoor air quality assessment (Murakami et al., 2003), building elements design (Manz, 2003) and for building energy and thermal comfort simulations (Bartak et al., 2002; Beausoleil-Morrison, 2002; Zhai and Chen, 2003).

4.2.1.1 Thermal comfort

By numerically solving the governing equations for fluid flow, CFD provides spatial-and temporal-distributed information of airflow, pressure, temperature, turbulence intensity, and moisture and contaminant concentration. These details can be used to evaluate the levels of thermal comfort, indoor air quality, and building system energy efficiency. Air velocity, temperature, and humidity ratio are the most important parameters in determining the predicted percentage dissatisfied (PPD) distribution in a building (Zhai, 2005).

Achieving an acceptable indoor environment with respect to energy use is one of the most difficult tasks when an office building is designed, especially if it is highly glazed. The main components that define the indoor environment are shown in Figure 4.1.

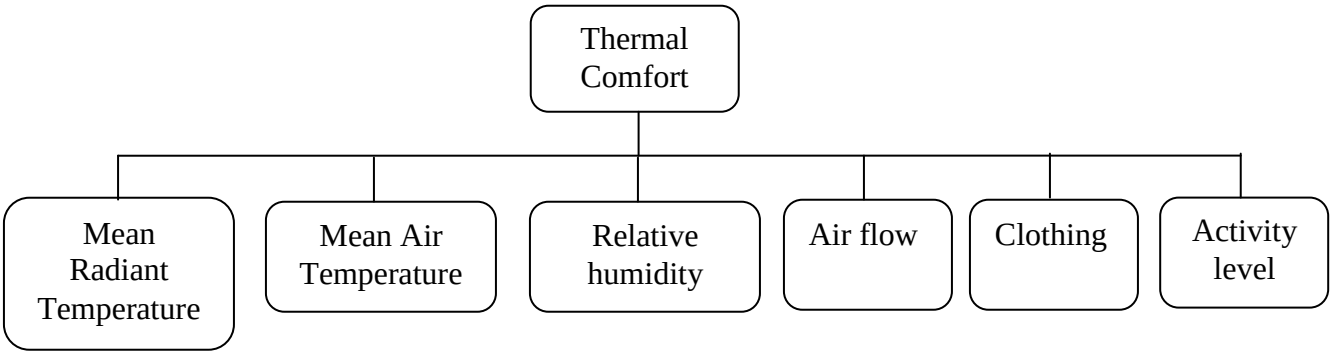

Figure 4.1 Components of thermal comfort

• Temperature and radiation (dry bulb, mean radiant):

Thermal sensation is dominated by the surrounding temperature. The standard dry bulb temperature, however, is not always a sufficient indicator for establishing a good indoor thermal environment, as it does not take into account the influence of radiant energy. The mean radiant temperature is a more appropriate thermal comfort indicator, as it is a measure of the average radiation exchange between the occupant and the surrounding surfaces.

• Relative humidity: Relative humidity is the ratio of moisture content at a certain temperature to the maximum possible moisture content at that temperature (until condensation starts). Generally, humidity affects heat loss by evaporation, which is most important at high temperatures and high metabolic rates (ASHRAE Fundamentals, 2005).

However, questionnaires have shown that even in comfort zones relative humidity has a large impact on the perception of the thermal environment. High relative humidity means that the moisture content of clothing increases, which alters their insulating properties. Usually the relative humidity in an office space varies between 30 and 60 percent.

• Air velocity and turbulence: The sensation of thermal comfort is influenced by air velocity and the scale of turbulence. Often the increased velocity can be an advantage in an office space, where the temperatures are higher than the comfort range. A typical way to increase air velocity

is to use circulation fans. However, at other times, draughts cause discomfort due to localized cooling.

• **Clothing**: Clothing provides thermal insulation and thus has an important influence on acceptable temperature. The choice of clothing can alter comfort preferences by as much as 2 to 3°K. The unit that expresses clothing insulation is clo; (1clo = 0.155 m^2KW^{-1}). According to the 2001ASHRAE Handbook Fundamentals, "because people change their clothing for the seasonal weather, ASHRAE Standard 55 specifies summer and winter comfort zones appropriate for clothing insulation levels of 0.5 and 0.9 clo respectively."

• **Activity:** activity level results in metabolic rates between 1.0 met and 1.3 met for office building.

• **Operative and resultant temperatures:** The operative and mean resultant temperatures empirically combine the dry bulb and the mean radiant temperatures. The operative temperature is the temperature at which a person emits the same heat output as before, but when air temperature (T*a*) = radiant temperature (T*r*) = operative temperature (T*op*) (Peterson, 1991). The T*op* does not have the same value for all parts of the room. Acceptable operative temperature ranges for naturally conditioned spaces

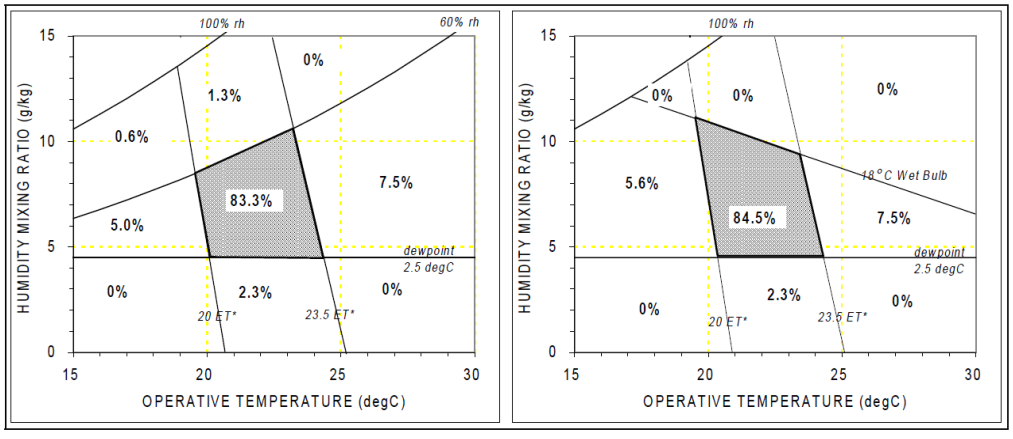

Figure 4.2 Relation between operative temperature and humidity

Distribution of winter indoor climatic measurements on the ANSI/ASHRAE Standard 55-1992 comfort chart defined in terms of ET (*an Effective Temperature, ET*, that is the dry-bulb temperature of a hypothetical environment at 50% relative humidity and uniform temperature (Ta = MRT) where the subjects would experience the same physiological strain as in the real environment.)*, dewpoint temperature and RH or wet bulb temperature. The chart on the left shows the comfort zone before the 1995.

Air speed < 0.2m/s			
Difference between radiant & air temp < 4 $°C$			
T*op* = A T*a* + (1-A) T*r*			
V	<0.2m/s	0.2-0.6m/s	0.6-1m/s
A	0.5	0.6	0.7

Table 4.1 Thermal Environment Conditions for Human Occupancy from ANSI/AHRAE Standard55-2004

• **Perception of thermal comfort:** It is important to clarify that thermal-comfort conditions are not easy to define, as it is a very subjective value. Thus, a thermal environment that is acceptable to some people may be totally unacceptable to others. According to Andresen (2000), it is not only that people are differently dressed and have different metabolic rates, but their assessment of comfort is also influenced by their psychosocial environment, which cannot easily be taken into account by any calculation method. The most commonly used calculation methods are the ASHRAE standard 55 (ASHRAE, 1992) and the ISO Standard 7730 (ISO, 1984). In order to describe this factor it is necessary to explain the concepts of predicted mean vote (PMV) index and predicted percent dissatisfied (PPD). Both ASHRAE and ISO standards are based on the concepts of PMV and PPD as developed by Fanger (1970).

The PMV index is a measure of thermal sensation, since it expresses the correlation between indoor environment parameters and human sensation of thermal comfort. It is a function of

activity, clothing, air temperature, mean radiant temperature, relative air velocity, and humidity. As described in ASHRAE Fundamentals (2001), "The PMV index predicts the mean response of a large group of people according to the ASHRAE thermal sensation scale." The ASHRAE sensation scale is presented below:

+3 = hot, +2 = warm, +1 = slightly warm, 0 = neutral, -1 = slightly cool, -2 = cool, -3 = cold.

The PPD of a large group is an indication of the number of persons who will be inclined to complain about the thermal conditions. After estimating the PMV, the PPD can also be estimated. Those persons not scoring +0.5, -0.5, or 0 are deemed to be dissatisfied. From this, the PPD of occupants can be determined. Liddament (1996) writes that, "the immediate conclusion of this work was that it was not possible to define a set of thermal conditions that would satisfy everyone. Even when the average of the predicted mean vote was zero, i.e. a neutral thermal environment, 5% of the test occupants were dissatisfied." Accepting that no single environment is judged satisfactory by everybody, the standards specify a comfort zone based on 90 percent acceptance or 10 percent dissatisfied occupants. Thus, the upper limit for operative temperature in summer is 26°C, given 50 percent relative humidity, sedentary activity, 0.5 clo and a mean air velocity of less than 0.15 m/s.

Based on the PMV index, the PPD index can be calculated. The PPD index predicts the percentage of occupants who will judge their thermal comfort unsatisfactory (corresponding to a vote below –2 or above +2). PPD as a function of PMV is shown in the functions below:

PPD is a major index for building thermal comfort judgment. It can be calculated via (4.1):

$$PPD = 100 - 95 \exp(0.03353\, PMV^4 - 0.2179\, PMV^2)\ [\%]. \qquad (4.1)$$

The PMV in the equation is determined by:

PMV= [0.303Exp (−0.036M) −0.028] L *(4.2)*

where M is body metabolism ($W \cdot m^{-2}$) and L is thermal load on the body ($W \cdot m^{-2}$).

M and L are the functions of air velocity, temperature, humidity ratio, and enclosure temperature. In addition, CFD results can be used to calculate the distribution of percentage dissatisfied (PD) people due to draft, another major thermal comfort index, through the equation:

PD = (34−T) (U − 0.05) $^{0.62}$ (3.14−0.37U Tu) [%] *(4.3)*

where T is local air temperature (°C), U is local air speed ($m \cdot s^{-1}$), and Tu is turbulence intensity (%). If the turbulence kinetic energy k ($m^2 \cdot s^{-2}$) is simulated by a turbulence model, the turbulence intensity can be estimated as:

Tu=100(2k) $^{0.5}$/U [%] *(4.4).*

CFD programs such as Fluent can provide detailed predictions of thermal comfort and indoor air quality, such as air-velocity distribution, temperature, and relative humidity. The distribution can be used further to determine thermal comfort and air quality indices such as described above plus the PMV, the PPD, and the PD.

4.2.2 CFD approaches in an outdoor airflow simulation

A CFD program can also calculate the pressure difference around buildings and these data can be used it as boundary conditions[2] for subsequent indoor airflow simulation. Ideally, the calculation should be performed for different wind directions under various wind speeds in a period suitable for natural ventilation, such as spring. For a site in Chicago Figure 4.3 illustrates pressure distribution pattern under a prevailing wind direction (southwest) and speed (10 m/s). In order to correctly take the impact of the surrounding buildings into account, the computational domain is much larger than the one shown in the Figure. Clearly, the pressure difference is the highest between the northern and southern facades. It is also interesting to note that CFD can help

[2] The set of conditions specified for the behavior of the solution to a set of differential equations at the boundary of its domain

develop natural ventilation by modeling and optimizing building site plans and indoor layouts. Jiang and Chen (2002) found that the outdoor environment has a significant impact on the indoor environment, especially in buildings with natural ventilation. They recommended that both the indoor and outdoor environments along with the combined indoor and outdoor airflow need to be studied together.

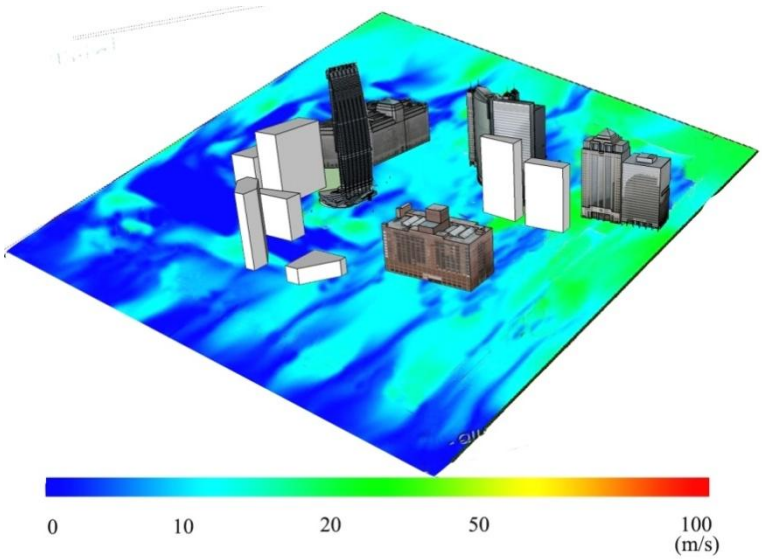

Figure 4.3 Urban pressure distribution (Wolf Point Chicago and surroundings)

4.2.3 CFD approaches in facade design

In the case of a naturally ventilated double-skin facade (DSF), wind speed and wind direction are important data required for correctly predicting the ventilation around and within a building. The facade system's solar performance is also critical as well as detailed solar-radiation data, which can be learned through building-energy simulation tools, such as EnergyPlus. Since these parameters are the driving force for natural convection, detailed data are required to study natural ventilation. A further difficulty is the prediction of the airflow rate in the facade cavity due to combined buoyancy (stack effect) and wind effects in natural convection. The airflow rate at any point is unknown and depends on the temperature profiles. This combined effect of wind and

temperature differences creates a pressure difference between the facade's inlet and outlet, which determines the airflow rate in the facade cavity. When wind velocities are low, the stack effect will be dominant; if wind velocities are high the wind effect will dominate. There is a "transition" regime between both effects that may assist or counteract the overall natural convection conditions.

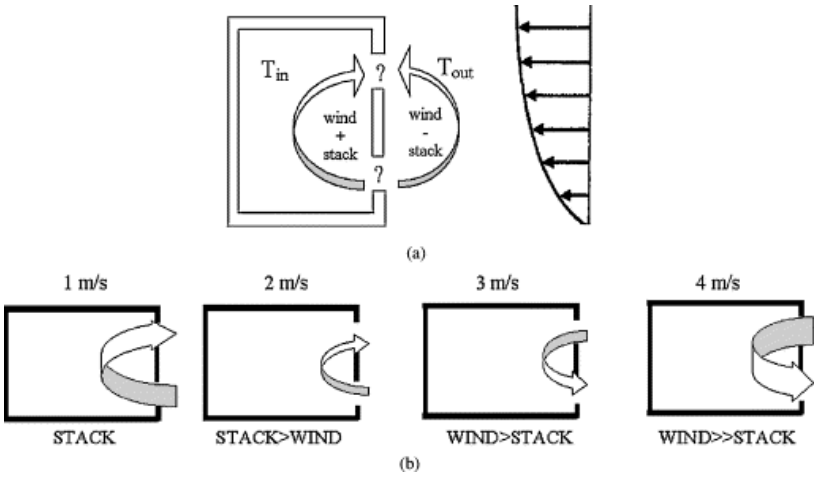

Figure 4.4 The effects of combined wind and stack forces: (a) reinforcing vs. counteracting effect (b) depiction of counteracting wind and stack effect over a progression of wind speeds (Alloca et al., 2003)

Fluent can calculate both driving forces through control volume system. Grabe et al. (2001) carried out a detailed study of the effects of ventilation with double-skin facades which provides important guidelines in using CFD simulation for facade investigation. They determined that the simulation of a double-skin facade must yield the following information:

a) The air mass flow through the facade gap to control the possibility of natural ventilation of the room behind.

b) The temperature of the facade air related to its height determines the temperature of the supply air in natural ventilation. It also helps in estimating the cooling load required in the case of air conditioning.

4.3 Simulation approach: Model set up

4.3.1 Fundamental of airflow modeling

Key parameters calculated as part of a CFD analysis include:

- Pressure distribution

Airflow is driven by pressure distribution; therefore the pressure field is fundamental to the whole flow process. Pressure is maintained by a combination of driven air or forced convection and buoyancy forces or natural convection. Free convection is driven by buoyancy forces created by an imbalance in temperature difference.

- Velocity field

Air movement is a vector having components in both speed and direction. To determine the air velocity distribution, air flow must usually be represented by three transport equations.

- Temperature field

The temperature field is sustained by thermal sources and sinks distributed about the enclosure. Buoyancy forces and free convection currents are generated by the temperature field.

- Boundary layer flow

Air flow close to surfaces is subjected to boundary later effects in which the rate of flow is influenced by surface friction.

- User input-boundary conditions

Flow, turbulence, temperature, and pollutant fields are unique to the prevailing boundary conditions. Input data must include:

- Location of openings
- Mass flow into and out of the building
- Type of flow boundary
- Velocity (speed and direction of flow through each opening)
- Thermal properties of surfaces and/or surface temperatures.

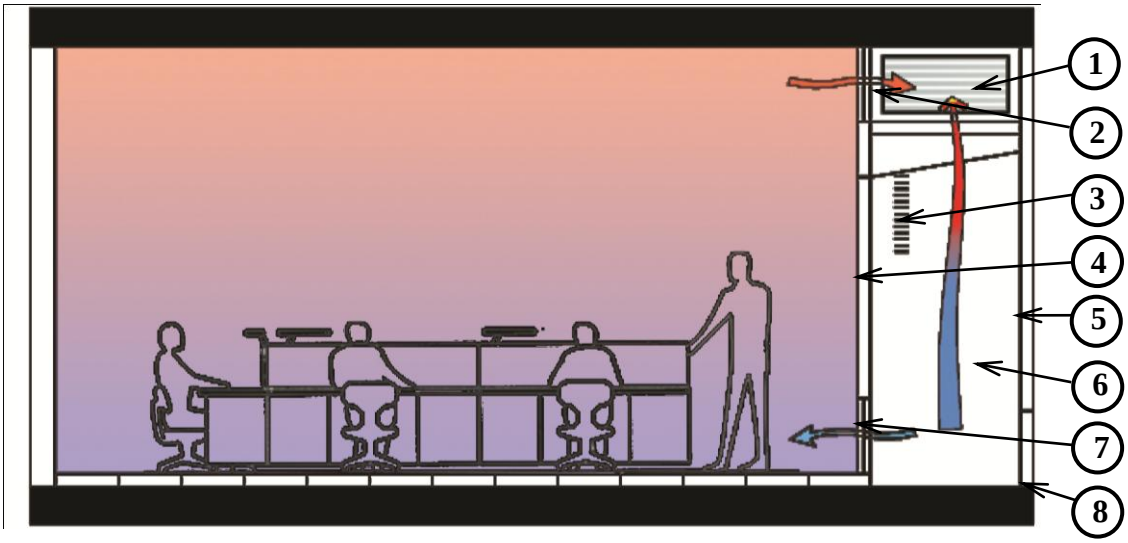

Figure 4.5 The schematic diagram of the office module's inputs: 1)upper air outlet to chimney; 2) interior upper operable window; 3) controllable solar control device; 4) interior operable or fixed view window; 5) exterior glazing layer; 6) air cavity; 7) interior

4.3.2 Creating a model geometry for CFD

In order to analyze the CFD model, geometry needs to be created in Gambit (Gambit is a meshing software program), which uses discrete points to describe the space. The Gambit model and the mesh grid are then exported to Fluent in order to conduct the CFD analysis.

4.3.2.1 Finite volume grid and geometric modeling considerations

To understand the model's applicability to architectural projects, it is important to understand what assumptions were made in the models and how researchers determined that they were satisfactory. The scope of CFD models includes modeling the DSF ventilation across the width of a floor plate, for a typical floor plate area, with three chimneys. Models are considered accurate once they have run a sufficient number of iterations as described by the researchers. In Fluent code, residuals are reported for each conservation equation. A discrete conservation equation at any cell can be written in the form LHS = 0[3]. For any iteration, if one uses the current solution to compute the LHS, it won't be exactly equal to zero, with the deviation from zero

[3] The LHS describe time rate of change of velocity and momentum flux.

being a measure of how far one is from achieving convergence. So Fluent calculates the residual as the (scaled) mean of the absolute value of the LHS over-all cells. Residual is the measure of farness from the conservation equation answer, typical number in architectural applications is less than 10^{-3}. As Hernandez (2006) mentioned that *"Simulations were considered converged when the normalized residuals were smaller than* 10^{-3} *and the solution field was stable. i.e. the values did not change by more than* 10^{-7} *(relative change) between iterations, and showed no visible fluctuation or changes after hundreds of iterations. The effects of turbulence were modeled using the standard k-e model. Results of simulations for different flow rates showed a linear variation of the air speeds in the room with inlet speed, as expected."*

4.3.2.2 Modeling and solvers

A practical approach to predict outdoor airflow is to decouple the outdoor and indoor airflow simulation. Outdoor airflow around buildings is first predicted and provides airflow and pressure information at the openings of buildings. With these values as the boundary conditions, indoor airflow for each space can be simulated independently and natural ventilation rate can be determined.

The decoupled simulation method is based on the assumption that indoor airflow and building openings have little impact on outdoor airflow and pressure distributions; indoor and outdoor flow fields can therefore be studied separately.

Stankovic[4] (2007) found that the accuracy of CFD results is critically dependent on boundary conditions. The highest accuracy of the boundary conditions is normally achieved by combining the measured specific site data with dynamic thermal simulations.

4 Internet page of Technology, *Environmental Engineering in the Tropics,* http://www.sia.org.sg

Jaros et al. (2002) established that the CFD characteristics of solved problems could be grouped under the following:

—where fluid flow is predominantly driven by buoyancy forces (natural or mixed convection);

—where heat transfer arrives simultaneously by conduction (in solids), convection, and thermal/solar radiation (in fluid).

The correct type of fluid flow is a very important aspect of the CFD simulation as well.

There are two radically different states of flows that are easily identified and distinguished: laminar flow and turbulent flow. Laminar flows are characterized by smoothly varying velocity fields in space and time in which individual "laminar" (sheets) move past one another without generating cross currents. These flows arise when the fluid viscosity is sufficiently large to damp out any perturbations to the flow that may occur due to boundary imperfections or other irregularities. These flows occur at low-to-moderate values of the Reynolds number[5]. In contrast, turbulent flows are characterized by large, nearly random fluctuations in velocity and pressure in both space and time. These fluctuations arise from instabilities that grow until nonlinear interactions cause them to break down into finer and finer whirls that eventually are dissipated (into heat) by the action of viscosity. Turbulent flows occur in the opposite limit of high Reynolds numbers.

The solver needs for this study are more likely to be turbulent due to irregularities of the surface. There are usually regions with and without turbulence in the same space. The turbulence model must be able to deal with laminar and transitional flow at the same time and the RNG k-e model of turbulence appears to be the most suitable choice among other models in Fluent.

[5] Reynolds number can be defined for a number of different situations where a fluid is in relative motion to a surface. (from Wikipedia: http://en.wikipedia.org/wiki/Reynolds_number).

Gan (1995a, 1995b) has carried out detailed research into the effects of displacement ventilation in building design using CFD simulation. He used the standard k-e turbulence model for the prediction of indoor air flow patterns, temperature and moisture distributions while taking account of heat transfer by conduction, convection, and radiation. The thermal comfort level and draught risk are predicted by incorporating Fanger's comfort equations in the airflow model. He found that common complaints of local thermal discomfort in offices with low turbulent air flow such as displacement ventilation often results from unsatisfactory thermal sensation rather than draught itself or alone.

In his research on thermal transmission through DSFs, Gan (2001) used CFD for predicting the convective heat transfer coefficient, thermal resistance, and thermal transmittance for a double-glazed unit. The unit was an unventilated enclosure and the flow within it would be buoyancy-induced natural convection.

Navier-Stokes (RANS) equation models and Large Eddy Simulation (LES) models to enhance the capabilities of CFD for use in indoor and outdoor environment design are used in Fluent.

A two-layer turbulence model, a single k- E equation turbulence model for near-wall flow, and the standard k-e model for flow in the outer-wall region could accurately predict heat transfer on a wall. The computing time needed is slightly higher than the standard k-e model but much lower than a low-Reynolds number k-e model. A zero equation model (a single algebraic function) is used to simulate transient flow that significantly reduces computational time. The coupling with an energy simulation program gives more accurate results for building energy analysis and indoor environment design. A new dynamic sub-grid-scale model is used to predict indoor airflow without a homogenous flow direction. The model uses two different filters to obtain the

model coefficient as a function of space and time. The model can accurately predict flow in a room with a heated floor and in an office with displacement ventilation.

The space to be simulated is discretized into a set of control volume or elements. The enclosed space may be divided into 30,000 to 50,000 control volumes or more, so each element represents only a fraction of the total enclosure volume. The system of discretization can be non-uniform so that clusters of elements can be located at areas of greatest interest. Direct solution techniques are not available, therefore iteration is applied. All parameters are initially given arbitrary values for which the iteration can commence. These values are then adjusted until each of the transport equations balance. The process of reaching a balance is referred to as convergence.

The accuracy of CFD prediction is highly sensitive to the boundary conditions supplied (assumed) by the user. The boundary conditions for CFD simulation of indoor air flows relate to the inlet (supply), outlet (exhaust), enclosure surfaces, and internal objects. The temperature, velocity, and air turbulence entering from diffusers or windows determine the inlet conditions, while the interior-surface, convective-heat transfers in terms of surface temperatures or heat fluxes are for the enclosures. These boundary conditions are crucial for the CFD accuracy.

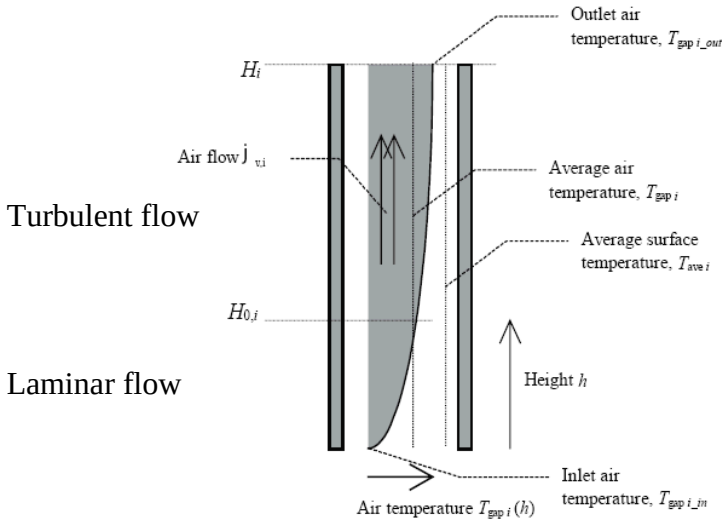

Figure 4.6 The air path inside the double skin facade transition from laminar to turbulent flow

4.3.2.3 A model grid in Gambit

The calculation method requires that the geometric space across which the calculations are to be conducted is first divided into a number of non-overlapping, adjoining cells which are collectively known as the finite volume grid.

When a CFD project is created, a grid is automatically generated for the required model domain by identifying all contained model object vertices, and then generating key coordinates from these vertices along the major grid axes. These key coordinates, extended from the X, Y, and Z axes across the width, depth, and height of the domain, respectively, are known as "grid lines." The distance between grid lines along each axis is known as a grid region and these regions are initially spaced employing user-defined, default grid spacing to complete the grid generation. The grid can have three different shapes but for a building application, a non-uniform rectilinear Cartesian grid would usually be used as shown in Figure 4.8, which means that the grid lines are parallel with the major axes and the spacing between the grid lines enables non-uniformity.

By default, grid regions are spaced uniformly using a system that is calculated to be as close as possible to the user-defined default grid spacing. In this case, the distance between these key coordinates is of an acceptable value. However, very narrow regions resulting in long, narrow grid cells or cells having a high aspect ratio should be avoided, as they tend to result in unstable solutions that can fail to converge. Highly detailed component assemblies can result in very large numbers of closely spaced key coordinates resulting in cells having high aspect ratios. Large numbers of key coordinates can also lead to overly complex grids and correspondingly high calculation run times and excessive memory usage, which can be avoided by replacing very detailed assemblies with cruder representations for the purpose of CFD calculation. However, where very narrow grid regions are unavoidable, adjacent grid lines formed from key coordinates

can be merged together using the merge tolerance setting which is accessed through the new CFD analysis dialogues.

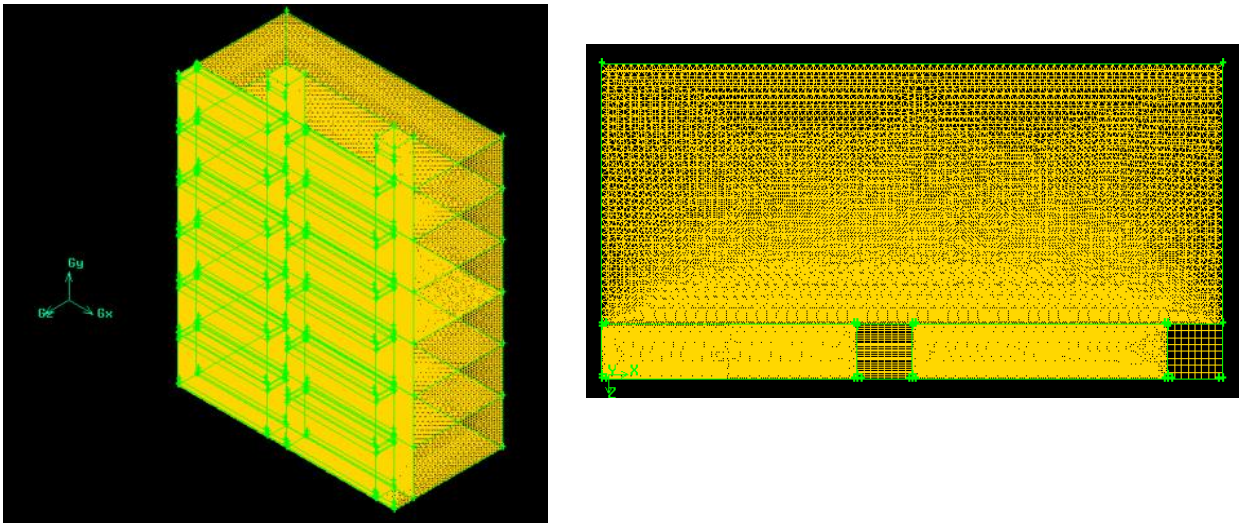

Figure 4.7 The mesh generated for a combined shaft-corridor DSF in Gambit.

As shown in Figure 4.8 the mesh has been mapped quads or triangles(unstructured solver). The number of grid is almost 5 million cells.

4.3.3 Boundary conditions of the three-dimensional model

An important initial concept for CFD analyses is that of boundary conditions. Each of the dependent variable equations requires meaningful values at the boundary of the calculation domain in order for the calculations to generate meaningful values throughout the domain. These values are known as boundary conditions, and can be specified in a number of ways. The specification of boundary conditions for two driving forces of wind and buoyancy effect can be defined as a pressure difference on inlet and outlet. To calculate the stack effect, the energy equation needs to be turned on (Fluent doesn't solve energy equations by default). By then setting the gravity vector correctly, the Boussinesq approximation calculates the natural convection effect. One drawback of this method is that it greatly slows down Fluent's solution-

convergence rate. Regarding the outdoor wind, by specifying pressure inlet and outlet conditions, the dynamic pressure of wind will be taken care of, therefore the outflow wind effect can be specified effectively there.

4.3.3.1 Wind speed, wind direction, and mean wind speed profile

The natural wind speed varies in time and space; the character of its variation is highly random and the wind flow is highly turbulent. At the same time, the wind speed is one of the main contributors to natural ventilation flow. The change of the mean wind velocity depending on height and intervening terrain is expressed through the mean wind speed profile, as one of the boundary conditions. Mean wind speed data for a specific time period is going to be used as one of the boundary conditions for the study, as stated in the previous section.

4.3.3.2 Outdoor air temperature, air humidity, and solar radiation

The mean outdoor air temperature is one of the other climate parameters that is required for the boundary condition. The table 4.2 shows a sample of the boundary conditions input.

Domain	
Domain Material	Incompressible flow-Air at 20°C, 1 atm
Reference Pressure	100,000 Pa (atmospheric pressure)
Reference Temperature	288 K
Sources	
Buoyancy Model	Boussinesq - calculates airflow from density difference
Buoyancy Reference Temperature	Outdoor air temperature in the specific time and date
Gravitational Acceleration	-9.81 m/s in the y-direction
Wind as the driving force	Wind velocity based on the external CFD modeling and weather date
Boundary Conditions	
Inlet Outlet	Inlet pressure = static pressure + $\frac{\rho V^2}{2}$ Outlet pressure = Gauge pressure(static)
Wall boundary conditions	Adiabatic solids (concrete) glass: standard 6mm clear glass for external and double low-e for internal layer
Velocity inlet	5 m/s
Cavity Details	
Cavity Size	3.5m high by 7m wide by 1.5m deep
Cavity External Facade	Internal plate with surface temperatures on both sides is going to be calculated based on heat source
Cavity Internal Facade	External plate with surface temperature base on heat source

Table 4.2 Boundary condition sample

4.4 Solution procedure

There are four turbulence models available in Fluent: the mixing length zero-equation model, the indoor zero-equation model, the two-equation (standard k-e) model, and the RNG k-e model. In turbulent flows, it computes the mass diffusion in the following form:

$$J_i = -\left(\rho D_{i,m} + \frac{\mu_t}{Sc_t}\right)\nabla Y_i \qquad (4.5)$$

where Sc_t is the turbulent Schmidt number, (with a default setting of 0.7).

In order to solve for buoyancy-driven flows and natural convection Fluent uses either the Boussinesq model or the ideal gas law in the calculation of natural convection flows. The importance of buoyancy forces in a mixed convection flow can be measured by the ratio of the Grashof and Reynolds numbers as follow:

$$\frac{Gr}{Re^2} = \frac{g\beta\,\Delta TL}{v^2} \qquad (4.6)$$

The terms radiant heat transfer and thermal radiation are commonly used to describe heat transfer caused by electromagnetic waves. All materials continually emit and absorb electromagnetic waves or photons. The strength and wavelength of emissions depends on the temperature of the emitting material. At absolute zero K no radiation is emitted from a surface. Fluent only consider the wavelengths in the infrared spectrum for heat transfer applications in its simulation and it provides two models for radiation heat transfer simulations, namely the surface-to-surface (S2S) radiation model and the discrete ordinates (DO) radiation model.

Fluent solves the governing integral equations for mass and momentum, and, when appropriate for energy, species transport, and other scalars such as turbulence. In summary, a control volume-based technique is used with the procedures as follows:

a) Division of the domain into discrete control volumes using a computational grid.

b) Integration of the governing equations in the individual control volumes to construct algebraic equations for the discrete dependent variables such as velocities, pressure, temperature, and conserved scalars.

c) Linearization of the discretized equations and solution of the resultant linear equation system to yield updated values of the dependent variables.

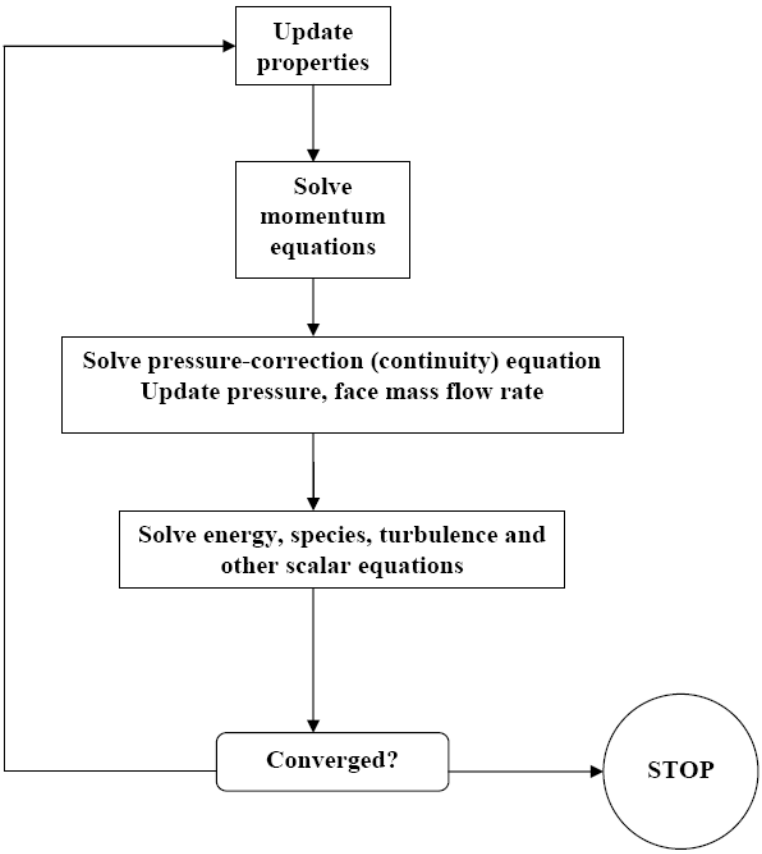

Figure 4.8 The CFD procedure of modeling to be converged

The governing equations continuity, momentum and energy are solved by Fluent:

Continuity: $\frac{\partial \rho}{\partial t} + \frac{\partial (\rho u)}{\partial x} + \frac{\partial (\rho v)}{\partial y} + \frac{\partial (\rho w)}{\partial z} = 0$ *(4.7)*

X-Momentum: $\frac{\partial (\rho u)}{\partial t} + \frac{\partial (\rho u^2)}{\partial x} + \frac{\partial (\rho uv)}{\partial y} + \frac{\partial (\rho uw)}{\partial z} = -\frac{\partial p}{\partial x} + \frac{1}{Re}\left[\frac{\partial \tau_{xx}}{\partial x} + \frac{\partial \tau_{xy}}{\partial y} + \frac{\partial \tau_{xz}}{\partial z}\right]$ *(4.8)*

Y-Momentum: $\frac{\partial (\rho v)}{\partial t} + \frac{\partial (\rho \mathrm{uv})}{\partial x} + \frac{\partial (\rho v^2)}{\partial y} + \frac{\partial (\rho vw)}{\partial z} = -\frac{\partial p}{\partial y} + \frac{1}{Re}\left[\frac{\partial \tau_{xy}}{\partial x} + \frac{\partial \tau_{yy}}{\partial y} + \frac{\partial \tau_{yz}}{\partial z}\right]$ *(4.9)*

Z-Momentum: $\frac{\partial (\rho w)}{\partial t} + \frac{\partial (\rho \mathrm{uw})}{\partial x} + \frac{\partial (\rho vw)}{\partial y} + \frac{\partial (\rho w^2)}{\partial z} = -\frac{\partial p}{\partial z} + \frac{1}{Re}\left[\frac{\partial \tau_{xz}}{\partial x} + \frac{\partial \tau_{yz}}{\partial y} + \frac{\partial \tau_{zz}}{\partial z}\right]$ *(4.10)*

Energy: $\frac{\partial (E_\gamma)}{\partial t} + \frac{\partial (uE_\gamma)}{\partial x} + \frac{\partial (vE_\gamma)}{\partial y} + \frac{\partial (wE_\gamma)}{\partial z} = -\frac{\partial (up)}{\partial x} - \frac{\partial (vp)}{\partial y} - \frac{\partial (wp)}{\partial z} - \frac{1}{Re\ Pr}\left[\frac{\partial q_x}{\partial x} + \frac{\partial q_y}{\partial y} + \frac{\partial q_z}{\partial z}\right] +$
$\frac{1}{Re}\left[\frac{\partial}{\partial x}\left(u\tau_{xx} + v\tau_{xy} + w\tau_{xz}\right) + \frac{\partial}{\partial y}\left(u\tau_{xy} + v\tau_{yy} + w\tau_{yz}\right) + \frac{\partial}{\partial z}\left(u\tau_{xz} + v\tau_{yz} + w\tau_{zz}\right)\right]$ *(4.11)*

The governing equations are solved sequential, and because the equations are not linear, several iterations of the solution loop must be performed before a converged solution is obtained. Each iteration consists of the steps outlined below and illustrated in Figure 4.9.

Fluid properties are updated based on the current solution. If the calculation has just begun, the fluid properties will be updated based on the initialized solution.

b) The u, v, and w momentum equations are each solved in turn using current values for pressure and face mass fluxes, in order to update the velocity field.

c) Since the velocity obtained in Step (b) may not satisfy the continuity equation locally, a Poisson-type equation for the pressure correction is derived from the continuity equation and the linearized momentum equations. This pressure correction equation is then solved to obtain the necessary corrections to the pressure and velocity fields and the face mass fluxes such that continuity is satisfied.

d) Where appropriate, equations for scalars such as turbulence, energy, species, and radiation are solved using the previously updated values of the other variables.

e) A check for convergence of the equation set is made.

f) The above steps are continued until the convergence criteria are met. (Fluent Tutorial)

Figure 4.10 shows how the residuals for each variable changes based on the number of iterations and reaches convergence.

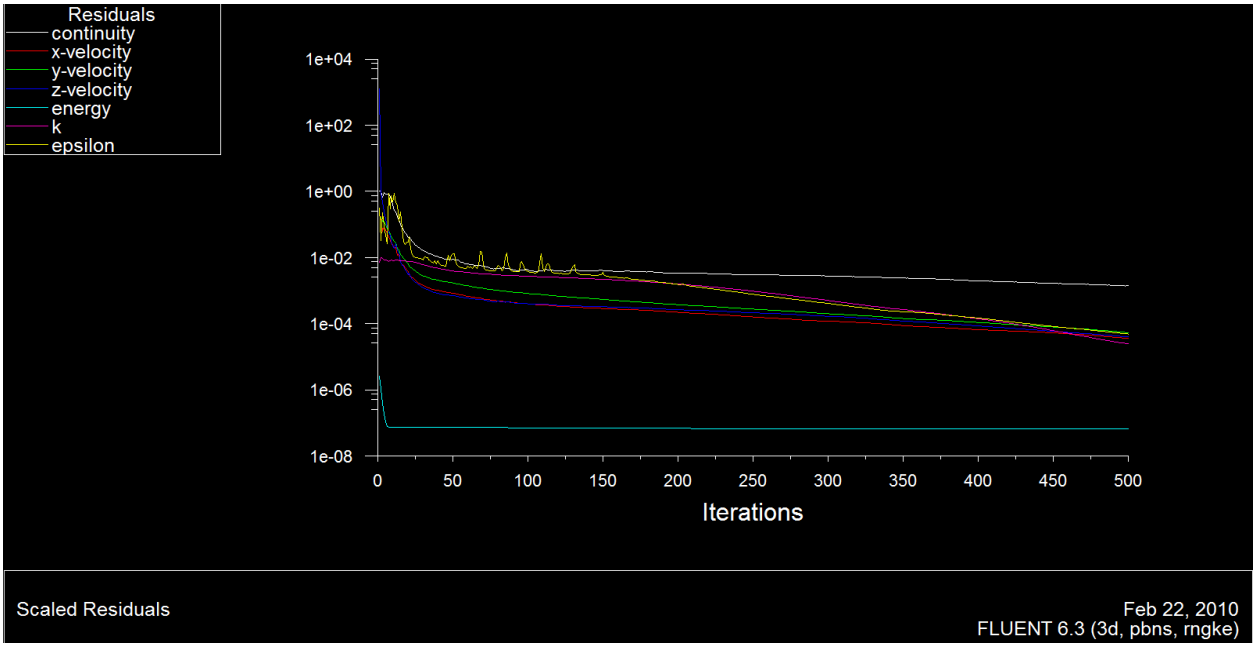

Figure 4.9 Convergence of residuals

4.5 Interpretation of CFD results

The simulation runs for an initial number of 1200 iterations typically. Then residuals will be plotted to check the residuals in the boundary definition would be converged. The simulation needs to be extended with at least all the residuals showing approximation to residuals of $1e^{-8}$. It is also necessary to carefully review the boundary settings and software mesh to solve the problem or trend to diverge of the continuity residual. As a result, the temperature can be plotted to illustrate the inlet-outlet temperature gradient. Also air-velocity magnitude inside the domain shows the influence of the convective forces. The results of the CFD simulation then can be used to calculate the thermal comfort based on the formula described at the beginning of this chapter. Figure 4.11 illustrates the example of the CFD results-Velocity profile within the DSF and the results show that the velocity in the offices is less than 1 m/s.

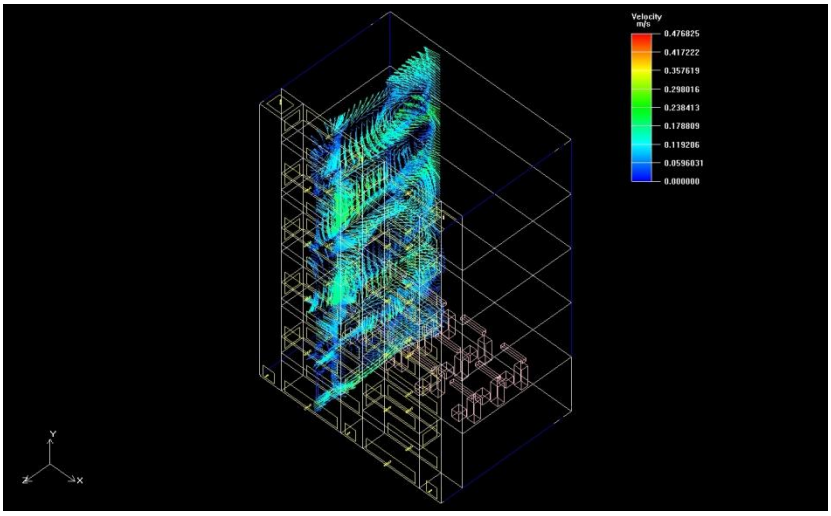

Figure 4.10 Velocity vector profile in the combined shaft-corridor DSF office spaces

4.6 Conclusions of CFD modeling

This chapter has provided background on CFD and demonstrated using Fluent to model airflow in buildings. The CFD modeling proved that airflow behavior could not have been intuitively estimated or assumed by the design team without the use of such tools. The major impact of CFD on the design is better airflow, and improved occupant satisfaction. In addition, the CFD was used to verify the effectiveness (avoiding high velocities and stagnation) of the airflow patterns at different wind speeds.

Chapter 5.0

Methodology

In previous chapters the principles of natural ventilation and DSF system was discussed and the application of CFD in built environment presented. This chapters provides the research methodology for the examining various parameters in the design of a combined shaft-corridor DSF investigating the energy performance through EnergyPlus and the behavior of airflow and an analysis of internal thermal comfort levels through CFD simulations.

In addition, this chapter presents the knowledge gap and research goals for the study. This will then lead to a discussion of the findings. The goal is to provide a process that can be applied at the earliest design stage to help a designer make better decisions that will result in more energy efficient buildings.

5.1 Introduction

This thesis addresses two major areas in energy efficient building design: technological aspects of airflow modeling and energy performance. Fig. 5.1 describes the methodology followed in conducting this research.

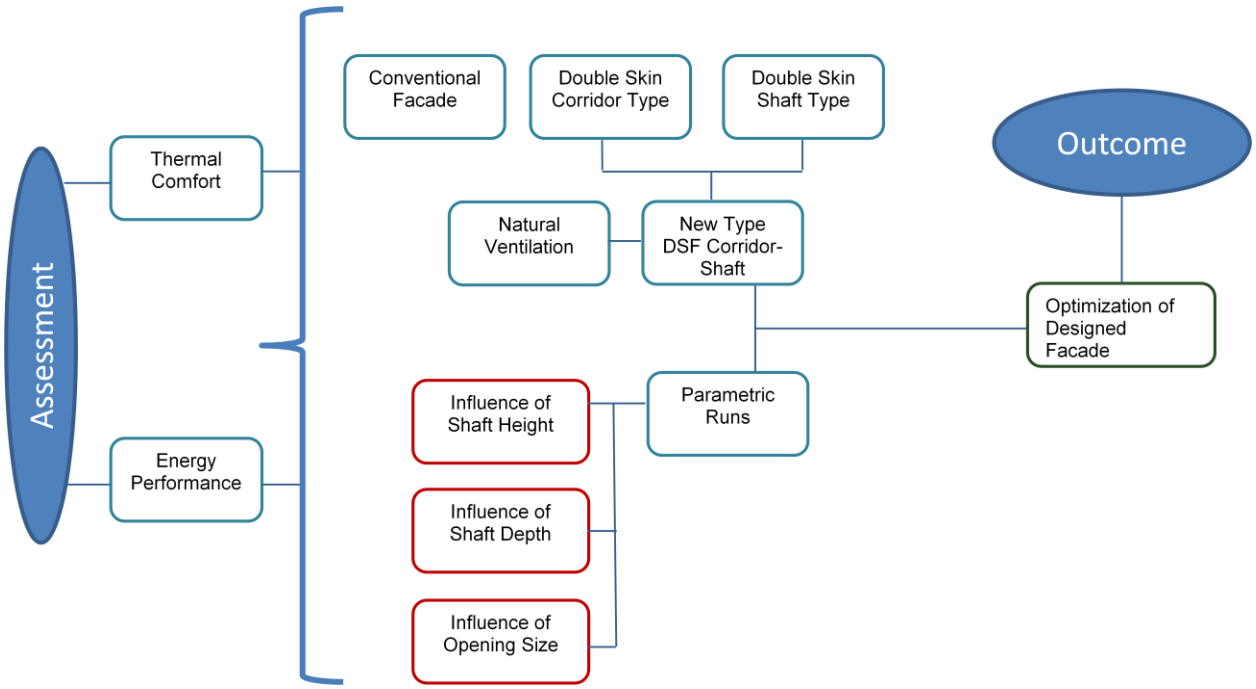

Figure 5.1 Diagram for methodology conducted in this research

5.2 Goals of the research

In attempting to answer the research questions raised in the Introduction, extensive research into the relevant subjects was carried out. The literature review was used to narrow the scope of the research field, and further, to come up with the right questions in identifying the knowledge gap. Issues such as natural ventilation strategies, human thermal comfort requirements, DSF technologies, building simulation tools, high-rise building designs in the urban context, and other built-environment criteria related to the research topic have been studied and critically reviewed. The research is attempting to incorporate natural ventilation techniques, combined with newly developed DSF technologies, and apply them onto high-rise office buildings in Chicago. A series of guidelines for DSF designs for Chicago high-rise office buildings are proposed to help designers make better decisions. This research will also help designers to make better selections

of DSF design featuers in terms of openings, sizes and locations, cavity depth, height of shaft, etc.

DSF energy-performance modeling is a complex problem. An accurate assessment of airflow and temperatures within the cavity requires detailed analyses of solar radiation transmitted through glazed facades, buoyancy, and wind pressure. Annual building simulation programs cannot provide accurate CFD simulations. For that reason, we discuss the application of CFD in the built environment in chapter 4.

The final objective of the research is to contribute to the energy performance and thermal comfort assessment of a combined shaft-corridor DSF by means of energy dynamic simulation and CFD tools. To achieve that goal, the following steps were taken.

First, a Chicago office building with a typical facade system-single skin was designed as the base case and it is described in detail in Chapter 6.

Then a numerical model was implemented to assess the energy performance of two typical DSF systems (shaft and corridor type) and a naturally ventilated combined shaft-corridor DSF, (which was a combination of the aforementioned ones) in comparison with the base case. In the next stage, all the variable parameters were studied to optimize the DSF energy performance. Finally, the results of the combined shaft-corridor DSF type with its variable parametric runs were compared to optimize both energy and comfort performance.

5.3 Developing inputs for the modeling process

The first step in the research procedure on energy performance of the combined shaft-corridor DSF configuration is to collect climate-condition data and information on the building under study which will be presented in detail in chapter 6. Chicago weather data was available through the U.S. Department of Energy. EnergyPlus, the software that was used as the dynamic building simulation, was also used that weather data for the energy analysis. These weather data includes temperature, relative humidity (RH), wind, solar insolation. They are collected from a location at Midway airport in Chicago which is close to the design site.

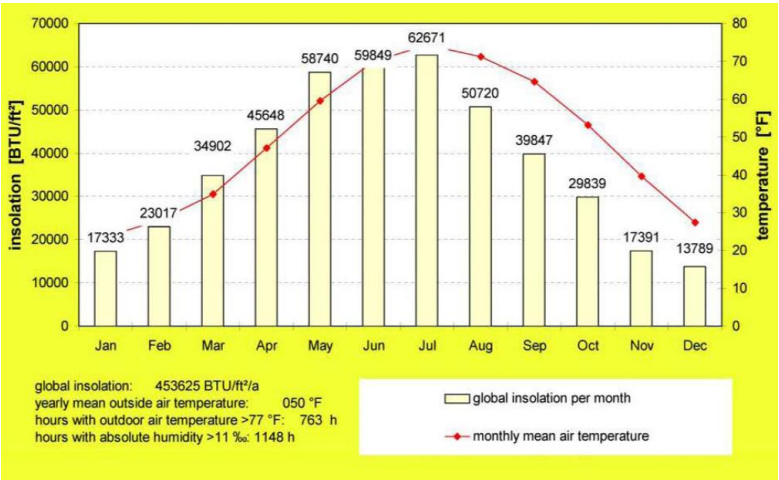

Figure 5.2 Chicago climate data

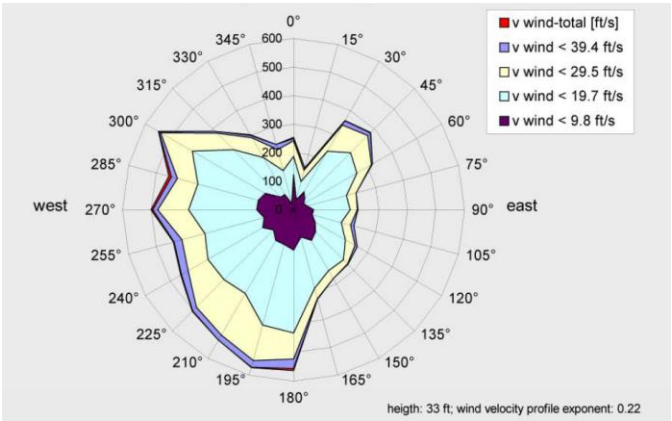

Figure 5.3 Wind rose

The wind data for Chicago shows that the dominant wind flows through the south and west and it is moving towards the North West.

5.4 Methodology for energy simulation and analyzing results

As suggested by Ternoey et al.(1985), the easiest way to evaluate energy improvements in building design is to appraise energy use patterns with a base case. For this purpose, a typical high-rise office building in Chicago was selected as a base case.

In this thesis, a parametric study was carried out focusing on energy use and thermal comfort. The base-case office building with double low-E pane windows was simulated to calculate the energy demand during the occupation stage. Then the same building with the combined shaft-corridor DSF was simulated. Moreover, parameters such as cavity depth, air inlet size, exhaust air opening size, as well as shaft height were all varied to study the impact of energy use and thermal comfort on the building. This study is divided into three main parts:

- Development and simulation of the reference single-skin building
- Simulations of the combined shaft-corridor DSF in terms of energy and comfort performance
- Simulation and analysis of the alternatives.

5.4.1 Simulation of the base case

After obtaining basic building and weather data, a simulation of the office building's energy performance was undertaken. This was the base case simulation for a single skin facade system. The simulation software used for this research was DesignBuilder with EnergyPlus as an engine. It provides a user friendly interface, also 3D visualization and has the capacity to simulate energy consumption from the basic input of the building shell, thermal zones, and climate data.

5.4.1.1 Input for energy simulation tool

The first step was to choose the metric (SI international System) or IP (Inch-Pound) unit systems. In order to build the model, the type of activity which is in this case is “Office”. Default building parameters was chosen by selection of building use type. Then the geometry is built by importing AutoCAD floor plans. DesignBuilder also follows a model data hierarchy.

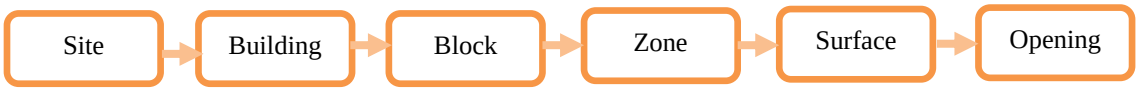

This arrangement allows users to make settings at different levels. For instance, a selection of wall type at the building level will affect all walls within the building while a selection at the block level only affect the walls within the particular block.

In order to build the model, the window wall ratio and the construction of wall types can be defined for all external and internal walls. Then based on information provided, the model can be run to calculate the annual energy consumption hourly.

5.4.1.2 Output

After providing the inputs, the results will be generated as a detailed report of the heating/cooling energies, peak and annual heating/cooling loads, and annual breakdown of energy consumption. For this research, a major focus of the analysis is on the breakdown of energy consumption and total annual cooling energy. It should be noted that the base-case energy consumption will be compared with the new configuration as the goal of naturally ventilated DSF is to reduce the cooling load by means of wind and natural convection.

5.4.2 Generation of building alternatives

In this section, a description of the methodology of the parametric study is given. To study the impact of design parameters on energy use and the thermal comfort performance of the combined shaft-corridor DSF in comparison with the base case, different building alternatives were simulated. The optimum alternative should facilitate the ventilation and be able to remove hot air continuously from the cavity while optimizing energy efficiency.

Studying a naturally ventilated system is much more difficult than studying a mechanically ventilated one, as the airflow rate depends on different parameters, such as the opening size, glazing type, the geometry of the cavity, etc. For this reason, a further parametric study was carried out for the naturally ventilated double-facade model to study the impact of parameters on the system performance (see diagram 7.1):

- Influence of cavity height and depth on air temperature profile
- Influence of opening size on airflows and air temperature profile
- Influence of shaft size on airflow and air temperature profile

5.5 Computational Fluid Dynamics

The computational fluid dynamics (CFD) software, Fluent, was used to analyze the Thermal performance of the combined shaft-corridor DSF cavity with wind and buoyancy-driven airflow. Developing a CFD model for this case was a lengthy process and typically taking 72 hours for each run. CFD has become a useful tool for designers in investigating the indoor environment conditions in building designs. The parameters such as air velocity and air temperature solved by CFD are critical for designing a comfortable environment. The application of Fluent in built environment has been introduced in Chapter 4. In order to investigate the DSF design three steps were taken:

- Step one: Establishing and assessing of the reference building.

Typical single skin facade office building (reference building) compared with two typical double skin facade systems shaft and corridor types. To study the facade design's impact on the space heating and cooling, a breakdown of energy components and overall energy consumption of a typical office building is presented in chapter 6.

- Step Two: Base case with Shaft-corridor DSF type assessment

To investigate the thermal performance of the combined shaft-corridor DSF, the boundary conditions and domain needed to be established based on the climatic condition. The initial simulation was concentrated on 7-story shaft height new configuration within a high-rise office building. The office module is constructed using Gambit and Fluent software which described in chapter 7 in details.

Instead of using the CFD software to model the whole high-rise building in one complete computer model, the office building has been 'divided' into several 'blocks' vertically since the height of the shaft is limited to a number of floors(7-story high for the first stage). Also just the half of the block (division occurs horizontally) is modeled. The reason for the simplification is to reduce the simulation time needed for each simulation run and any problem in the modeling process or domain settings will be identified easier.

The high-rise office building can be 'divided vertically' into four office blocks of 7-storey each. One of the 'office blocks' of 7-storey shaft height modeled with the similar boundary conditions and simulations were runs to study the thermal comfort of the internal spaces. Results were analyzed and details of the step-by-step modeling process were documented in Chapter 7.

- Step three: Parametric runs

This level of simulation is to optimizing the Shaft-corridor DSF of double-skin facade (combined shaft-corridor) which is presented in Chapter 8. The parameters used for the optimization are the opening size, the shaft height and the cavity depth. These parameters are found to be most important in affecting the facade system in providing optimum thermal comfort.

Chapter 6.0

Energy Performance Assessment

6.1 Introduction

This chapter provides a detailed description of the reference building model as designed and used for energy analysis in EnergyPlus- DesignBuilder. The building is modeled to assess the energy performance of incorporating of three types of DSFs in comparison with the reference building. A naturally ventilated combined shaft-corridor DSF and two typical corridor and shafts are studied and compared with a single skin facade. The building is assumed to be in Chicago for simulation and weather-data purposes.

To study the facade design's impact on the space heating and cooling, a breakdown of energy components and overall energy consumption of a typical office building is presented.

First, the components of the reference building will be described. The next section discusses the influence of different types of DSFs on space heating and cooling in comparison with the base case office building. Finally, the results are compared with a traditional facade and with each other in terms of energy performance and thermal condition.

6.2 Energy use in office buildings

In general, energy consumption in buildings is determined by function, climate, building components, construction, control, and settings. The climate and the ambiance are considered as-boundary conditions in energy simulation. Building function also has an important impact on energy use. As shown in Chapter One, significant amounts of energy (50 percent) go into the buildings and 23 percent of that goes into the office buildings. High occupancy and amounts of equipment increase the energy consumption as compared with residential buildings. Building

components and construction both provide great potential for improvement of energy demand in such areas as adequate thermal insulation, a key component of energy consumption. In office buildings, a careful choice of windows and shading devices should help to avoid additional solar gains. Incorporating efficient HVAC equipment and heat recovery techniques may also reduce the energy use. Designing a high-performance facade system will make a tremendous impact in minimizing energy consumption and optimizing the thermal condition. To illustrate different energy components in offices, Figure 6.1 presents a breakdown of a typical Chicago office building. The results of this benchmark are presented in KW/ $m^2\,yr$ and based on a survey of a large number of occupied office buildings. Typical patterns are representative for the median energy use of 2003 office buildings.

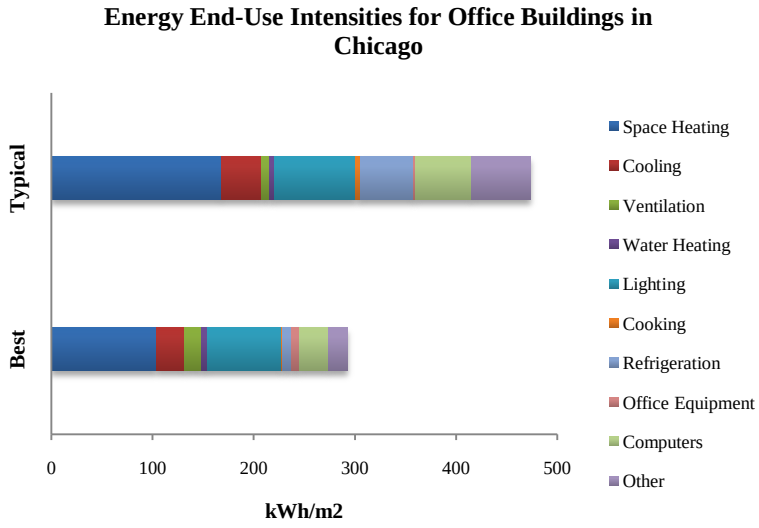

Figure 6.1 Energy components of typical office buildings (US Department of Energy, 2003)

CASE	Space Heating	Cooling	Ventilation	Water Heating	Lighting	Cooking	Refrigeration	Office Equip.	Computers	Other	total
Typical	168.1	39.7	7.9	5.0	80.1	4.10	53.0	2.2	54.9	58.7	**473.8**
Best	103.5	28.1	16.4	6.3	72.9	0.9	9.1	8.2	28.4	19.2	**293.1**

Table 6.1 Energy components of typical and best practice office building in Chicago

Total energy consumption is split up into nine end uses and two energy resources (gas and electricity). Gas is used for space heating and electricity consumption includes HVAC related consumption (cooling, ventilation), and other building services (lighting, equipment, catering, and water heating). In the Chicago climate, most of the energy goes into heating, as shown in the pie chart below; as 36 percent of the typical office building's energy is for heating and 20 percent for cooling (there is no natural ventilation in typical office building).

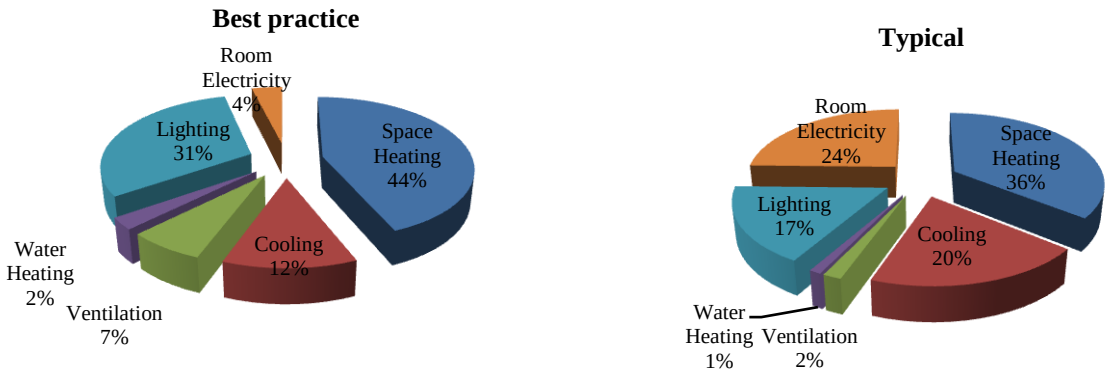

Figure 6.2 Energy breakdown of a typical (right) and best-practice (left) building based on DOE surveys

In order to assess the impact of the DSF in this research, a reference building was constructed and modeled. The results show that the model of reference building consumes 305.1 KWh/ $m^2 yr$, which assumes that all traditional energy saving technologies are employed. Therefore, in this study, the DSF impact is compared with the best-practice as the reference building.

6.3 Description of the reference building

The description concerns the real (designed) building, and the simulated model created for the energy and indoor-climate simulations.

The baseline facade configuration was a traditional, double glazed, low-E single skin facade.

Initially, the reference building was a 28-story building as shown in Figure 6.3. It is a rectangular shape with an open plan. In terms of geometry and installations, the floors are completely identical. However, floors 1-27 are connected (floor, ceiling) with other internal building zones, while the roof on the 28th floor is connected to the outside, and the ground floor is the ground (i.e., no basement).

The height of the building is 98m, with a length of 78m, and a width of 32m. Architectural drawings (floor plans, cross sections, facades) are presented in Appendix A. Room height is 3.5 m with a suspended ceiling. For this study, however, only part of the plan will be modeled both in energy simulation and airflow modeling analysis. It was assumed that the building divided into four blocks of 7-story high shaft modules. To simplify, the module to be studied is a rectangle 28 m by 8.5 m. The module area is 229.5 m^2 and includes 7 stories, making a total of 1,607m^2. The window area (including the frames) comprises 100 percent of the south facade. The interior design and the work places were not in the scope of the study. The four alternatives based on external skin types were compared in terms of energy use and the quality of thermal condition.

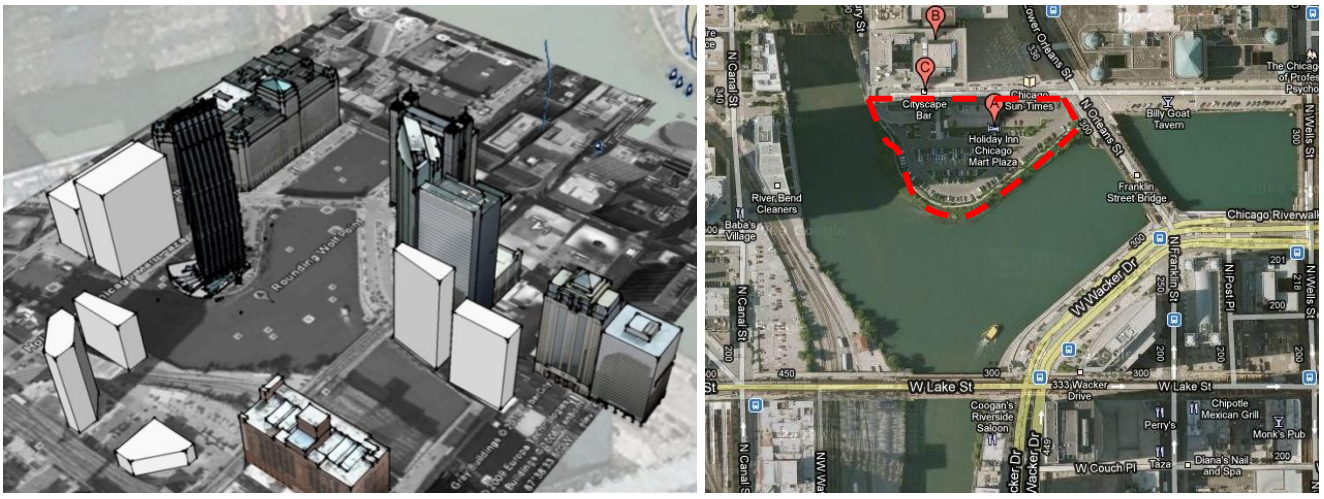

Figure 6.3 Left: View of the building in the site Right: Site Plan (Source: www.maps.google.com)

6.3.1 Office layouts

Floor layouts for both single and double skin facade were designed with open plan offices and shown in Figure 6.4. For the sake of simplicity, the simulation was created with as few thermal zones as possible. Adiabatic conditions were assumed between the ceiling and floor on all floors, which are identical zones, with similar temperatures.

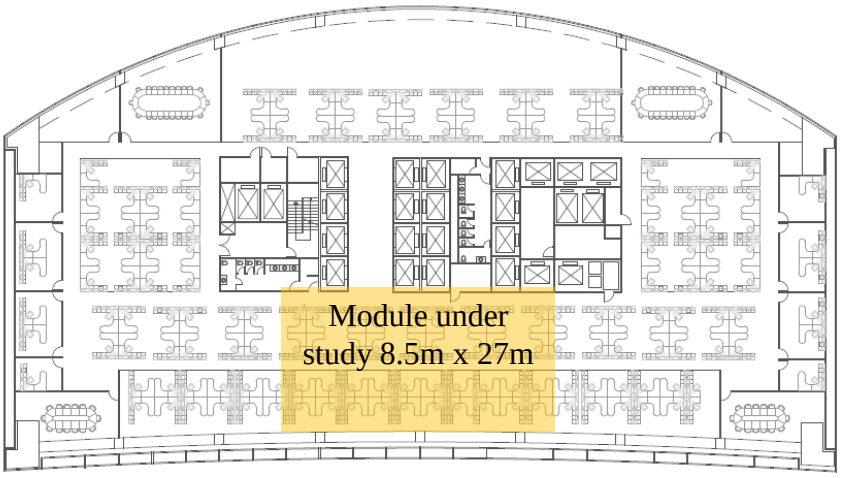

Figure 6.4 Office Layout

The building's total floor area for the number of working places (only office rooms) is 15.4 m^2/occupant.

6.4 Simulation of single skin facade

After obtaining basic building and weather data, this information was used to simulate the energy performance of the single skin facade model.

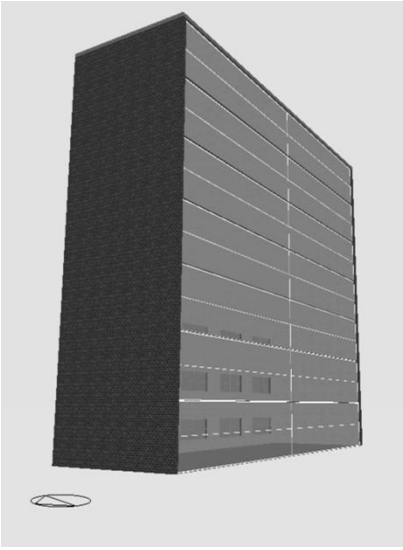

Figure 6.5 View of the modled proportion of the single skin facade in DesignBuilder

6.4.1 Input

First, the site needed to be chosen as illustrated in Figure 6.3. The site defines the building's geographical location and weather data. Then the activity template, selected: open office space. The occupancy schedules and other data, such as metabolic rates and levels of equipment use, were set based on the office space requirements.

The occupants' schedules, activity levels, clothing and room use are shown in Table 6.2.

Schedule for offices	08:00 -12:00, 13:00 – 17:00
Winter schedule	50% working during the Christmas vacations, otherwise 100% weekends closed
Summer schedule	75% working during July otherwise 100%, weekends closed
Activity level	Office Activity : 1 met = 108 W / occupant (1 met corresponds to 58.2 W / m^2 body surface)Task: sitting, reading
Clothing	For winter conditions: 1 clo For summer conditions: 0.6 clo

Table 6.2 Occupants schedule and activity level

6.4.1.1 Zone Identification

To simplify the simulation, only one zone per story was identified. The office building faces south with 100 percent glazing.

6.4.1.2 Zone properties description

The two main components of the energy simulation model are the building fabric and elements (walls, floors, ceilings, occupants, and equipment) and the plant components (HVAC equipment, and other environmental control systems). Ventilation, lighting and equipment, type of HVAC system, use of natural ventilation and daylighting should all be set in describing zone properties, For all of these values, office-building defaults were used, except for the HVAC system, which

had a VAV system with terminal reheat that had been chosen for the base case. However, the base case was simulated with no natural ventilation.

Then specific properties of each zone in terms of the wall properties (type, R-value, exposure, and construction), shading, window properties (type, glazing area, size and layout) needed to be set. The description of building's construction is shown in Table 6.2.

The glass area in the base case is 100 percent in the south facade and double-pane low-E insulation was chosen for the glazing type.

Building construction	Material type(from outside to inside)	Thickness (m)	Density (kgm^{-3})	U-value ($Wm^{-2}K^{-1}$)
External wall	Exposed concrete	0.10	1500	0.35
	Polystyrene	0.08	16	
	Concrete block	0.10	1000	
	Gypsum plastering	0.013	758	
Internal wall	Gypsum Plaster	0.025	970	1.9232
	Airgap 10mm	0.10	1.2	
	Gypsum Plaster	0.025	1090	
Floor	Cast concrete	0.10	2300	4.7
Ground floor	UF Foam	0.087	1200	0.35
	Cast concrete	0.10	2300	
	Creed	0.07	900	
	Wooden Flooring	0.03	1000	
Roof	Asphalt	0.01	930	0.25
	MW Glass wool	0.145	16	
	Airgap 25mm	0.20	2.5	
	Plasterboard	0.013	720	

Table 6.3 Description of building construction

The thermal properties of materials were initially calculated by EnergyPlus-DesignBuilder. It should be noted that thermal losses due to thermal bridges were not included in these calculations. In order to be accurate, practical values should be used instead of theoretical values.

6.4.1.3 Windows

The property of the reference window is as follows:

Window properties	Description	Aluminum window
	U value (W/m^2K)	4.719
Glazing properties	Description	Dbl LoE(e3=0.1) Clr 6mm/13Air
	U value(W/m^2K)	2.44
	SHG	0.643
Frame properties	Description	Aluminum
	Thickness	0.02
	Surface resistance(m^2K/W)	0.040
Shading device	Description	Blinds with high reflectivity slats
	Control	Scheduled and positioned inside

Table 6.4 Properties of window on south facade

6.4.1.4 Other settings

Control points for the indoor environment were set at 22 ℃ minimum for winter and 24.5 ℃ for summer. The infiltration rate assumed for the reference building was 0.5 ACH (air changes per hour). There were 300 occupants in the building. The lighting was assumed to be florescent with a power of 10 W/m^2 200lux and the annual equipment energy use for the open plan was 57 kWh/m^2. Another parameter was a control set for artificial lights, assuming that they are switched on according to occupant schedules.

6.4.2 Output

6.4.2.1 Simulation results for the reference building

After the appropriate input to best define the typical office building was entered, the base case was simulated for the year's annual performance. EnergyPlus generates a detailed report of the heating/cooling energies, peak and annual cooling/heating loads, costs, and annual breakdown of energy consumption.

For this thesis, only the most relevant output graphs were analyzed. The number of heating degree days far exceeded the number of cooling degree days and clearly showed the heating-season dominance. (Please refer to the detailed weather data for Chicago in the Appendix B). It was apparent that due to the cold conditions, the most significant loads and maximum energy use was for heating. In terms of breaking down annual energy consumption, the largest components were space heating, cooling, and lighting. A building cost analysis was omitted, as the major research objective was to study facades' thermal effects. The key point of adding a naturally ventilated DSF was to take some of the grid's cooling loads out. Therefore, the major focus of the analysis was on the following three output graphs:

a) Comfort

b) Annual Cooling and Heating Loads

c) Breakdown of Energy Consumption

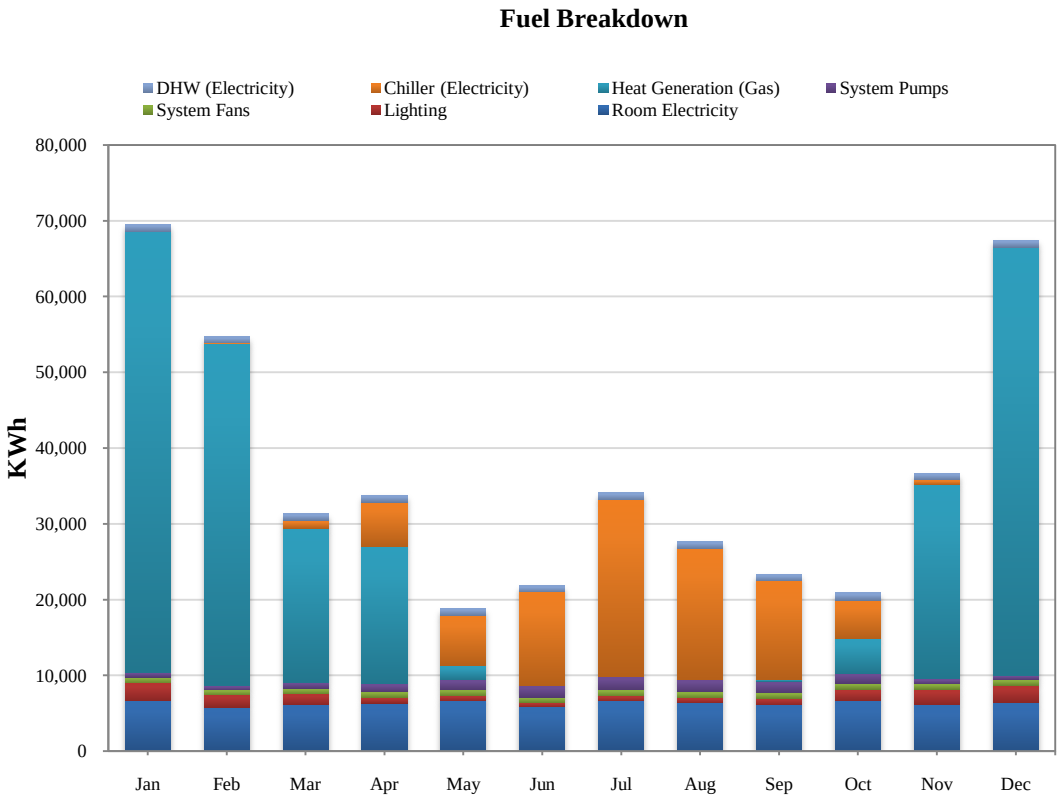

Figure 6.6 Fuel use break down of the reference building

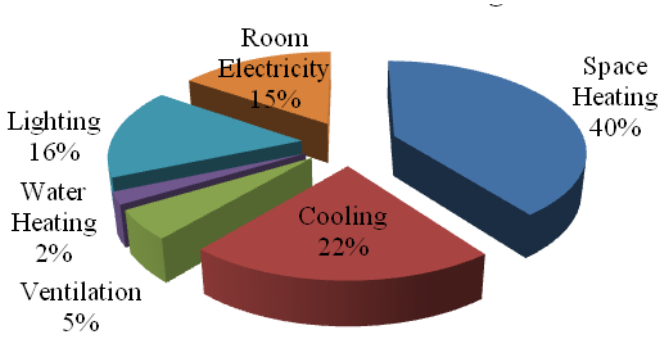

Figure 6.7 Fuel breakdown of the simulated result with percentage of usage 274 total energy intensity use

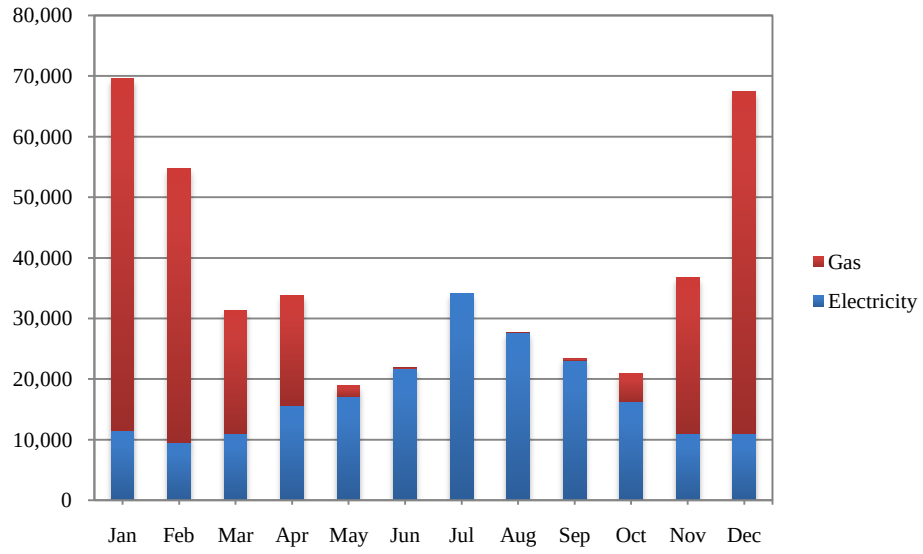

Figure 6.8 The reference building's heating and cooling consumption

KWh	Jan	Feb	Mar	Apr	May	Jun	Jul	Aug	Sep	Oct	Nov	Dec
Electricity	11,435	9,560	11,024	15,634	17,047	21,820	34,112	27,658	23,095	16,310	11,004	10,962
Gas	58,107	45,143	20,314	18,141	1,807	15	0	4	250	4,568	25,674	56,468

Table 6.5 Reference building simulation results, heating and cooling energy

6.5 Simulation of facade alternatives

6.5.1 Description of double skin facade alternatives

In this section, the energy performance of 7-story DSFs were studied and compared to the 7 story section of the reference building. The energy demands of the following facades were studied:

- A seven-story naturally ventilated cavity shaft type
- A seven-story sealed outer skin-corridor type comprised of a single pane of clear glazing, wherein the facade acts as an external air curtain
- A seven-story naturally ventilated new DSF configuration combination of corridor and shaft type.

Two DSF construction types were assumed: a corridor type and a shaft type. In both cases, the cavity depth was assumed to be 1.5m and the shaft height was assumed to be 7 stories (3.5m height). The main difference of the alternative facades is that a double skin has been added to the building; with the internal skin the same as the reference building and the external skin as a single pane window (6mm). The shadings were located inside the cavity. In both DSF types, the building was mechanically ventilated, yet the cavity was naturally ventilated. The shading devices were considered to be white with a slat angle of 45. Figure 6.9 shows these three alternatives for energy simulation.

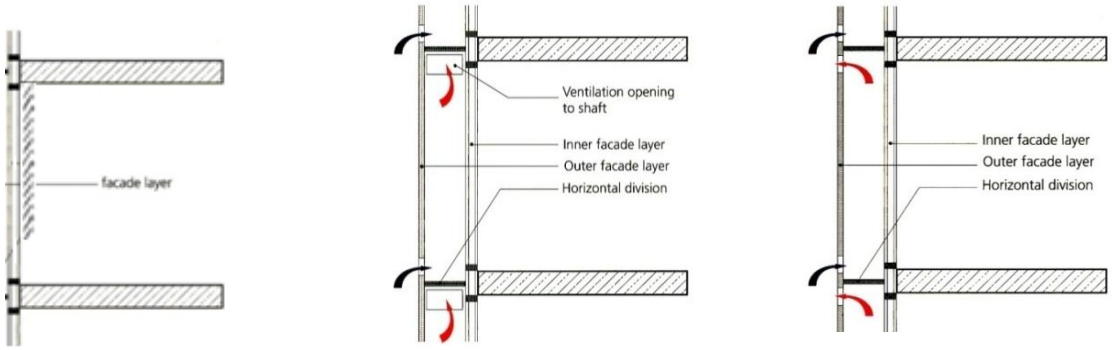

a: Base case facade b: Shaft type c: Corridor type

Figure 6.9 Diagram of the simulated double skin facades

The base case consists of a well insulating glazing with a U-value of 2.44 W/m^2K and a solar transmittance of 0.634. The window is equipped with roller blind as shown in the Figure 6.9a. If we added a clear glass pane (6mm) in front of the base case with divisions along each story that allowed the exterior air to enter, the cavity a double skin facade corridor type is created (Figure 6.9-b). In the case of a shaft type, single glass was added to the exterior a small distance from the insulated internal glazing, while the extracted air goes to a shaft that goes through multiple stories and takes the exhaust air outside (Figure 6.9-c). The office was equipped with a

mechanically ventilated system in case of variable weather condition and the natural airflow was not enough to provide cooling.

Almost all the literature studies noted advantages regarding the reduction of heating/cooling losses over traditional single facade systems. The lower radiant temperature increased building's thermal comfort. Also, during the winter, the cavity can act as a buffer zone and capture incident solar energy, which further improves the energy efficiency.

6.5.2 Combined shaft-corridor DSF

This study looks beyond typical shaft and corridor DSF solutions and provide a new type shaft-corridor configuration. The combined shaft-corridor DSF configuration takes advantage of strategies such as ventilation driven by different combinations of wind and external stack. The most distinguishing visual feature of this configuration is it can pronounce a module by projecting or taking back the towr on the facade as presented in Figure 6.10. This configuration combined both shaft box and corridor types on the building's facade while trying to avoid their disadvantages. The cooling stacks allow for further ventilation on hot, stagnant, summer days so the building always remains within reasonable temperature levels, like that of an air-conditioned building.

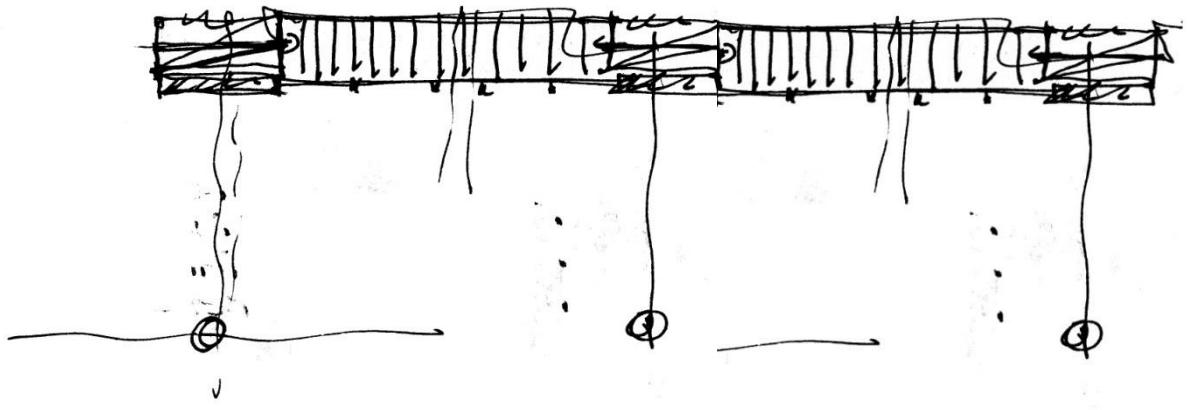

Figure 6.10 Sketch plan of the new configuration

One of the disadvantages of a shaft-type window is that the narrow width makes it difficult to clean and maintain. A corridor type can simply act as an internal or external air curtain. As a result, natural wind cannot be introduced to the interior space; if we open the internal screen the air inlet and exhaust air will mix. With the combined shaft-corridor DSF we tried to avoid the disadvantages mentioned above. To avoid air mixing, the inlet and exhausted air are separated through a channel. Exhausted office air will go directly into the transparent channel, which is connected to the shaft. In addition, the shaft width is increased up to 1.5m, the same as the corridor depth. Ventilation effectiveness is driven by thermal buoyancy, or stack effect, which is determined by the inlet air temperature, the height between inlet and outlet openings, and size of these openings.

Figure 6.11 shows how air flows through the chimney and provides ventilation inside each office module. The air gap inlet draws in fresh air at a low level and directs it into the room. The air is exhausted through the outlet at the high-level gap of the inner pane. The multi-story chimneys sucks the exhausted air through a bypass opening at the top of the corridor facade. The vertical height of the glass chimney creates a stronger uplift force due to the increased stack effect.

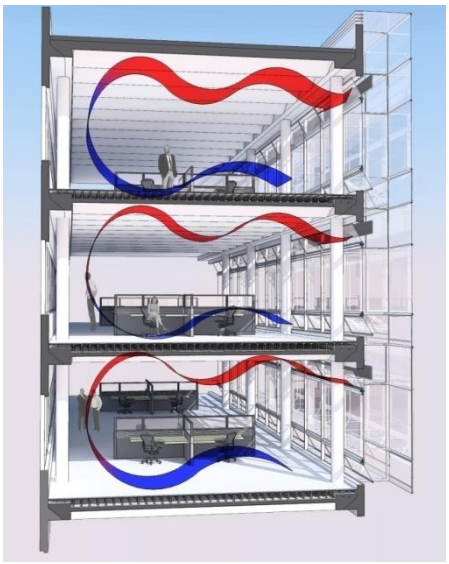

Figure 6.11 The combined shaft-corridor DSF configuration and show air flows within the building

6.5.3 Energy use simulation results

An annual energy simulation on an hourly basis under Chicago climatic conditions was performed for different DSF alternatives. All inputs were the same as the reference building, with the same floor area. In the case of the corridor facade, the width of the corridor was 1.5m and the width of the shaft-type facade was 0.3m that passed through 7 stories. The energy performances of the different DSFs will be discussed in detail in this section.

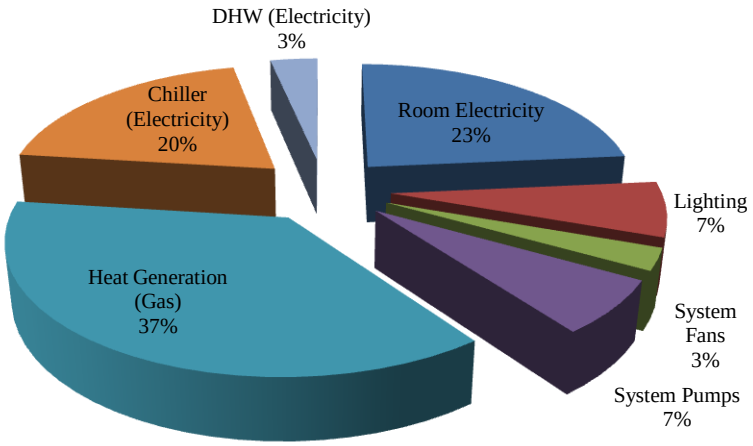

Figure 6.12 Energy breakdown in the combined shaft-corridor DSF configuration

The annual cooling and heating energy consumption of the combined shaft-corridor DSF is presented in Figure 6.12. When heating and cooling loads were compared, it is apparent that heating is the largest component of energy consumption. The heating season period is longer than the cooling season in Chicago.

6.5.3.1 Energy demand results

The net annual gas consumption was reduced by 18 percent through the shaft, 16 percent through the corridor type, and 35 percent in the new type (Shaft-corridor DSF). As shown in Figure 6.13, the heating energy (gas consumption) was reduced in comparison with the two other typologies;

however, in terms of cooling demand, electricity consumption decreased by five percent in the shaft type and nine percent in the corridor type. Total electricity was reduced by 15 percent in the combined shaft-corridor DSF. Cooling and heating demands will be discussed in detail for each month in the following section.

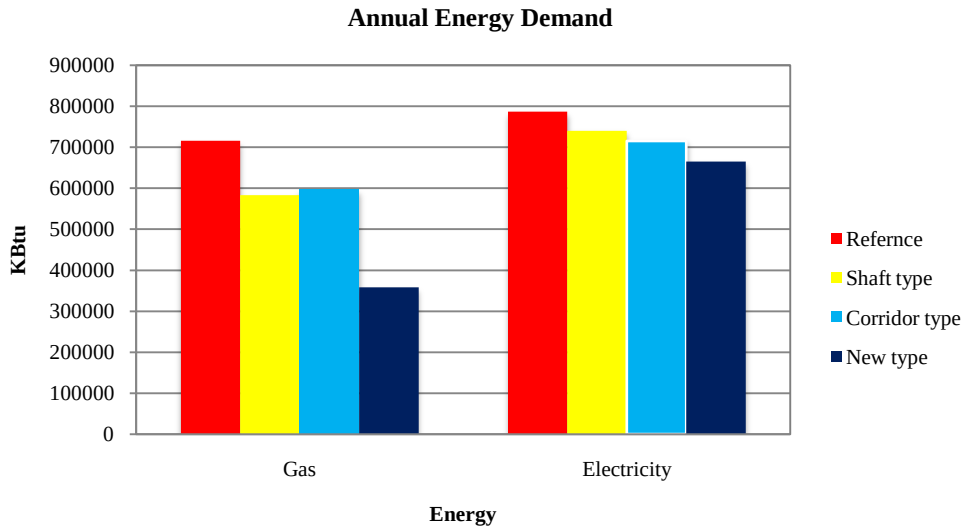

Figure 6.13 Annual gas and electricity demands

6.5.3.2 Cooling demand

It should be emphasized that the results represent the space heating and cooling energy demands. Cooling efficiency differs from heating. The cooling demand is reduced each month in comparison with the base case, except for the month of July, when it is lower than the shaft and corridor types. However, the total annual cooling load was reduced by adding the DSF, as the exterior shading devices decreased the heat solar gain, and made it easier to lose the indirect solar gain. The results, consequences of the different climate, contradict Saelen's (2002) findings. They also indicate that the combined shaft-corridor DSF increased the natural ventilation even in hot summer months and would be a good option for the building.

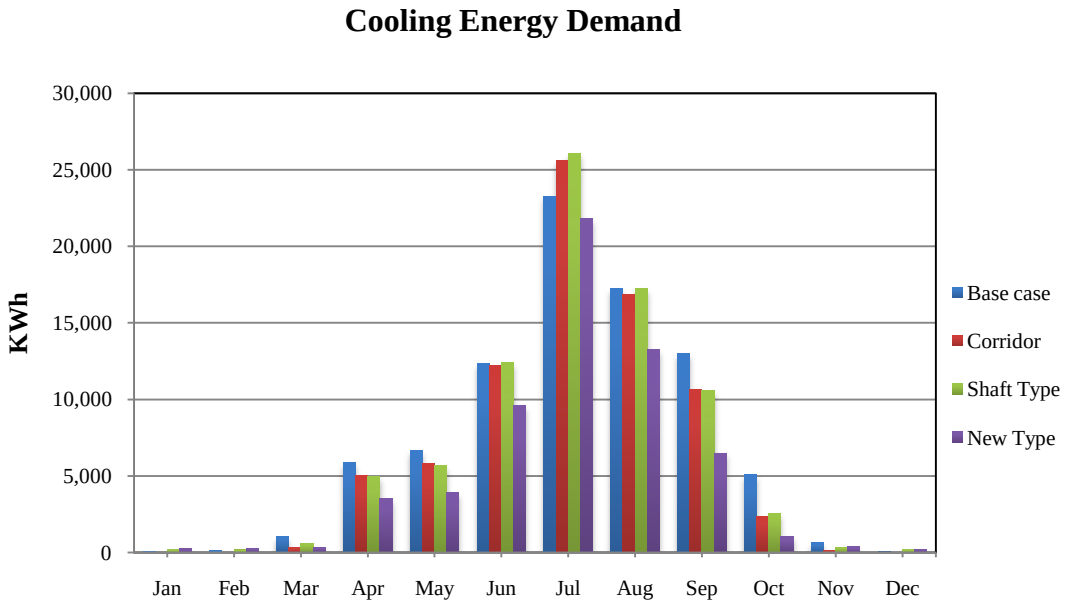

Figure 6.14 Annual net cooling demand for each month

The Figure above shows the cooling demand of each month for the four different alternatives. The total energy use for cooling has been reduced by 28 percent in the combined shaft-corridor DSF and by almost five and seven percent in the shaft and corridor types, respectively. Based on the energy simulation in Belgium by Saelens the south-oriented DSF requires 32 percent more for cooling energy than the traditional facade (Saelens, 2002), while the combined shaft-corridor DSF reduces cooling energy by 28 percent. Because of the extra pane, the DSF has a lower direct solar gain, and the shading devices situated outside while in the base case the blinds located inside which doesn't reduce the solar heat gain. In addition, with the combined shaft-corridor DSF we can take advantage of both wind and natural convection that has occurred in the stack, which improves the air velocity in eliminating the hot stuffy air from the building.

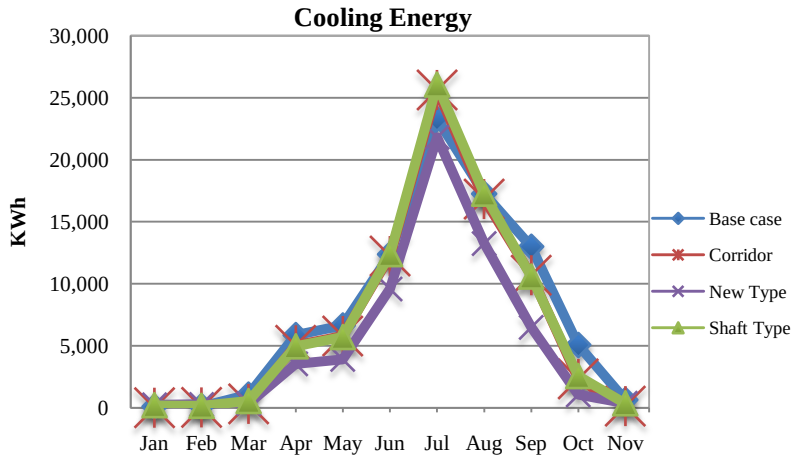

Figure 6.15 Cooling energy demand for four different enclosures

The total cooling energy is reduced by almost 28 percent, although this trend is not the same for all the types in each month, as shown in the Figure above. The shaft and corridor types almost save the same amount, however, the total annual reduction in the corridor type is seven percent and five percent in the shaft type from the base case.

6.5.3.3 Heating demand

Comparing the DesignBuilder Heating and cooling demand for the four enclosures occurs in Figure 6.16. The energy use for heating in the combined shaft-corridor DSF configuration is several times lower than the base case demands and other DSF alternatives. In general, the results seem to be remarkably different than the cooling savings and can be explained by the following reasons: during the heating season the system would be closed thus no air is moving in the cavity. The cavity then heats up and increases the temperature of the inner pane and thereby reducing conductive, convective, and radiant losses. In addition, the whole system increases the R-value of the enclosure by providing a buffer zone in front of the inner pane. The difference between the maximum and minimum heating load is more pronounced than it was for the

cooling demand. It can be concluded that in the Chicago climate, the extra pane can lower the heating load by 22 percent annually.

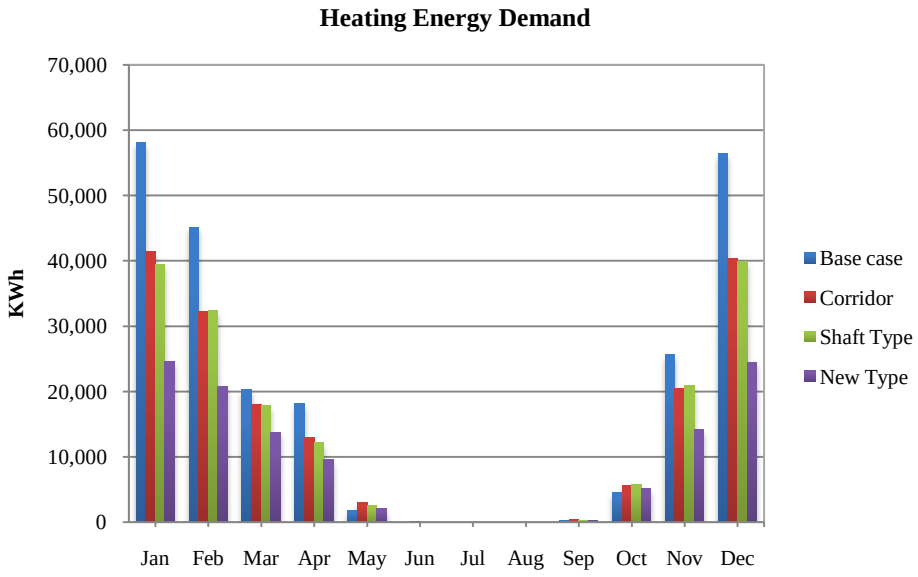

Figure 6.16 Heating energy demand for each month

6.5.3.4 Simulation results for the building

In this section, the energy-use difference for heating, cooling, and lighting is compared with the three alternative facades and the base case. The energy use for heating in the reference building is 34.7KWh/m^2 (25%) higher than the shaft and corridor types and 72 KWh/m^2 (50%) higher than the combined shaft-corridor type, respectively. As expected, in all cases the energy use for heating and cooling was higher than the reference building. However, Figure 6.17 shows DesignBuilder results for lighting increased in the shaft and in the combined shaft-corridor DSF in comparison with the base case by one percent. It can be concluded that 100 percent glazing provides more daylight than the combined shaft-corridor DSF and shaft types, which makes sense.

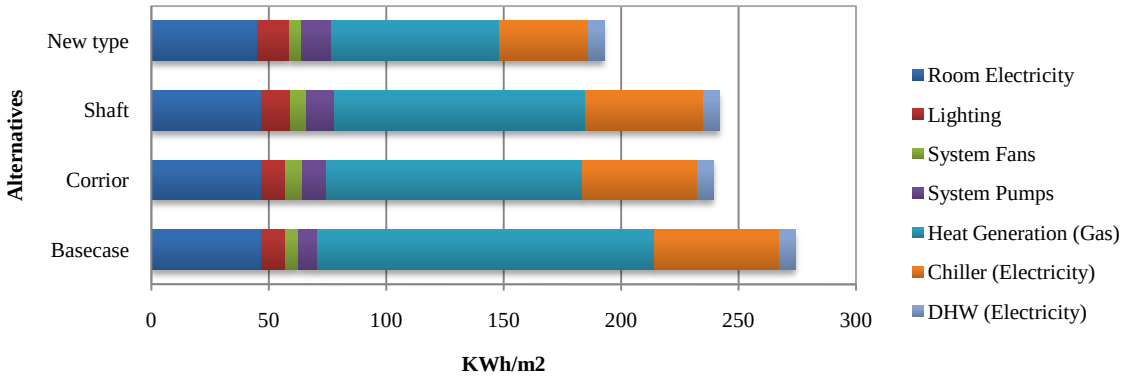

Figure 6.17 Impact of facade types on energy use

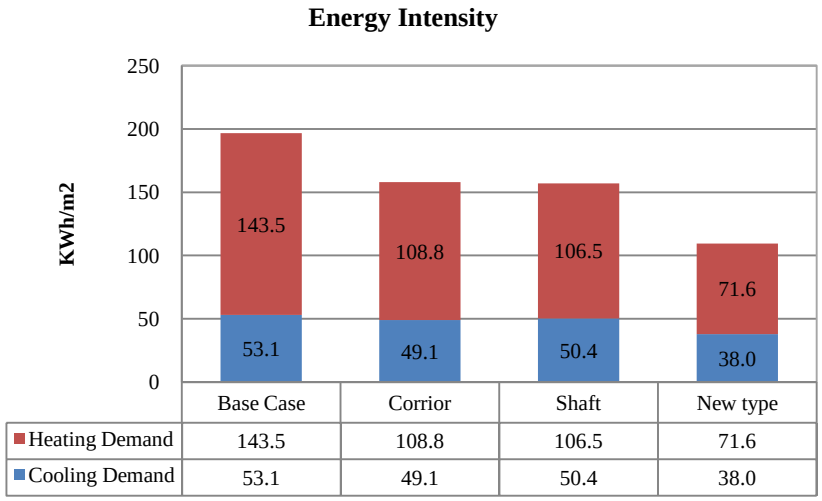

Figure 6.18 Energy intensity of alternatives

The heating energy intensity was reduced by 50 percent in the new type (Shaft-corridor DSF) and 28 percent in cooling energy intensity. In total, compared with the base case, the corridor type reduced energy by 12 percent, shaft by 11 percent and the combined shaft-corridor DSF by 29 percent.

Case	Energy Intensity KWh/m^2 yr	Percent Savings (%)
Base	274.1	
Corridor	239.3	12
Shaft	241.7	11
combined shaft-corridor	192.7	30

Table 6.6 Energy intensity of 4 cases and the percentage of savings

6.5.4 Impact of enclosure on the perception of thermal comfort

The section evaluates the indoor comfort of the different facade alternatives. The monthly average values presented below are good indicators of the indoor thermal condition on the building level, while the local discomfort is not in the scope of this study.

6.5.4.1 Average mean air temperatures

The mean air temperature difference between the new DSF type and the base case is very small. As expected, the new configuration and other DSF alternatives provided a lower temperature than the base case during the summer months, although they also reduced the cooling loads. With strict temperature-set points for all alternatives, the PMV and PPD values are quite similar, and just a few degrees lower than the base case.

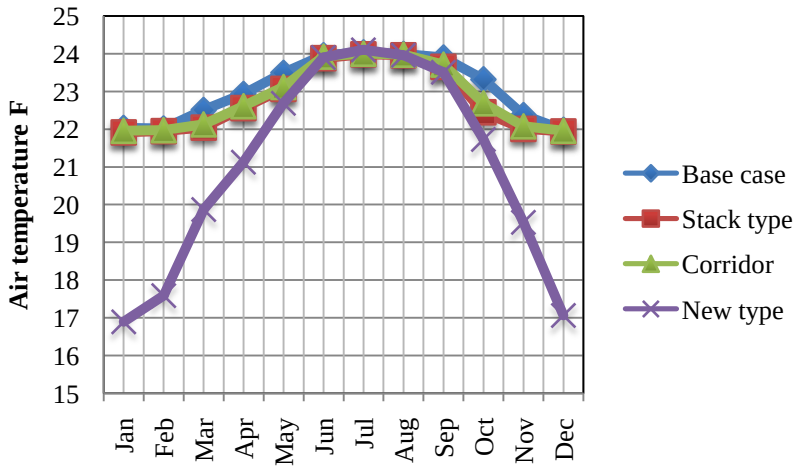

Figure 6.19 Average mean temperatures for reference and alternatives

6.5.4.2 Perception of thermal comfort

The thermal comfort indices, PMV and PPD values, were calculated in DesignBuilder to study the thermal comfort inside the office building. Since the building was assumed to be the open plan type, average radiant temperatures of the external walls were calculated and the occupants' position was not considered. The average PMV varied between -1 and 1 for the base case, slightly different for the Shaft-corridor type. The base case was slightly hotter than the DSF alternatives and the new configuration was slightly colder during the winter months than the base case and the other two DSFs. The single and double skin enclosures performed similarly due to the strict temperature-set points.

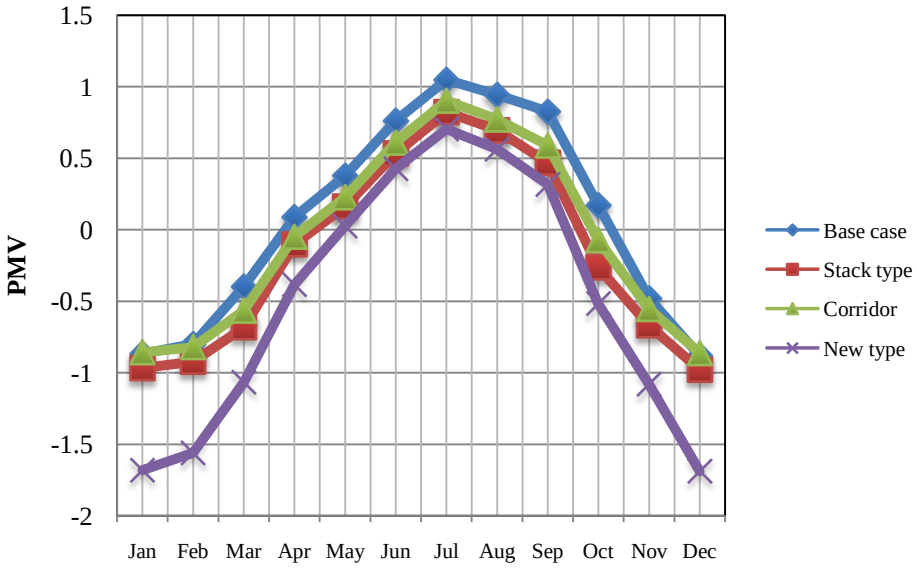

Figure 6.20 PMV differences in four enclosures

The results in Figure 6.20 shows that during the winter months, the PMV results of Shaft-corridor type is lower than the other types and the reason is that the cavity is not mechanically heated and the sun space effect can not warm the cavity enough during the months December,

January, February. For climate of Chicago, the warm air needs to be introduced to the cavity during these months to provide a better comfort for the occupants.

6.6 Summary of the energy use simulation results

The analysis of the basic DSF typologies shows their potential to lower the building's heating demand. Heating energy consumption was higher than cooling energy consumption. The reduction of energy losses and the possibility of providing a sunspace to take advantages of the solar heat gain caused the combined shaft-corridor DSF and the other two DSF alternatives to lower the heating needs more than the reference building.

In the Chicago climate, both heating and cooling loads were reduced simultaneously, which contradicts with what Saelens (2002) found in Belgium for a south-oriented facade. Since the exterior shading devices performed best during cooling season, the cooling demand was reduced about 15 percent in the new configuration. The results indicate that natural ventilation of offices is feasible in minimizing cooling energy and would be a good option in the summer time.

CASE	Energy Intensity KWh/m^2	Heating Consumption KWh/m^2	Heating Reduction %	Cooling Consumption KWh/m^2 yr	Cooling Reduction %
Reference building	274.1	143.5		53.0	
Corridor type	239.3	108.8	24	49.2	7
Shaft type	241.7	106.6	25	50.5	5
Shaft-corridor type	192.7	71.6	50	37.9	28

Table 6.7 Summary of results

Chapter 7.0

CFD Modeling of the combined shaft-corridor DSF

7.1 Introduction

To preserve thermal comfort and reduce cooling loads, natural cooling strategies can be incorporated into buildings. In this chapter, the behavior of natural ventilation in a new double skin facade (DSF) configuration will be studied. To that end, Fluent, computational fluid dynamics software (CFD), was used to study the office airflow path. Developing a CFD model is a lengthy process. First, EnergyPlus-DesignBuilder was used to solve some boundary conditions, such as solar thermal energy. Then a strategy was developed to reduce computation time, in which half of the model was analyzed instead of running the whole model (the building is symmetrical). The temperature profile and air velocity within the DSF's cavity and the internal office space were simulated by Fluent, and, as a result, the offices' thermal comfort was calculated and presented.

7.2 CFD modeling

Some researchers (Wong, 2008) argue that DSFs are the only means of natural ventilating in buildings. In general, incorporating natural ventilation into high-rise buildings is prohibitive due to high outdoor noise levels and/or high-wind speed levels. But under what conditions is incorporation of natural ventilation possible with this combined shaft-corridor in a hot summer continental climate? How are offices next to a DSF ventilated?

7.2.1 Climate data assumptions for the site

Simulations were performed with climatic data of Chicago (Midway airport). Weather data were recorded by the World Meteorological Organization and includes 12 actual months. Natural ventilation is possible during the shoulder season in Chicago. For this study, the months of May, June, September, and October were explored.

Daily wind and hourly weather data is presented in the Figures7.1 through 7.4.

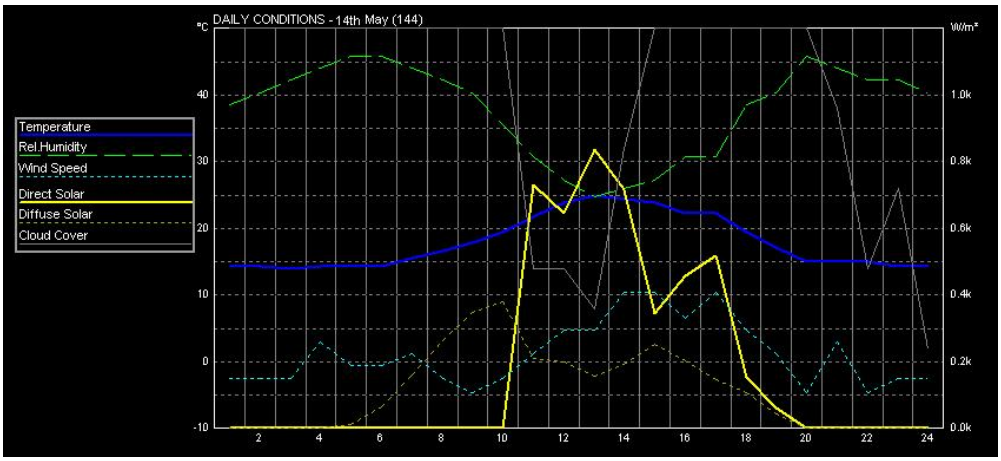

Figure 7.1 Weather data for May 14th, 2009, Chicago, Il

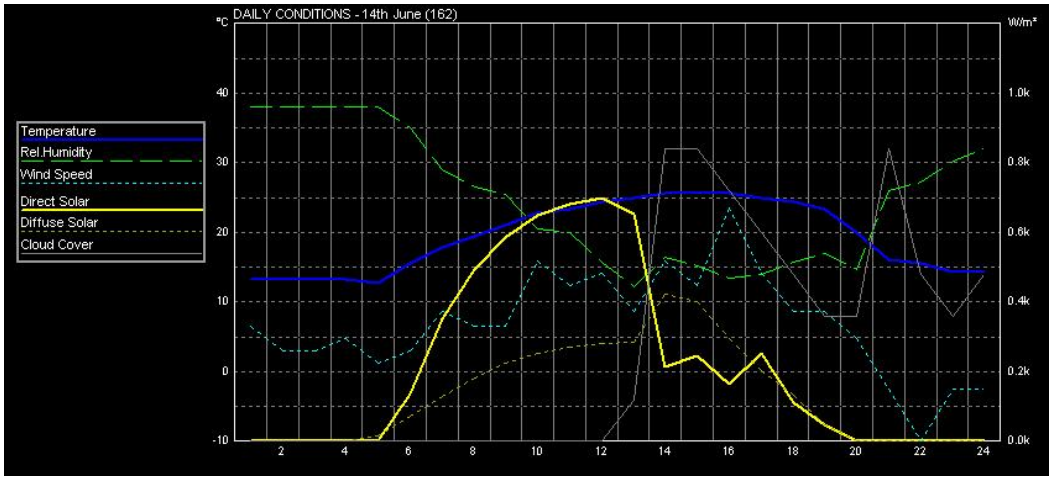

Figure 7.2 Weather date for June 14th, 2009, Chicago, Il

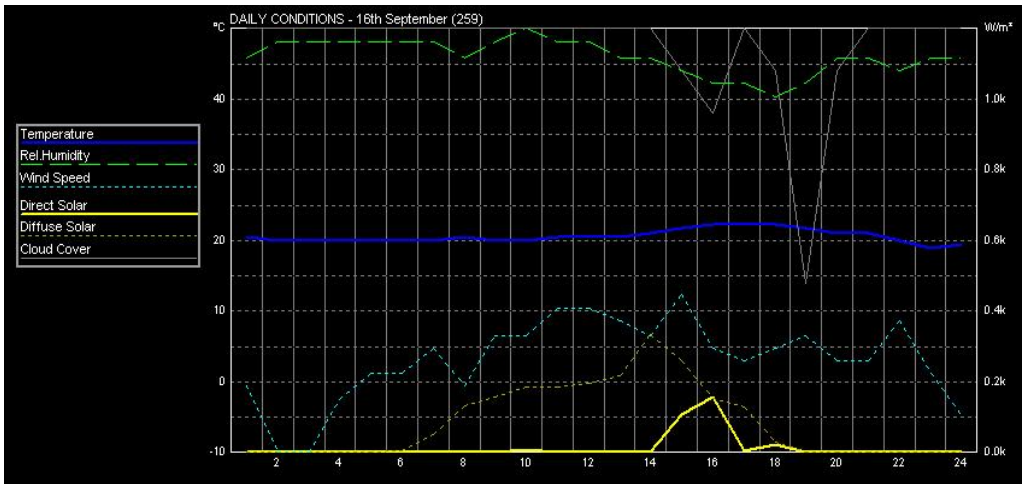

Figure 7.3 Weather data for Sep 16th, 2009, Chicago, Il

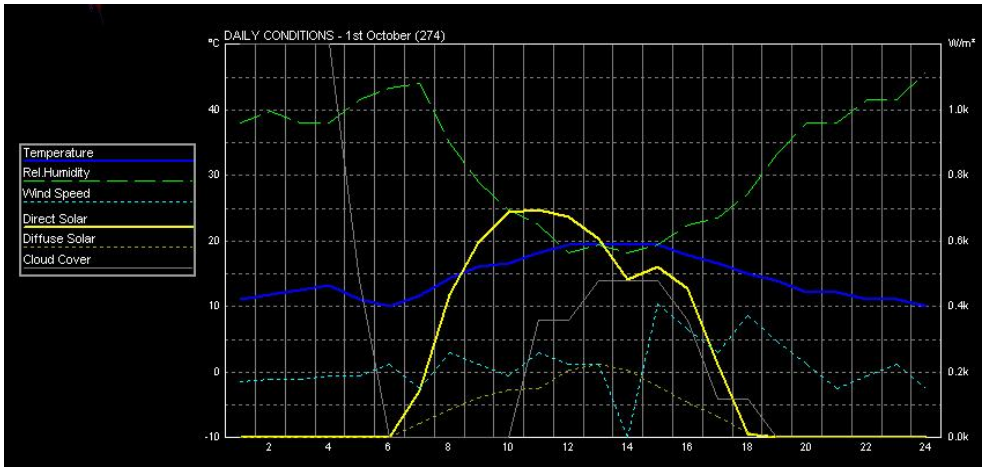

Figure 7.4 Weather data for Oct 15th, 2009, Chicago, Il

The first stage of the air flow modeling is to construct a simple model of the combined shaft-corridor DSF configuration in Gambit (for detail information refer to Chapter 4). The numerical model is three-dimensional and the model is based on a control volume method. The geometric model of the entire building is constructed using a matrix of numbers to represent the points at which surfaces meet.

In the next stage, the boundary conditions were solved, the grid size refined, and number of necessary iterations determined. Fluent then generate a model that solved for wind velocity along with buoyancy forces. The model used to solve the iteration was bousinesqe in order to consider the buoyancy forces and in order to include wind force, the pressure at the surface boundary was calculated (refer to Chapter 4 for more details). In order to define the external boundary condition, the airflow needed to be solved for the external wind to be entered in Fluent.

7.2.2 External airflow modeling

In designing a naturally ventilated building, the site-condition effects such as adjacent buildings, walls, and vegetation on wind velocity needs to be studied. One approach to study the external airflow path is to build the building in its context in the CFD software. In this strategy, the reference office building was modeled to analyze the wind pressure variable. The model was run with a number of reference wind velocities to solve for air velocities near cavity openings. These velocities could then be used as boundary conditions for a cavity model. The modeled wind pressure around the building was used as a boundary condition for internal airflow modeling. The image below shows the CFD model of the building located in the larger domain.

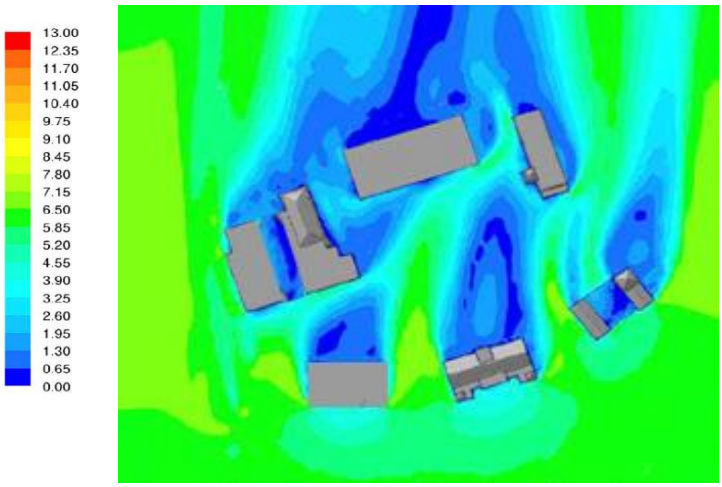

Figure 7.5 Wind distribution around the office at ground level (yellow: high wind speed, green: moderate wind speed, and blue: low wind speed). The date of the simulation is May 1st

The surrounding buildings can either block or enhance wind speed around the site. The computational domain for the building and its surroundings is shown in the Figure 7.5. The domain length is about five times that of site length in four horizontal directions. The wind distributions around the building were calculated for all directions with a typical wind speed for each one. The grid number was too coarse so wind information was not sufficiently detailed. Nevertheless, the results converged with a mass residual no higher than one percent.

In assessing wind effects on buildings, it is important to consider the characteristic wind nature and the speed with height variability. The second approach to include the urban context effect on airflow path is to solve the equation for specific airflow terrain. Vertical profiles of mean wind speed for boundary layers are approximated by assuming the speed to be proportional to the height raised to some power – a power-law variation (Davenport, 1965). The simple expression used extensively has the following form:

$$V_h = \mathrm{a} V_{\mathrm{met}} h^{\mathrm{b}}. \qquad (7.1)$$

Wind speed from the meteorological data corresponds to the speed at 10 m height in open country. Since the building is located in an urban environment, the appropriate wind profile was assumed to be (a=0.35 and b=0.25 are the constants which depends on the terrain in the vicinity of the buildings),

$$V_h = 0.35 V_{\mathrm{met}} h^{0.25}.$$

Where V_h is the local wind speed at height, h, and V_{met} are the meteorological wind speed. Based on this formula, wind has been calculated by Fluent for the specific times that the CFD analysis was performed.

7.2.3 Wind pressure assessment

The wind-pressure distribution around a building depends very closely upon the local variation in wind velocity that the building produces. In accordance with the elementary pressure-velocity relationship, the pressure distribution is represented by a dimensionless pressure coefficient C_p:

$$P_w = C_p \frac{\rho U_r^2}{2}. \qquad (7.2)$$

Where,

P_w= wind pressure, Pa

ρ = air density, $^{kg}/_{m^3}$

V_r = wind speed at specified height, $^{m}/_{s}$.

These formulas have been used to calculate the boundary conditions for the inlet pressure in Fluent. This pressure plus static pressure is the total inlet pressure. There are default C_p values provided in the airflow network-model simulation tools. These are based on the Air Infiltration and Ventilation Centre's (AIVC) Guide to Energy Efficient Ventilation (Liddament, 1996), which consists of a number of wind tunnel tests for generic, low-rise buildings. Typically, these $C_p$values only apply as acceptable initial approximations for buildings that are close to rectangularly shaped. The other approach to calculate more accurate pressure coefficients is to analyze the external CFD analysis to provide the air velocity distributions and pressure around the building due to wind effect. For simplicity, this investigation used an external CFD to calculate the pressure difference as the boundary conditions for indoor airflow simulation. Wind profiles one cell away from the building was recorded as inputs for the cavity model. These are shown graphically in Figure 7.6, and values for x, y, z, and net velocities one cell away from the building at the chimney entrance. These velocities are used as boundary conditions for a cavity

model, allowing for the analysis of cavities at any height. The results shown are for reference velocities of 5 m/s and 10 m/s at 10 m above ground.

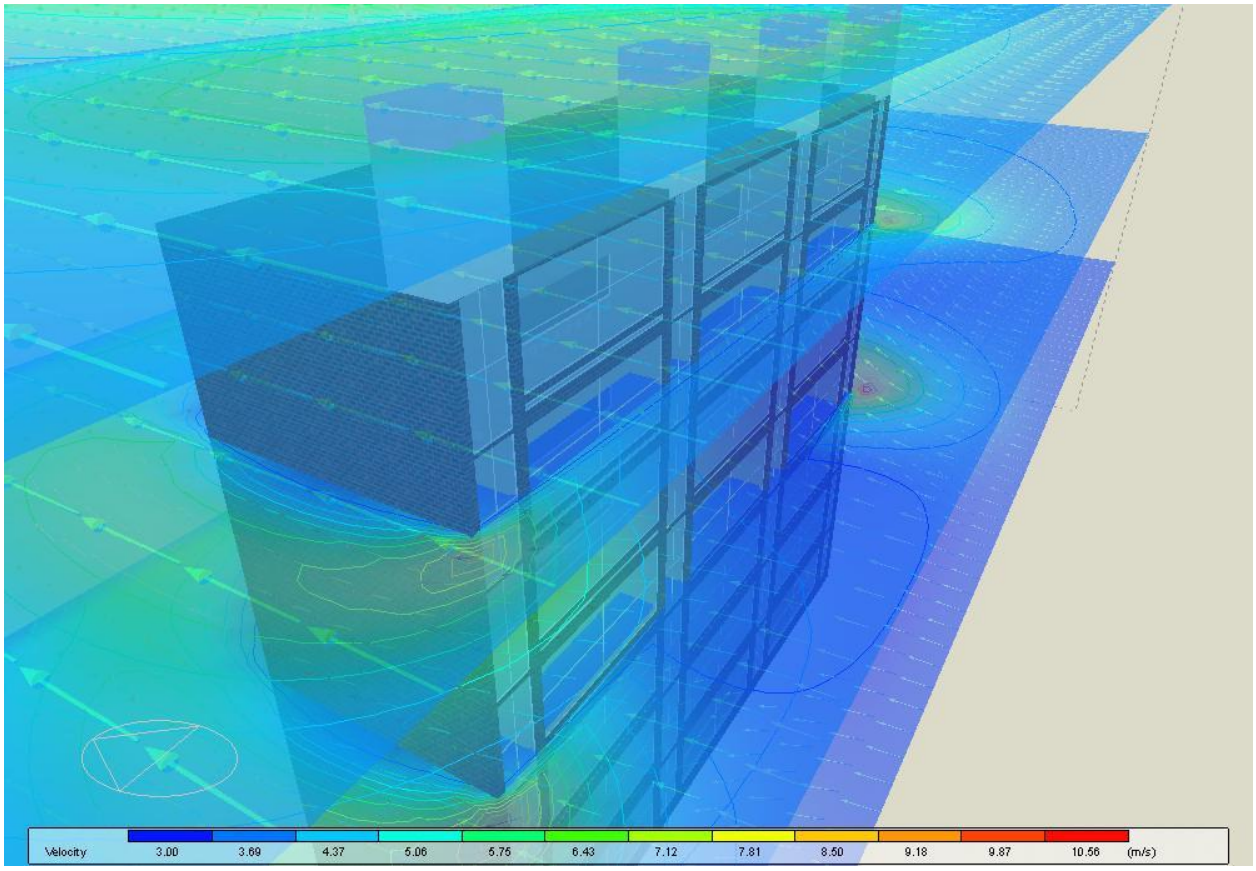

Figure 7.6 Velocity distribution around the building the prevailing wind, south at 5m/s

7.3 The geometry of the CFD model

The first stage of the internal CFD modeling is to construct a seven-story office module with geometrical dimensions of 27x7 m, with 3.5 m ceiling height and 1.5 m cavity corridor in front of the offices in the Gambit. The simplified single skin facade of the model has openings on panes with 6mm thick glass. The DSF construction has one opening (inlet) at the outer pane and two openings (air inlet and exhaust) at the inner pane. The model is constructed in 3-D in Gambit as shown in the Figures 7.7, 7.8 and 7.9.

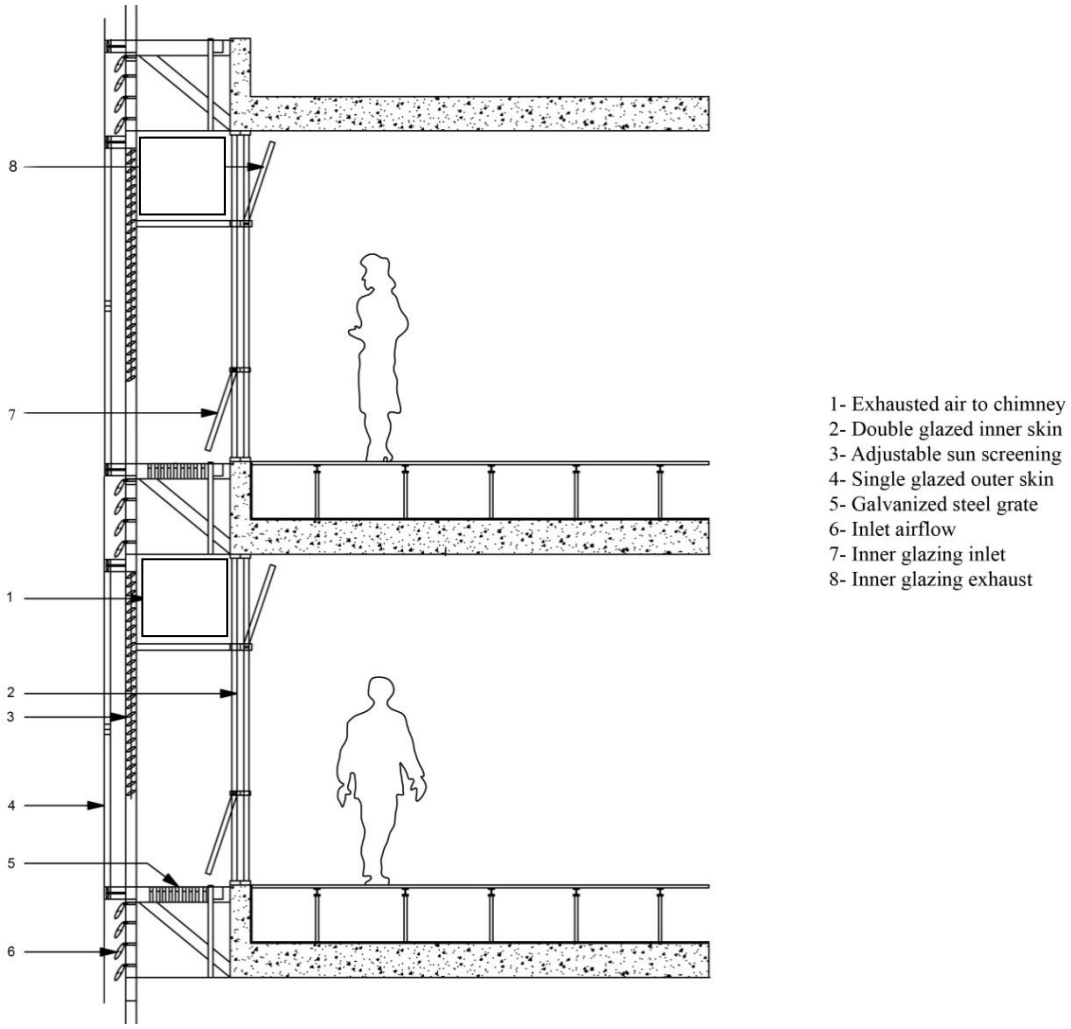

Figure 7.7 Vertical cross section of the combined shaft-corridor DSF

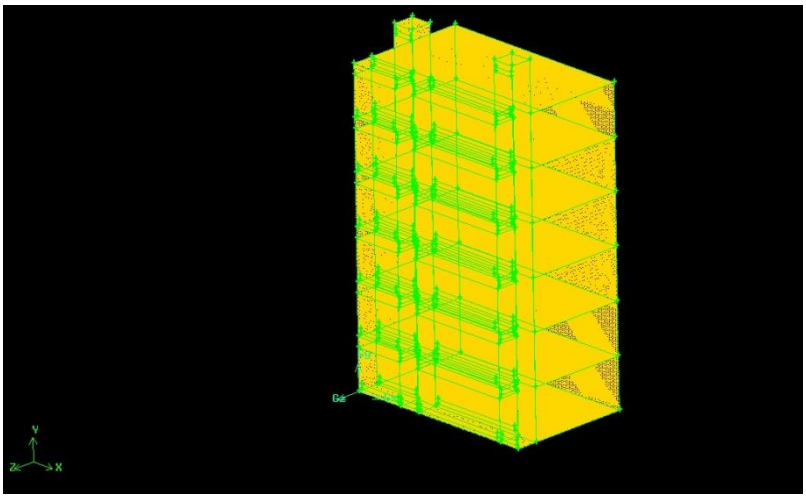

Figure 7.8 Three-dimensional grid model of the seven-story building with combined shaft-corridor DSF configuration shown the gambit output

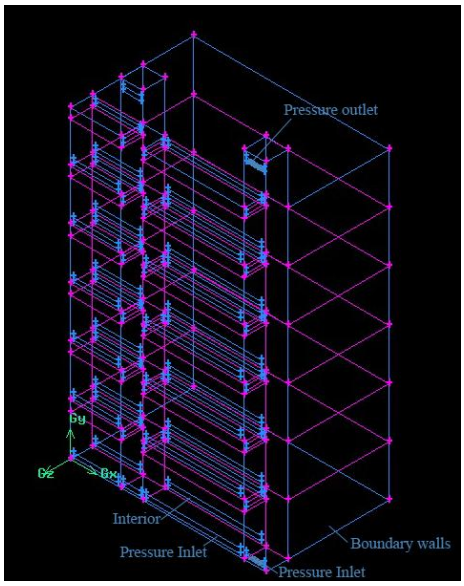

Figure 7.9 Model boundary settings

7.3.1 Model construction materials and components

The external walls of the office consisted of concrete with a density of 2,130 kg/m^3 and thermal conductivity of 0.7 W/m-K. The outer pane of the DSF consists of single pane 6 mm clear glass, and the inner pane, as described in Chapter 6, is a double pane low-E glazing. Simulations are performed under steady state conditions using the k-epsilon turbulent model. Simulated wind speeds are used to model expected wind velocities at the levels under study with corresponding ambient and radiant temperatures shown later in this chapter. For this study, only wind direction which is perpendicular to the DSF has been considered.

7.3.2 CFD model boundary conditions

This study is going to model levels from the sixteenth to the twenty-third stories of a high-rise building. In the new configuration, the DSF has a ventilated shaft, which is 1.5x1.5 m with two openings on the lower and high chimney levels. This study introduces a shaft to improve the

possibility of natural-ventilation stack effect to extract heat from the offices and improve airflow rates required to reach thermal comfort level within the interior.

The results of Fluent model of this seven story block looked at the velocity profile, airflow patterns, temperature within the double skin, and the internal office space. To calculate thermal comfort, the boundary conditions for wind velocity, external temperature and relative humidity were set to the ranges similar to Chicago climatic conditions and the inputs and assumptions are presented in the Table 7.1.

Domain	
Domain material	Air at 20°C, 1 atm
Reference pressure	100,000 Pa (atmospheric pressure)
Reference temperature	295 K
Sources	
Buoyancy model	Boussinesq-calculates airflow from temperature difference rather than density difference.
Buoyancy reference temperature	Outdoor air temperature.
Gravitational acceleration	-9.81 m/s in the y-direction.
Boundary Conditions	
Side, top, bottom, & front domain boundary conditions	Openings with "deduced" air velocities, external temperature = outdoor air temperature at inflow only, external pressure at atmospheric pressure.
Back boundary conditions	Adiabatic solids (concrete) with depth = cavity Depth, glass: standard 6 mm clear glass.
Heat source(external glass)	11.43 W/m^2
Heat source(internal glass)	7.93 W/m^2
Walls heat	25 W/m^2
Velocity inlet	5 m/s
Cavity Details	
Cavity size	3.5 m high by 7 m wide by 1.5 deep.
Cavity external facade	Internal plate with surface temperatures on both sides is calculated based on heat source.

Table (cont.)

Cavity internal facade	External plate with surface temperature base on heat source.
Shaft and opening details	
Shaft size	1.5 m deep,1.5 long, 24.5 m high
DSF opening size for inner pane, air gap size (inlet and exhaust).	300 mm

Table 7.1 Model assumptions and inputs required by Fluent

7.4 Fluent simulation results demonstration

For the analysis of airflow and temperature in DSF and adjacent space, the base case with the combined shaft-corridor DSF has been generated and airflow patterns and temperature profile within the DSF has been illustrated for specific times of the year. Based on those data, the level of thermal comfort within the space will be predicted. To study thermal comfort, the specific internal space temperature and velocity at a particular height has been derived from the Fluent analysis. The chimney opening size and inlets and outlets are 0.3 m; the chimney size is 1.5 m.

7.4.1 Cavity and room air temperature

The location of the chimney openings in this shaft-corridor type in relation to the chimney exhaust will have an effect on the indoor thermal comfort and airflow velocity. It is a fact that the higher the exhaust opening is located from the inlet, the stronger the stack effect will be within the air gap. This effect will then pull more air from office spaces to circulate throughout the building. The other factor that impacts on air velocity are inlet and outlet sizes. Due to the venturi effect, the smaller the size, the more the velocity. Figure 7.10 illustrates the room's temperature gradient, which is clearly lower than the outside temperature of 20 ˚C. There is some temperature variation as the cavity is ventilated. The room air temperature increases towards the top as shown in Figure 7.10.

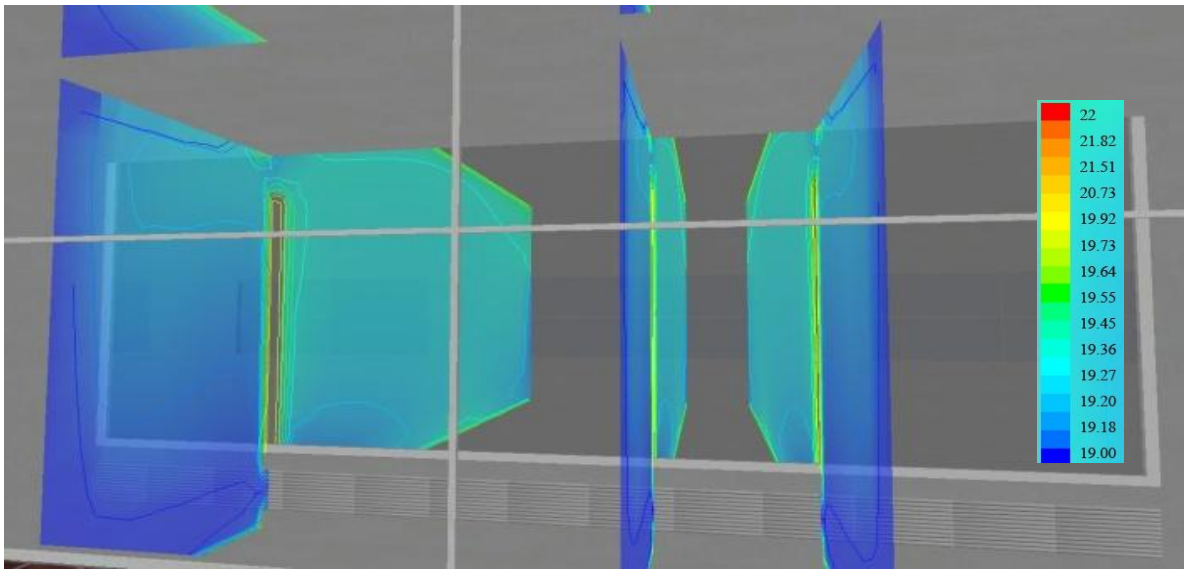

Figure 7.10 As displayed in Fluent analysis of room temperature profile

Figure 7.11 clearly illustrates an increase in the gradient temperature from the inlet to the outlet where higher-surface temperatures were reached due to accumulated heat and buoyancy effect.

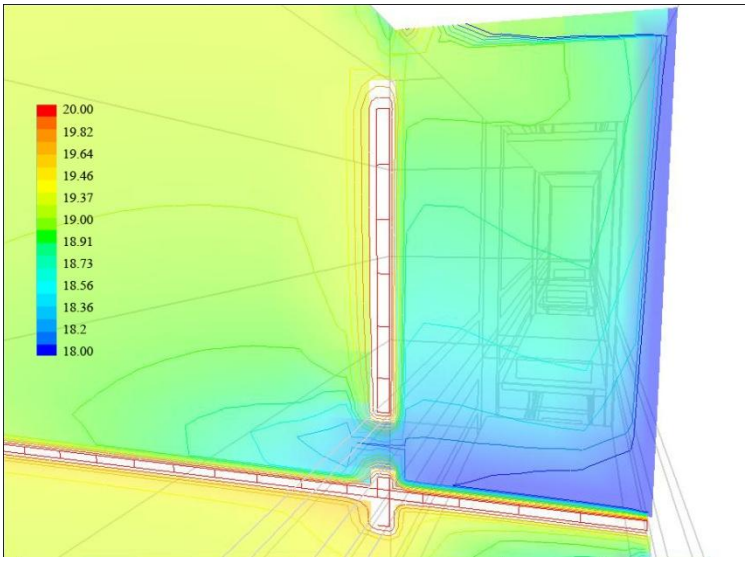

Figure 7.11 Cavity temperature gradient

As illustrated in Figures 7.10 and 7.11, the interior air temperature is slightly higher than the exterior in the half of the room closer to the cavity and also in the half upper part. The

temperature goes from 19 °C at the bottom opening to about 19.9 °C at the top opening. Figure 7.12 illustrates the temperature stratification from lowest on the floor to highest close to the ceiling.

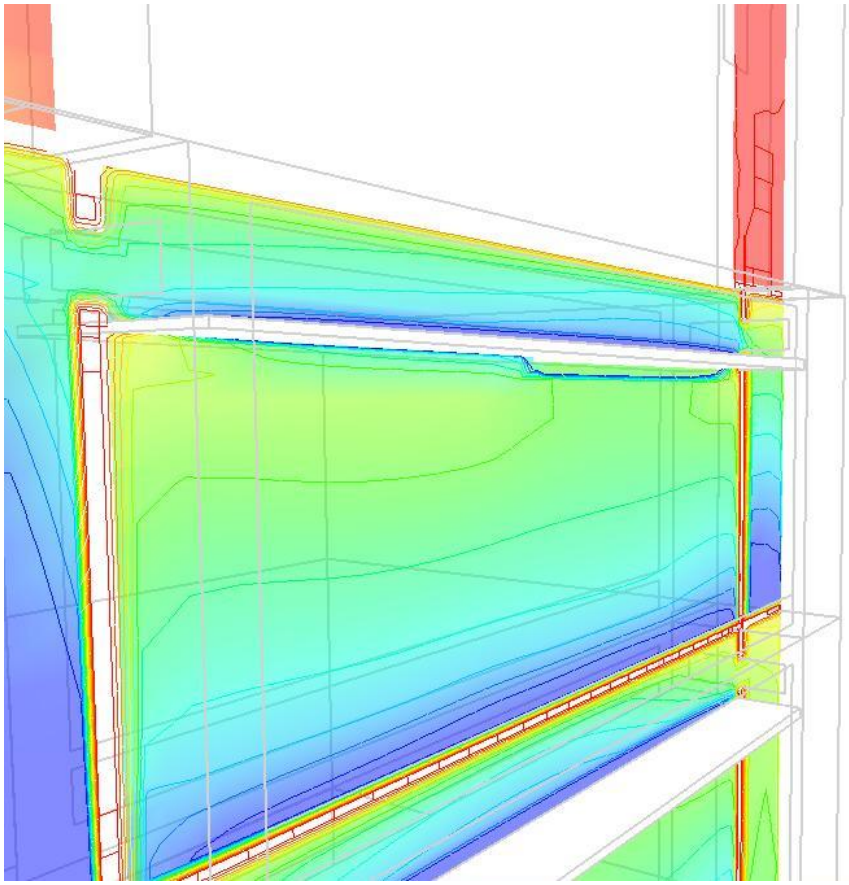

Figure 7.12 Cavity temperature profile-output from Fluent

Figure 7.12 also shows the cavity air temperature near the interior glazing. The temperature goes from 18 °C at the bottom opening to about 19.5 °C at the top opening. The stack air temperature increases towards the top of the chimney in a fairly linear progression, as shown by gradients in Figure 7.13. Figures 7.10,7.11,7.12,and 7.13 depict the cavity model with 20° C outdoor air temperature and 480 watts/m^2 incident solar energy obtained from the weather data. Figure 7.12 shows the interior air temperature is slightly higher than the lower half of the chimney air in average 1°C per floor.

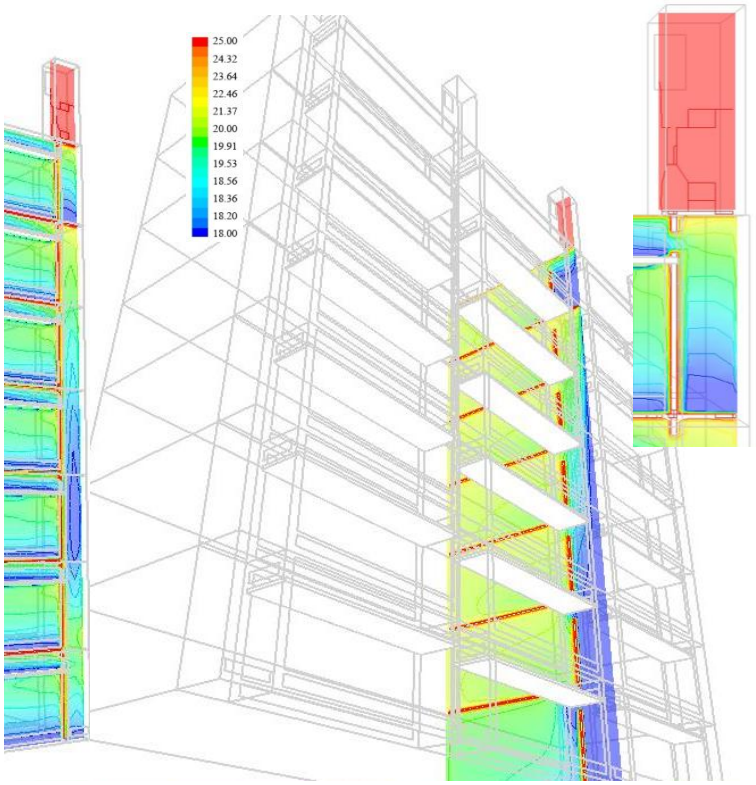

Figure 7.13 Chimney air temperature profile

Figure 7.14 shows a horizontal temperature profile at the level of 1 m from the floor (this is the height of the body mass of a seated person). The air temperature varies in this direction from about 20 ˚C near the glazing to about 19.3 ˚C in the center, and 18.5 ˚C in the back of the room. The air reaches the higher temperature near the middle of the room, the point at which air velocity is lowest. This Figure also illustrates how the concentration of heat is accumulated mostly towards the center of the space.

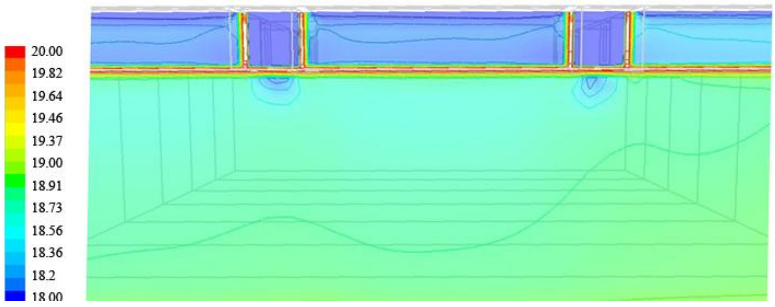

Figure 7.14 The horizontal temperature profile of the room

A temperature contour study has shown that the office space's lower floors have lower internal temperatures compared to the higher floors. As we increase the shaft height, the upper floors would be hottest and probably uncomfortable for occupants during the summer month. It is interesting to discover that the office's mid-portion floor areas for all the floors are having higher temperatures when compared to the floor area of the front part. This could be due to the airflow pattern shown in the next section.

7.4.2 Airflow

The air velocity through the cavity is due to buoyancy and wind forces, and it is quite high. Figure 7.15 shows the building's air velocity model. The velocity in this model ranges from 7 m/s inlet to 2.3 m/s outlet of the chimney. The inflow from the external screen is 1 m/s and the internal screen inflow velocity is 0.45 m/s, while the exhaust airflow is 0.46 m/s on average. The exhaust air velocity to the chimney averages 1.3 m/s. The greatest velocity is near the inlet to the chimney and exhaust from the stack. As shown in the Figure below, the velocities are increased relative to the one-story high cavity.

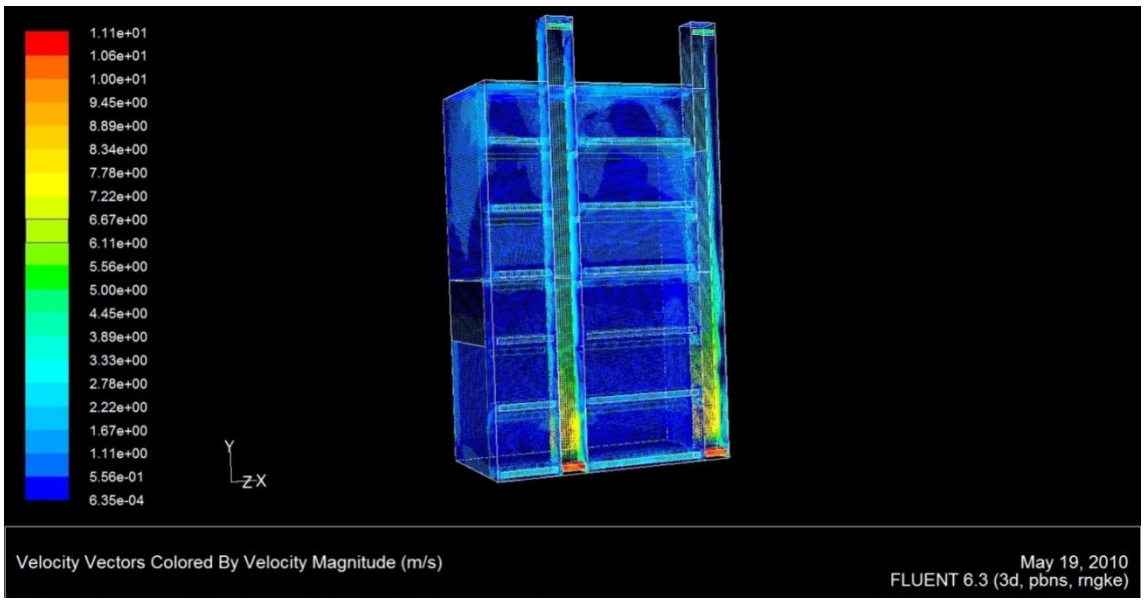

Figure 7.15 Model of air velocity vector in the building

Figure 7.16 shows the section of airflow at the opening of one story horizontally. Velocities are greatest near the opening, when the air is forced through the smaller area. In the back of the room, air velocities are high as they move toward the exhaust to get out from the stack. As illustrated in the Figure 7.15, air velocity in the chimney is higher close to the back wall of the chimney, and it is generally laminar when driven only by buoyancy without wind effects.

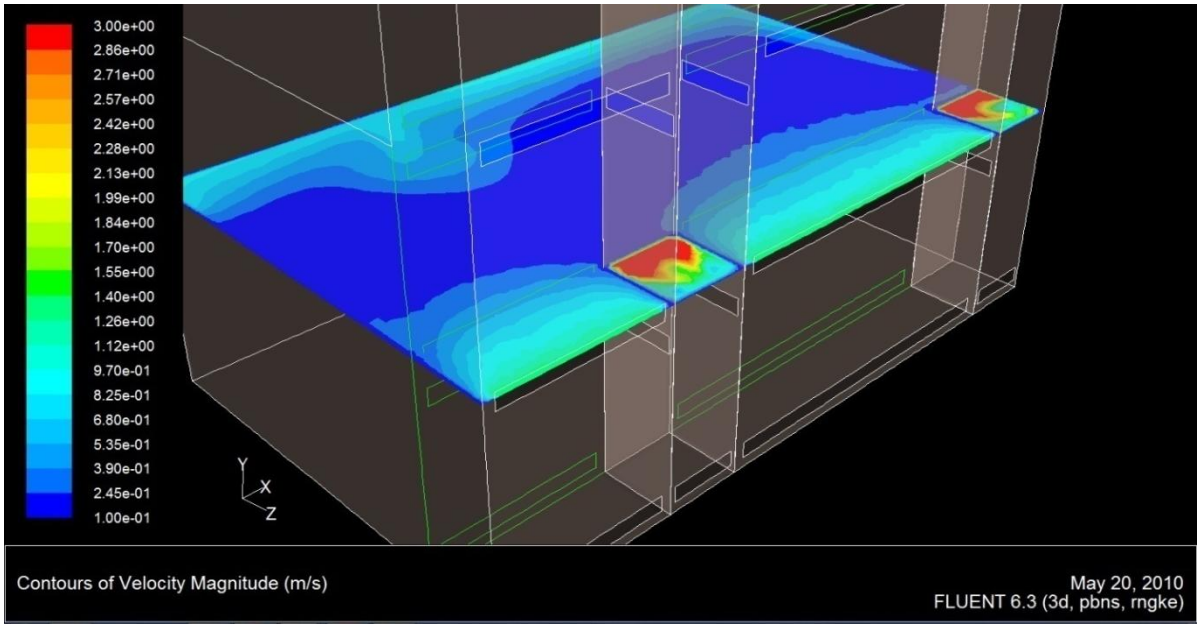

Figure 7.16 Horizontal velocity profiles

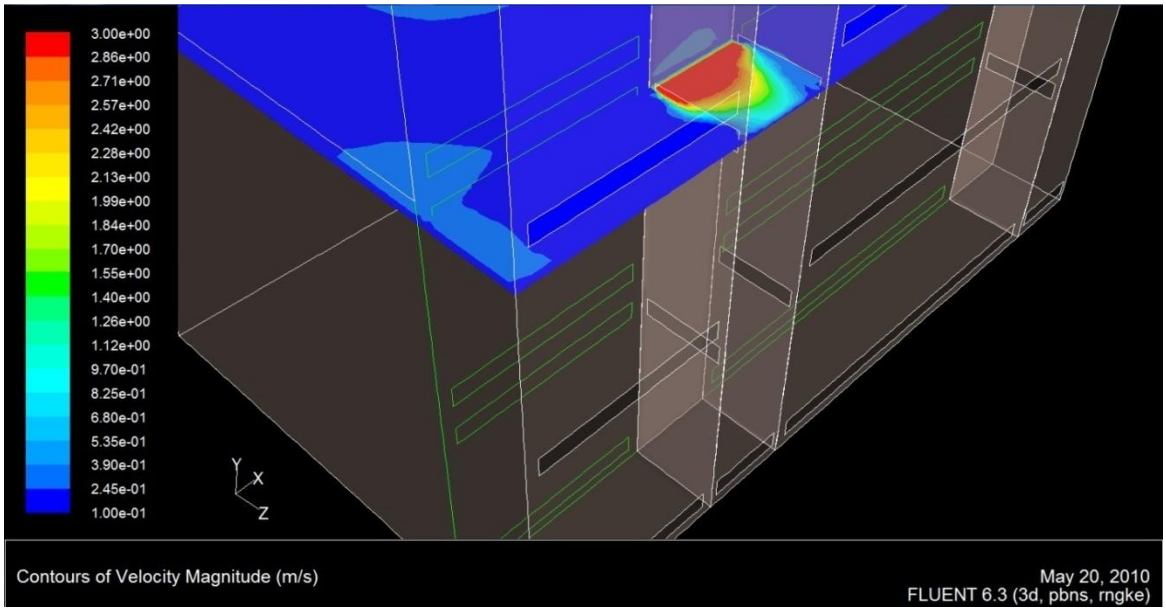

Figure 7.17 Horizontal velocity gradient

Figure 7.17 shows the horizontal velocity profile in the cavity and chimney. The velocity ranges from 0.46 m/s away from the surface and 0.97m/s near the opening. The variation from the greatest to the least velocity magnitude are in the range of perception (0.1-1m/s) based on the ASHRAE standard (2004).

The greatest velocities are near the cavity openings where the wind impacts the airflow rate.

Figure 7.18 shows velocity vectors at the openings of the chimney cavity model as analyzed in Figure 7-1. Velocities are greatest near the openings, when air is forced through the smaller area. In this model, the maximum velocity at the inlet is about 11 m/s. Other than at the openings, airflow through the chimney well is around 5 m/s and is driven by both wind and stack effect.

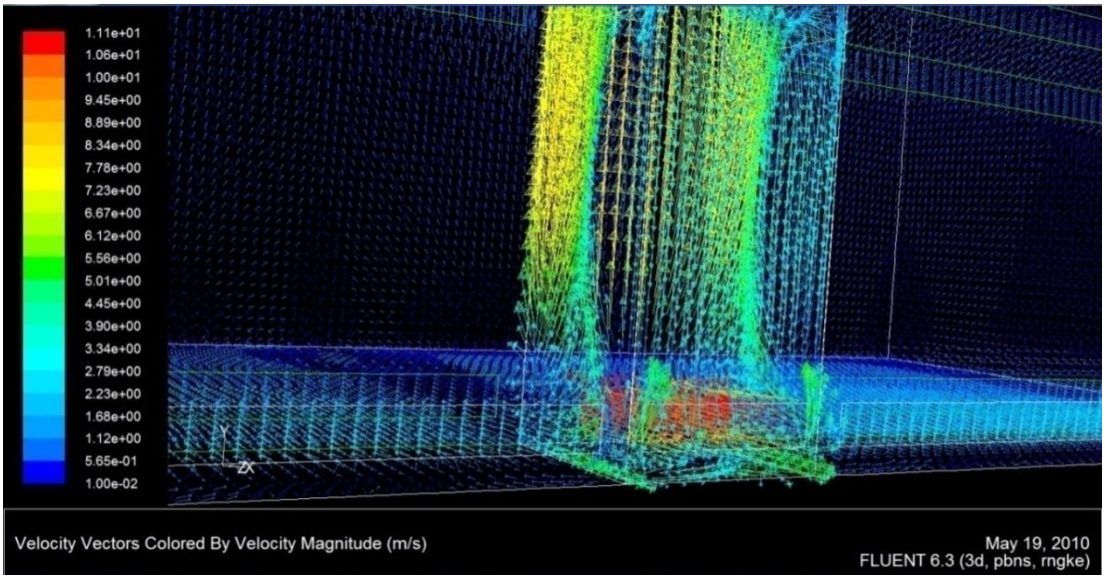

Figure 7.18 Model of air velocity close to the inlet opening

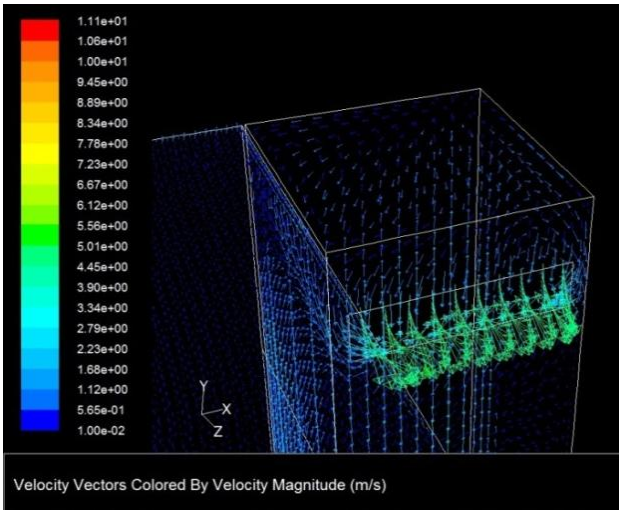

Figure 7.19 Airflow patterns and velocity at the chimney's outlet opening

A small turbulent flow forms at the stack inlet and outlet, and stack airflow is generally laminar when it is only driven by buoyancy.

Figure 7.20 shows a vertical profile of air velocity vectors to the stack from the cavity. The velocity is quite high and it extracts hot stuffy air from offices to the stack and outdoors. The airflow is likely to be more effective in extracting heat when the wind velocity is high and the temperature gradient occurs in the shaft increase the buoyancy effect.

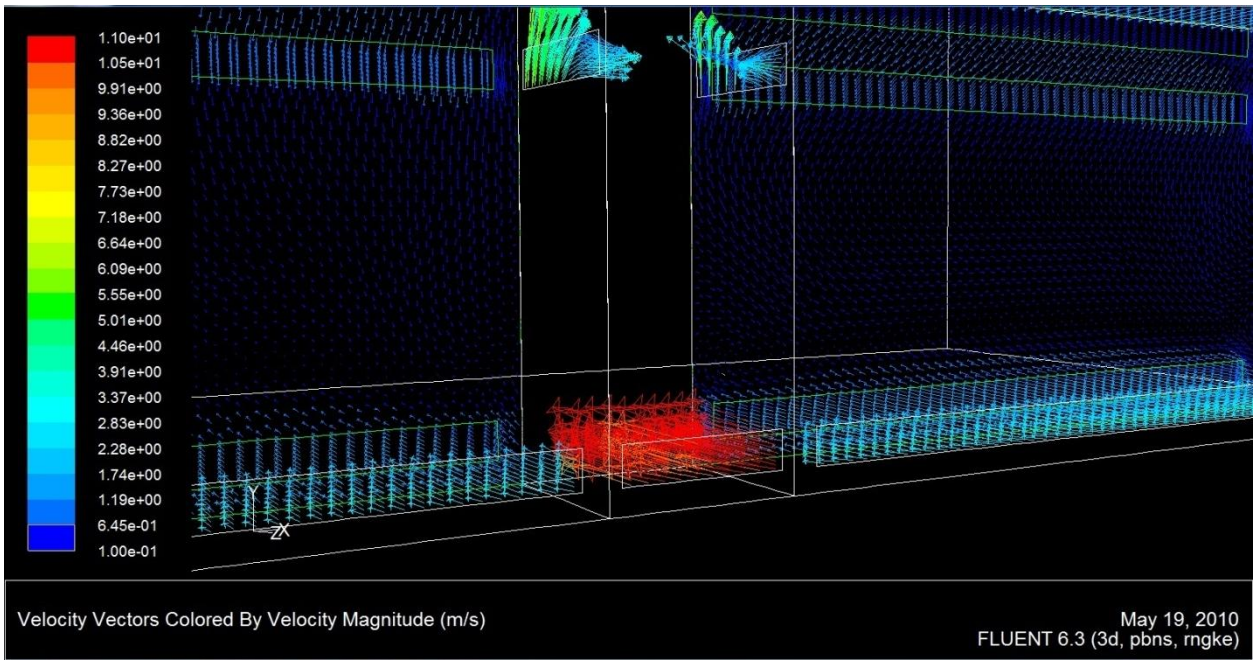

Figure 7.20 Air velocity vectors in the cavity and chimney

Figure 7.20 shows how air comes inside the chimney, which is then extracted from the offices through the chimney opening.

Figure 7.21 shows the section of air-flow path inside the cavity and shafts and how air from the office outlet is directed outside. The air is basically induced to flow upwards by a buoyancy effect created by the accumulated heat. Figure 7.21 illustrates how the flow reaches higher velocities within the inlet and outlet where pressures are higher. As depicted, flow tends to be turbulent near the glazed surfaces and openings where forces are higher. The airflow inside the cavity is much higher than what is measured by typical examples in the literature.

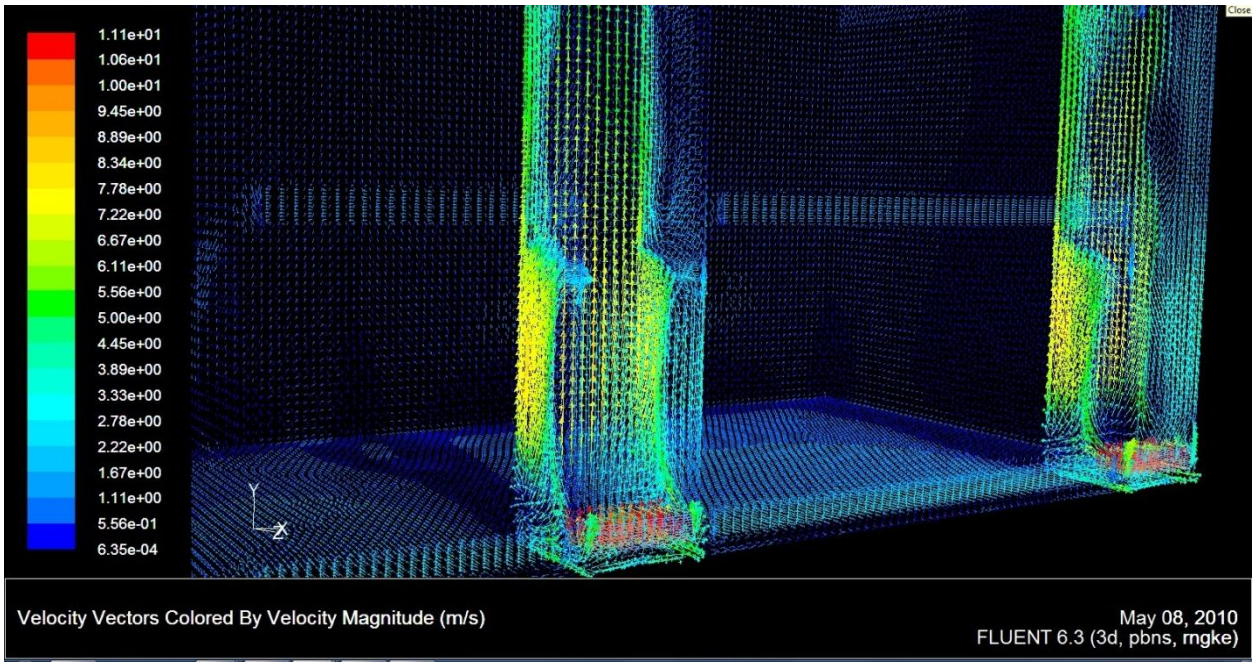

Figure 7.21 Velocity vectors in the chimney and cavity

The airflow inside the room is illustrated in Figure 7.22. The Figure shows an air-movement trend from laminar close to the wall boundaries to turbulent in the room's center. The airflow inside the rooms is less than 1 m/s and more than 0.1 m/s.

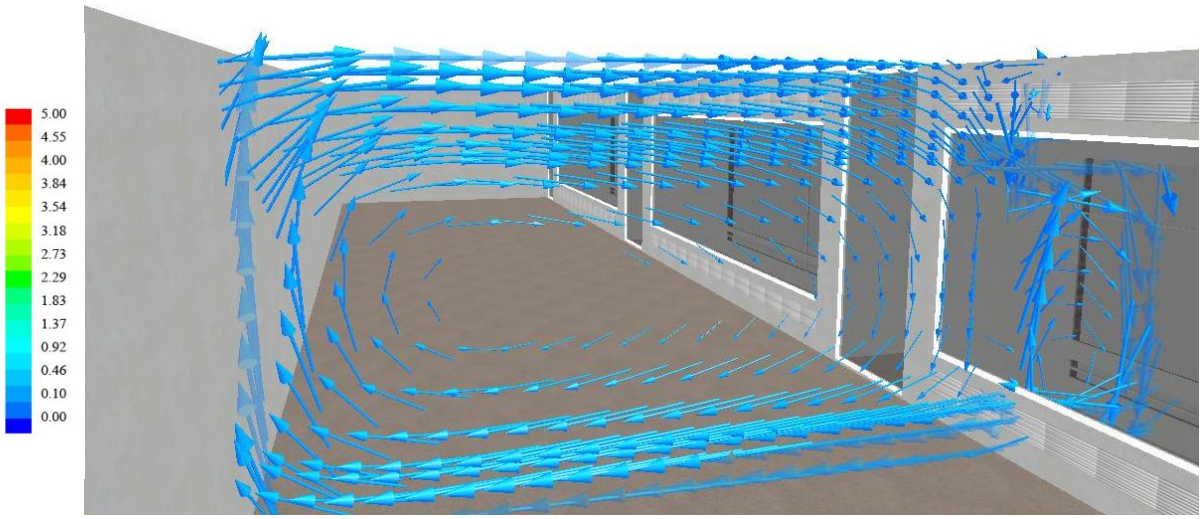

Figure 7.22 Velocity vectors in the room

7.5 Analysis of the model solved by Fluent

k-e RNG Turbulence Model					
	Run Details			Model Results	
Model	Grid number	Run time	iterations	ΔT cavity inlet and exhaust	Airflow rate($\frac{m^3}{hr}$)
	5,000,000	72 hours	1000	13.2	102.5

Table 7.2 The Fluent model information

Simulation	Floor Level	Temp. C	Air Velocity	Radiant Temp	RH %	PMV	OT
May	3	20	0.28	22.53	40.7	0.18	20.22
	5	22.4	0.16	22.93	47.3	0.29	20.3
	7	24.8	0.11	23.64	45.59	0.37	20.56
June	3	23.7	0.20	27	51.1	0.5	20
	5	24	0.19	27.50	50.68	0.66	21.30
	7	24.6	0.15	28.19	56.60	0.76	21.09
Sep	3	23.4	0.27	26.3	50.3	0.4	24
	5	23.7	0.20	26.25	57.40	0.54	25.38
	7	24.2	0.13	26.98	56.35	0.71	25.20
Oct	3	22	0.27	23.3	36.4	-0.32	22
	5	22.3	0.20	23.4	42.4	0.11	22.80
	7	22.8	0.19	24.6	45.4	0.23	22.04

Table 7.3 Calculated air velocity in the office room: 0.5 meter from the windows and 1 meter from the floor.

7.6 CFD result findings and analysis of the combined shaft-corridor DSF

The results for a south-facing, combined shaft-corridor DSF with external wind velocity of 5 m/s and 50 percent air humidity, respectively, are tabulated in Tables 7.1. Results for the combined shaft-corridor DSF type as shown in Figure 7.23 indicate that the DSF air gap size of 0.3m gives a comfortable result for these particular conditions in a natural ventilated space.

The office space's lower floors would generate the lowest operative temperature due to the stack effect provided by the DSF configuration. This has enhanced the natural ventilation strategy to provide better internal thermal comfort condition.

There is an internal temperature difference of 1 ˚C for the DSF mid-floor, which could be due to slower internal air velocity generated. The south-facing DSF configuration produced an 82 percent acceptability limit for the 0.3 m opening for external temperature 20℃, according to the Thermal Environmental Conditions for Human Occupancy from ANSI/ASHRAE Standard 55-2004.

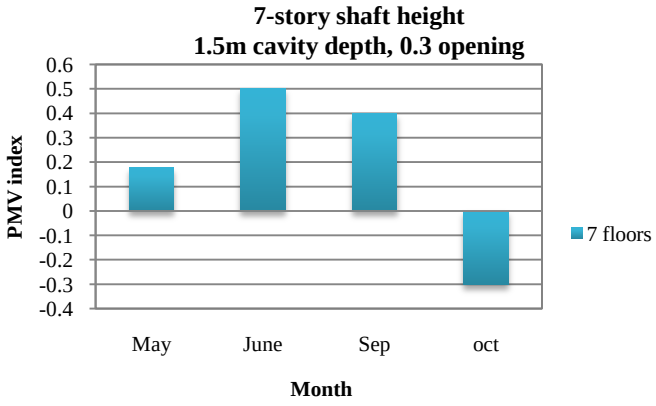

Figure 7.23 Average PMV index first floor months under study

Figure 7.24 shows the distribution of PMV values calculated by DesignBuilder for the combined shaft-corridor naturally ventilated DSF office spaces with values within 80 percent acceptable limits. This distribution is for the third floor in May. For air velocity lower than 1m/s and a temperature difference between radiant and ambient of lower than 4°K, the operative temperature (T_{op}) would need to be adjusted according to the formula T_{op}=AT_a + (1-A) T_r, where T_r is the ambient air temperature and T_r is the radiant temperature.

V	<0.2m/s	0.2-0.6m/s	0.6-1m/s
A	0.5	0.6	0.7

Table 7.4 Calculated air velocity in the office room: 0.5 meter from the windows and 1 meter from the floor.

Air movements determine convective heat and mass exchange of the human body with the surrounding air. In the Chicago climate, high air velocities will increase the evaporation rate at the skin surface, which results in a cooling sensation. The recommended upper limit of indoor air movement is usually 0.8 m/s for human comfort; such air velocity permits the interior space to be 1-2 degrees higher than the human comfort temperature to maintain desirable a comfort level (Hien et al, 2005).

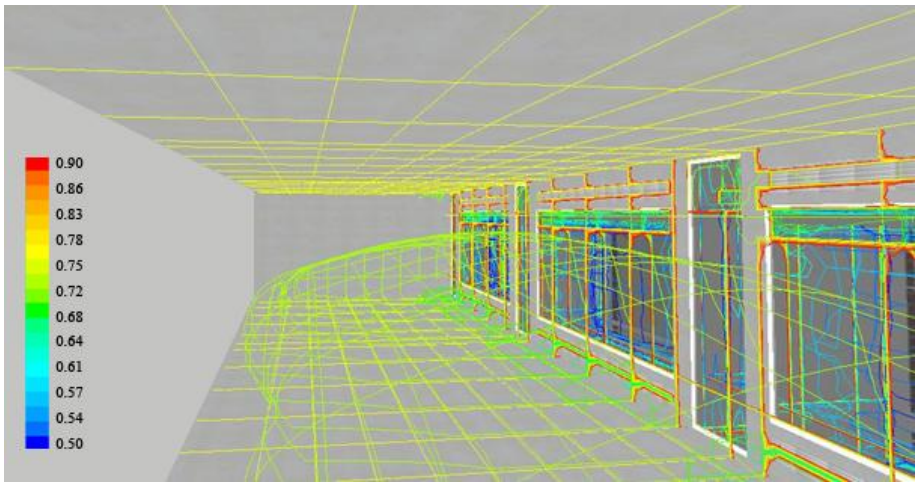

Figure 7.24 Average PMV as calculated in the room

It was found that the combined shaft-corridor DSF will generate a strong stack effect within the air gap, which, in turn, will pull more air out from the office space through rear-wall vents. The temperature generated within the office space is then desirable and close to the human comfort requirement. The airflow pattern created will have a good ventilation effect with cool air coming from the vents, and across and above the internal space, and discharge through the inner pane high level opening.

7.7 Conclusion

The first stage of simulation of the combined shaft-corridor DSF was carried out on seven story stack high to investigate the thermal behavior of this new design facade and evaluate the

processes involved in thermal comfort. This will become the base case for parametric studies in chapter 8. Fluent was used to simulate turbulent airflow.

In order to verify the results, the precise approach of the CFD model depends on the the boundary conditions-settings accuracy. Simulation of fluid dynamics based on natural convection with air velocities requires extensive calculation time to get desired converged residuals.

A process was also described to use pre-determined wind pressure values at the cavity's openings to model a DSF cavity in a CFD model. This method reduces computation time that would be needed to analyze wind effects along with buoyancy forces. CFD models were used to determine velocities at various points on the reference building for wind velocity of 5 m/s based on the weather data. These values can be implemented in models using the process described earlier in this chapter.

Based on airflow modeling of the combined shaft-corridor DSF, it was found that the stack encourages buoyancy and induces air movement. Convective forces inside the cavity could be used to promote air extraction from the room, although it is needed to promote air movement within the room to release the excess heat.

The CFD results appear to confirm the design's effectiveness in two ways. First, the airflow follows the ceiling and exits through the chimney openings, which suggests that the cool night air will effectively draw the heat out of the ceiling slab. The second outcome of the airflow staying near the ceiling is the avoidance of high air velocities in the occupied zone during the day. The main driving forces in the cavity are buoyancy and wind pressure. The pressure differences resulting from these forces can be determined with the following equations:

$$\Delta p_{bouyancy} = \rho_{\circ} * g * H(\frac{T_{cav}}{T_e} - 1)$$

where ρo is outdoor air density in kg/m^3, g is gravitational acceleration (9.8 m/s^2), H is the cavity height in meters, *Tcav* is the average cavity temperature, and *Te* is the outdoor air temperature in Kelvin. Thus,

$$\Delta p_{wind} = \frac{\rho_\circ \, U_{met}{}^2}{h_{met}} \left(\frac{\partial_{met}}{h_{met}}\right)^{2a_{met}} \left(h^{2a} - (h+H)^{2a}\right) \quad \text{(Pa)}$$

Where *Umet* is measured wind speed at height *hmet*, *δmet* is the wind boundary-layer thickness, *a* is the ASHRAE local terrain exponent, *h* is the height of the lower cavity opening, and *H* is the distance between inlet and outlet openings. The airflow rate through the cavity can then be determined with:

$V = a\Delta pb$ (m^3/hr),

where *a* and *b* are pressure loss characteristics of the cavity and openings.

This chapter has shown that the combined shaft-corridor DSF has a possibility of providing acceptable internal thermal comfort through natural ventilation strategy in a hot summer continental climate. These results answered the first question posed in the introduction of this chapter. The next chapter explores the parameters that can optimize the thermal condition and energy performance of this new configuration for shoulder season.

Chapter 8.0

Parametric Optimization Studies of the Combined Shaft-corridor DSF

8.1 Introduction

The energy analysis of the new DSF combined shaft-corridor configuration presented in the previous chapters revealed that the new system is viable in terms of providing acceptable internal thermal comfort through natural ventilation while also improving energy consumption. The analysis was confined to a combined shaft-corridor DSF-system design that could provide the significant extraction force required to ventilate the office spaces through combined wind and buoyancy effects. In this chapter the results of systematically varying the base case are presented to further investigate possibilities to improve the office airflow by modifying the new DSF configuration system. The strategies include:

a) Modifying the ventilated stack by varying openings of the DSF system. Investigating different sizes for openings and their effects on internal thermal comfort for office spaces and energy performance. It should be noted that opening sizes are the same for the inlet, exhaust, and chimney openings.

b) Varying the shaft height by extending the stack through a different number of stories to see the effect on ventilation rates within internal office spaces.

c) Investigating the effect of cavity depth on airflow velocity.

e) Last, but not least, comparing the best performing alternatives in terms of energy and comfort.

8.2 Parameters examined

The modeling process described in Chapter 7 was used to analyze the performance of a number of DSF cavity geometries with a range of variables. The main goals were to determine general airflow and temperature profiles by varying the cavity geometry. In this analysis, the driving forces for airflow are buoyancy and wind pressure based on the weather data in each of the models. This allows for correlations to be developed for different parameters and can be used in an annual DesignBuilder energy simulation.

Variables analyzed include:

- Cavity Depth: 0.5 m, 0.9 m, 1.2 m and 1.5 m
- Shaft height: 5 to 9 stories (3.5 m each story)
- Opening Size: 0.3, 0.6 and 0.9m.

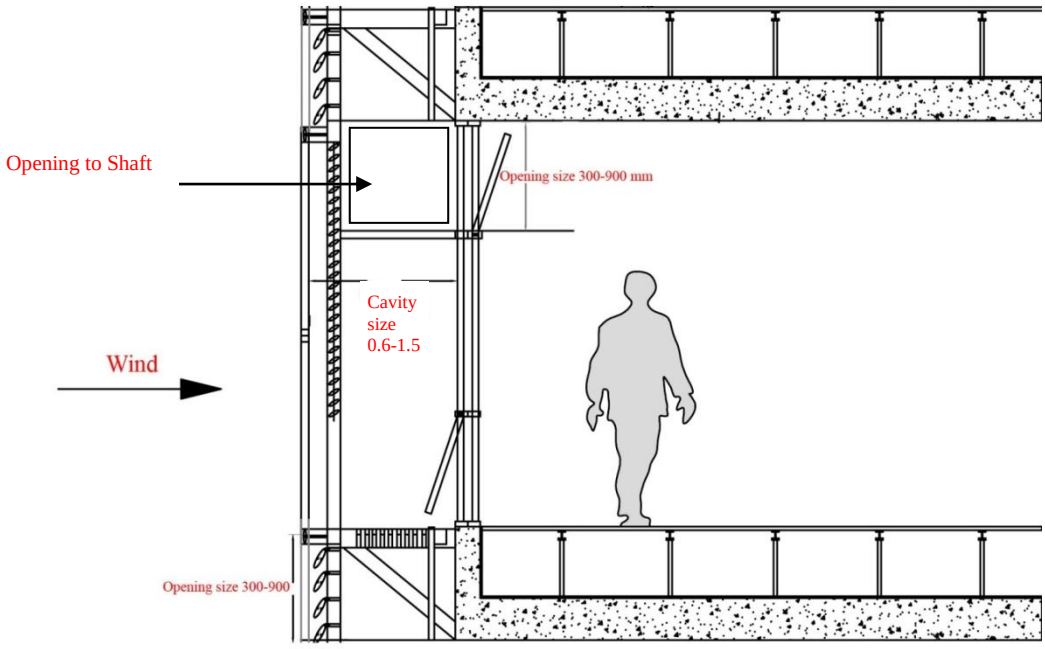

Figure 8.1 Parametric variables used in CFD.

Thirty-six different gambit models were developed to analyze the cavity geometry variables. Each of the models was run in Fluent under a number of different environmental conditions to determine trends in the cavity's airflow and temperature performance as described in the previous chapter. All of the models are summarized in Table 8-1. Data from all of the runs are included in Appendix D.

8.3 Parametric runs: Simulation results

Results from each of the thirty six fluent analyses provide values of indoor conditions for air temperature, air velocity, and relative humidity were investigated at 1.2 m above floor level and at the office space's center. Table 8.1 shows all alternatives taken from the simulations with constant input conditions included an external temperature of 20 $° C$, wind velocity of 5 m/s and relative humidity of 52%.

			Opening size		
Cavity	Height	Parameters	0.3	0.6	0.9
1.5 m cavity	7-story	Radiant Temp.	23.99	23.74	23.07
		Velocity	0.3	0.3	0.35
		RH	57.6	52.1	59.9
		PMV	0.18	0.15	0.05
	9-story	Radiant Temp.	23.94	23.75	23.07
		Velocity	0.4	0.45	0.54
		RH	57.6	59.73	52.31
		PMV	0.18	0.15	0.11
	5- story	Radiant Temp.	23.55	23.76	23.76

Table cont.

		Velocity	0.25	0.12	0.35
		RH	57.39	52.99	52.53
		PMV	0.18	0.15	0.15
1.2 m cavity	7- story	Temperature	23.50	23.96	22.98
		Velocity	0.35	0.44	65
		RH	52.46	57.39	52.99
		PMV	0.11	0.14	0.06
	9- story	Temperature	23.45	23.92	22.94
		Velocity	0.2	0.33	0.35
		RH	52	52.46	58.78
		PMV	0.1	0.1	0.02
	5- story	Temperature	23.55	24	22.95
		Velocity	0.45	0.47	0.57
		RH	52.14	57.39	52.99
		PMV	0.11	0.19	0.03
0.9 m cavity	7- story	Temperature	23.63	23.72	23.73
		Velocity	0.25	0.45	0.55
		RH	52.46	48.78	53.14
		PMV	0.12	0.14	0.06
	9- story	Temperature	23.95	23.74	23.14
		Velocity	0.45	0.6	0.55
		RH	52.46	48.78	53.14
		PMV	0.18	0.3	0.4

Table cont.

	5- story	Temperature	23.81	23.74	23.2
		Velocity	0.35	0.45	0.48
		RH	54.15	54.17	55
		PMV	0.15	0.46	0.06
0.5 m cavity	7- story	Temperature	23.8	23.67	23.91
		Velocity	0.3	0.3	0.4
		RH	52.1	47.84	49.91
		PMV	0.15	0.13	0.17
	9- story	Temperature	23.77	22.52	22.85
		Velocity	0.3	0.4	0.6
		RH	50.65	52.99	52
		PMV	0.15	0.18	0.16
	5- story	Temperature	23.65	23.9	25.9
		Velocity	0.5	0.3	0.35
		RH	50.65	52.14	47.84
		PMV	0.11	0.18	0.16

Table 8.1 Simulation results for different scenarios of the combined shaft-corridor DSF.

8.3.1 Impact of opening size on energy use and thermal comfort

In order to study the impact of the opening area on energy use, openings of 0.3, 0.6, and 0.9 m (as described in Chapter 7, results were taken for May, June, Sep and Oct) were generated. A cross-comparison diagram of energy use of these alternatives is presented in Figure 8.2. The results show that cooling energy use for the 0.6 opening size is 9% and 15% for the 0.9 m

opening size, respectively, and decreased in comparison with the 7-story, 0.3 opening size as the cavity depth remained constant. The heating load increased by 11 % for 0.6 and 27% for 0.9 m.

One of the main arguments for using increased opening areas in buildings is the provision of better natural ventilation. However, the increased opening area leads to a reduction in energy use for cooling but not for heating in the building. To make use of airflow more efficiently, attention has to be paid to how the opening works with the chimney, which will be discussed in the next section. In terms of energy use, the simulation shows that the best cases would be 0.3 m and 0.6 m opening sizes.

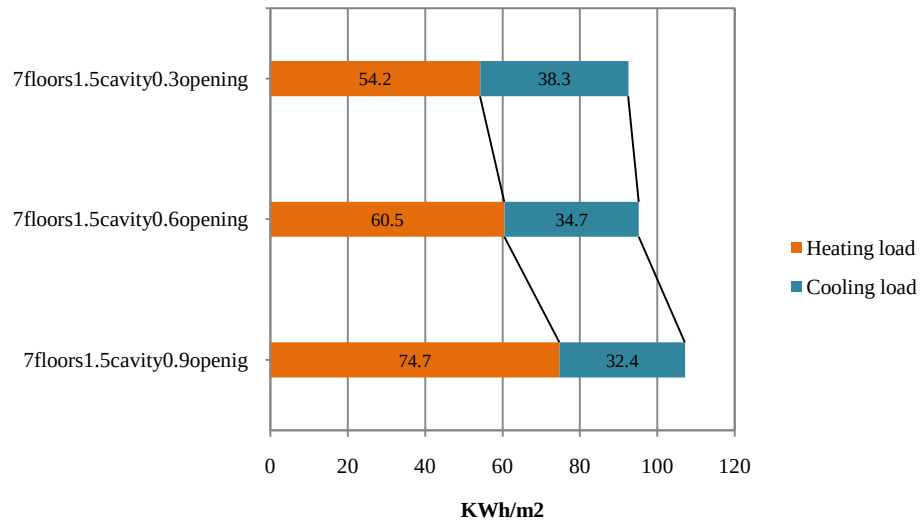

Figure 8.2 Impact of opening size on energy use

As previously stated, the perception of thermal comfort depends not only on the mean-air temperatures, but also on the surface temperatures that surround the occupant. Thus, the opening size is crucial for the perception of thermal comfort as it influences the airflow and radiant temperature as seen in Figure 8.3. For the reference building, the monthly average PMV varies from -0.3 to 0.5, while for the alternatives the monthly average PMV varies from -0.41 to 0.5 and -0.55 to 0.36, respectively.

Different opening sizes are tested to optimize energy and comfort for the combined shaft-corridor DSF.

The findings show that an opening size of 0.6 provides optimum ventilation rates for the internal office space and the most desirable thermal comfort conditions. In terms of energy consumption, the 0.3 m opening reduces total consumption. Although a 0.3 opening size uses less energy, the comfort levels of 0.9 and 0.6 m openings are better during the shoulder season. However, the larger the opening sizes, the colder during the winter month. As illustrated in Figure 8.3,comfort as shown by the PMV index is lower for the bigger opening size, which can be favorable during warm months but not during the winter season.

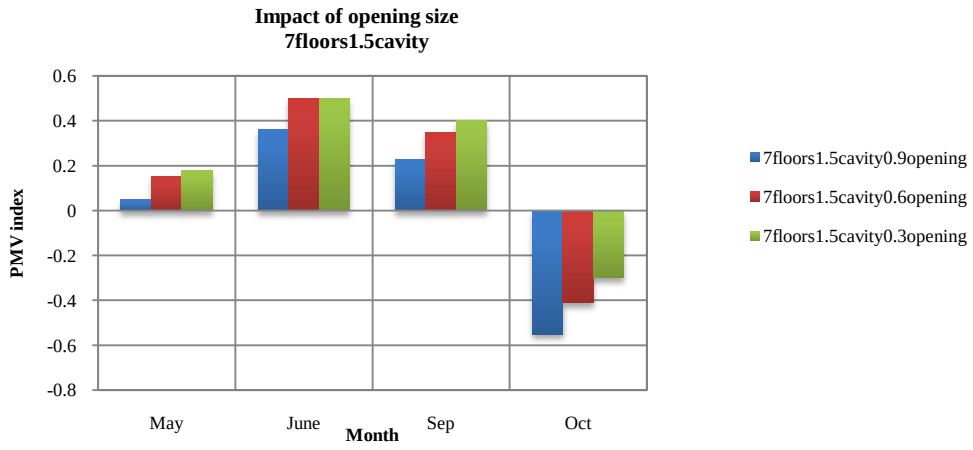

Figure 8.3 Impact of opening size with shaft height (7-story), cavity depth (1.5 m) on comfort

For 7-story shaft height and 1.5 m cavity depth, the best case would be a 0.6 m-opening size.

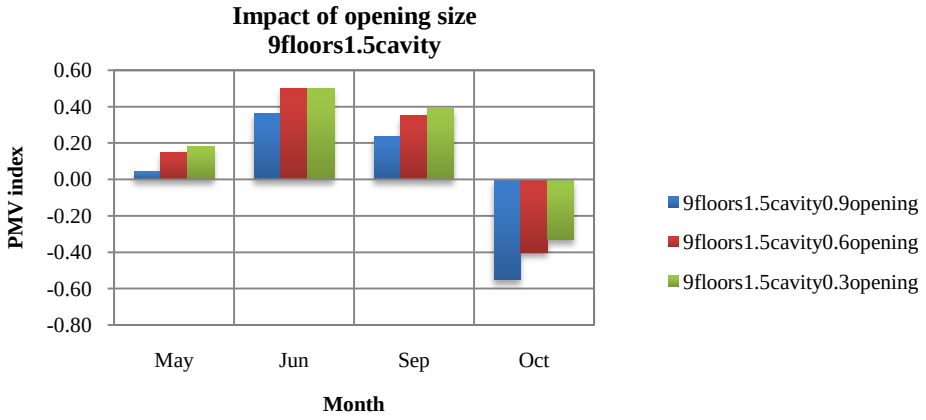

Figure 8.4 Impact of opening size with 9-story shaft height, 1.5 m cavity depth on comfort

For Nine story shaft height and 1.5 m cavity depth the best scenario for the opening size would be 0.9 m.

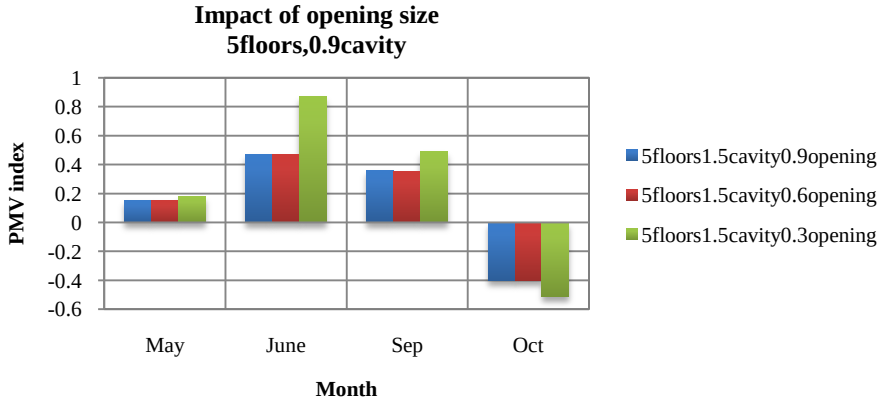

Figure 8.5 Impact of opening size with 5-story shaft height, 1.5 m cavity depth on comfort

But for a shorter shaft height, the variability of opening size from 0.6 m to 0.9m does not impact much on the PMV.

As we reduce the shaft height and keep the cavity depth intact, the best case for an opening size would be 0.6 m. As the shaft height decreased for the same cavity size, the smaller opening size cannot provide the same thermal comfort for occupants.

Figure 8.6 shows the configurations of the CFD model for simulations under specific conditions.

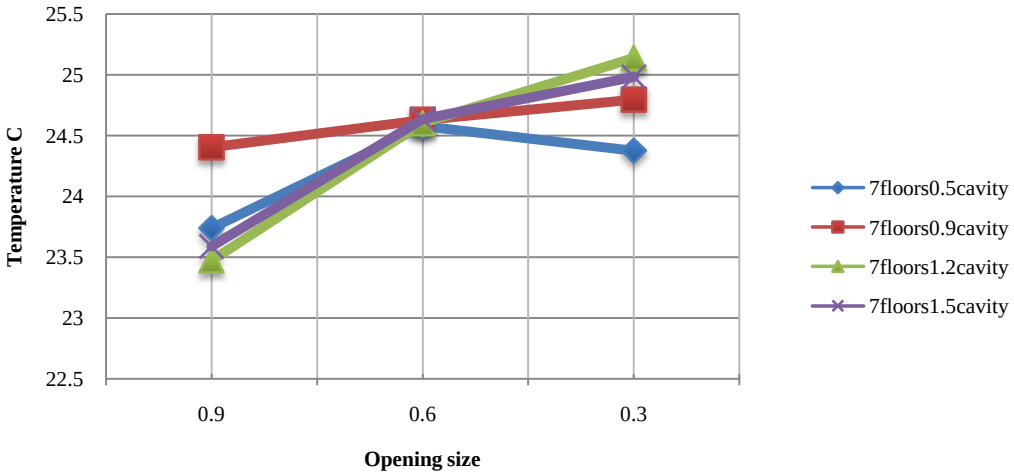

Graph 8.1 Temperature comparisons for different opening sizes (Shaft height: 7-story)

Graph 8.1 shows temperature comparisons for different opening sizes. The 0.9 m opening for the bigger cavity depth shows lower indoor temperature, but as we reduce the cavity size (to 0.9m), the opening has not impacted the operative temperature. As for a 0.5 m cavity, the temperature of the 0.6 m opening increased in comparison with a 0.3m opening size, while the case 0.9 m cavity depth the temperature has not changed much by increasing the opening size.

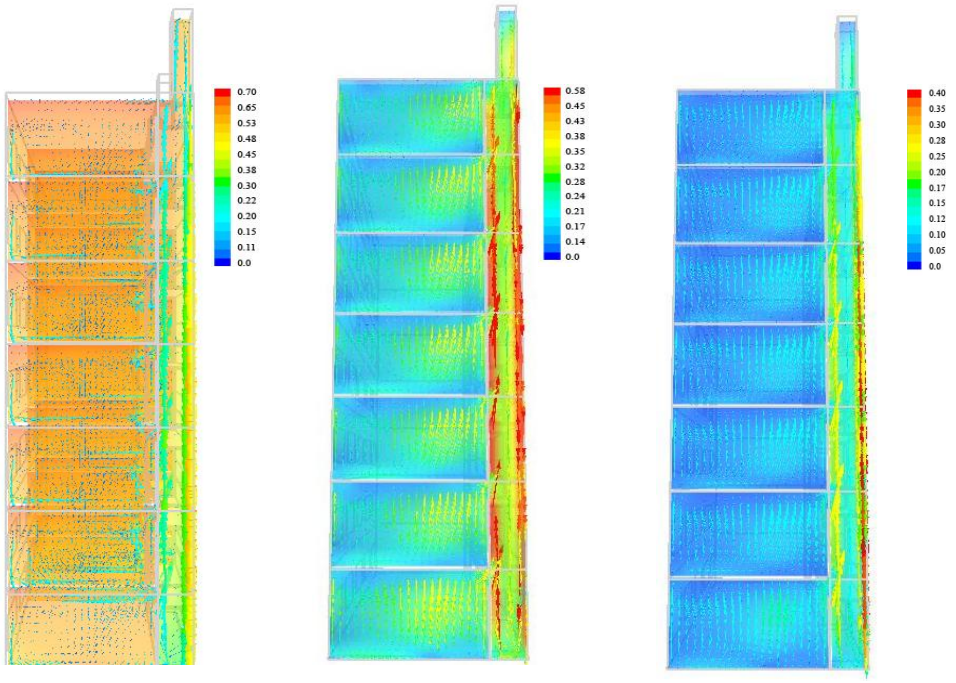

Figure 8.6 Airflow for different opening sizes (from right: 0.3m-0.6m-0.9m)

After taking all thermal comfort parameters into consideration, an opening of 0.3 m would provide optimum results.

8.3.2 Impact of cavity depth on airflow, energy use, and thermal comfort

After establishing the optimum opening size for the combined shaft-corridor DSF, the second parameter to investigate is the effect of different cavity depths on indoor thermal comfort and energy use. Different cavity depth sizes of 0.5 m, 0.9 m, 1.2 m, and 1.5 m will be introduced to the DSF system, with an optimum outer skin opening size of 0.6 m, and 0.3 m. It should be noted that the inner pane and shaft exhaust openings are also equal to the outer skin opening size.

Figure 8.7 show simulation results for thermal comfort under the weather data presented in the previous chapter. The results show that the optimum cavity sizes are between 0.9 and 1.2 m, as presented in Figures 8.8, 8.9.

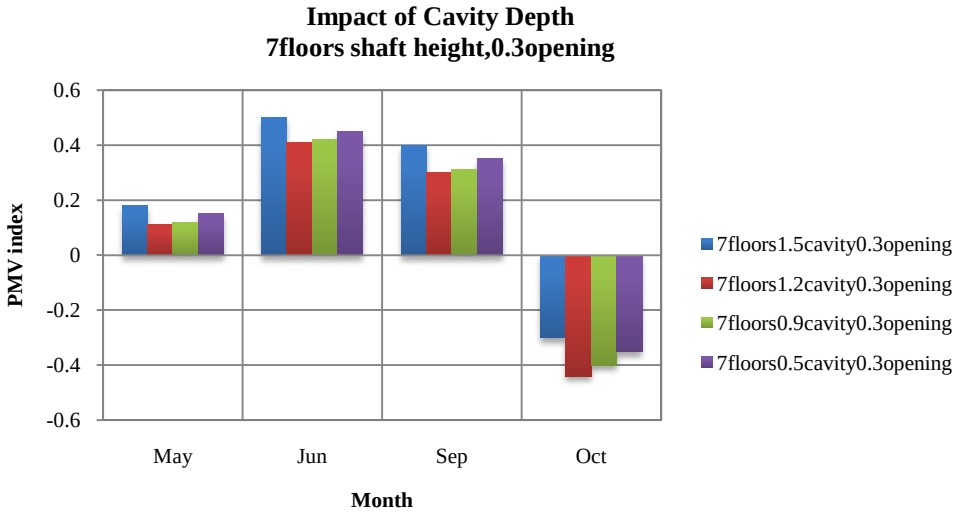

Figure 8.7 Impact of cavity depth on comfort with constant 7-story shaft height, 0.3m opening size

The research found that the optimum cavity width for maximizing the buoyancy-induced flow rate was 0.5 m, as the height of the shaft remained 7-story. However, due to maintenance issues for a 0.5 m cavity depth, the next optimum sizes would be 0.9 and 1.2 m. Research also found

that velocity rate in a DSF of a 7-story shaft height increased as cavity width increased from 0.5 m to 0.9 m but then the increase would be so small as the depth is increased further than 0.9.

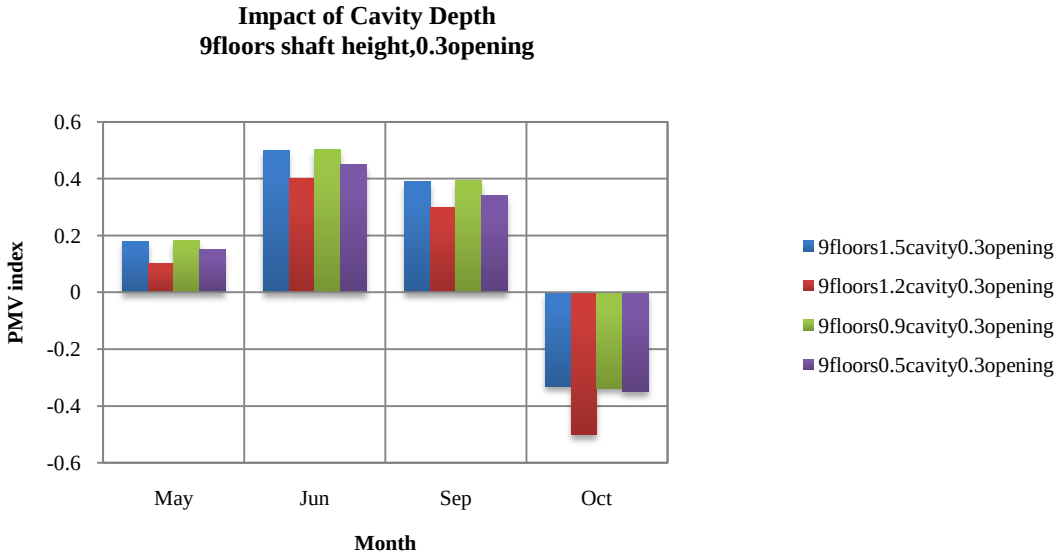

Figure 8.8 Impact of cavity depth on comfort with constant 9-story shaft height, 0.3 m opening size

As we increase the shaft height with an 0.3 m opening size, the buoyancy flow rate will be increased and lead to better thermal comfort as illustrated in Figure 8.9.

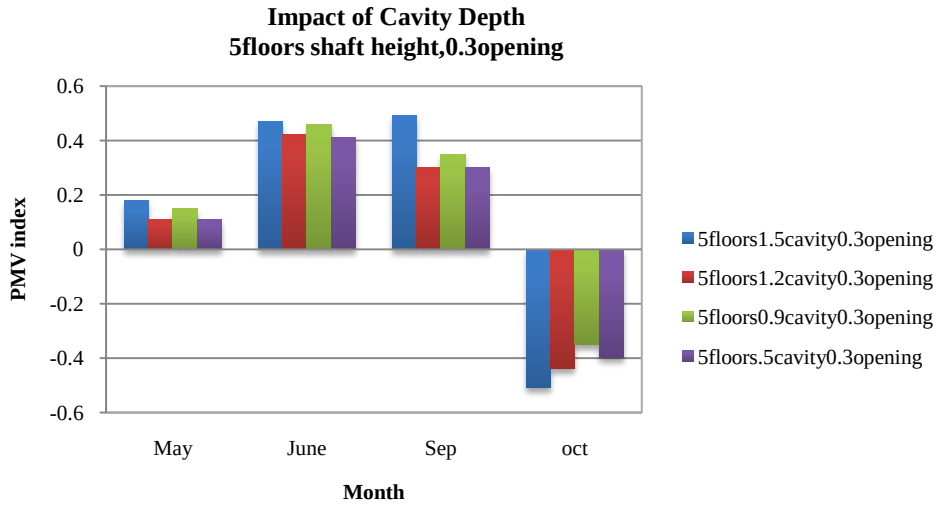

Figure 8.9 Impact of cavity depth on comfort with constant 5-story shaft height, 0.3 m opening size

It was expected that as the shaft height increased, the comfort level would be higher. However, the results do not show much difference. This does not mean that air velocity has not increased by adding to the shaft height. Air speed has increased but there are several other issues that impact thermal comfort. The results in Figures 8.10 to 8.12 indicate a slightly better comfort level in a 7-story shaft height with cavity depth of 1.2 m.

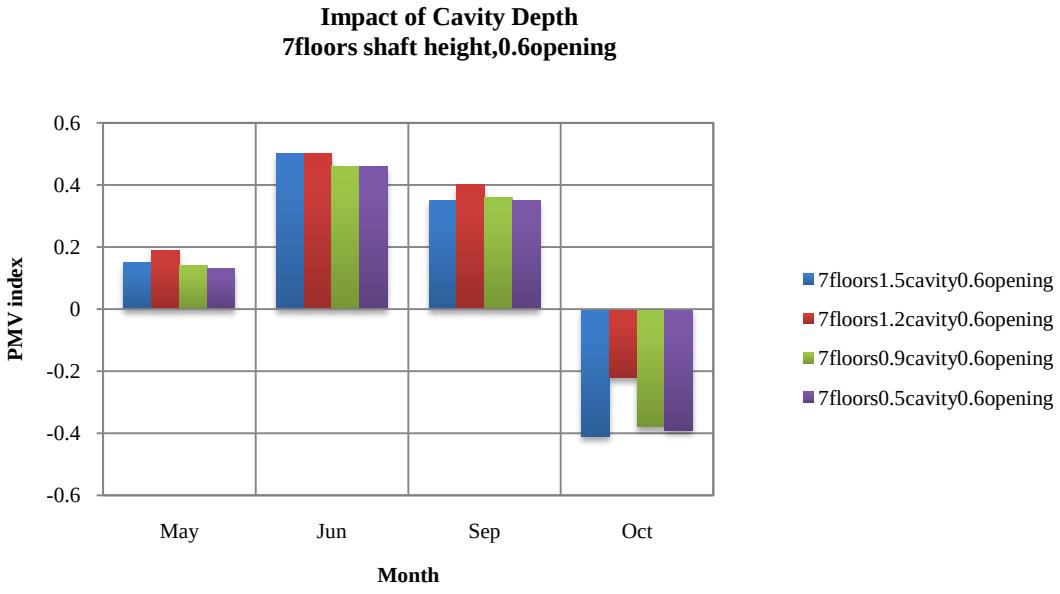

Figure 8.10 Impact of cavity depth on comfort with constant 7-story shaft height, 0.6 m opening

The results show better thermal comfort as opening size increased to 0.6 m -optimum opening size- in comparison with 0.3 m. The cavity depth of 0.5 m shows better comfort with 0.6m opening and the second best option would be 0.9 m with 0.3 m opening size.

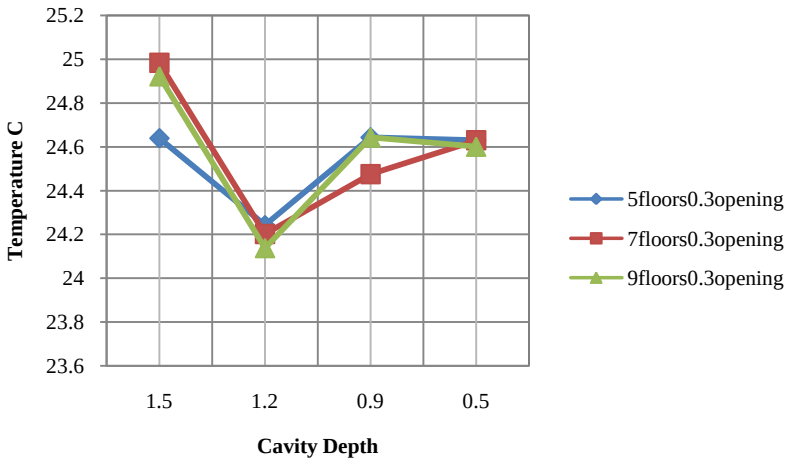

Graph 8.2 Temperature comparisons for different cavity depth and shaft height

Comparing the operative temperature of different cavity depths shows that 1.2 m provides a lower temperature and would be the optimum choice.

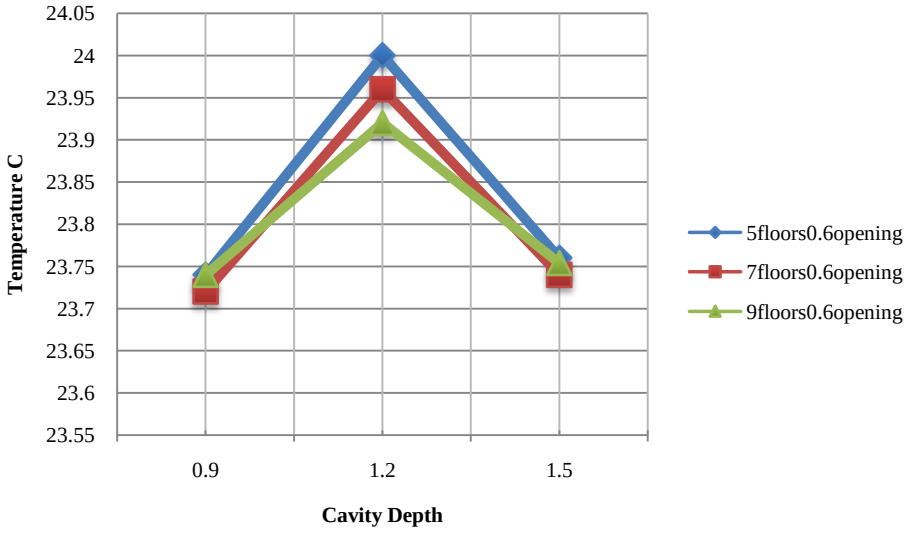

Graph 8.3 Temperature comparisons for different cavity depth and shaft height

In comparison of air temperature values shown in the graphs above for a 0.6 m opening, the optimum cavity size would be 0.9 m and the results doesn't show much difference as the shaft heights varied .

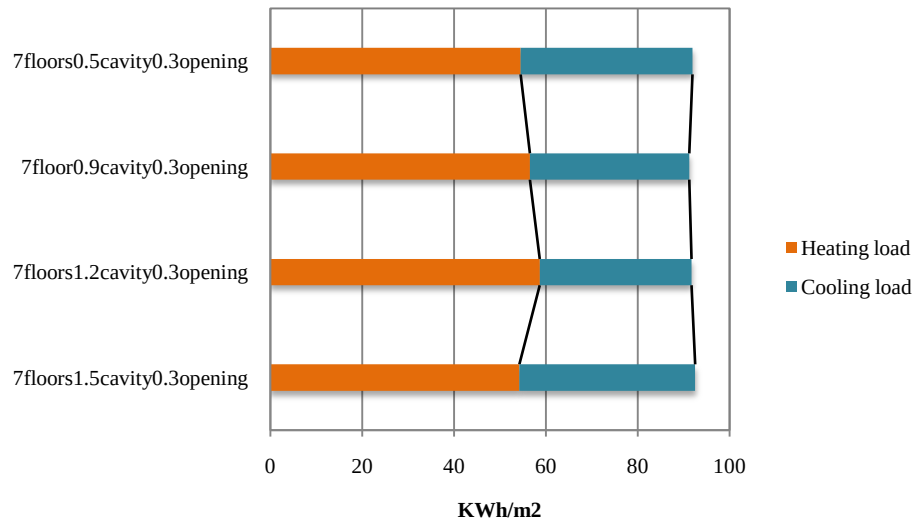

Figure 8.11 Impact of cavity depth on energy use

In terms of energy use the best case would be a 1.2 m cavity depth, which reduces the cooling loads 13%, while a 10% reduction by introducing a 0.9 m cavity depth and 8 % reduction in a 0.5 m cavity depth, but in terms of heating energy use the best case is 1.5m cavity depth.

The findings show that a cavity depth of 1.2 m provides optimum ventilation rates for the internal office space and the most desirable thermal comfort occupant conditions.

8.3.3 Impact of shaft height on energy use and thermal comfort

In order to investigate the shaft height on the combined shaft-corridor DSF, three different shaft heights have been introduced to the system. Boundary conditions are the same as the reference building in the previous chapter. The shaft height will be tested to provide the better thermal comfort and energy use. At this stage, the shaft height will also be tested on the optimum openings size and cavity depth obtained for the system in previous sections. The optimum opening size for the outer pane is 0.3 m–0.6 m and the cavity depth size is set to 0.9–1.2 m.

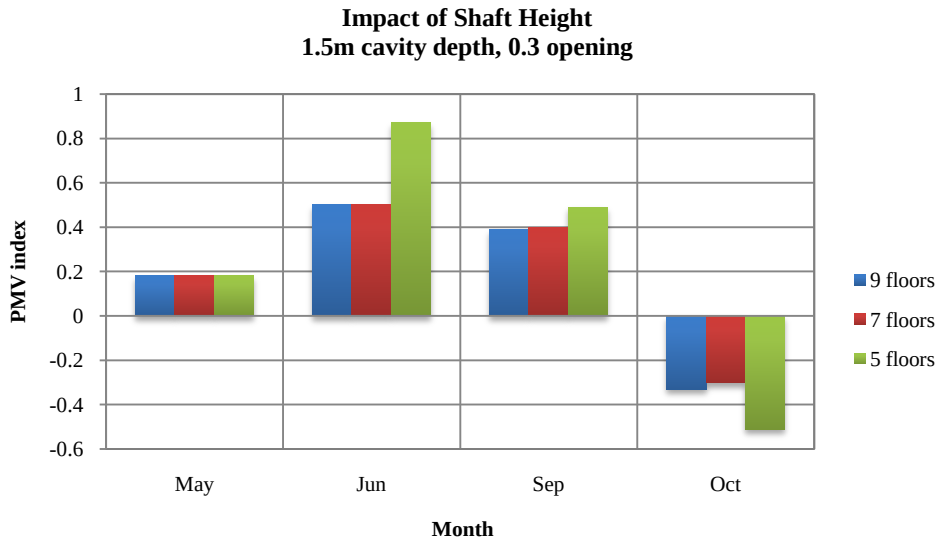

Figure 8.12 Impact of shaft height on comfort with constant 1.5 m cavity depth, 0.3 m opening size

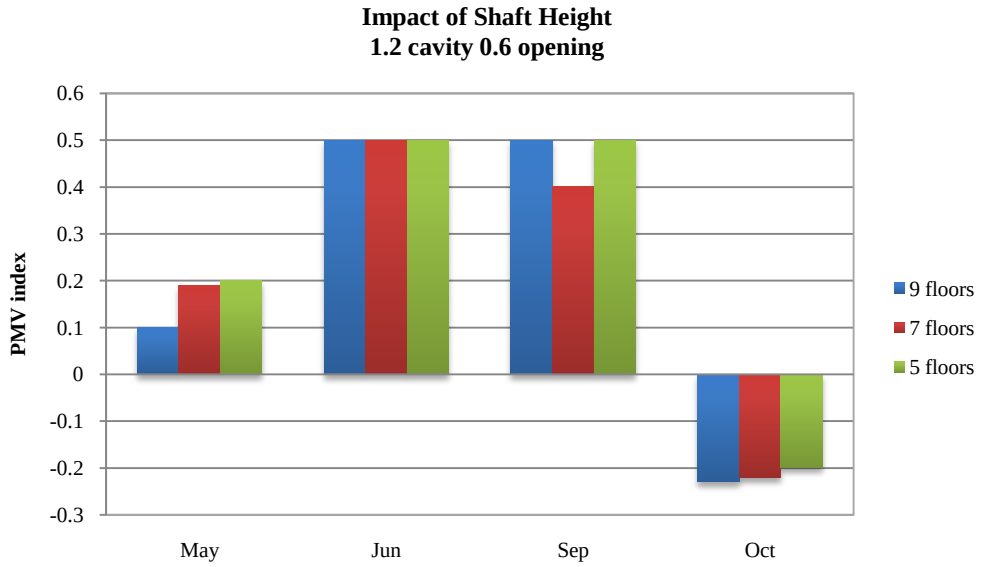

Figure 8.13 Impact of shaft height on comfort with constant 1.2 m cavity depth, 0.6 m opening size

It was found out the 7-story shaft height provides a slightly better comfort than the 9-story shaft height. Although the air velocity will be increased in a 9-story shaft, the top floor would be slightly warmer when the shaft height is increased more than 7 stories as illustrated in the graph 8.4.

The temperatrue graph of different shaft heights shows that the 1.2 m cavity size in the case of an 0.3 opening has a lower operative temperature in comparison with other depths. In the case of a 1.2 m cavity depth, the 9-story shaft high has a lower temperature than the 7-story high.

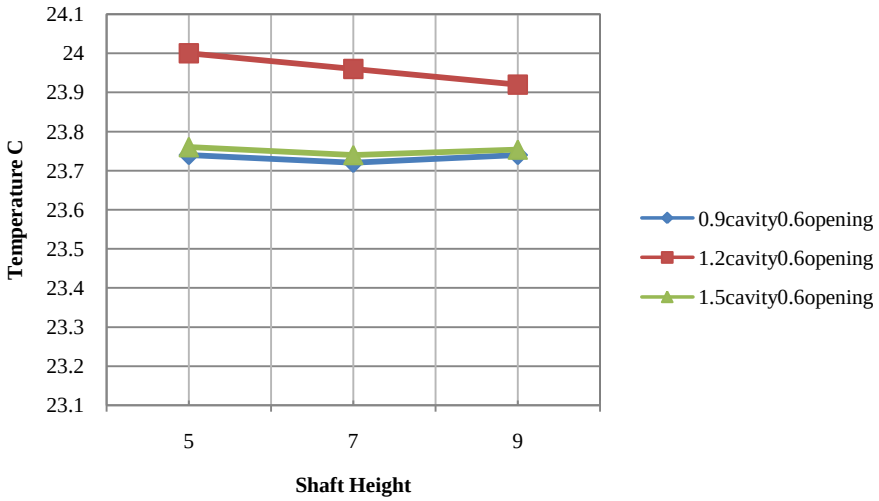

Graph 8.4 Temperature comparisons for different shaft height and cavity depth

It was found out that a 0.9 m cavity depth performed better when the opening size increased from 0.3 to 0.6 m. In the case of 0.9 m cavity depth and 0.6 opening size, the shaft height has not had much impact on the temperature.

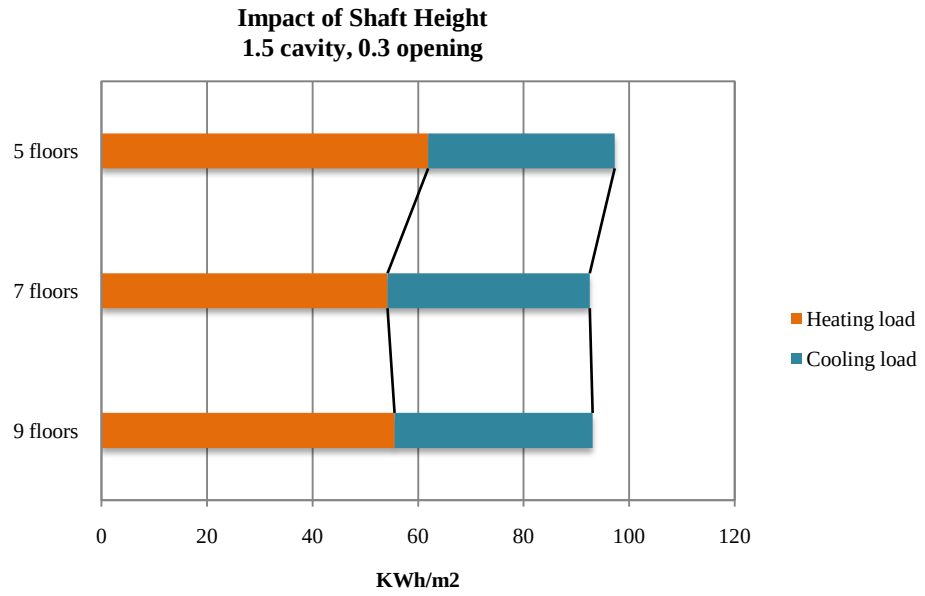

Figure 8.14 Impact of shaft height on energy use with 1.5 m cavity depth and 0.3 m opening size

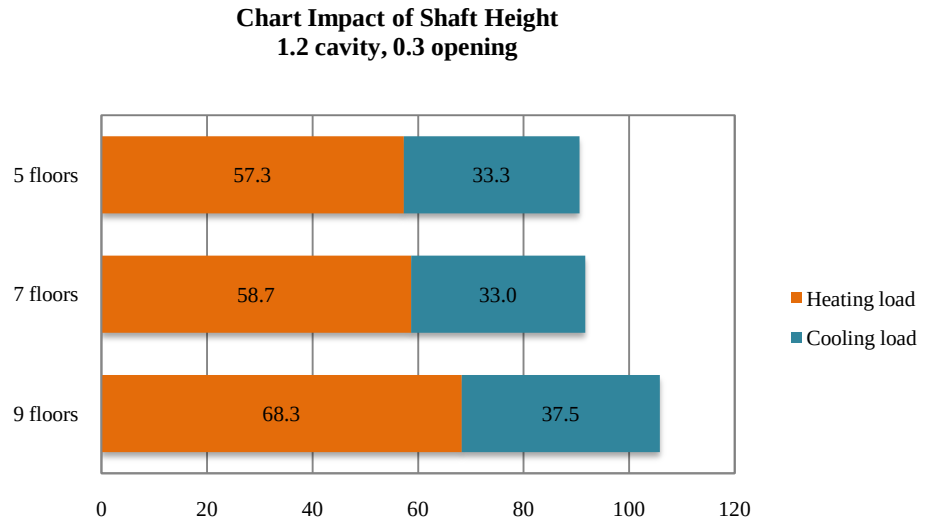

Figure 8.15 Impact of shaft height on energy use with 1.2 m cavity depth and 0.3 opening size

After analyzing all simulation results and taking thermal comfort parameters into consideration, a 9-story shaft high provides in average better comfort during naturally ventilated month but in terms of energy, the 5-story shaft high performs better.

Both of graphs' energy and comfort analysis show that the 7-story shaft high is the optimum solution and provides better indoor operative temperatures for offices spaces.

8.4 Double skin facade performance assessment

8.4.1 Comparison of the best comfort performance alternatives

In regards to the quality of indoor thermal comfort, it is evident that smaller opening areas provide a more stable environment with fewer dissatisfied occupants. The percentage of dissatisfied occupants increases mainly due to low inner surface temperatures during winter, which is the result of bigger openings. When the monthly average PMV values for different alternatives compared, the case with 9-story shaft height, 1.2m cavity depth, 0.9m-opening size performs similarly with slightly lower PMV values than the case with 7-story shaft height, 1.2m cavity depth and 0.9 m opening size. It can be concluded that for 1.2 m cavity depth with 0.9 opening, the shaft height does not impact thermal comfort.

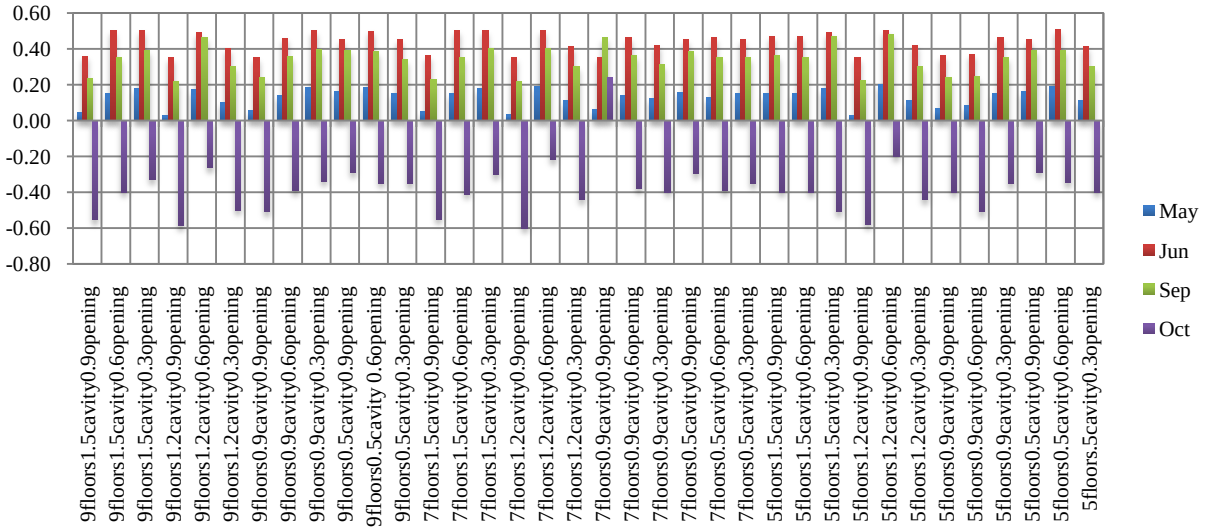

Figure 8.16 Monthly average PMV for the different alternatives

In addition, the case of a 7- story shaft height 1.5 m cavity depth, 0.9 opening size performs the same as 5 story shaft,1.2m cavity depth and 0.9 opening size and it can be concluded that increasing two stories to the shaft height is similar to decreasing the cavity depth by 0.3 m.

8.4.2 Comparison of the best energy performance alternatives

8.4.2.1 Cooling season

During this period, heat needs to be extracted from the space to the cavity, and as the cavity depth increases, the more heat can be extracted to the outside. Generally, solutions with larger opening sizes and smaller cavity depths (models 0.9 m cavity depth) perform slightly better in the Chicago climate. The larger opening size allows a greater airflow rate through the cavity, thereby extracting more heat, and the smaller depth causes greater air velocities near the cavity surfaces. In the case of a smaller cavity depth, the insolation helps extract heat because of a greater buoyancy force. It is also notable that the taller shaft enhances the DSF performance. It was expected that the taller shafts would result in more heat extraction and lead to lower temperature but that is not always the case. Apparently the solar heat gain offset this to some extent. However, the results in future show that a larger opening size would make these cavities perform better.

The five-story high shaft performs well and it can be concluded that the solar heat gain trapped in this type can be extracted more efficently with a large opening. This type of DSF is more successful in extracting heat through the buoyancy effect.

8.4.2.2 Heating season

The DSF models that perform best in this season are those with the lowest airflow rate. This rate can be due to smaller opening sizes or larger cavity depth. In these models, the solar heat gain trapped within the cavity cannot be extracted from the stack. For instance By closely comparing the energy performance of these two cases 5-story, 0.9 cavity, 0.3 m opening size, and 5-story 1.2 m cavity and 0.9 opening, it is notable that the larger the opening size the higher the heating load.

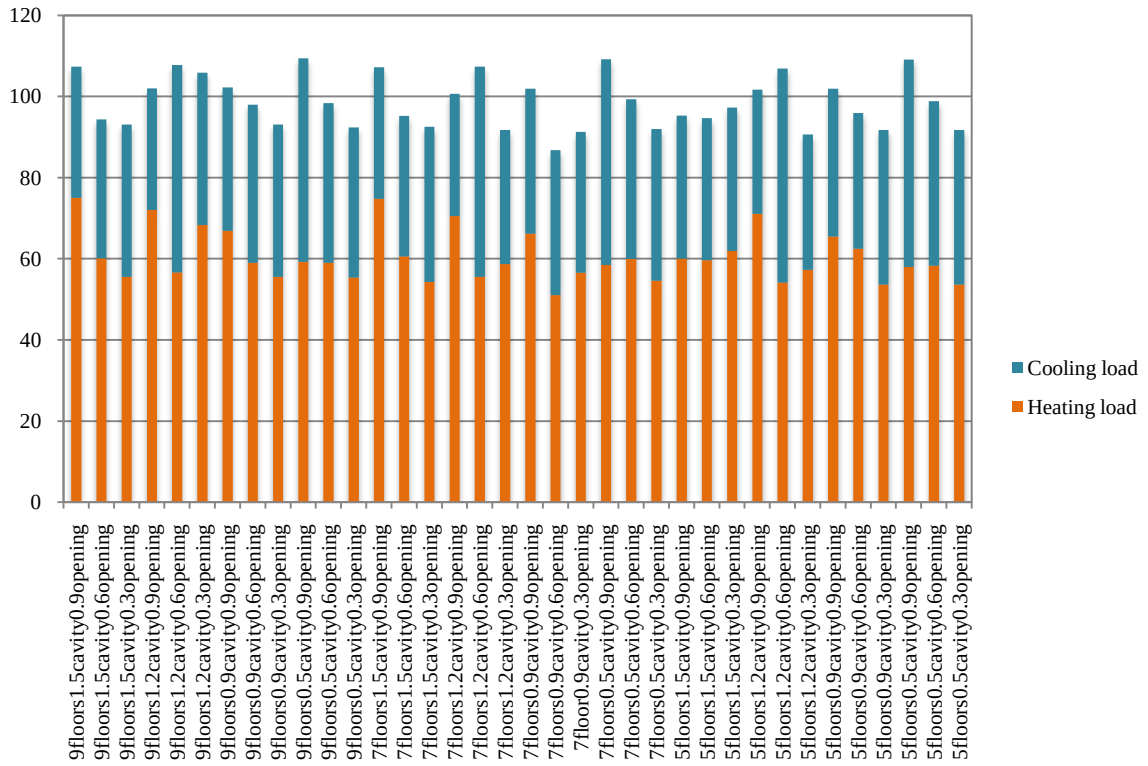

Figure 8.17 Energy use comparisons for different alternatives

The two cases of 7-story shaft height, 0.9m cavity depth and 0.6m opening size and 5-story shaft height, 1.5m cavity depth and 0.9m opening size performs the best. In addition the case 7-story shaft height 0.9m cavity depth and 0.3m opening size also would be an optimum choice. These three alternatives are going to be investigated based on the

8.5 Comparison of the three optimum performance alternatives

Finally, a comparison of the best performing alternatives of energy use and thermal comfort has been performed. An improved version of the reference single skin building was simulated.

The smaller area of windows and cavity depth resulted in a lower (compared with the rest of the cases) heating and cooling demand, and the lowest total demand (91.7kWh/m^2a) occurred in a 5--story shaft, and 0.9 cavity, and 0.3 opening. The next two alternatives had the same shaft height

but a larger opening size and cavity depth. For buildings with a larger opening area, the total energy use increased by4 kWh/m^2a for the 0.6 m opening size, and by 10 a for the 0.9 m opening size. Comparing the 7-story shaft height case, it was seen that a 0.9 cavity and 0.3 opening use 91.2 kWh/m^2a due to a decrease in the cooling demand. By taking into consideration both energy and thermal comfort, the optimum cases were the 7-story shaft height with 1.2 cavity depth and 0.6 opening size, or 7-story shaft height with 0.9 cavity depth and 0.3 opening size, or 5-story shaft height with 1.5 cavity and 0.3 opening size. The Case 7-story shaft height with 1.2 cavity depth and 0.6 opening size has the lowest cooling energy use and the case 5-story shaft height with 1.5 cavity and 0.3 opening size has the lowest heating energy use.

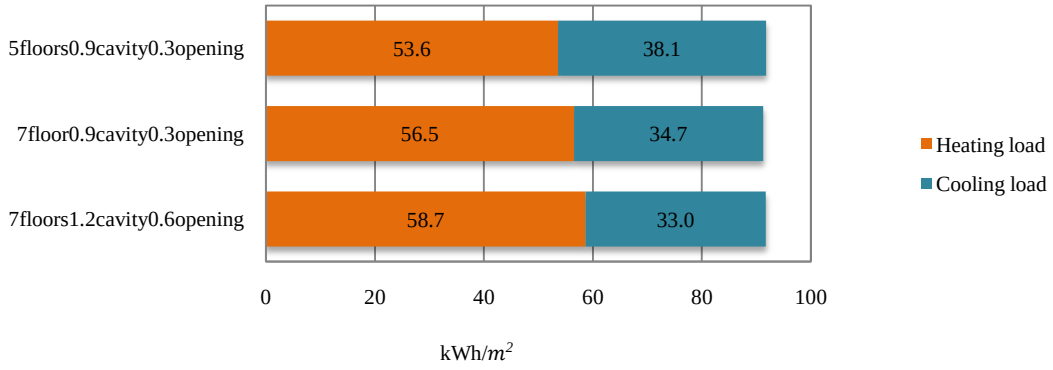

Figure 8.18 Energy use of optimum alternatives

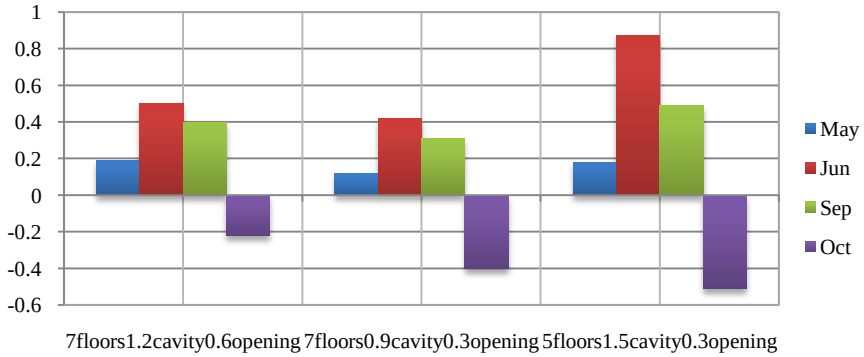

Figure 8.19 PMV index of optimum alternatives

8.6 Optimization results and findings

After numerous attempts and comparisons to optimize DSF configurations to find acceptable indoor thermal comfort conditions for office occupants, a number of positive findings were observed. These results and findings will be of utmost importance as indications of whether this new type of facade (Shaft-corridor DSF configuration) can be used as a mean to introduce natural ventilation to high-rise buildings in a cold climate.

Optimization findings are summarized below:

a) The optimum opening size for the outer pane of the DSF system is 0.3–0.6 m.

b) The optimum air gap sizes for the DSF system with the optimum shaft height are between 0.9 m–1.2 m.

e) The optimum shaft height is 7-story and the thermal comfort of the upper floors is better than the other cases.

The optimized DSF for Chicago climate is 7-story high shaft, 1.2m cavity depth, and 0.6m opening size.

The parametric studies in optimizing the configurations of the DSF system have lead to the construct of an improved DSF system for use in a cold climate.

Some of the important findings are tabulated below:

a) A DSF system with openings vs. cavity depth (shaft height constant).

As the opening size increased, the comfort improved with the same cavity depth.

In order to get the same results in thermal comfort, as the cavity depth is decreased, the opening size should be increased.

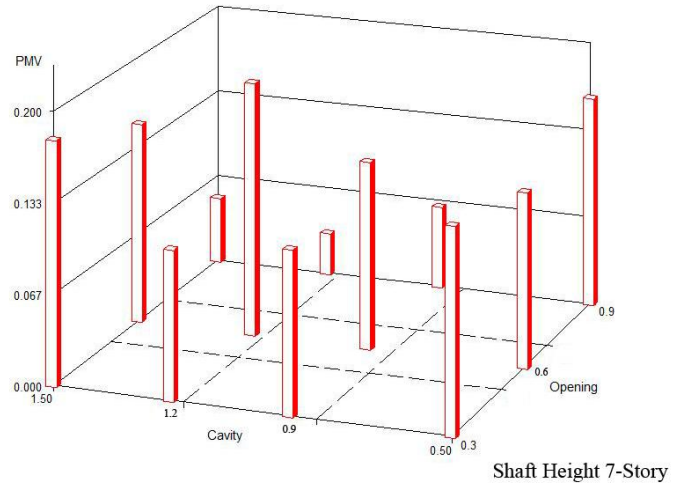

Figure 8.20 Opening size vs. cavity depth

b) A DSF system with opening size vs. shaft height (cavity depth constant).

Increasing the shaft height improved the thermal environment and as the shaft height increases the opening size needs to increase to provide the same results.

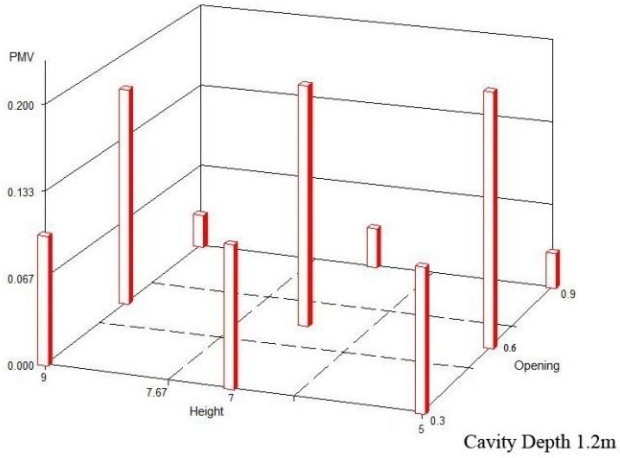

Figure 8.21 Opening size vs. shaft height

c) DSF system cavity depth vs. shaft height (opening size constant).

As the shaft height increases, the cavity depth should be decreased with a constant opening size to provide the same results.

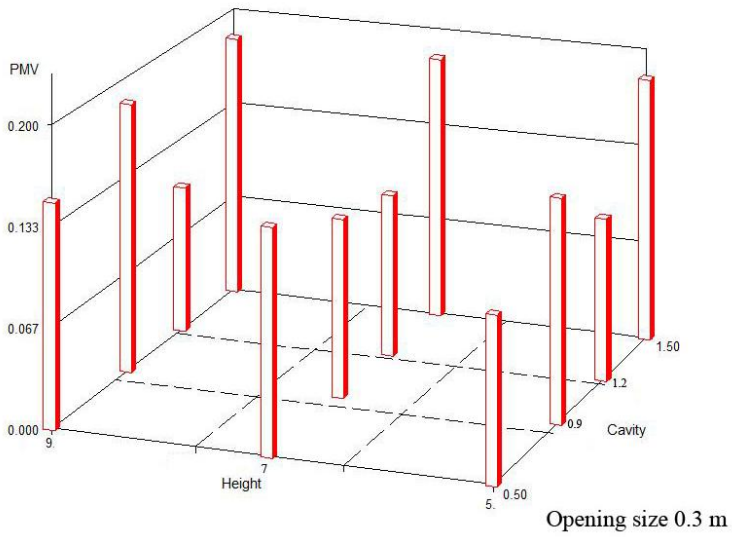

Figure 8.22 Cavity depth vs. shaft height

8.7 Summary and Conclusions

While there is a great deal of interest in transparent building in current architecture, larger areas of glazing area results in higher building heating and cooling loads, and higher levels of energy consumption. The advent of the double skin facade is a response to these problems. A DSF provides the potential to introduce daylighting and natural ventilation to the building, resulting in reduced energy consumption associated with those loads. In addition, a DSF could provide a buffer zone between the outdoor and indoor environment, allowing it to act as a sunspace to reduce the heating load. Annual energy savings of above 50% have been found.

In this research, the buoyancy and wind-driven energy flows through the cavity have been analyzed with CFD.

A modeling process using CFD and EnergyPlus was developed to assess the performance of a combined shaft-corridor DSF cavity that combines the shaft and corridor to take advantage of

buoyancy-driven airflow. The model uses EnergyPlus to determine boundary conditions, including glazing surface temperatures and heat flux, and CFD to analyze airflow rate and cavity patterns in an iterative process. It was determined that a single iteration between the two models provides sufficient convergence and accuracy. The combined shaft-corridor DSF strategy does not yet have data from actual implementation from physical models. Construction of full scale or reduced scale DSF structures has substantial capital requirements and considerable temporal requirements for constructions and monitoring. The use of computer models and simulations can provide an economical and efficient first assessment of the feasibility of a combined shaft-corridor DSF strategy.

A process was also described to use pre-determined wind pressure values at the cavity's openings to model a DSF cavity in a simpler CFD model than would otherwise be required. This method reduces computation time that would be needed to model a cavity in a domain large enough to analyze wind affects along with buoyancy forces. CFD models were used to determine velocities at various points on a 10-story building for reference wind velocities of 5.0 and 10.0 m/s. These values can be implemented in models using the described process.

Simulations using the developed model were run for a number of different cavity configurations in order to optimize the performance of this combined shaft-corridor DSF. The model was used to develop correlations that describe a DSF cavity performance. Key correlations were also described in the last section.

8.7.1 Energy performance assessment

In order to reduce energy use and improve indoor thermal environment, combined shaft-corridor DSF were introduced. The combined shaft-corridor DSF is a system consisting of corridor and shaft types. In this combined shaft-corridor DSF, chimneys are placed in such a way that air can

flow through the intermediate cavity with no mixing of inlet and exhaust air. In principle, the main purpose of the DSFs (as to energy use and thermal comfort) is to allow useful solar gains into the building and to introduce natural ventilation during the shoulder season. This research investigated the possibility of introducing natural ventilation and buoyancy in order to reduce the cooling loads.

The distance between the skins in the parametric study was varied from 0.5 m up to 1.5 m. For protection and heat extraction reasons, solar shading devices were placed inside the cavity. The two driving forces, wind and buoyancy, were incorporated to enhance the building's ventilation. A main requirement when designing ventilated DSF cavities is efficient heat extraction during summer months. For naturally ventilated cavities, the key parameters are the characteristic height of the cavity (height to depth ratio) and opening sizes. For naturally ventilated cases, the position of a shading device inside the cavity has only a limited impact on the thermal comfort (Gen, 2003). Movable external louvers decrease cooling and the heating demands. The effect is opposite for internally placed venetian blinds, resulting in the highest total energy use due to the drastic increase in cooling demand. The location of shading devices in regards to the external or internal screen was not in the scope of this study but a previous study shows that there is not much impact on energy use (Afonso, 2003).

The energy savings achieved for this combined shaft-corridor DSF has been investigated by changing those parameters to see how they can enhance the natural ventilation via buoyancy. Regarding thermal comfort, the double facade alternatives performed slightly better due to the higher (and closer to the 0 axis) PMV values during the swing months in comparison with the reference combined shaft-corridor DSF. Introducing buoyancy and wind effect to the cavity enhanced the airflow and results in lower cooling loads.

Often, increasing the opening size doesn't improve the energy performance of the DSF system. Since as the larger openings reduces cooling loads, the heating loads increases respectively. Finding the optimum opening size for each cavity is essential for improving the building's thermal and energy performance, especially as with a bigger shaft depth and larger opening size a building's energy use may vary substantially, depending upon the design. The external louvers are located in the cavity with the same window properties. The difference in total energy use between the reference combined shaft-corridor DSF (0.3 opening size, 1.5 m cavity, 7- story shaft height) and the best performing alternative could be 158.8 kWh/$m^2\,yr$. This is the same alternative as the base case but the optimum opening size results in a reduction of energy by 10 kWh/$m^2\,yr$.

8.7.2 Thermal comfort performance

The majority of this research focused on developing correlations that can be used to analyze the energy performance of a DSF within an annual building energy simulation program. The most notable finding is that a DSF cavity is successful in extracting more heat from the facade of a building at an outdoor air temperature of 20 °C and insolation rates of 250 watts/m^2more than a single facade of equivalent insulating glazing. As a result, the thermal comfort level during the shoulder season is within 80% acceptable. It was hypothesized that the combined shaft-corridor DSF would show significant improvements in terms of enhancing the airflow and shading the interior glazing. This is promising for the combined shaft-corridor DSF in its ability to reduce cooling season loads by implementing natural ventilation to the interior.

Other conclusions:

• A 7-story cavity, with greater airflow rates from greater buoyancy-driven airflow, does not show improved cooling season performance over a 5-story height cavity.

• The cavity models analyzed with larger opening sizes (0.9 m) and smaller cavity depths (0.5 m) performed slightly better in the cooling season than the bigger cavity depth (0.9 m) and smaller opening sizes (0.6 m). This is due to greater airflow rates with the larger opening size, and slightly higher airflow velocities with a thinner cavity.

• The cavity depth has very little effect (from 0.9-1.5 m) on the airflow rate through the cavity; the rate is largely driven by the cavity opening size with buoyancy-driven airflow.

• A closed cavity (buffer zone) in the heating season assumed in this study. The best performing cavities in heating season have larger cavity depth to collect solar gain, and small opening sizes, as expected.

Also, the correlations developed for airflow rate can also be used to make cavity design decisions about depth and opening size. The equations will give a range of airflow rates from buoyancy-driven and wind airflow from a given DSF cavity configuration.

Regarding the quality of the indoor environment, it is evident that the optimum opening size in relation to shaft height and cavity depth areas provides a more stable environment, with fewer dissatisfied occupants.

Chapter 9.0
Contribution and Future Works

9.1 Contribution

The building facade plays an important role in achieving the critical goals of thermal comfort and energy efficiency. Due to technological advances, transparency, and the use of glass have become an attractive option for building envelopes. Designing glass facades can provide outdoor views, abundant natural light as well as the potential for natural ventilation. With the use of glass, however, both heating and cooling loads increase due to heat loss during the cold season and solar gain during the summer. The development of DSFs is one of the more promising responses to this problem.

The combined shaft-corridor DSF incorporates natural ventilation between the interior and exterior skin. It provides cooling by convective heat extraction and wind as a natural driving force. It can provide a buffer zone between the indoor and outdoor air during heating season.

This dissertation proposed a new configuration of a DSF system by combining two typical facade systems in hot summer continental climate. This can be used as a guideline in the initial design of a DSF system in that context.

In literature, numerous studies have shown DSFs should work to improve energy efficiency without calculation results or experiments (Arons and Glicksman, 2001) Gertis correctly points out that few simulations have been made and few measurements are available to support the benefits that have been claimed. Other researchers have provided models to simulate specific DSF typologies but did not link the envelope-level results to the building energy performance. Only a few combinations of building performance analysis and envelope performances are

available that were restricted to one typical configuration or one story building (Saelens, 2003). Most studies on thermal performance of DSFs have been carried out in moderate climates and in one-story buildings. Only one study (Hasse, 2006) has been done on refurbishing of buildings in hot summer continental climates. My study departs from previous investigations in the following aspects:

This study designed a new DSF configuration and coupled a dynamic energy simulation program with airflow modeling of a control volume model. Further, it investigates the thermal performance of a double skin facade in different configurations and in a different climate.

This research has bridged the gap of investigating a combined shaft-corridor DSF to provide and improve natural ventilation in a high-rise office building in humid continental climate. The research found that this Shaft-corridor DSF has advantages over the typical curtain wall system in reducing the cooling load by allowing wind to be introduced as the driving force in combination with the stack effect to enhance natural ventilation. This combined shaft-corridor DSF combined a corridor facade and a shaft type as described in Chapter 2. The findings have concluded that this Shaft-corridor DSF of facade system provides better thermal comfort in terms of radiant temperature reduction and energy savings as much as 30 percent with a seven-story shaft extension.

9.2 Limitation and recommendations for future work

Regarding the complexity of analyzing DSFs, a few assumptions have been made and limitations are acknowledged. Following are some of the research areas that were not in the scope of this study, which might be addressed in the future to reduce energy usage in high-rise buildings with DSFs:

First, in addition to the whole building energy simulation, measurements on the actual model is highly recommended. The results and findings from the research needed to be validated directly with experimental results. This shortcoming could be overcome to some extend by installing full size experimental model in Chicago climate and monitor the experimental results for a specific period of time. Due to the time and cost constraints for the research, the simulation tools have been used to study the different parameters in terms of energy savings and thermal comfort analysis.

Second, the research has looked at overall comfort through different parameters such as air temperature, air velocity, radiant temperature, relative humidity, and by calculating the PMV and PPD to achieve indoor thermal comfort. Other issues associated with a DSF such as daylighting and condensation, are not within the scope of this research. In addition, the local discomfort has not been investigated within this research.

Third, this study has not looked at different internal partitions' positions. The internal airflow patterns would be affected based on different layout spaces that can be investigated to point out the stagnant points and thermal comfort conditions. In other words, the influence of geometrical characteristics on airflows can be investigated and presented as a guideline for architects.

The next recommendation is to consider the integration of other technologies such as phase change materials, PV, and aero gel transparent insulation to the DSF system. Some research has been done in the integration of PV and DSF for low-rise buildings. However, further work need to be done in humid continental climate for high-rise buildings.

Furthermore, it is necessary to investigate the energy life cycle and economic analysis, which are the ultimate tools in assessing DSF impact on a global scale. Further, it is useful to identify the

importance of other parameters such as control strategies-dashboard system that may validate and monitor the actual building performance.

Last but not least, the incorporation of nighttime ventilation to the DSF system has been addressed in the literature. However, the impact of nighttime ventilation on the cooling loads has not been investigated in this study.

9.3 Conclusion

This research has achieved the goals that were set out at the onset. The question of the viability of naturally ventilated DSFs in high-rise buildings in a hot summer continental climate has been answered.

In this unique type of DSF, there is no mixing of intake and exhausted air. Natural ventilation strategies (wind and natural convection) could be enhanced to provide satisfactory indoor thermal conditions for high-rise buildings in particular periods (shoulder seasons).

CFD as a feasible tool has been used to test the uncertainty in building design and the possibility of solutions for a particular problem.

In order to reduce energy consumption and improve the indoor thermal environment of highly glazed buildings, DSFs can be implemented for Chicago's climate.

During the parametric studies, the ventilation rate should be considered to estimate the inner pane temperature. On one hand, reducing the heating demand is essential for office buildings located in Chicago; on the other hand, sufficient ventilation results in efficient heat extraction and low cooling demand.

In this study, i.e. detailed CFD calculations on a combined shaft-corridor DSF, the influence of geometrical characteristics on airflows also was studied and a single case compared with the

combined shaft-corridor DSF. The obtained results presented as the energy performance of the building and thermal comfort of occupants.

9.4 Final note

The development of new technology plays a major role in response to energy issues. To that end, resources must be used wisely, while new ways of generating energy are being developed. Consumption must be reduced and more types of renewable energies should be incorporated. Technology and architecture should be integrated to face the challenge of the future. In the worlds of the master architect of all time, Le Corbusier, “The question of window hasn’t been solved yet.”

References

Afonso, C., & Oliveira, A. (2000). Solar chimneys: Simulation and experiment. *Energy and Buildings, 32*(1), 71-79.

Allocca, C., Chen, Q., & Glicksman, L. R. (2003). Design analysis of single-sided natural ventilation. *Energy & Buildings, 35*(8), 785.

Allard, F. (1998). *Natural ventilation in buildings - a design handbook* . London, UK: Earthscan Publications Ltd.

Al-Mumin, A. A. (2001). Suitability of sunken courtyards in the desert climate of Kuwait. *Energy and Buildings, 33*(2), 103-111.

Alnaser, N. W., Flanagan, R., & Alnaser, W. E. (2008). Potential of making over to sustainable buildings in the kingdom of Bahrain. *Energy and Buildings, 40*(7), 1304-1323.

Angus, H.H. & Associates Limited, Consulting Engineers. (2001). University of Toronto Centre for Cellular and Biomedical Research: Draft Study of a Double Wall Facade.

Arens, E., Blyholder A. & Schiller, G. (1984). Predicting Thermal Comfort of People in Naturally Ventilated Buildings. *ASHRAE Transactions.* Vol. 90, Pt. 1B, 1984, 12 pp.

Arons, D. (2000a). Properties and Applications of Double-Skin Building Facades. MSc thesis in Building Technology, Massachusetts Institute of Technology (MIT), USA. Retrieved from http://libraries.mit.edu/docs

Arons, D. M., & Glicksman, L. R. (2000b). Double Skin, Airflow Facades: Will the Popular European Model Work in the USA? Proceedings of the ACE3 2000 summer study on energy efficiency in buildings. New York.

ASHRAE Handbook of Engineering Fundamentals. (1993). American Society of Heating, Refrigeration and Air Conditioning, Atlanta. pp. 336-338.

ASHRAE. (2001). *ANSI/ASHRAE Standard 562-2001*, Ventilation for Acceptable Indoor Air Quality, Atlanta: American Society of Heating, Refrigerating, and Air-Conditioning Engineers, Inc.

ASHRAE. (2004). *ANSI/ASHRAE Standard 55-2004*, Thermal Environmental Conditions for Human Occupancy, Atlanta: American Society of Heating, Refrigerating, and Air-Conditioning Engineers, Inc.

Awbi, H.B. (1991). Ventilation of Buildings, E &FN SPON.

Baldinelli, G. (2009). Double skin facades for warm climate regions: Analysis of a solution with an integrated movable shading system. *Building and Environment*, *44*(6), pp. 1107-1118.

Ballestini, G., Carli, M. D., Masiero, N., & Tombola, G. (2005). Possibilities and limitations of natural ventilation in restored industrial archaeology buildings with a double-skin facade in Mediterranean climates. *Building and Environment, 40*(7), 983-995.

Ballinger, J. A. (1988). The 5 star design rating system for thermally efficient, comfortable housing in Australia. *Energy and Buildings, 11*(1-3), 65-72.

Balocco, C., & Colombari, M. (2006). Thermal behavior of interactive mechanically ventilated double glazed facade: Non-dimensional analysis. *Energy and Buildings*, *38*(1), 1-7.

Bartak, M., Dunovská, T., & Hensen, J. (2001). Design Support Simulations for a Double Skin Facade. Proceedings of the 1st Int. Conf. on Renewable Energy in Buildings "Sustainable Buildings and Solar Energy 2001," pp. 126-129, Brno, 15-16 November, Brno University of Technology / Czech Academy of Sciences in Prague, Czech Republic. Retrieved from: http://www.bwk.tue.nl/fago/hensen/publications/01_brno_dskin_design_support.pdf

Bartak, M., Beausoleil-Morrison, I., Clarke, J. A., Denev, J., Drkal, F., Lain, M., et al. (2002). Integrating CFD and building simulation. *Building and Environment, 37*(8-9), 865-871.

Beausoleil-Morrison, I.(2002). The adaptive conflation of computational fluid dynamics with whole-building thermal simulation, *Energy and Buildings*, *34*(9), 857-871.

Boake, T. M., Chatham, A., Harrison, K., & Lum, K. (2003). Doubling up II. *Canadian Architect, 48*(8), 38-39.

Bouchet, B., & Fontoynont, M. (1996). Day-lighting of underground spaces: Design rules. *Energy and Buildings*, *23*(3), 293-298.

Burek, S. A. M., & Habeb, A. (2007). Air flow and thermal efficiency characteristics in solar chimneys and trombe walls. *Energy and Buildings*, *39*(2), 128-135.

Calderaro, V., & Agnoli, S. (2007). Passive heating and cooling strategies in an approaches of retrofit in rome. *Energy and Buildings, 39*(8), 875-885.

Cen, X.-R., Zhan, J.-M., Yang, S.-C., Ma, Y. (2008). CFD simulation and optimization design of double skin facade *Zhongshan Daxue Xuebao/Acta Scientiarum Natralium Universitatis Sunyatseni, 47* (SUPPL.2), pp. 18-21.

Cetiner, I., & Özkan, E. (2005). An approach for the evaluation of energy and cost efficiency of glass facades.*Energy & Buildings*, *37*(6), 673-684. doi:10.1016/j.enbuild.2004.10.007.

Champagne, C. (2002). Computational Fluid Dynamics and Double Skin Facades. Assignment for the Architectural Engineering Computer Labs, Pennsylvania State University, USA. Retrieved from: http://www.arche.psu.edu/courses/ae597J/Champage-Hw1.pdf

Chan, A.L.S., Chow, T.T., Fong, K.F., Lin, Z. (2009). Investigation on energy performance of double skin facade in Hong Kong. *Energy and Buildings, 41* (11), pp. 1135-1142.

Chandra, S., et al. (1986). Cooling with ventilation, Solar Energy Research Institute, Golden Co.

CIBSE- Chartered Institution of Building Services Engineers, . (1997).*Natural ventilation in non-domestic buildings*. Chartered Institution of Building Services Engineers.

Chow, W. K., Hung, W. Y., Gao, Y., Zou, G., & Dong, H. (2007). Experimental study on smoke movement leading to glass damages in double-skinned facade. *Construction and Building Materials, 21*(3), 556-566.

Chow, W. K., & Hung, W. Y. (2006). Effect of cavity depth on smoke spreading of double-skin facade. *Building and Environment, 41*(7), 970-979.

Chow, W. K. (1996). Application of computational fluid dynamics in building services engineering. *Building and Environment, 31*(5), 425-436.

Chou, S. K., Chua, K. J., & Ho, J. C. (2009). A study on the effects of double skin facades on the energy management in buildings. *Energy Conservation and Management, 50* (9): 2275-2281.

Crespo, A.M.L. History of the Double Skin Facades. Retrieved from the web: http://envelopes.cdi.harvard.edu/envelopes/content/resources/PDF/doubleskins.pdf

Daniels, Klaus. (1998) Low-tech light-tech high-tech : building in the information age Basel ; Birkäuser

Davenport A.G. (1965). Proceedings of the conference on wind effects on buildings and structures, vol 1. HMSO.

Dawson, L. (2005). Banking on Frankfurt. *Architectural Review, 217*(1299), 40-40.

De Dear, R. J., & Brager, G. S. (2002). Thermal comfort in naturally ventilated buildings: Revisions to ASHRAE standard 55. *Energy and Buildings, 34*(6), 549-561.

Di Maio, F., & van Paassen, A.H.C. (2000). Second skin facade simulation with Simulink code. International symposium air conditioning in high rise buildings (Shanghai).

Ding, W., Hasemi, Y., & Yamada, T. (2005). Natural ventilation performance of a double-skin facade with a solar chimney. *Energy & Buildings, 37*(4), 411-418.

Djunaedy, E., Hensen, J.L.M., & Loomans, M.G.L.C. (2002). Towards a Strategy for Airflow Simulation in Building Design Center for Building & Systems TNO - TU/e. Technische Universiteit Eindhoven, the Netherlands. Retrieved from: http://sts.bwk.tue.nl/erdj/papers/roomvent2002.pdf

Djuric, N., Novakovic, V., & Frydenlund, F. (2008). Heating system performance estimation using optimization tool and BEMS data. *Energy and Buildings, 40*(8), 1367-1376.

Dorigati, R. (2005). Effetto urbano/New bayer HQ,leverkusen. *L'Arca*, (207), 2-11.

Duarte N, et al. (2001). An interferometric study of free convection at a window glazing with a heated venetian blind. HVAC&R Research, *7*(2):169–84.

Etheridge, D., Mat. (1996) Building ventilation: theory and measurement Chichester ; John Wiley & Sons.

Faggembauu D., Costa M., Soria M., and and Oliva A.(2003). *Numerical analysis of the thermal behaviour of ventilated glazed facades in Mediterranean climates. Part I: development and validation of a numerical model.* Solar Energy. *75*(3), 217-228.

Fanger, P.O. 1970. *Thermal Comfort*. Copenhagen: Danish Technical Press.

Farías, O., Jara, F., & Betancourt, R. (2008). Theoretical and experimental study of the natural draft in chimneys of buildings for domestic gas appliances. *Energy and Buildings, 40*(5), 756-762.

Fluent 6.2 User's Guide. 2001. Fluent Inc.

Fuliotto, R., Cambuli, F., Mandas, N., Bacchin, N., Manara, G., Chen, Q. (2010). Experimental and numerical analysis of heat transfer and airflow on an interactive building facade. *Energy and Buildings, 42* (1), pp. 23-28.

Gan, G. (1998). A parametric study of Trombe walls for passive cooling of buildings. *Energy and Buildings, 27*(1), 37-43.

Gan, G. (1995). Numerical investigation of local thermal discomfort in offices with displacement ventilation. *Energy and Buildings, 23*(2), 73-81.

Gavan, V., Woloszyn, M., Kuznik, F., Roux, J.-J. (2010). Experimental study of a mechanically ventilated double-skin facade with Venetian sun-shading device: A full-scale investigation in controlled environment. *Solar Energy*, *84*(2), pp. 183-195.

Givoni, B. (1981). Conservation and the use of integrated-passive energy systems in architecture. *Energy and Buildings, 3*(3), 213-227.

Givoni, Baruch. (1998) Climate considerations in building and urban design /New York : Van Nostrand Reinhold.

Gosselin, J. R., & Chen, Q. (2008). A computational method for calculating heat transfer and airflow through a dual-airflow window. *Energy and Buildings, 40*(4), 452-458.

Gratia, E., & De Herde, A. (2007a). Are energy consumptions decreased with the addition of a double-skin? *Energy and Buildings, 39*(5), 605-619.

Gratia, E., & De Herde, A. (2007b). Greenhouse effect in double-skin facade. *Energy and Buildings, 39*(2), 199-211.

Gratia, E., & De Herde, A. (2007c). Guidelines for improving natural daytime ventilation in an office building with a double-skin facade. *Solar Energy, 81*(4), 435-448.

Gratia, E., & De Herde, A. (2007a). The most efficient position of shading devices in a double-skin facade. *Energy and Buildings, 39*(3), 364-373.

Gratia, E. (2004a). Is day natural ventilation still possible in office buildings with a double-skin facade? *Building and Environment, 39*(4), 399.

Gratia, E., & De Herde, A. (2004b). Natural cooling strategies efficiency in an office building with a double-skin facade. *Energy & Buildings, 36*(11), 1139-1152.

Gratia, E., & De Herde, A. (2004c). Optimal operation of a south double-skin facade. *Energy & Buildings, 36*(1), 41.

Gratia, E., and De Herde, A. (2004d). Natural ventilation in a double-skin facade. *Energy and Buildings, 36*(2), 137-146

Haase, M., Amato, A. (2009). A study of the effectiveness of different control strategies in double skin facades in warm and humid climates. *Journal of Building Performance Simulation, 2* (3), pp. 179-187.

Haase, M., da Silva, F. Marques and Amato, A. (2009). Simulation of ventilated facades in hot and humid climates. *Energy & Buildings, 41*(4): 361-373

Haase, M., & Amato, A. (2008). Ventilated airflow windows for comfort in a hot and humid climate. *International Journal of Ventilation, 7*(2), 113-124.

Haggag, M. A. (2007). Building skin and energy efficiency in a hot climate with particular reference to Dubai, UAE. *1st International Conference on Energy and Sustainability, ENERGY 2007, 105* (287-2970.

Hamza, N. (2008). Double versus single skin facades in hot arid areas. *Energy and Buildings, 40*(3), 240-248.

Hamza, N., & Underwood, C. (2005). "CFD supported modeling of double skin facades in hot arid climates", 9th International IBPSA Conference Building Simulation 2005, *Vol. 1,* Montreal (Canada). 365-372.

Hanby, V. I., Cook, M. J., Infield, D. G., Ji, Y., Loveday, D. L., Mei, L., et al. (2008). Nodal network and CFD simulation of airflow and heat transfer in double skin facades with blinds. *Building Services Engineering Research and Technology, 29*(1), 45-59.

Hasselaar, B. L. H. (2006). Climate adaptive skins: Towards the new energy-efficient facade. *1st International Conference on the Management of Natural Resources, Sustainable Development and Ecological Hazards, RAVAGE OF THE PLANET 2006, RAV06,* Bariloche. *, 99* 351-360.

Hensen, J. (2003). Paper Preparation Guide and Submission Instruction for Building Simulation 2003 Conference, Eindhoven, Netherlands.

Hensen, J., & Augenbroe, G. (2004). Performance simulation for better building design. *Energy and Buildings, 36*(8), 735-736.

Hernandez, M. T. (2006). *Cfd simulation of a double skin facade model* [Short-term Research Report].

Hien, W. N., Liping, W., Chandra, A. N., Pandey, A. R., & Xiaolin, W. (2005). Effects of double glazed facade on energy consumption, thermal comfort and condensation for a typical office building in Singapore. *Energy & Buildings, 37*(6), 563-572.

Hill, D. (2007). David Adjaye's MCA/Denver opens. *Architectural Record, 195*(12), 34-34.

Hoseggen, R., Wachenfeldt, B. J., & Hanssen, S. O. (2008). Building simulation as an assisting tool in decision making. Case study: With or without a double-skin facade? *Energy and Buildings, 40*(5), 821-827.

Huckemann, V., Kuchen, E., Leão, M., Leão, E.F.T.B. (2010). Empirical thermal comfort evaluation of single and double skin facades. *Building and Environment, 45*(4), pp. 976-982.

Janssens, A., & Hens, H. (2007). Effects of wind on the transmission heat loss in duo-pitched insulated roofs: A field study. *Energy and Buildings, 39*(9), 1047-1054.

Jenkins, D., Liu, Y., & Peacock, A. D. (2008). Climatic and internal factors affecting future UK office heating and cooling energy consumptions. *Energy and Buildings, 40*(5), 874-881.

Jiru, T. E., & Haghighat, F. (2008). Modeling ventilated double skin facade: A zonal approach. *Energy and Buildings, 40*(8), 1567-1576.

Jones, J., & West, A. W. (2001). Natural ventilation and collaborative design. *ASHRAE Journal, 43*(11), 46-51.

Kaluarachchi, Y., Jones, K., James, P., Jentsch, M., Bahaj, A. S., Clements-Croome, B., et al. (2005). Building facades: Sustainability, maintenance and refurbishment. *Engineering Sustainability, 158*(2), 89-95.

Khan, N., Su, Y., & Riffat, S. B. (2008). A review on wind driven ventilation techniques. *Energy and Buildings, 40*(8), 1586-1604.

Knowles, R. L. (2003). The solar envelope: Its meaning for energy and buildings. *Energy and Buildings, 35*(1), 15-25.

Kuznik, F., & Rusaouen, G. (2007). Numerical prediction of natural convection occurring in building components: A double-population lattice Boltzmann method. *Numerical Heat Transfer; Part A: Applications, 52*(4), 315-335.

Lechner, N. (2009). *Heating, cooling, lighting: design methods for architects*. Hoboken, New jersey: Wiley.

Li, D. H. W., & Lam, J. C. (2000). Solar heat gain factors and the implications to building designs in subtropical regions. *Energy and Buildings, 32*(1), 47-55.

Liddament, MW. (1992). The role and application of ventilation effectiveness in design. Proceedings of International Symposium on Room Air Convection and Ventilation Effectiveness, University of Tokyo, 59-75.

Lou, W., Li, H., Wei, K., Chen, Y., & Li, H. (2008). Wind tunnel test study on wind pressure distribution on double-skin facades of high-rise buildings with typical shapes. *Harbin Gongye Daxue Xuebao/Journal of Harbin Institute of Technology, 40*(2), 296-301.

Lou, W., Hu, W., Wang, W. (2009). Numerical analyses for scale effect on wind pressure of double-skin facades and its mechanism. *Tongji Daxue Xuebao/Journal of Tongji University, 37* (10), pp. 1291-1295+1301.

Manz, H., & Frank, T. (2005). Thermal simulation of buildings with double-skin facades. *Energy & Buildings, 37*(11), 1114-1121.

Manz, H. (2003). Numerical simulation of heat transfer by natural convection in cavities of facade elements. *Energy & Buildings, 35*(3), 305.

Marques da Silva, F., & Glória Gomes, M. (2008). Gap inner pressures in multi-story double skin facades. *Energy and Buildings, 40*(8), 1553-1559.

Masoso, O. T., & Grobler, L. J. (2010). The dark side of occupants' behavior on building energy use. *Energy and Buildings, 42*(2), 173-177.

Ménézo, C., Fossa, M., & Leonardi, E. (2007). An experimental investigation of free cooling by natural convection of vertical surfaces for building integrated photovoltaic (BIPV) applications. *1st International Conference on Thermal Issues in Emerging Technologies, Theory and Applications; Proceedings - ThETA1,* Cairo. 125-131.

Mitchell, J.W., Beckman, W.A. (1995). Instructions for IBPSA Manuscripts, SEL, University of Wisconsin, Madison, WI.

Murakami, S. 1992. *New scales for ventilation efficiency and their application based on numerical simulation of room airflow,* In: Proceedings of International Symposium on Room Air Convection and Ventilation Effectiveness, University of Tokyo, 22-38.

Navvab, M. (2005). Full scale testing and computer simulation of a double skin facade building. 9th International IBPSA Conference Building Simulation 2005, Vol 2, Montreal (Canada). 831-838.

Navvab, M., Varodompum, J., & Arch, M. (2006). Thermal performance of a double skin façade using full scale testing, computer simulation and actual building. *ASME International Solar Energy Conference - Solar Engineering 2006,* Denver, CO.

Orme, M.(1999). Applicable Models for Air Infiltration and Ventilation Calculations, AIVC Technical Reports.

Oesterle, E., Leib, R.D., Lutz, G., Heusler, B. (2001). Double skin facades: integrated planning: building physics, construction, aerophysics, air-conditioning, economic viability, Prestel, Munich.

Osanyintola, O. F., Talukdar, P., & Simonson, C. J. (2006). Effect of initial conditions, boundary conditions and thickness on the moisture buffering capacity of spruce plywood. *Energy and Buildings, 38*(10), 1283-1292.

Pappas, A., Zhai, Z. (2008). Numerical investigation on thermal performance and correlations of double skin facade with buoyancy-driven airflow *Energy and Buildings, 40* (4), pp. 466-475.

Park, C., Augenbroe, G., Sadegh, N., Thitisawat, M., & Messadi, T. (2004). Real-time optimization of a double-skin facade based on lumped modeling and occupant preference. *Building and Environment, 39*(8), 939-948.

Park, C., Augenbroe, G., Messadi, T., Thitisawat, M., & Sadegh, N. (2004). Calibration of a lumped simulation model for double-skin facade systems. *Energy & Buildings, 36*(11), 1117-1130.

Pasquay, T. (2004). Natural ventilation in high-rise buildings with double facades, saving or waste of energy. *Energy and Buildings, 36*(4), 381-389.

Platt, G., Li, J., Li, R., Poulton, G., James, G., & Wall, J. (2010). Adaptive HVAC zone modeling for sustainable buildings. *Energy and Buildings, 42*(4), 412-421.

Poirazis, H. (2004). *Double Skin Facades for Office Buildings: Literature review*, Report EBD-R-04/3, Department of Construction and Architecture, Lund University.

Radhi, H. (2008). A systematic methodology for optimizing the energy performance of buildings in Bahrain. *Energy and Buildings, 40*(7), 1297-1303.

Rey, E. (2004). Office building retrofitting strategies: Multicriteria approach of an architectural and technical issue. *Energy & Buildings, 36*(4), 367.

Rijal, H. B., Tuohy, P., Humphreys, M. A., Nicol, J. F., Samuel, A., & Clarke, J. (2007). Using results from field surveys to predict the effect of open windows on thermal comfort and energy use in buildings. *Energy and Buildings, 39*(7), 823-836.

Roth, K., Lawrence, T., Brodrick, J. (2007). Double-skin facades. *ASHRAE Journal*, *49* (10), pp. 70-73.

Saelens, D., Roels, S., & Hens, H. (2008). Strategies to improve the energy performance of multiple-skin facades. *Building and Environment, 43*(4), 638-650.

Saelens, D., Carmeliet, J., & Hens, H. (2003). Energy performance assessment of multiple skin facades. International Journal of HVAC&R Research 9 (2): 167-186. Retrieved from: http://www.bwk.kuleuven.ac.be/bwf/pdf_artikels/I_J_HVACR_DS_2003.pdf

Saelens, D. (2002). Energy Performance Assessments of Single Storey Multiple-Skin Facades. PhD thesis, Laboratory for Building Physics, Department of Civil Engineering, Catholic University of Leuven, Belgium. Retrieved from: http://envelopes.cdi.harvard.edu/envelopes/content/resources/pdf/case_studies/PhD_Dirk_Saelens.pdf

Saelens, D., & Hens, H. (2001). Experimental evaluation of airflow in naturally ventilated active envelopes. *Journal of Thermal Envelope and Building Science, 25*(2), 101-127.

Saelens, D., Carmeliet, J., & Hens, H. (2001). Modeling of Air and Heat Transport in Active Envelopes, Proceedings of ICBEST 2001, International Conference on Building Envelope Systems and technologies, Ottawa, Canada, pp. 243-247.

Safer, N., Woloszyn M., Roux J.J., Kuznik F. (2005). Modeling of the double skin facades for building energy simulation: radiative and convective heat transfers. 9th International IBPSA Conference Building Simulation 2005, Vol. 2, Montreal (Canada). 1067-1074.

Santamouris, M. (2007). *Advances in building energy research.* London Sterling VA: Earthscan.

Scartezzini, J. (2004). Foreword. *Energy and Buildings, 36*(4), 319-320.

Shang-Shiou L. (2001). A Protocol to Determine the Performance of South Facing Double Glass Facade System A Preliminary Study of Active/Passive Double Glass Facade Systems, master thesis, Virginia Polytechnic Institute and State University.

Stec, W. J., & Paassen, A. H. C. v. (2005). Symbiosis of the double skin facade with the HVAC system. *Energy & Buildings, 37*(5), 461-469.

Stec, W.J., Van Paassen, A.H.C., Maziarz, A. (2005). Modeling the double skin facade with plants. *Energy and Buildings, 37*(5), pp. 419-427.

Stec, W., & Passen D. (2003). Defining the performance of the double skin facade with the use of the simulation model. 8th International IBPSA Conference Building Simulation 2003, Vol 2, Eindhoven (Netherlands). 1243-1250.

Stec, W., & van Paassen, D. (2003). Integration of the double skin facade with the buildings. 674-681.

Straube, J. F., & Straaten, R.V. (2002). The technical Merit of Double Skin Facades for office Buildings in cool humid climates. School of Architecture, University of Waterloo, USA. Retrieved from: http://www.civil.uwaterloo.ca/beg/Downloads/DoubleFacadesPaper.pdf

Subject index of volume 37. (2005). *Energy and Buildings, 37*(12), 1292-1304.

Subject index of volume 38, (2006). *Energy and Buildings, 38*(12), 1495-1509.

Suma, A. B., Van Herwijnen, F., & Voorthuis, J. C. T. (2007). 3D adaptable building skin: Adaptive space as a guide through a corridor. *International Journal of Space Structures, 22*(3), 169-177.

Supic, P. (1982). Vernacular architecture: A lesson of the past for the future. *Energy and Buildings, 5*(1), 43-54.

Szokolay, S. V. S. V. (1980). *Environmental science handbook for architects and builders*, Construction Press, Lancaster.

Szucs, E. (1980). *Similitude and Modeling*. Amsterdam, Netherlands: Elsevier Scientific Publishing Co.

Tanaka, H., Okumiya, M., Tanaka, H., Young Yoon, G., Watanabe, K. (2009). Thermal characteristics of a double-glazed external wall system with roll screen in cooling season. *Building and Environment, 44*(7), pp. 1509-1516.

Ternoey, S. and Bicle L., Robbins C., Busch R., and McCord, K.(1985). The design of energy responsive commercial buildings. New York: Wiley &Sons.

Todorovic, B., & Maric, B. The influence of double facades on building heat losses and cooling loads. Faculty of Mechanical Engineering, Belgrade University, Belgrade, Yugoslavia.

Torres, M., Alavedra P., Guzman A., 2007, "Double skin facades-cavity and exterior openings dimensions for saving energy in a Mediterranean climate." IBPSA Proceedings of Building Simulation 2007, 198-205.

Turner, F. (2009). Air tightness in buildings. *ASHRAE Journal*, *51*(4), 5. Retrieved from Academic Search Premier database.

Von Grabe, J. (2002). A prediction tool for the temperature field of double facades. *Energy & Buildings, 34*(9), 891.

Wei, J., Zhao, J., & Chen, Q. (2010). Energy performance of a dual airflow window under different climates. *Energy and Buildings, 42*(1), 111-122.

Wenting Ding, & Hasemi, Y. (2006). Smoke control through a double-skin facade used for natural ventilation. *ASHRAE Transactions, 112*(1), 181-188.

Wigginton, M. (1996). *Glass in architecture*, Phaidon Press, London, England.

Wigginton, M. (2002). *Intelligent skins*, Butterworth-Heinemann, Oxford.

Wittkower, W. J. (1984). Climate-adapted building in Israel: How far has our knowledge influenced building practice? *Energy and Buildings, 7*(3), 269-280.

Wong, P.C., Prasad, D., Behnia, M. (2008). A new type of double-skin facade configuration for the hot and humid climate. *Energy and Buildings, 40*(10), pp. 1941-1945.

Xamán, J., Álvarez, G., Lira, L., & Estrada, C. (2005). Numerical study of heat transfer by laminar and turbulent natural convection in tall cavities of facade elements. *Energy & Buildings, 37*(7), 787-794.

Xu, X., & Yang, Z. (2008). Natural ventilation in the double skin facade with venetian blind. *Energy and Buildings, 40*(8), 1498-1504.

Yellamraju, V. (2004). *Evaluation and design of double-skin facades for office buildings in hot climates* (Master's thesis), Available from Dissertations and Theses database at Texas A&M University.

Yılmaz, Z., & Çetintaş, F. (2005). Double skin facade's effects on heat losses of office buildings in istanbul. *Energy & Buildings, 37*(7), 691-697.

Zerefos, S. C. (2007). On the performance of double skin facades in different environmental conditions. *International Journal of Sustainable Energy*, *26*(4), 221-229.

Zhang, M., Lou, W., & Chen, Y. (2008). Wind pressure distribution and gust factor on double-skin facades of high-rise building with rectangular shape. *Zhejiang Daxue Xuebao (Gongxue Ban)/Journal of Zhejiang University (Engineering Science), 42*(1), 54-59.

Zhou, J., Chen, Y. (2010). A review on applying ventilated double-skin facade to buildings in hot-summer and cold-winter zone in China. *Renewable and Sustainable Energy Reviews, 14* (4), pp. 1321-1328.

Zhou, J., Chen, Y.-M., Fang, S.-S. (2009). Ventilated double skin facades in hot-summer and cold-winter zones in China *Hunan Daxue Xuebao/Journal of Hunan University Natural Sciences, 36* (SUPPL.), pp. 160-162.

Zöllner, A., Winter, E. R. F., & Viskanta, R. (2002). Experimental studies of combined heat transfer in turbulent mixed convection fluid flows in double-skin-facades. *International Journal of Heat and Mass Transfer, 45*(22), 4401-4408.

Zrudlo, L. R. (1988). A climatic approach to town planning in the arctic. *Energy and Buildings, 11*(1-3), 41-63.

APPENDIX A: Drawings

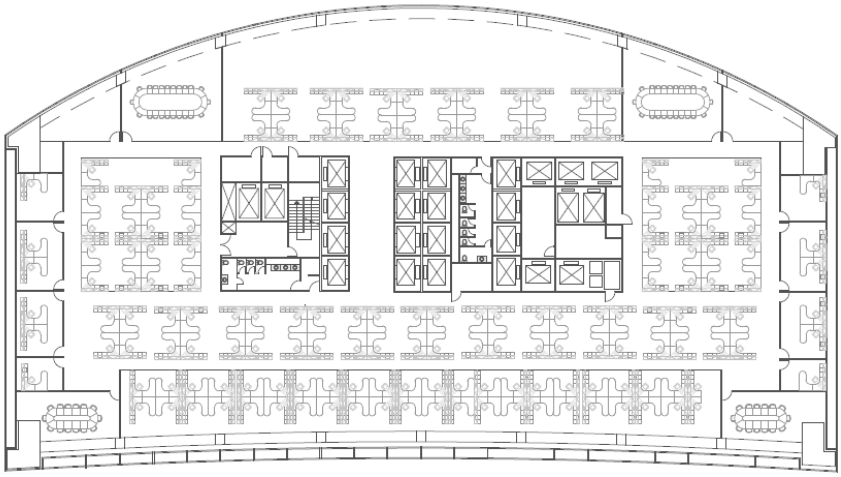

Plan of the office building designed in Chicago

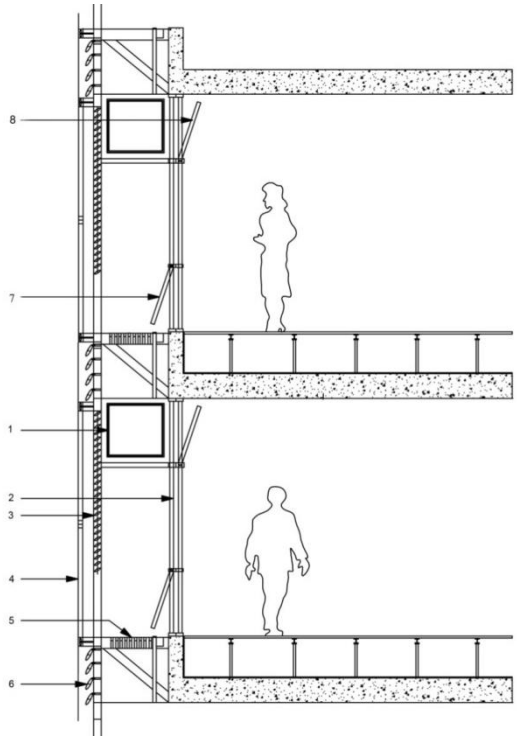

Section of new DSF

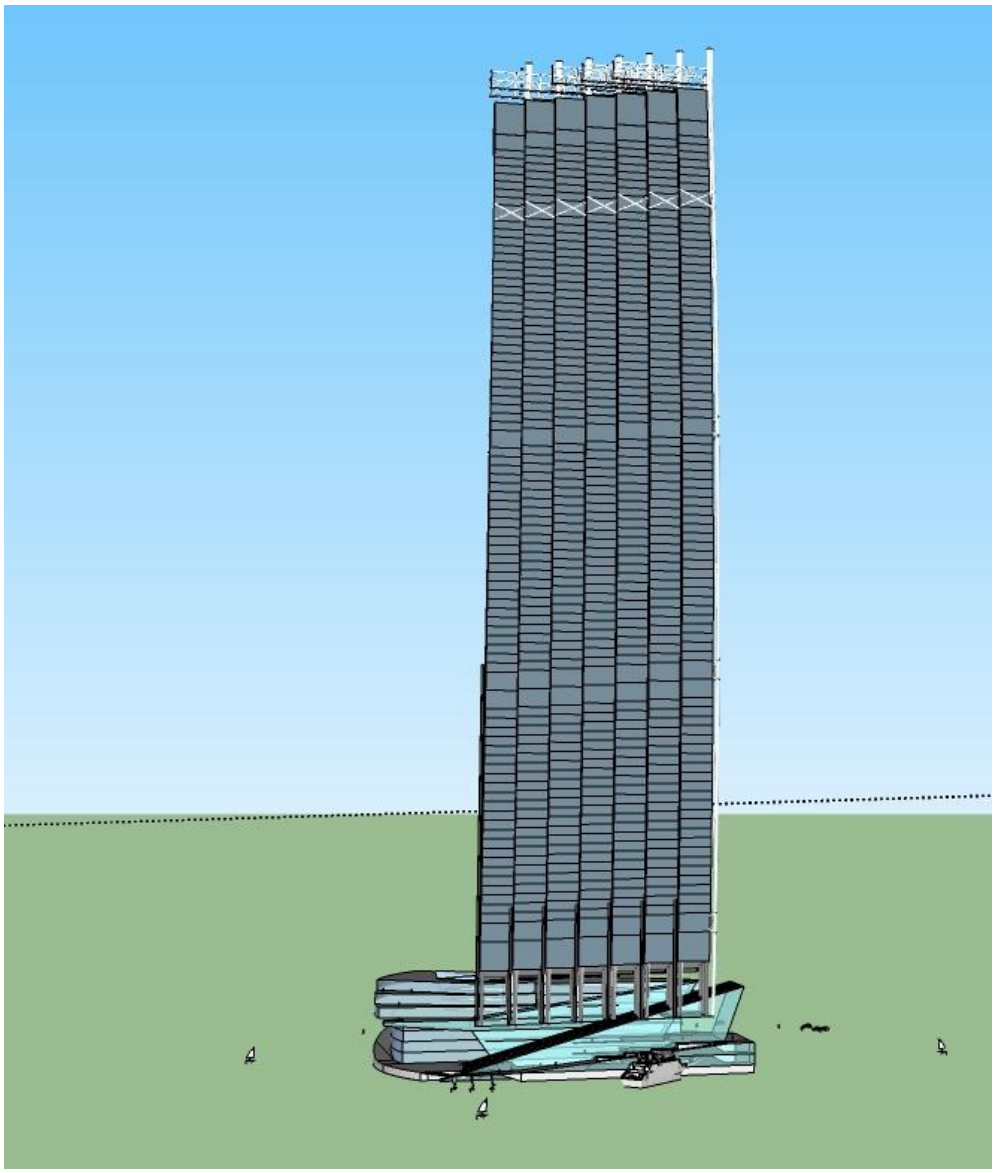

Elevation view of the shaft-corridor DSF configuration of office building

APPENDIX B: Weather data

Statistics for USA_IL_Chicago-Midway.AP.725340_TMY3
Location -- Chicago Midway Ap IL USA
{N 41° 46'} {W 87° 45'} {GMT -6.0 Hours}
Elevation -- 186m above sea level
Standard Pressure at Elevation -- 99110Pa
Data Source -- TMY3

WMO Station 725340

- Using Design Conditions from "Climate Design Data 2009 ASHRAE Handbook"

- If the design condition source is ASHRAE, the design conditions are carefully generated
- from a period of record (typically 30 years) to be representative of that location and
- be suitable for use in heating/cooling load calculations. If the source is not ASHRAE,
- please consult the referenced source for the reasoning behind the data.

- Monthly Statistics for Dry Bulb temperatures °C

	Jan	Feb	Mar	Apr	May	Jun	Jul	Aug	Sep	Oct	Nov	Dec
Maximum	16.0	15.5	23.8	26.0	29.0	34.0	40.0	34.0	34.0	31.0	24.0	14.0
Day:Hour	2:18	23:15	14:14	7:16	9:15	13:15	24:15	1:12	6:14	4:13	1:12	31:01
Minimum	-21.0	-27.3	-11.2	3.0	4.0	9.0	15.0	15.0	10.0	2.0	-4.0	-18.0
Day:Hour	30:04	3:07	1:07	17:04	2:24	4:19	28:04	20:05	23:02	23:04	30:04	24:05
Daily Avg	-5.7	-1.8	4.9	11.2	13.9	21.4	25.2	24.2	21.2	13.5	8.6	-0.8

- Maximum Dry Bulb temperature of 40.0°C on Jul 24
- Minimum Dry Bulb temperature of -27.3°C on Feb 3

- Average Hourly Statistics for Dry Bulb temperatures °C

	Jan	Feb	Mar	Apr	May	Jun	Jul	Aug	Sep	Oct	Nov	Dec
0:01- 1:00	-5.9	-3.6	3.1	9.4	11.9	18.6	22.7	22.0	18.9	12.0	6.7	-1.7
1:01- 2:00	-6.1	-3.9	2.7	9.3	11.5	18.1	22.3	21.7	18.5	11.5	6.5	-1.9
2:01- 3:00	-6.3	-4.1	2.4	8.9	11.2	17.9	21.9	21.4	18.1	11.2	6.1	-2.0
3:01- 4:00	-6.7	-4.4	2.2	8.6	11.0	17.5	21.5	21.0	17.9	10.9	5.8	-2.4
4:01- 5:00	-7.0	-4.5	2.2	8.4	11.0	17.4	21.3	20.8	17.6	10.5	5.7	-2.7
5:01- 6:00	-7.2	-4.4	1.9	8.7	11.6	18.3	22.1	21.1	17.6	10.3	5.5	-2.8

6:01- 7:00	-7.5	-4.3	2.2	9.6	12.5	19.4	23.6	22.1	18.2
10.7	5.4	-2.9							
7:01- 8:00	-7.4	-3.8	3.6	10.6	13.4	20.6	25.0	23.5	19.9
11.9	6.3	-2.5							
8:01- 9:00	-7.2	-2.8	4.7	11.6	14.3	21.4	26.1	24.6	21.2
13.4	7.8	-1.7							
9:01-10:00		-6.4	-1.5	5.9	12.2	15.0	22.5	26.9	25.6
22.3	14.6	9.4	-0.9						
10:01-11:00		-5.7	-0.3	6.7	12.6	15.9	23.5	27.8	26.5
23.6	15.5	11.0	0.1						
11:01-12:00		-5.0	0.5	7.2	13.3	16.6	23.8	28.7	27.2
24.4	15.9	12.0	0.7						
12:01-13:00		-4.5	0.9	8.0	13.6	16.9	24.6	28.6	27.4
25.1	16.5	12.6	1.2						
13:01-14:00		-4.2	1.4	8.3	14.0	17.2	25.0	28.7	27.6
25.2	16.9	12.9	1.3						
14:01-15:00		-4.0	1.6	7.9	14.1	17.0	24.9	28.5	27.5
24.8	16.9	12.6	1.4						
15:01-16:00		-4.1	1.2	7.8	13.9	16.6	24.7	28.2	27.4
24.6	16.4	12.0	1.1						
16:01-17:00		-4.5	0.7	7.3	13.1	16.0	24.3	27.5	26.7
23.8	15.7	10.8	0.5						
17:01-18:00		-4.6	-0.1	6.2	12.5	15.2	23.8	26.9	25.7
22.9	14.9	10.0	0.3						
18:01-19:00		-4.7	-0.7	5.4	11.8	14.2	22.9	26.1	24.7
22.1	14.2	9.2	0.1						
19:01-20:00		-5.0	-1.2	5.0	11.4	13.4	22.0	24.8	24.2
21.4	14.0	8.7	-0.1						
20:01-21:00		-5.2	-1.7	4.6	10.8	12.9	21.3	24.4	23.6
20.8	13.3	8.2	-0.4						
21:01-22:00		-5.5	-2.0	4.3	10.5	12.6	20.8	24.0	23.4
20.2	13.1	7.8	-0.8						
22:01-23:00		-5.7	-2.6	4.0	10.2	12.4	20.3	23.7	22.9
19.8	12.7	7.4	-0.9						
23:01-24:00		-6.1	-2.9	3.9	9.9	12.2	19.5	23.1	22.4
19.3	12.2	6.7	-1.4						
Max Hour		15	15	14	15	14	14	14	14
14	15	14	15						
Min Hour		7	5	6	5	5	5	5	5
6	6	7	7						

- Monthly Statistics for Extreme temperatures °C

#Days	Jan	Feb	Mar	Apr	May	Jun	Jul	Aug	Sep
Oct	Nov	Dec							
Max >= 32						4	8	6	4
Max <= 0	21	11	3						
		10							
Min <= 0	30	19	12						
	5	21							
Min <=-18	3	4							
		1							

- Monthly Statistics for Dew Point temperatures °C

Jan	Feb	Mar	Apr	May	Jun	Jul	Aug	Sep
Oct	Nov	Dec						

	Maximum	13.0	15.5	12.7	18.3	20.0	23.0	24.4	24.0	
	23.0	20.0	14.0	11.0						
	Day:Hour	2:16	23:15	20:08	3:09	10:21	11:23	25:21	1:20	
5:20	3:10	1:10	30:24							
	Minimum	-26.0	-32.8	-18.9	-8.0	-8.0	6.0	7.0	7.0	
	3.0	-3.3	-12.0	-24.4						
	Day:Hour	30:03	3:01	2:05	24:20	2:19	3:07	2:11	18:10	
	23:10	15:15	30:13	24:09						
	Daily Avg	-10.8	-6.8	-1.2	5.9	6.9	13.9	16.0	17.0	
	14.8	6.6	0.9	-6.0						

- Maximum Dew Point temperature of 24.4°C on Jul 25
- Minimum Dew Point temperature of -32.8°C on Feb 3

- Monthly Statistics for Relative Humidity %

		Jan	Feb	Mar	Apr	May	Jun	Jul	Aug	
	Sep	Oct	Nov	Dec						
	Maximum		100	100	100	100	100	100	94	94
	100	94	100	100						
	Day:Hour	2:05	7:23	5:07	1:01	1:14	1:01	5:02	13:20	
7:02	12:01	21:05	6:04							
	Minimum	31	25	25	24	25	26	25	28	31
	20	15	34							
	Day:Hour	21:24	18:13	1:17	26:15	3:15	17:18	10:15	18:15	
	12:15	15:14	6:14	20:15						
	Daily Avg	65	68	66	73	65	65	59	66	69
	65	60	67							

- Average Hourly Relative Humidity %

		Jan	Feb	Mar	Apr	May	Jun	Jul	Aug	
	Sep	Oct	Nov	Dec						
	0:01- 1:00	66	73	72	82	74	75	69	77	
78	72	68	71							
	1:01- 2:00	66	73	74	82	74	77	70	78	
79	73	69	71							
	2:01- 3:00	68	72	76	84	76	79	72	79	
80	74	69	71							
	3:01- 4:00	67	75	77	86	77	81	73	79	
80	74	69	71							
	4:01- 5:00	68	75	77	86	77	82	74	80	
81	75	69	72							
	5:01- 6:00	68	75	77	85	75	79	71	79	
81	76	69	71							
	6:01- 7:00	68	76	76	82	72	74	65	74	
79	74	70	72							
	7:01- 8:00	69	75	71	76	68	70	59	68	
73	70	68	71							
	8:01- 9:00	68	72	66	71	65	66	55	63	
68	65	64	69							
	9:01-10:00		65	68	62	67	62	62	52	
59	64	60	58	66						

	10:01-11:00		61	62	59	68	60	58	48
57	60	57	52	63					
	11:01-12:00		61	60	57	64	57	57	46
53	57	55	48	60					
	12:01-13:00		61	60	55	63	57	55	46
52	54	53	47	59					
	13:01-14:00		61	59	54	62	55	52	45
51	55	52	45	59					
	14:01-15:00		61	59	54	62	54	52	45
51	57	52	46	59					
	15:01-16:00		61	60	55	62	55	52	46
51	58	54	48	61					
	16:01-17:00		64	61	56	64	56	53	49
55	60	57	53	64					
	17:01-18:00		65	64	60	65	57	55	51
58	62	60	56	65					
	18:01-19:00		66	66	64	68	60	58	55
63	65	63	59	65					
	19:01-20:00		67	67	66	69	64	61	60
67	68	64	60	66					
	20:01-21:00		67	70	68	72	67	64	63
71	70	67	61	67					
	21:01-22:00		66	70	69	75	68	67	65
72	72	68	62	68					
	22:01-23:00		66	72	71	78	69	70	66
74	74	69	63	68					
	23:01-24:00		65	72	72	80	71	72	69
76	76	71	66	70					
	Max Hour		8	7	5	5	4	5	5
5	6	6	7	7					
	Min Hour		12	15	14	14	15	15	15
15	13	15	14	15					

- Monthly Indicators for Precipitation/Moisture (kPa)

		Jan	Feb	Mar	Apr	May	Jun	Jul	Aug
	Sep	Oct	Nov	Dec					
		0.3	0.5	0.6	1.0	1.1	1.6	1.7	1.9
1.8	1.0	0.7	0.5						

- Monthly Statistics for Wind Chill/Heat Index temperatures °C **

		Jan	Feb	Mar	Apr	May	Jun	Jul	Aug
	Sep	Oct	Nov	Dec					
	Minimum WC		-37	-46	-25	-8	-5	2	
		-5	-12	-37					
	Day:Hour	6:09	3:07	1:07	16:09	2:06	4:19		
	25:07	29:09	19:08						
	Average WC		-16	-13	-4	2	2	5	
		3	0	-10					
	Avg Del WC		10	10	7	6	5	4	
		4	5	8					
	# Hours WC		723	613	557	270	92	4	
		194	418	679					
	Maximum HI						28	37	40
39	39	32							

	Day:Hour					9:14	13:15	24:11	1:16	6:14	4:13	
	Average HI						28	30	30	31	31	29
	Avg Del HI						1	1	1	2	2	1
	# Hours HI						2	133	186	165	75	34

- **WindChill/HeatIndex Temps -- statistics...only those different from Air Temps

- Monthly Wind Direction % {N=0 or 360,E=90,S=180,W=270}

	Jan	Feb	Mar	Apr	May	Jun	Jul	Aug	Sep	Oct	Nov	Dec
North	9	11	16	15	27	7	16	10	17	20	14	9
NorthEast	6	9	14	23	21	11	21	20	10	8	3	1
East	8	2	10	23	17	11	16	20	9	10	3	3
SouthEast	8	2	2	11	7	7	4	8	4	3	3	3
South	7	7	11	10	5	17	10	9	11	15	15	14
SouthWest	13	19	13	6	3	24	14	19	25	16	26	22
West	22	24	14	6	10	15	13	10	14	9	17	21
NorthWest	26	26	19	7	10	8	6	4	10	19	21	26

- Monthly Statistics for Wind Speed m/s

	Jan	Feb	Mar	Apr	May	Jun	Jul	Aug	Sep	Oct	Nov	Dec
Maximum	11.3	11.8	12.8	14.9	17.0	9.8	11.3	10.8	11.3	9.8	11.3	15.4
Day:Hour	14:16	11:06	20:15	6:14	11:12	15:12	20:13	22:01	6:21	19:10	10:24	12:18
Minimum	0.0	0.0	0.0	0.0	0.0	1.0	0.0	0.0	0.0	0.0	0.0	0.0
Day:Hour	1:02	6:05	3:03	7:04	4:02	8:03	9:01	3:11	2:23	2:16	1:04	2:09
Daily Avg	5.2	5.6	4.7	4.9	4.9	3.9	4.0	4.0	3.6	4.2	4.3	5.2

- Maximum Wind Speed of 17.0 m/s on May 11
- Minimum Wind Speed of 0.0 m/s on Jan 1

- Monthly Statistics for Liquid Precipitation mm

	Jan	Feb	Mar	Apr	May	Jun	Jul	Aug	Sep	Oct	Nov	Dec
Total	17	11	38	141	128	46	44	66	57	12	10	27

- Monthly Statistics for Albedo

	Jan	Feb	Mar	Apr	May	Jun	Jul	Aug	Sep	Oct	Nov	Dec
Average	0.170	0.160	0.150	0.160	0.170	0.160	0.150	0.150	0.180	0.160	0.170	0.180

- Monthly Statistics for Solar Radiation (Direct Normal, Diffuse, Global Horizontal) Wh/m²

	Jan	Feb	Mar	Apr	May	Jun	Jul	Aug	Sep	Oct	Nov	Dec
Direct Avg		2082	2670	2734	3407	4330	4813	5124	4735	4552	3024	3424
2675												
Direct Max		5848	7837	8544	8726	8720	8651	8585	8009	7757	6722	5259
5035												
Day	19	24	3	30	22	17	8	7	4	1	4	29
Diffuse Avg		936	1118	1572	1951	2454	2646	2642	2251	1791	1391	1017
772												
Global Avg		1649	2236	3003	4066	5413	5985	6196	5373	4451	2832	2341
1644												

- Maximum Direct Normal Solar of 8726 Wh/m² on Apr 30

- Average Hourly Statistics for Direct Normal Solar Radiation Wh/m²

	Jan	Feb	Mar	Apr	May	Jun	Jul	Aug	Sep	Oct	Nov	Dec
0:01- 1:00	0	0	0	0	0	0	0	0	0	0	0	0
1:01- 2:00	0	0	0	0	0	0	0	0	0	0	0	0
2:01- 3:00	0	0	0	0	0	0	0	0	0	0	0	0
3:01- 4:00	0	0	0	0	0	0	0	0	0	0	0	0
4:01- 5:00	0	0	0	0	12	43	13	0	0	0	0	0
5:01- 6:00	0	0	1	24	94	146	114	16	0	0	0	0
6:01- 7:00	0	3	66	216	202	247	282	216	142	37	9	0
7:01- 8:00	40	108	217	273	202	305	370	338	309	240	145	30
8:01- 9:00	191	234	282	328	281	370	434	401	402	342	353	263
9:01-10:00		213	305	302	328	299	425	433	449	445	337	422
330												
10:01-11:00		254	334	304	345	375	402	515	490	460	350	491
387												
11:01-12:00		310	311	328	326	457	418	487	444	505	374	507
426												
12:01-13:00		301	313	314	285	446	459	513	495	465	352	478
388												
13:01-14:00		229	335	291	303	450	448	424	453	487	301	437
334												

	14:01-15:00		257	310	250	299	425	408	430	422	476	276	359	307					
	15:01-16:00		219	280	204	289	402	379	395	395	441	291	212	210					
	16:01-17:00		68	129	140	225	332	335	305	348	299	123	10	0					
	17:01-18:00		0	9	36	157	259	273	265	221	105	0	0	0					
	18:01-19:00		0	0	0	8	93	156	145	48	0	0	0	0					
	19:01-20:00		0	0	0	0	0	0	0	0	0	0	0	0					
	20:01-21:00		0	0	0	0	0	0	0	0	0	0	0	0					
	21:01-22:00		0	0	0	0	0	0	0	0	0	0	0	0					
	22:01-23:00		0	0	0	0	0	0	0	0	0	0	0	0					
	23:01-24:00		0	0	0	0	0	0	0	0	0	0	0	0					
	Max Hour*		12	14	12	11*	12	13	11*	13	12	12	12	12					
	Min Hour		1	1	1	1	1	1	1	1	1	1	1	1					

- Monthly Calculated "undisturbed" Ground Temperatures** °C

	Jan	Feb	Mar	Apr	May	Jun	Jul	Aug	Sep	Oct	Nov	Dec
0.5 m	3.4	-1.4	-2.7	-1.5	4.9	12.1	18.9	23.8	25.3	23.0	17.4	10.4
2.0 m	7.7	3.2	1.1	1.0	4.4	9.4	14.7	19.2	21.6	21.2	18.0	13.2
4.0 m	10.5	7.0	4.9	4.3	5.5	8.4	12.0	15.5	17.8	18.4	17.0	14.2

- **These ground temperatures should NOT BE USED in the GroundTemperatures object to compute building floor losses.
- The temperatures for 0.5 m depth can be used for GroundTemperatures:Surface.
- The temperatures for 4.0 m depth can be used for GroundTemperatures:Deep.
- Calculations use a standard soil diffusivity of 2.3225760E-03 {m**2/day}

- Monthly Heating/Cooling Degree Days/Hours

	Jan	Feb	Mar	Apr	May	Jun	Jul	Aug	Sep	Oct	Nov	Dec
HDD base 10C	487	330	179	22	4	0	0	0	0	19	83	334
HDD base 18C	734	554	406	206	133	36	0	0	7	166	281	581
CDD base 10C	1	0	21	59	123	341	471	441	335	129	43	0
CDD base 18C	0	0	0	2	5	138	223	193	103	28	0	0
CDH base 20C	0	0	32	80	146	2528	3997	3239	1759	562	65	0

	CDH base 23C		0	0	1	13	34	1396	2185
1531	773	246	2	0					
	CDH base 27C		0	0	0	0	6	433	665
417	216	51	0	0					

- 1964 annual cooling degree-days (10°C baseline)
- 1458 annual heating degree-days (10°C baseline)

- 691 annual cooling degree-days (18°C baseline)
- 3106 annual heating degree-days (18°C baseline)

- Climate type "Dfa" (Köppen classification)**
- Humid continental (hot summer, cold winter, no dry season, lat. 30-60°N)
- Unbearably hot dry periods in summer, but passive cooling is possible
- **Note that the Köppen classification shown here is derived algorithmically from the source weather data.
- It may not be indicative of the long term climate for this location.

- Climate type "5A" (ASHRAE Standards 90.1-2004 and 90.2-2004 Climate Zone)**
- Cool - Humid, Probable Köppen classification=Dfa, Humid Continental (Warm Summer)
- **Note that the ASHRAE classification shown here is derived algorithmically from the source weather data.
- It may not be indicative of the long term climate for this location.

- Typical/Extreme Period Determination

- Summer is Jun:Aug
  Extreme Summer Week (nearest maximum temperature for summer)
  Extreme Hot Week Period selected: Jul 20:Jul 26, Maximum Temp= 40.00°C, Deviation=|12.812|°C
  Typical Summer Week (nearest average temperature for summer)
  Typical Week Period selected: Aug 24:Aug 30, Average Temp= 23.62°C, Deviation=| 0.079|°C

- Winter is Dec:Feb
  Extreme Winter Week (nearest minimum temperature for winter)
  Extreme Cold Week Period selected: Jan 27:Feb 2, Minimum Temp= -27.30°C, Deviation=|11.760|°C
  Typical Winter Week (nearest average temperature for winter)
  Typical Week Period selected: Dec 15:Dec 21, Average Temp= -2.77°C, Deviation=| 0.655|°C

- Autumn is Sep:Nov
  Typical Autumn Week (nearest average temperature for autumn)
  Typical Week Period selected: Oct 13:Oct 19, Average Temp= 14.45°C, Deviation=| 0.597|°C

- Spring is Mar:May
  Typical Spring Week (nearest average temperature for spring)
  Typical Week Period selected: Apr 19:Apr 25, Average Temp= 9.97°C, Deviation=| 0.303|°C

APPENDIX C: DesignBuilder's input -Shaft-corridor type facade

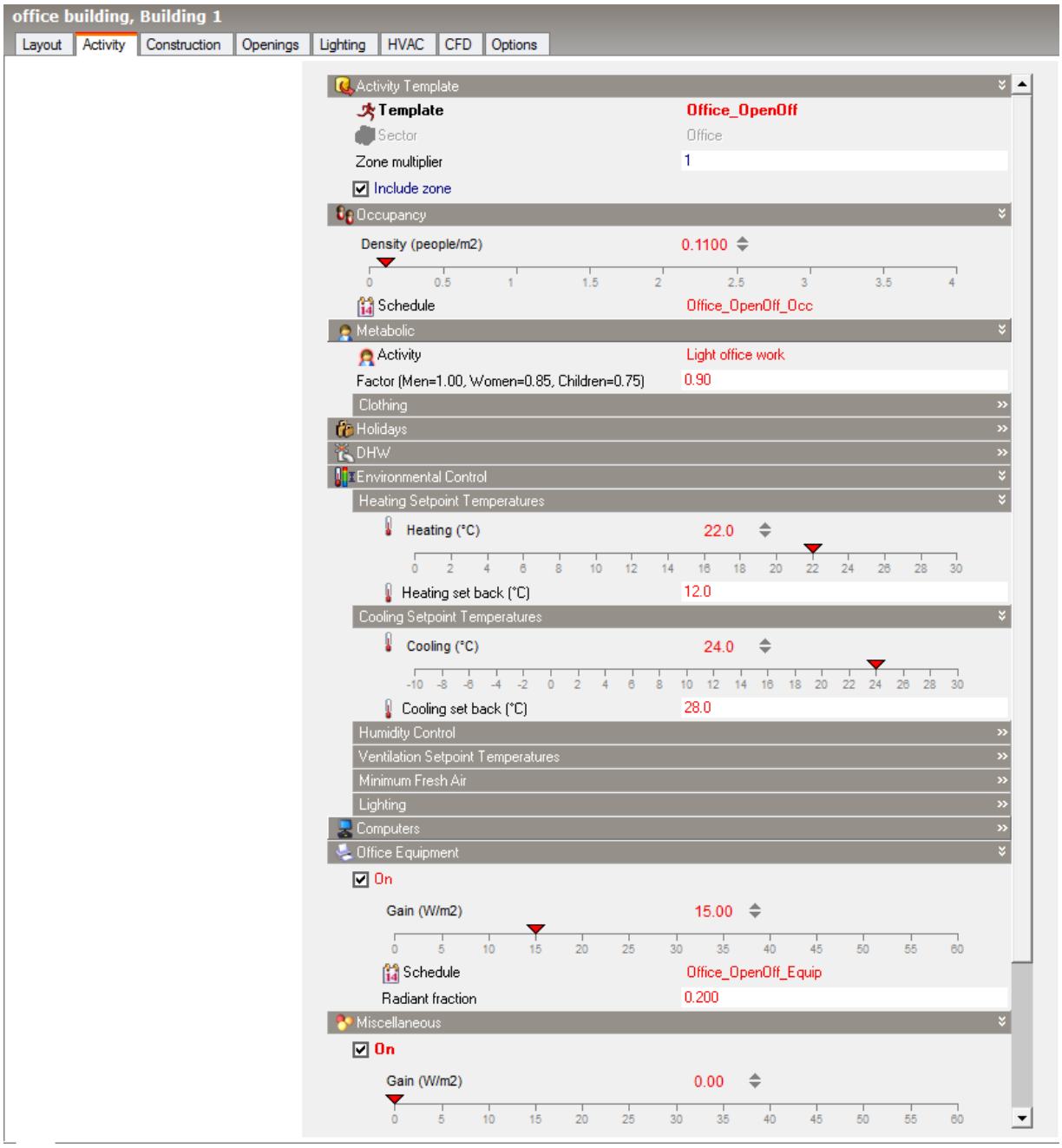

Activity settings

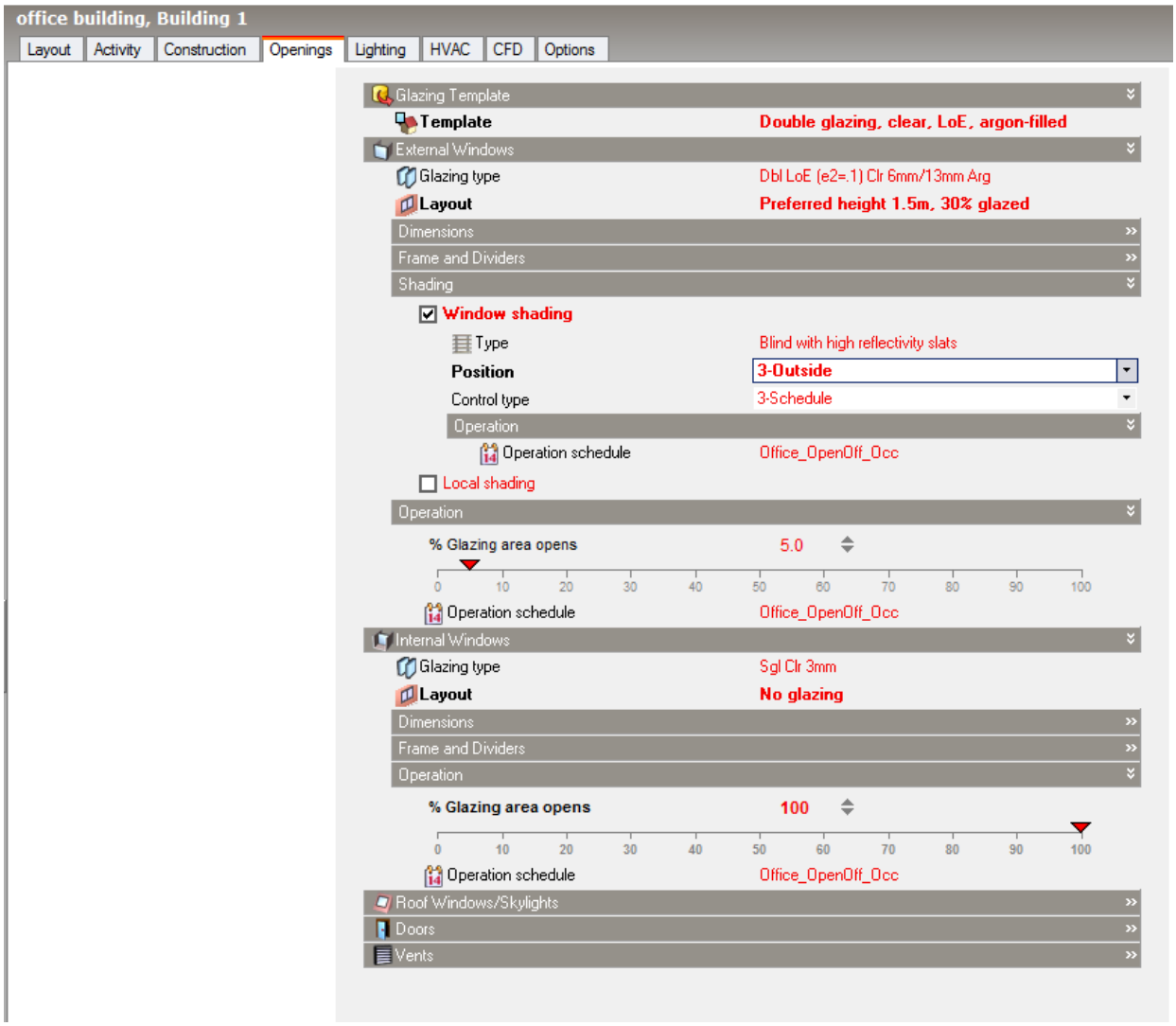

Opening settings

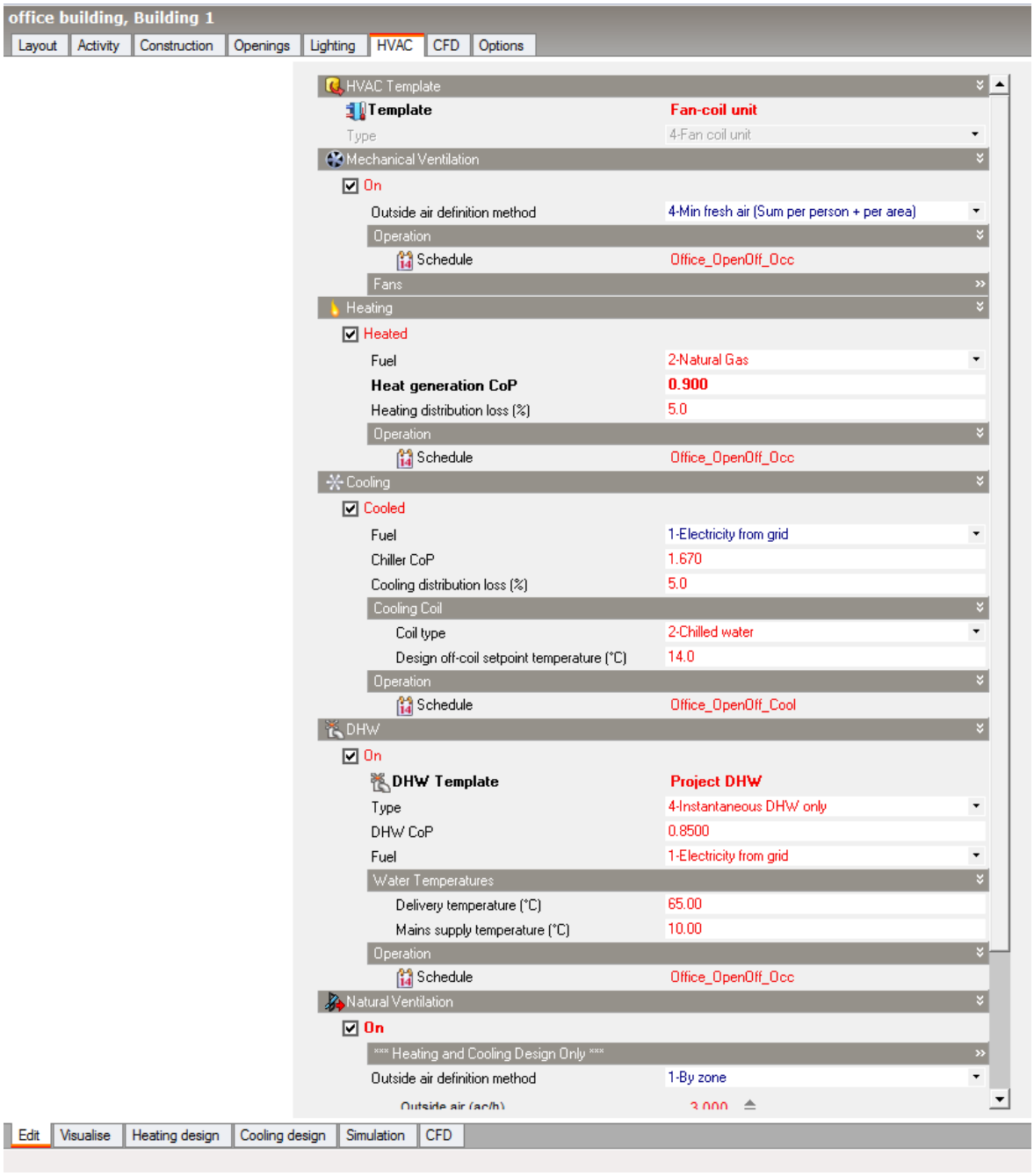

HVAC setting

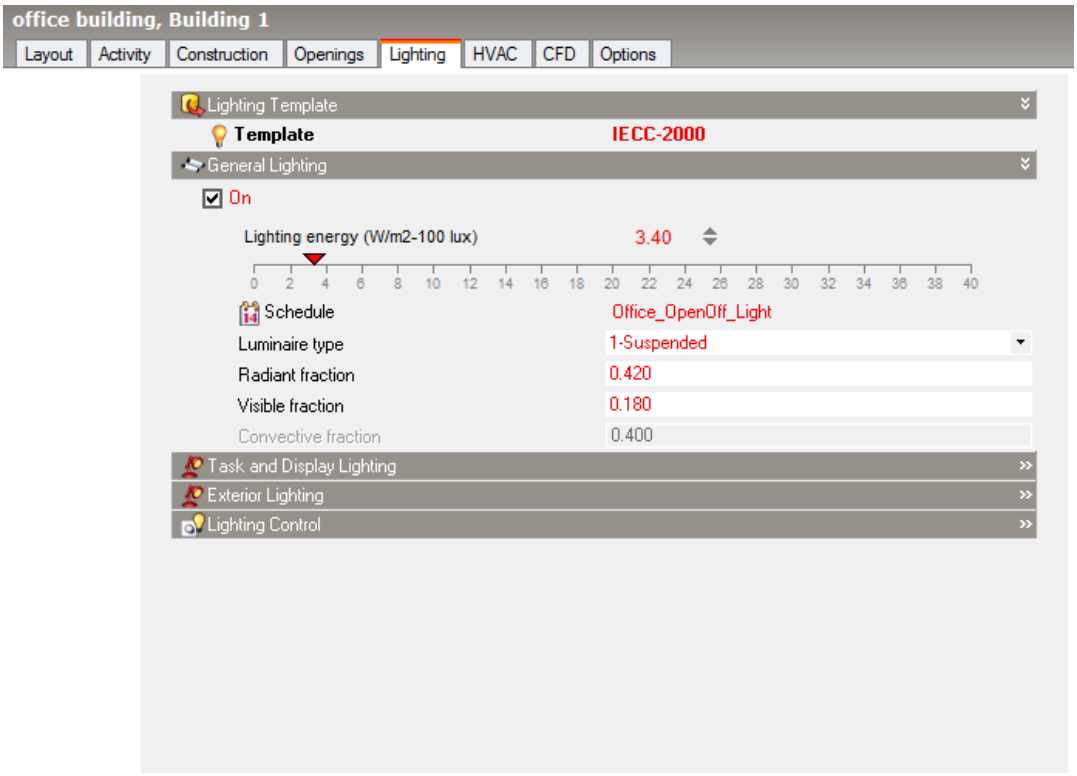

Lightings

For the other alternatives just the geometry has been changed, the rest of the inputs remains the same.

APPENDIX D: PMV graphs of all 36 simulations

General parameters: One parameter constant and show the correlation for the other two parameters

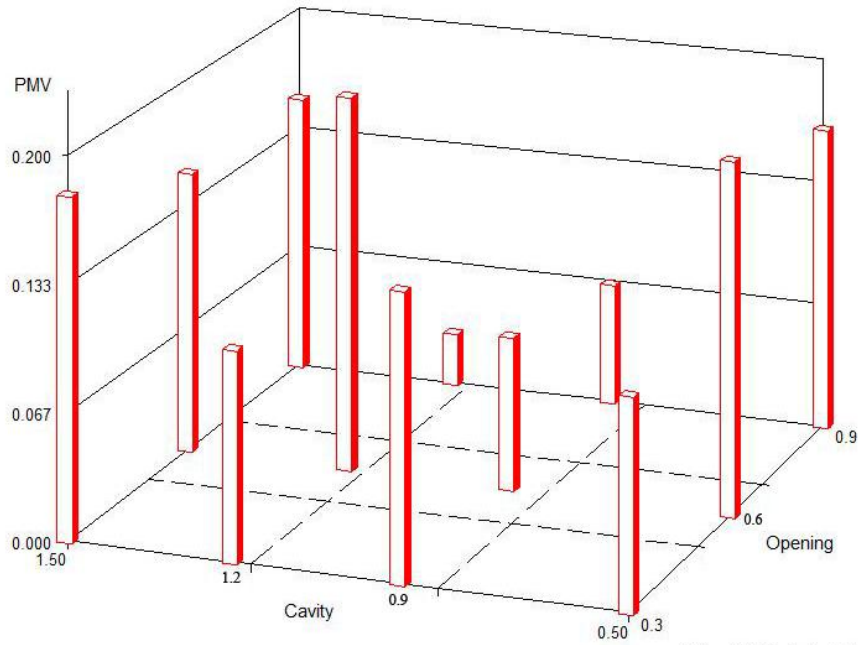

Shaft Height 5-Story

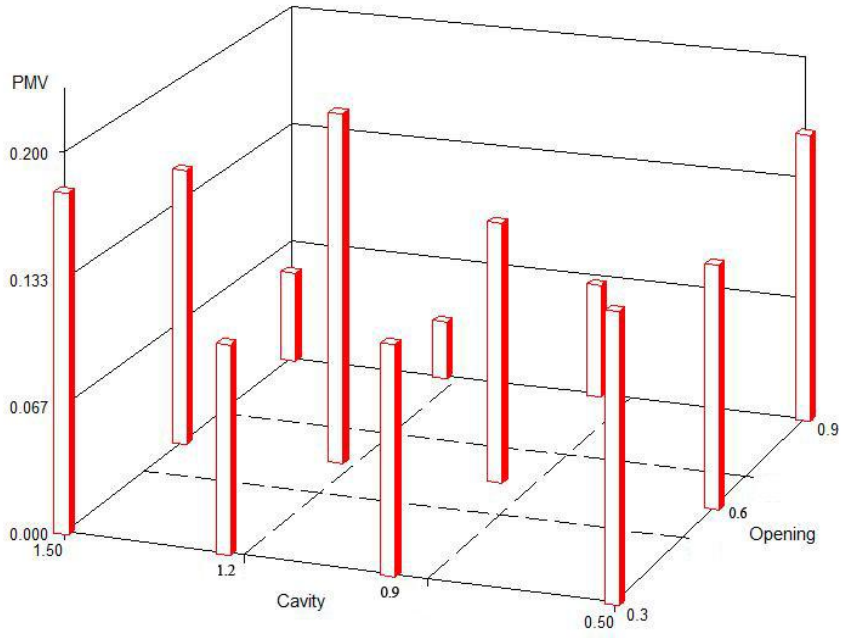

Shaft Height 7-Story

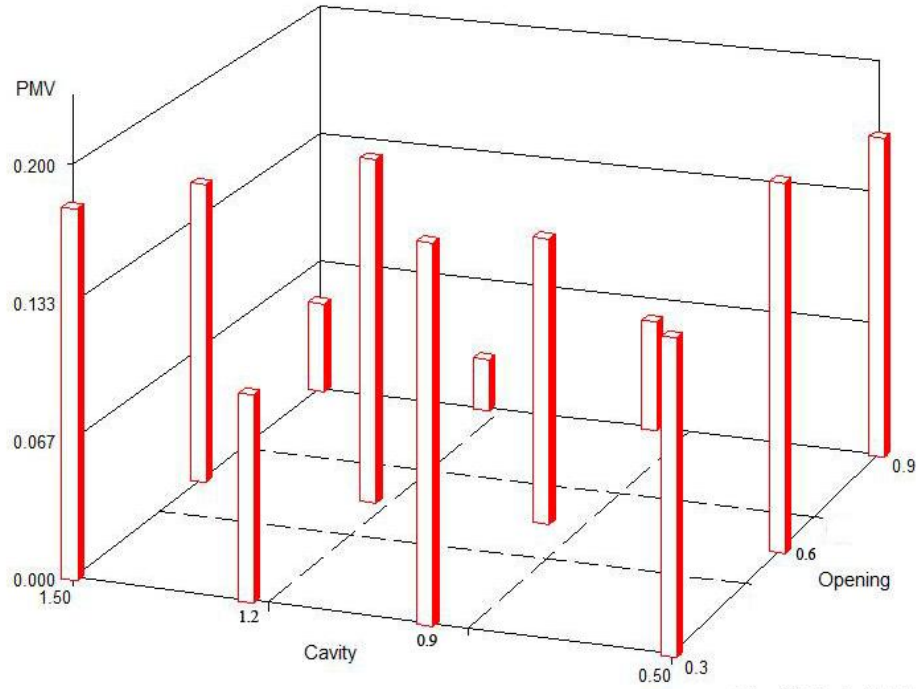

Shaft Height 9-Story

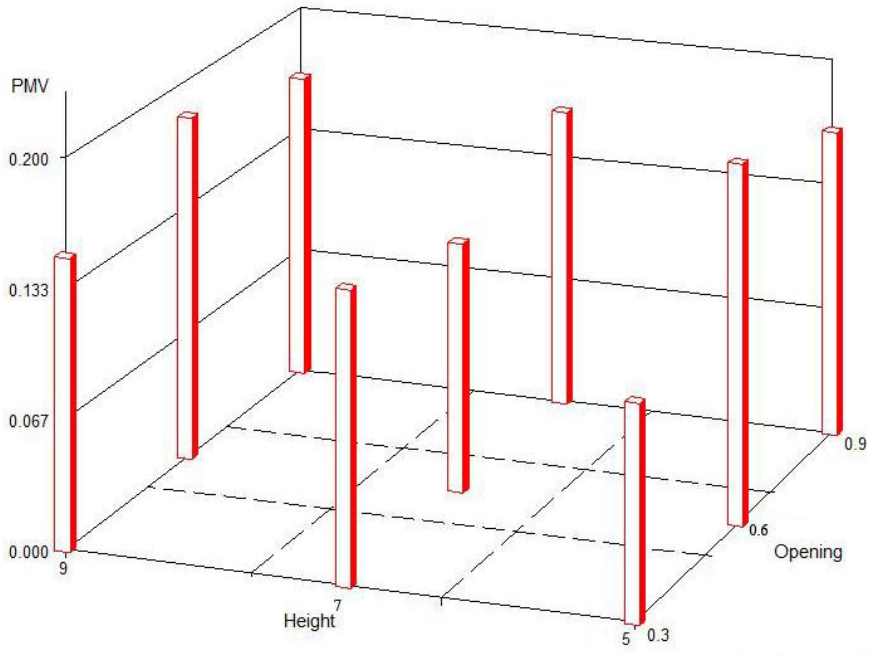

Cavity Depth 0.5m

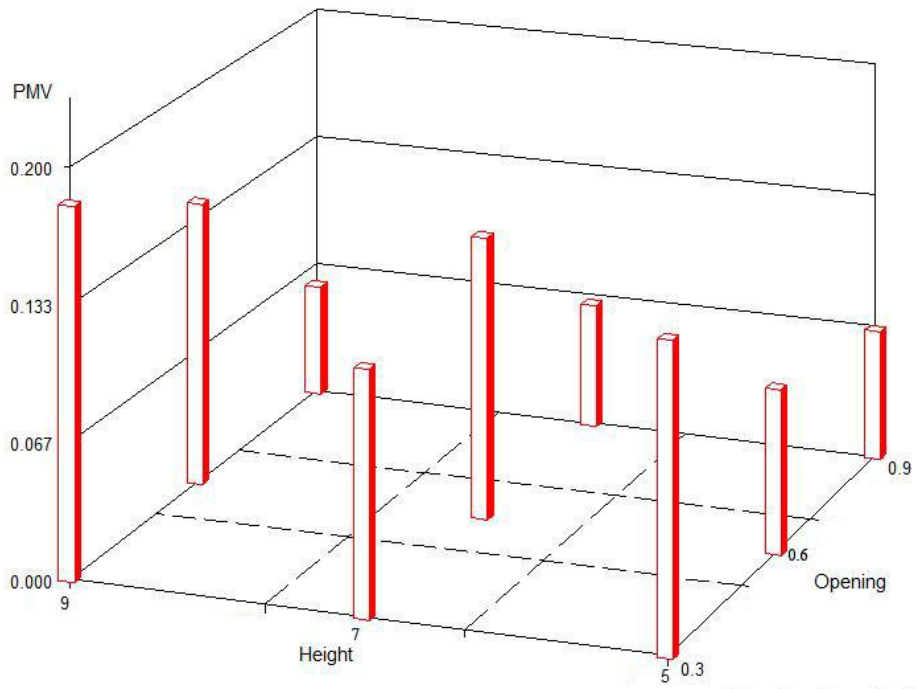

Cavity Depth 0.9m

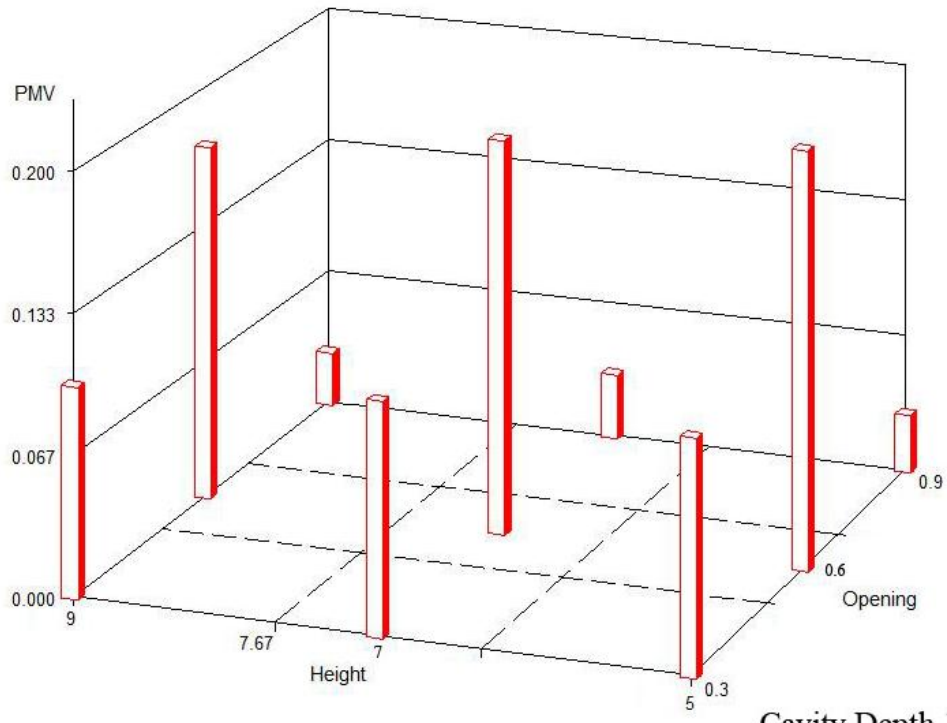

Cavity Depth 1.2m

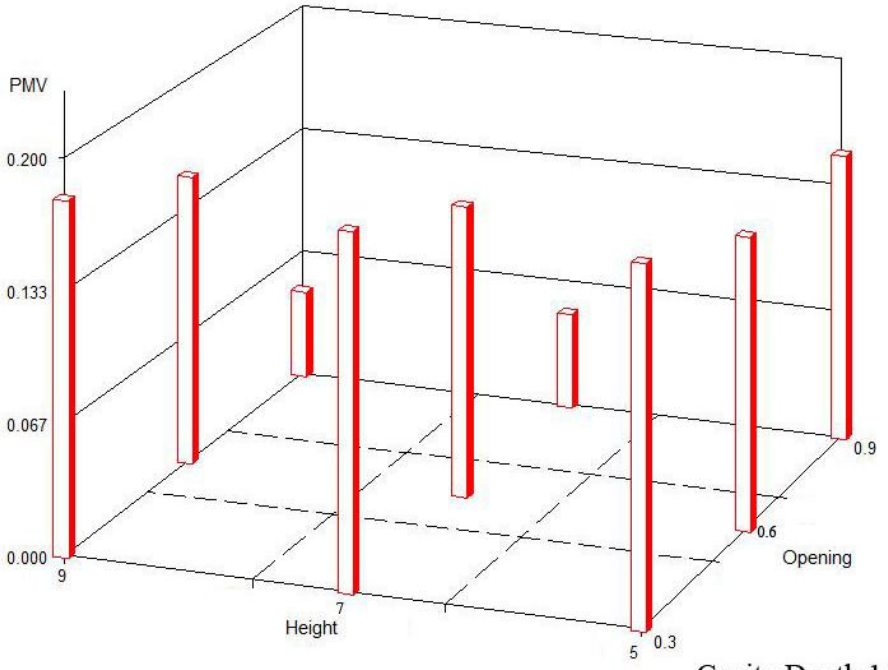

Cavity Depth 1.5m

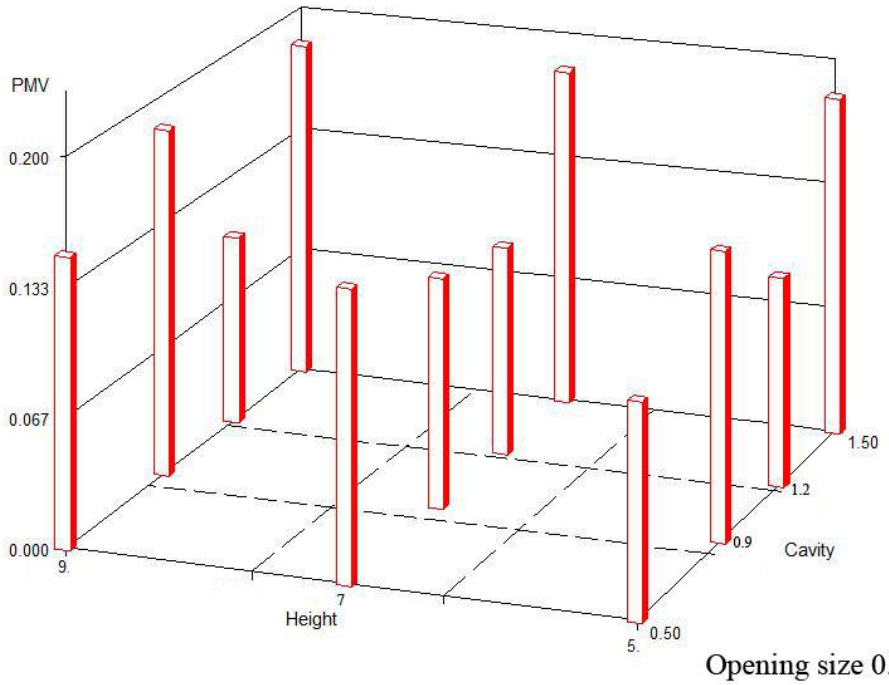

Opening size 0.3 m

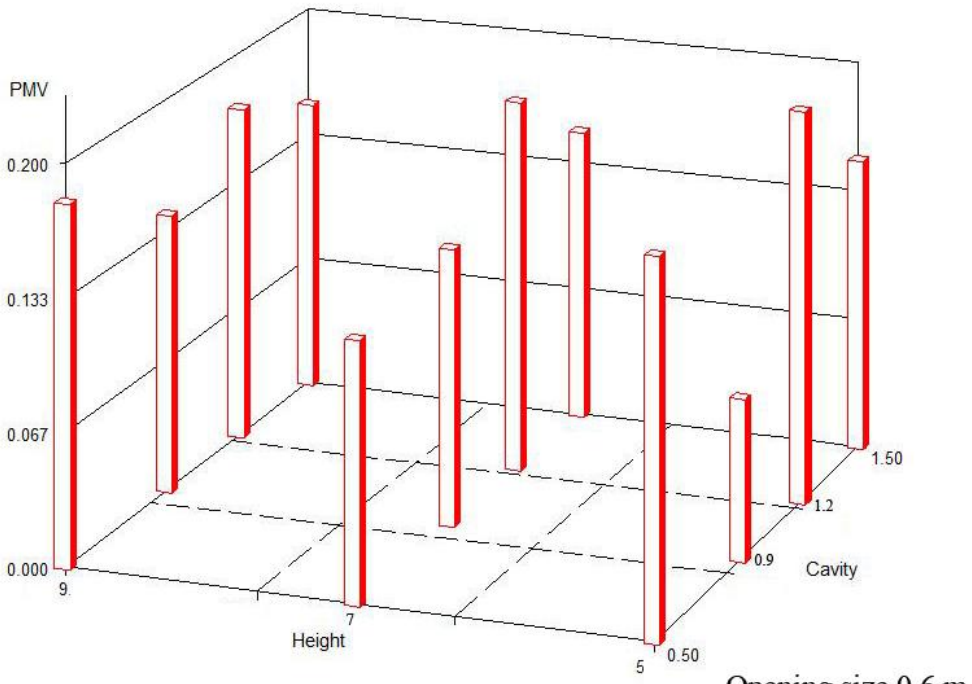

Opening size 0.6 m

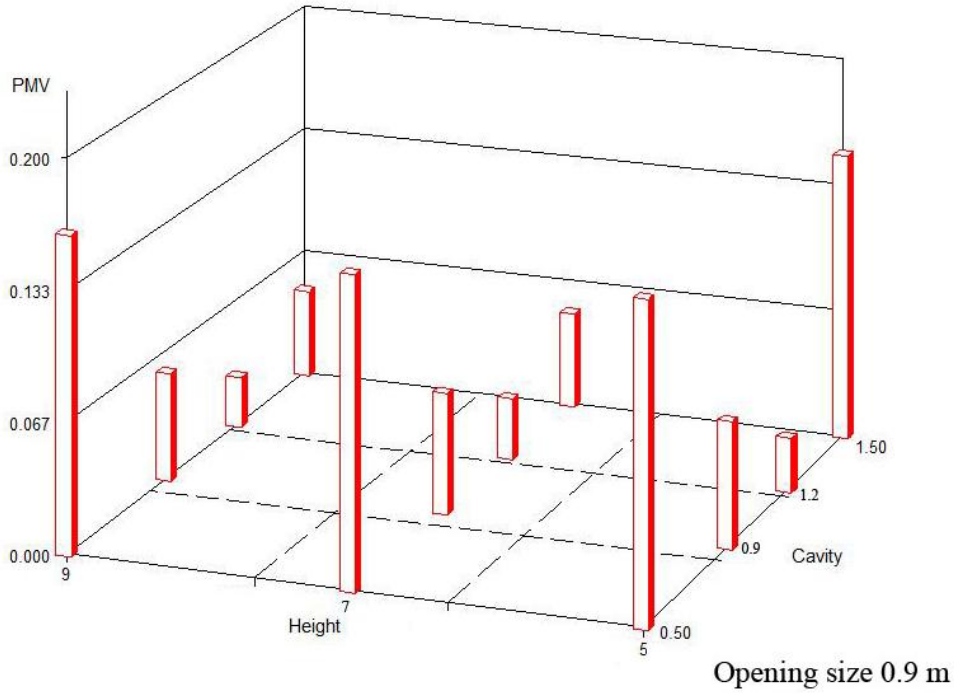

Opening size 0.9 m

APPENDIX E: Impact of parameters on cooling and heating energy

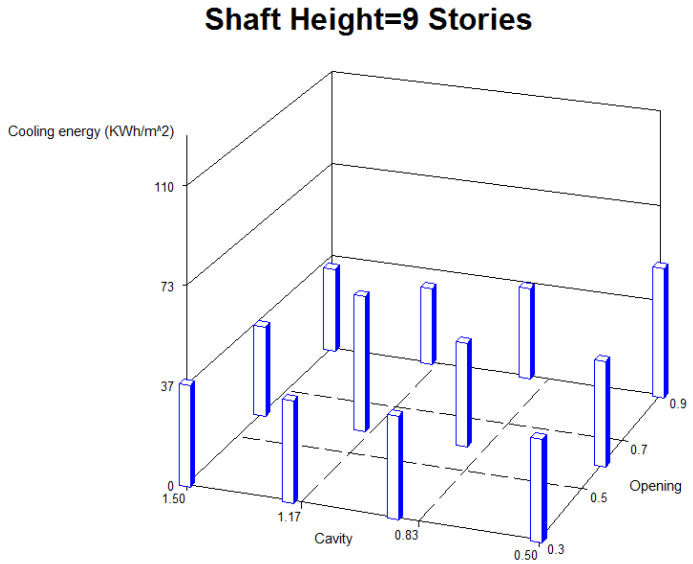

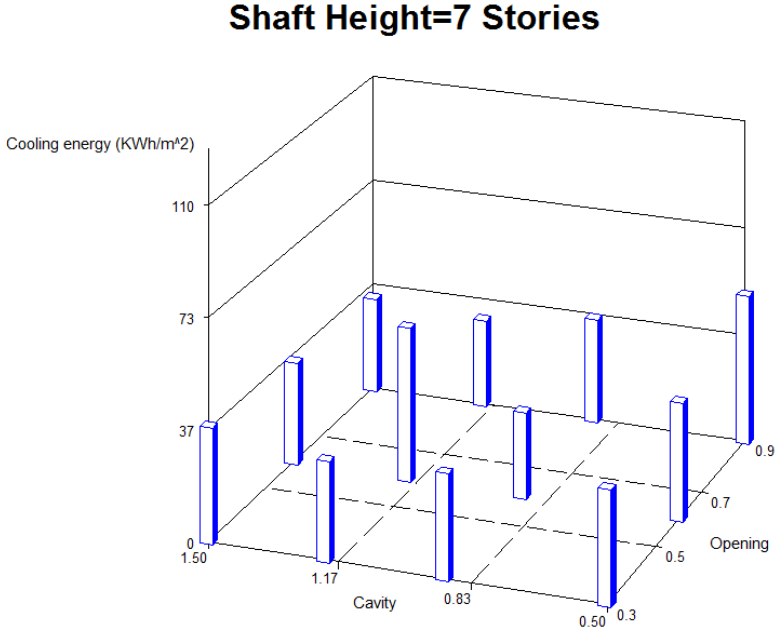

Shaft Height=5 Stories

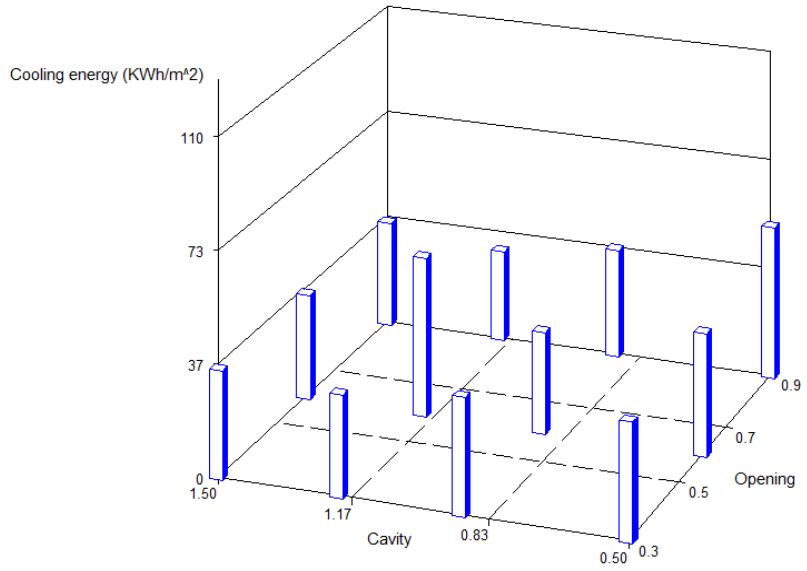

Opening Size=0.9 m

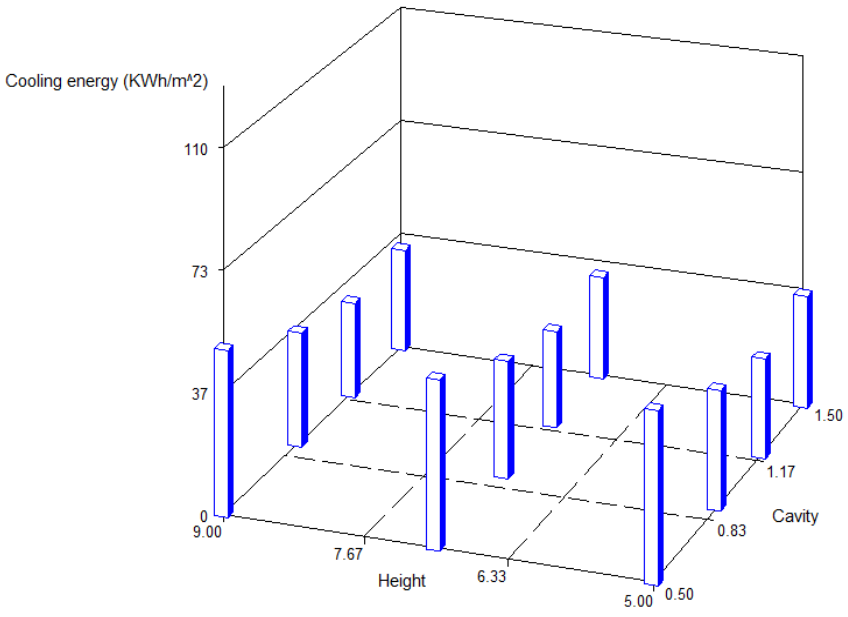

Opening Size=0.3 m

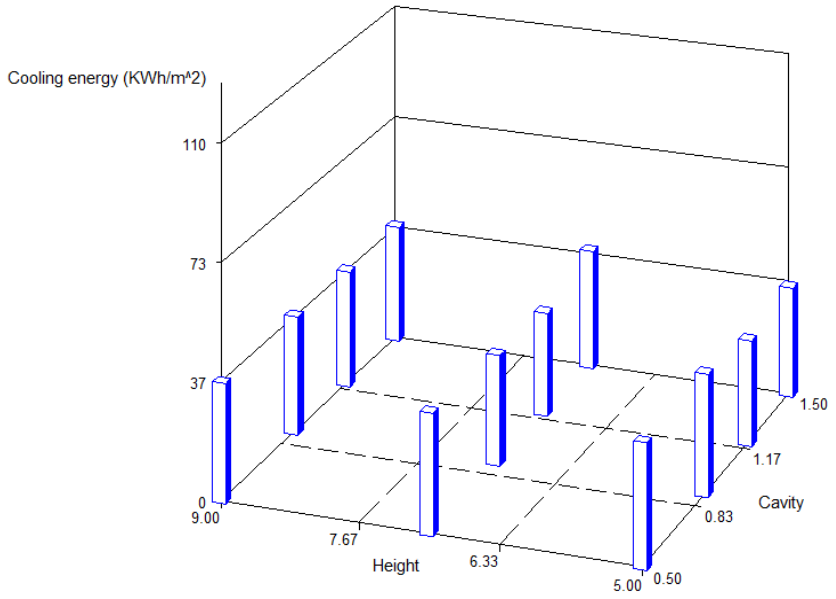

Opening Size=0.6 m

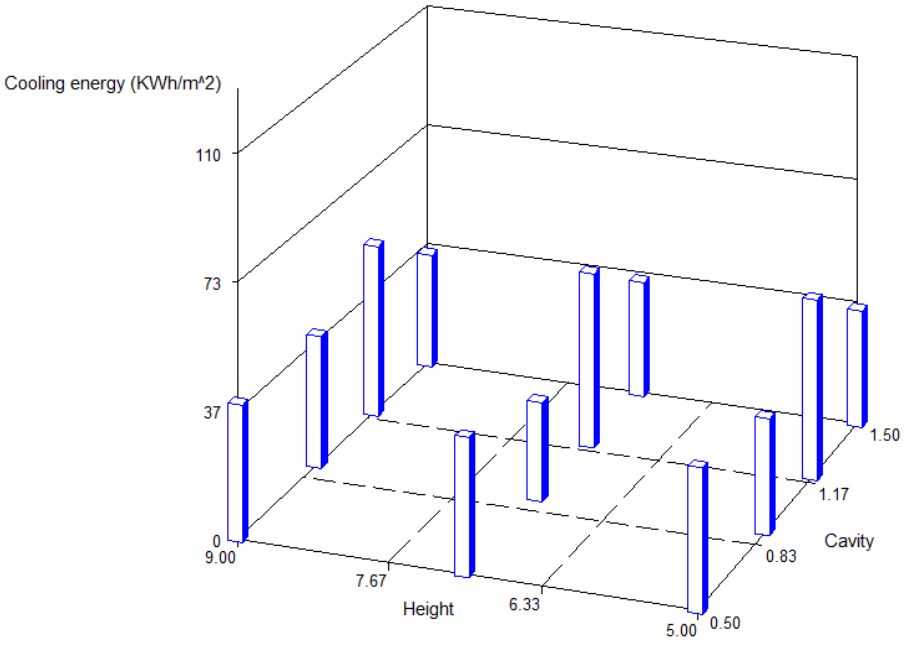

Cavity Depth=1.2 m

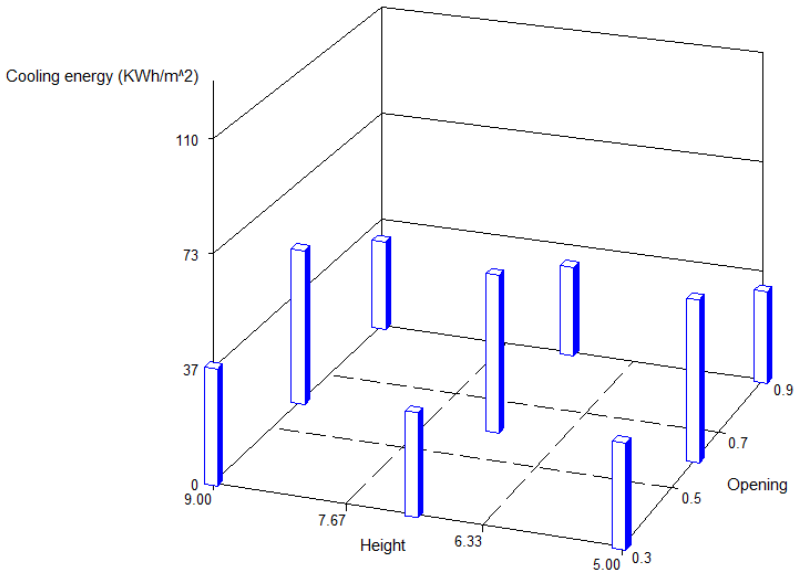

Cavity Depth=1.5 m

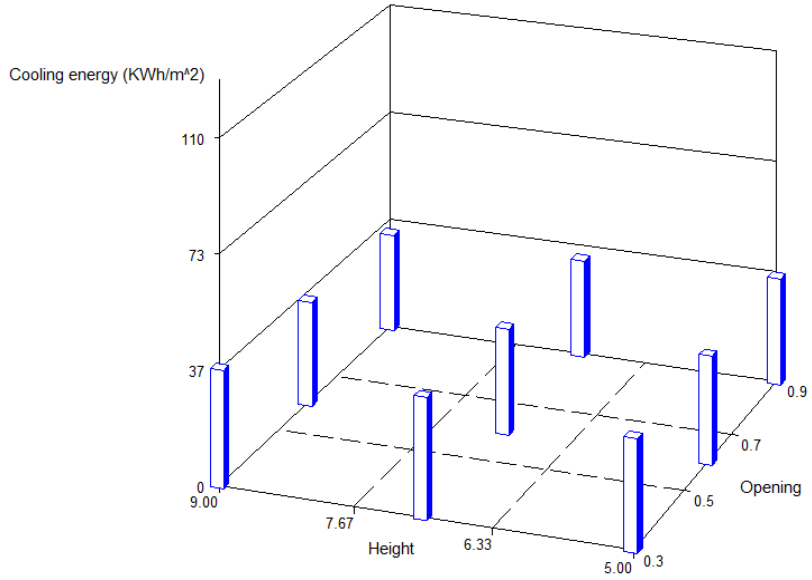

Cavity Depth=0.9 m

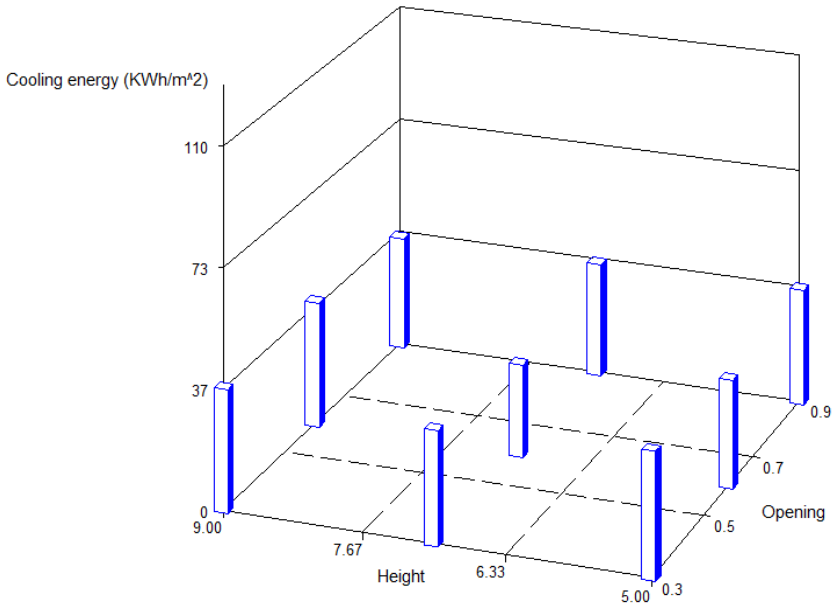

Shaft Height=7 Stories

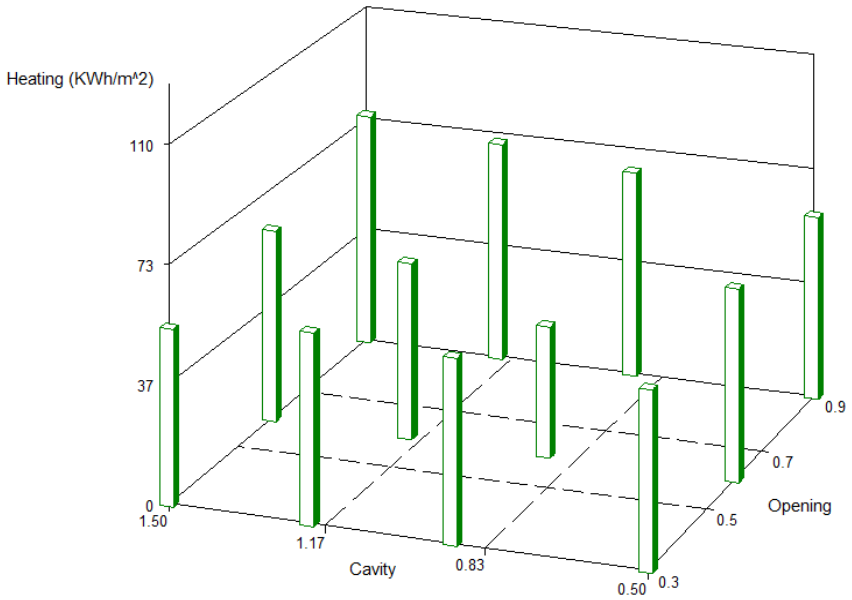

Shaft Height=5 Stories

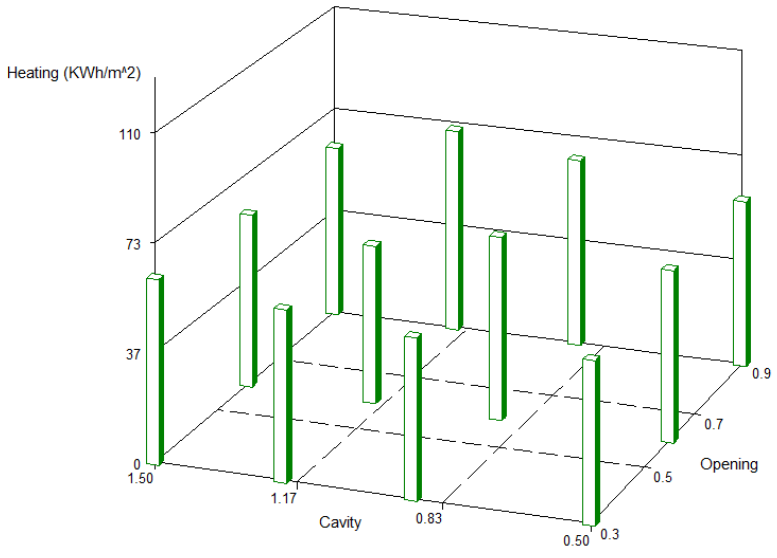

Shaft Height=9 Stories

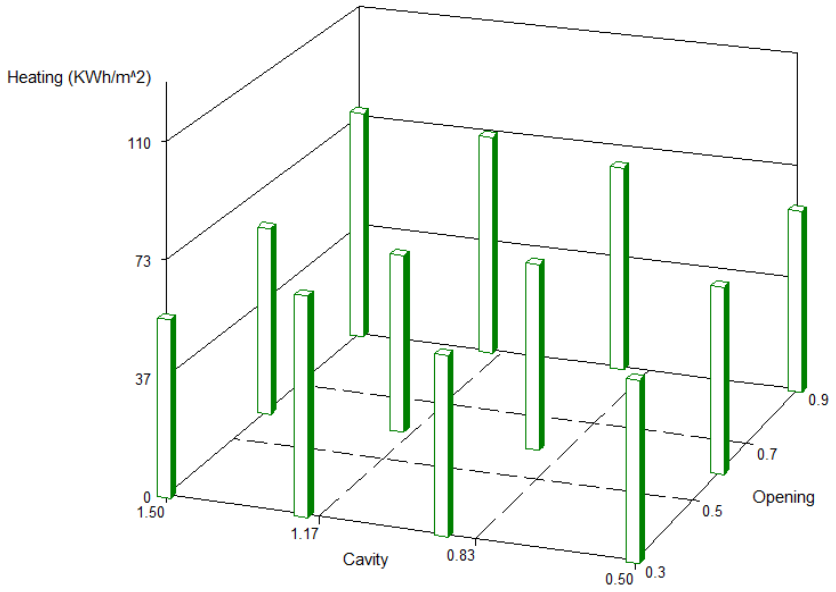

Opening Size=0.3 m

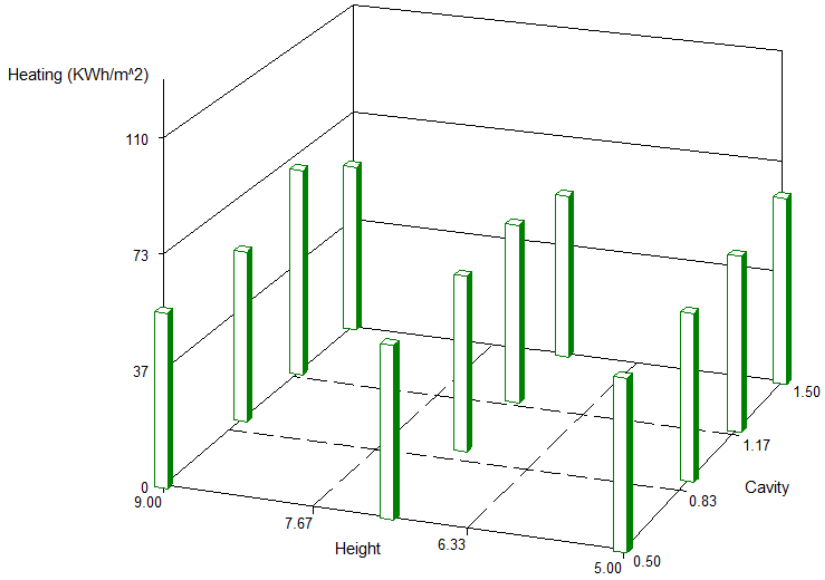

Opening Size=0.9 m

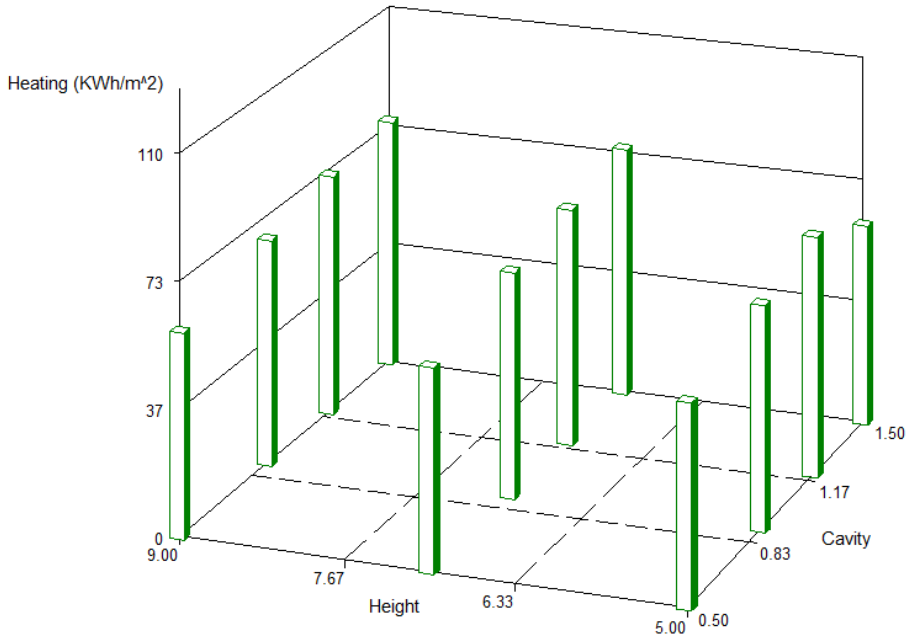

Opening Size=0.6 m

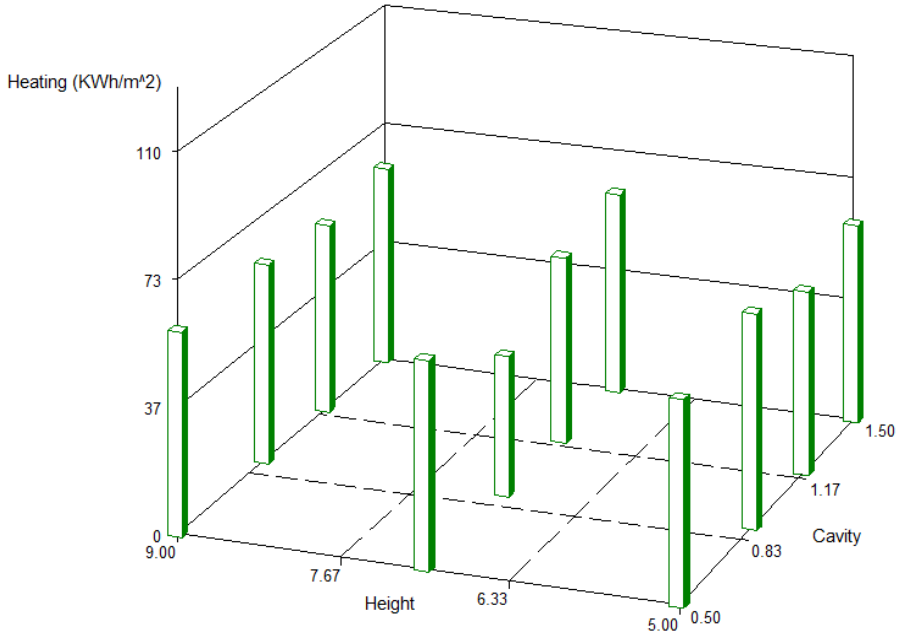

Cavity Depth=1.5 m

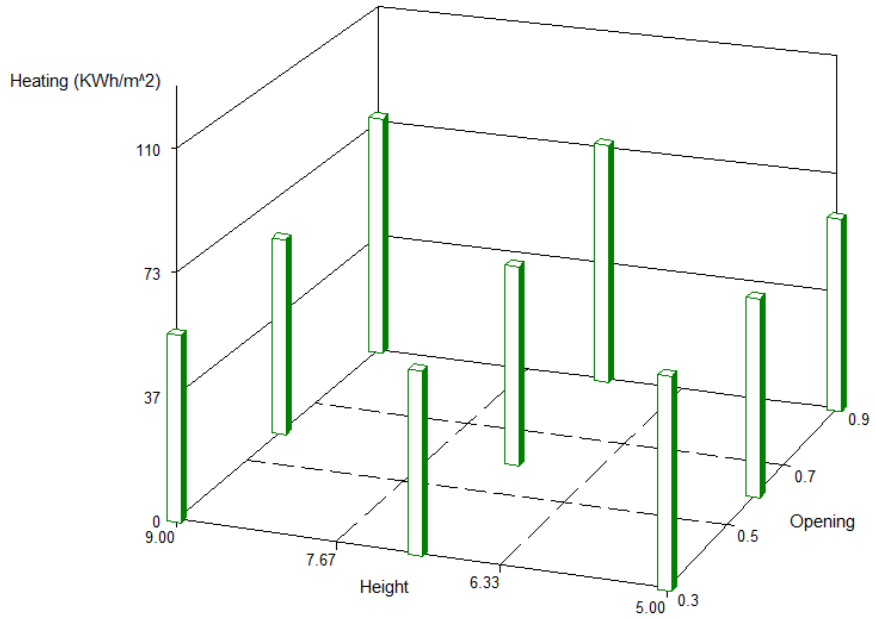

Cavity Depth=1.2 m

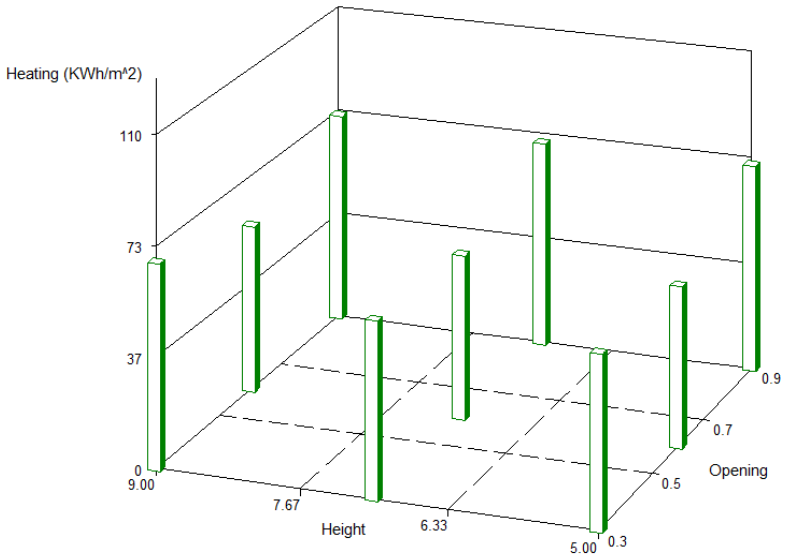

Cavity Depth=0.5 m

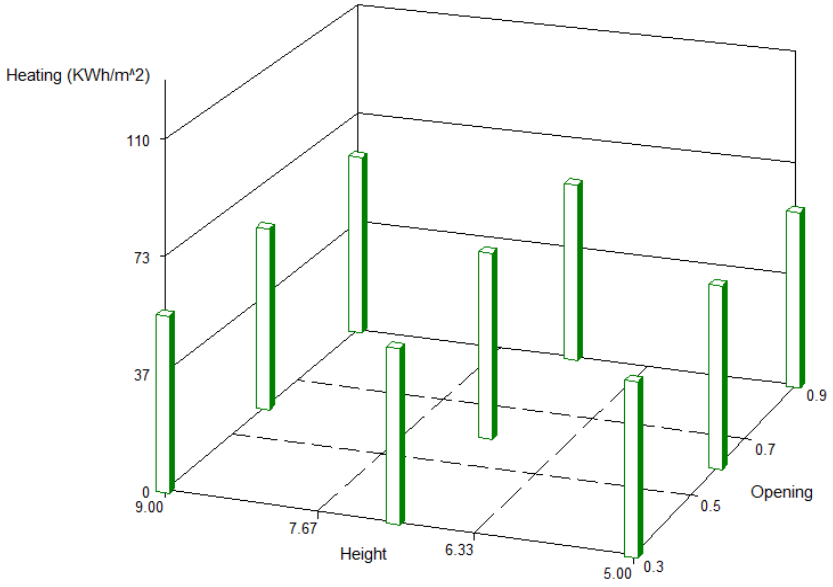

Cavity Depth=0.9 m